Final Report

to

California Department of Food and Agriculture
Fertilizer Research & Education Program,

Evaluating the Impact of Nutrient Management on Groundwater Quality in the Presence of Deep Unsaturated Alluvial Sediment

Sevim Onsoy
Thomas Harter
Timothy R. Ginn
Jan W. Hopmans
William R. Horwath

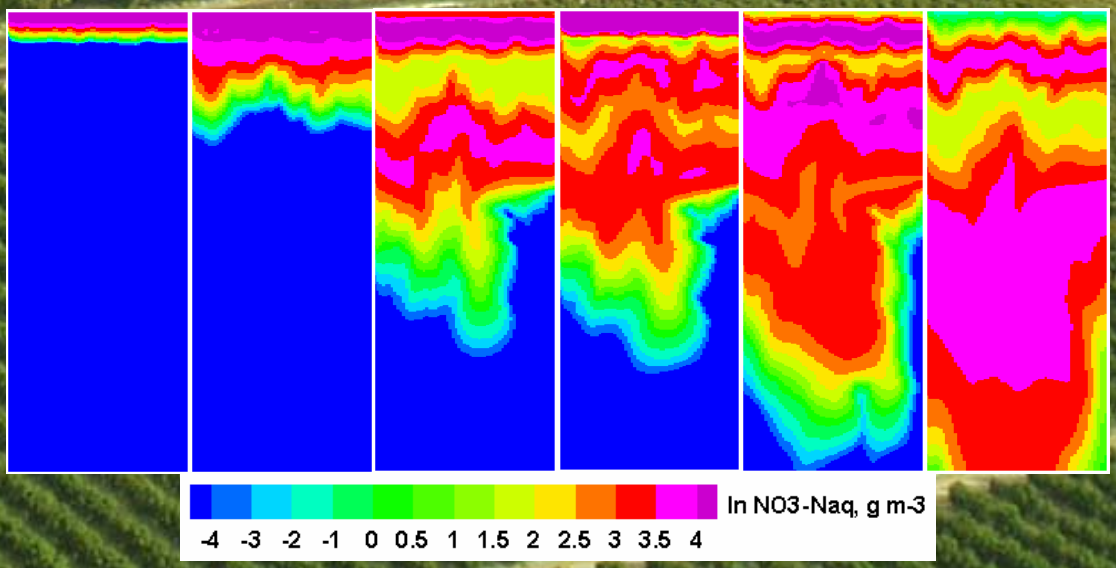

August 2005

FINAL REPORT / TECHNICAL COMPLETION REPORT

to

California Department of Food and Agriculture
Fertilizer Research and Education Program (FREP), Project 01-0584

Project Title: **Evaluating the Impact of Nutrient Management on Groundwater Quality in the Presence of Deep Unsaturated Alluvial Sediment**

Project Location Kearney Agricultural Center, Parlier, California

Project Scientist Sevim Onsoy, Graduate Research Assistant, University of California, Davis

Project Leaders

Thomas Harter, Ph.D.
Assoc. CE Specialist, Subsurface Hydrology
thharter@ucdavis.edu

Tim Ginn, Ph.D.
Professor, Water Resources Modeling
trginn@ucdavis.edu

Jan Hopmans, Ph.D.
Professor, Water Management
jwhopmans@ucdavis.edu

William R. Horwath, Ph.D.
Assoc. Prof., Soil Biogeochemistry
wrhorwath@ucdavis.edu

Department of Land, Air, and Water Resources
& Department of Civil and Environmental Engineering
University of California
Davis, CA 95616-8628

Funding Support

Fertilizer Research and Education Program, *Project 01-0584*, 2002-2005 **$ 58,468.-**

TABLE OF CONTENTS

LIST OF TABLES **7**

LIST OF FIGURES **8**

EXECUTIVE SUMMARY **13**

1. INTRODUCTION **17**

2. OVERVIEW OF MULTI-DIMENSIONAL VADOSE ZONE FLOW AND TRANSPORT MODELING APPROACHES **17**

2.1 Governing Equations for Flow 18

2.2 Governing Equations for Solute Transport 19

2.3 Overview of Existing Deterministic Flow and Transport Models 19

2.4 Overview of Existing Stochastic Flow and Transport Models 21

2.4.1 Upscaling of Solute Flux Predictions 21
2.4.2 Monte Carlo Approach 22

3. MODEL DEVELOPMENT: WATER FLOW **23**

3.1 Unsaturated Soil Hydraulic Properties for Homogeneous Lithofacies 23

3.1.1 Average Soil Hydraulic Properties 24
3.1.2 Effective van Genuchten Parameters for Homogenous Lithofacies 25

3.2 Unsaturated Soil Hydraulic Properties for Heterogeneous Lithofacies 27

Random Field of Scaling Factors within Lithofacies 27
Two-Dimensional Distribution of Scaling Factors 28

3.3 Plant Water Uptake 30

3.3.1 Tree Root Distribution 31

3.4 Initial Condition 32

3.4.1 Initial Pressure Profile: No Flow vs. Steady State Flow Conditions 32
3.4.2 Pseudo Steady State Flux in the Kearney Site Deep Vadose Zone . 34
3.4.3 Initial Pressure Profile for Two-Dimensional Layered Vadose Zone 35

3.5 Boundary Conditions 35

3.5.1Upper Boundary Condition 36
3.5.2 Lower and Vertical Boundary Conditions 42

3.6 Time and Domain Discretization 43

4. NITROGEN TRANSPORT IN THE VADOSE ZONE 43

4.1 Plant Nitrogen Nutrient Uptake 44

4.2 Initial Condition 45

4.3 Upper Boundary Condition 45

4.3.1 Fertilizer N Applications 45
4.3.2 Irrigation N Applications 46

4.4 Lower and Side Boundary Conditions 46

5. RESULTS AND DISCUSSION OF NUMERICAL SIMULATIONS 47

5.1 Numerical Mass Balances for Water Flow 47

5.2 Numerical Mass Balances for Nitrogen Transport 48

5.2.1 Numerical Stability of Nitrogen Transport Model 50

5.3 Surface Water Flux 50

5.3.1 Soil Evaporation 54

5.4 Plant Water Uptake 55

5.5 Pressure Head and Soil Water Content in the Vadose Zone 57

5.5.1 Mean Pressure Head in the Root Zone and in the Deep Vadose Zone 57
5.5.2 Effect of Lithofacies on Soil Water Content and Pressure Head 59

5.6 Soil Water Content 60

5.7 Pressure Head 62

5.8 Two-Dimensional Spatial Distribution of Soil Water Content 63

5.8.1 Homogeneous Lithofacies Model 63
5.8.2 Heterogeneous Lithofacies Model 65

5.9 Two-Dimensional Spatial Distribution of Pressure Head 67

5.10 Recharge from the Root Zone 67

5.11 Irrigation Efficiency 70

5.11.1 Role of Plant Water Uptake in the Root Zone Water Budget Analysis 70

5.12 Long-term Water Recharge to Groundwater 73

5.13 Two-dimensional Spatial Distribution of Water Flux 74

5.13.1 Homogeneous Lithofacies Model 74
5.13.2 Heterogeneous Lithofacies Model 77

5.14 Plant Nitrogen Uptake..... 81

5.14.1 Effects of Applied Irrigation on Plant Nitrogen Uptake 82
5.14.2 Model Estimated versus Measured Plant Nitrogen Uptake 84

5.15 Temporal Variations of Nitrogen in the Root Zone 85

5.15.1 Average Nitrogen Concentration 85
5.15.2 Total Nitrogen Mass 87
5.15.3 Annual Root Zone Nitrogen Budget 89

5.16 Nitrogen Concentration at the Root Zone 89

5.16.1 Standard Subplot 91
5.16.2 High Subplot 92

5.17 Temporal Variations of Nitrogen in the Deep Vadose Zone 93

5.17.1 Average Nitrogen Concentration 93
Total Nitrogen Mass 95
5.17.3 Annual Deep Vadose Zone Nitrogen Budget 95

5.18 Two-Dimensional Spatial Distribution of Nitrogen in the Vadose Zone 96

5.18.1 Homogeneous Lithofacies Model 96
5.18.2 Heterogeneous Lithofacies Model 102

5.19 Nitrogen Concentration and Travel Time in the Lithofacies 108

5.20 Average Nitrogen Concentration at Water Table 111

5.21 Nitrogen Travel Time to Groundwater 111

5.22 Nitrogen Flux to Groundwater 112

5.22.1 Cumulative Nitrogen Flux to Groundwater 113

5.23 Annual Vadose Zone Nitrogen Budget 114

6. SYNTHESIS OF MODELING APPROACHES: METHODS, RESULTS, AND DISCUSSION 119

6.1 Homogeneous vs. Heterogeneous Lithofacies 120

6.1.2 Effect of Correlation of Soil Hydraulic Properties on Model Results 121
6.1.3 Effect of Scaling Analysis on Model Results 121
6.1.4 Effect of Lack of Third Dimension on Model Results 122
6.2 Root Zone Mass Balance Approach vs. Numerical Modeling 122

6.3 Measured vs. Model Predicted Deep Vadose Zone N Mass 123

6.3.1 Effect of Denitrification on Deep Vadose Zone N Mass 124

6.3.2 Effect of Preferential Flow on Deep Vadose Zone N Mass..... 125
6.3.3 Effect of Layered Lithofacies on Deep vadose Zone N Mass 126

7. FUTURE WORK 127

EXTENSION ACTIVITIES RELATED TO THIS PROJECT 129

TECHNICAL/SCIENTIFIC CONFERENCE PRESENTATIONS 129

APPENDICES

Appendix 1. Onsoy, Y. S., T. Harter, T. R. Ginn, W. R. Horwath, 2005. Spatial variability and transport of nitrate in a deep alluvial vadose zone. Vadose Zone J. 4:41-55.

Appendix 2. Harter, T., Y. S. Onsoy, K. Heeren, M. Denton, G. Weissmann, J. W. Hopmans, W. R. Horwath, 2005. Deep vadose zone hydrology demonstrates fate of nitrate in eastern San Joaquin Valley, California Agriculture 59(2):124-132.

Appendix 3: Onsoy, Y. S., T. Harter, 2005. Spatial Variability of Soil Hydraulic Properties and Scaling Factors.

LIST OF TABLES

Table 1 Homogeneous soil hydraulic properties of the lithofacies given in the form of the van Genuchten parameters 25

Table 2 Basic statistics of scaling factors categorized by the lithofacies 27

Table 3 Records of irrigation applications at the fertilizer subplots from 1990 to 1996 38

Table 4 Records of fertilizer applications at the fertilizer subplots from 1990 to 1996. N concentrations are evaluated based on the amount of surface water flux (either irrigation, I, precipitation, P, or both, irrigation and precipitation, I+P) at the orchard……..45

Table 5 Annual root zone water mass balance from 1990 to 1996 based on simulation results in the a) homogeneous and b) heterogeneous lithofacies models 72

Table 6 Annual and cumulative NO_3-N uptake values at the standard subplot based on simulation results in the a) homogeneous and b) heterogeneous lithofacies models.....82

Table 7 Annual and cumulative NO_3-N uptake values at the high subplot based on simulation results in the a) homogeneous and b) heterogeneous lithofacies models 83

Table 8 Plant NO_3-N uptake measured at the standard and high subplots during the period from 1983 to 1985 and from 1991 to 1994 84

Table 9 Annual root zone NO_3-N mass balance at the standard subplot based on simulation results in the a) homogeneous and b) heterogeneous lithofacies models 89

Table 10 Annual root zone NO_3-N mass balance at the high subplot based on simulation results in the a) homogeneous and b) heterogeneous lithofacies models 90

Table 11 Annual root zone and vadose zone NO_3-N mass balance at the standard subplot based on simulation results in the a) homogeneous and b) the heterogeneous lithofacies models.....116

Table 12 Annual root zone and vadose zone NO_3-N mass balance at the high subplot based on simulation results in the a) homogeneous and b) the heterogeneous lithofacies models 117

Table 13 Comparison of the measured and model predicted deep vadose zone NO_3-N mass at the control, standard, and high subplots.....123

LIST OF FIGURES

Figure 1 a) East-west lithofacies cross section at y = 53.7 m (D-D' in Figure 2.1) identified at the fertilizer experimental site; b) boundaries of eight lithofacies identified from three boreholes shown inside the box in a) are used to characterize the site subsurface in the transient, variably saturated numerical model. Each layer is treated as a homogeneous unit with average soil hydraulic parameters that are defined in the form of the van Genuchten model.....26

Figure 2 A single realization of scaling factors generated individually for each lithofacies, a) log-transformed scaling factors and b) scaling factors 29

Figure 3 Schematic of the S-shaped plant water stress response function *a(h)* as defined by van Genuchten (1987).....31

Figure 4 Hypothetical pressure head profile as a function of depth in deep vadose zones.....33

Figure 5 Temporal variations of water flux at the bottom (at z =15.8 m) during the period from 1984 to 1996 based on simulation results in the one-dimensional numerical simulation 35

Figure 6 Initial condition pressure profile established for the eight-layered soil domain under a steady flux of 0.05 cm d^{-1} 35

Figure 7 Daily values of precipitation from 1990 to 1996 as obtained from the Parlier CIMIS station in Fresno, California 36

Figure 8 A typical irrigation application at the orchard: a) irrigation pipe is located from north to south direction on the east side of the orchard; b) irrigation is almost complete.....37

Figure 9 Crop coefficient curve for nectarine plotted together with precipitation and irrigation schedule for year 1990; K_{cb}: basal crop coefficient (solid blue line) varying as a function of the crop development stage, $K_{cb} + K_e$: combined effect of both transpiration coefficient K_{cb} and evaporation coefficient shown by solid green line.....41

Figure 10 Daily values of potential transpiration and evaporation plotted with daily precipitation and irrigation data for 1990 42

Figure 11 Daily potential transpiration and evaporation rates during the simulation period (1990 – 1996) .42

Figure 12 Hydrograph of a monitoring well (with the state well identification number 15S23E30B001M), located near the site.....43

Figure 13 Variations of relative water mass balance (in percentages) during the period from 1990 to 1996 based on simulation results in the homogeneous and heterogeneous lithofacies models.....47

Figure 14 Variations of relative N mass balance (in percentages) at the standard subplot during the period from 1990 to 1996 based on simulation results in the homogeneous and heterogeneous lithofacies models.....48

Figure 15 Variations of relative N mass balance (in percentages) at the high subplot during the period from 1990 to 1996 based on simulation results in the homogeneous and heterogeneous lithofacies models.....49

Figure 16 Variations of time step during the period from 1990 to 1996 based on simulation results in the a) homogeneous and b) heterogeneous lithofacies models 50
Figure 17 Variations of Peclet number during the period from 1990 to 1996 based on simulation results in the homogeneous and heterogeneous lithofacies models 51
Figure 18 Variations of Courant number during the period from 1990 to 1996 based on simulation results in the homogeneous and heterogeneous lithofacies models 51
Figure 19 Variations of mean pressure head at the top boundary (ground surface, z = 0 m) during the period from 1990 to 1996 based on simulation results in the a) homogeneous and b) heterogeneous lithofacies models 52
Figure 20 Variations of cumulative actual and potential surface fluxes during the period from 1990 to 1996 based on simulation results in the homogeneous and heterogeneous lithofacies models. a) Actual cumulative surface flux in the homogeneous and heterogeneous lithofacies models and b) potential and actual cumulative surface fluxes in the homogeneous lithofacies model. 53
Figure 21 Daily values of model simulated (actual) transpiration and evaporation during the period simulation period (1990 – 1996) in the a) homogeneous and b) heterogeneous lithofacies models 54
Figure 22 Comparison of daily values of potential and model simulated (actual) transpiration during the simulation period (1990 – 1996) in the a) homogeneous and b) heterogeneous lithofacies models 56
Figure 23 Cumulative potential and model simulated (actual) transpiration during the simulation period (1990 – 1996) in the homogeneous and b) heterogeneous lithofacies models 57
Figure 24 Variations of mean pressure head simulated in the root zone (0 m) during the simulation period (1990 – 1996) in the a) the homogeneous and b) heterogeneous lithofacies models 58
Figure 25 Variations of mean pressure head in the deep vadose zone of the standard and high subplots (1.8 m < z 15.8 m) during the simulation period (1990 – 1996) in the homogeneous and heterogeneous lithofacies models 59
Figure 26 Variations of pressure head at eight observation points located at various depths of the standard and high subplots based on simulation results in the a) the homogeneous and b) heterogeneous lithofacies models. Root Zone at z = 1.8 m; SL1 at z = 2 m; Var1 at z = 3.05 m; HP1 at z = 4.3 m; S at z = 6.75 m; Var2 at 7.9 m; C-Si-L at z = 12.65 m; and SL2 at z = 15.2 m. All points are located at the same horizontal distance of x = 3.1 m. 61
Figure 27 Variations of pressure head at eight observation points located at various depths based on simulation results in the homogeneous lithofacies model. Root Zone at z = 1.8 m; SL1 at z = 2 m; Var1 at z = 3.05 m; HP1 at z = 4.3 m; S at z = 6.75 m; Var2 at 7.9 m; C-Si-L at z = 12.65 m; and SL2 at z = 15.2 m. All points are located at the same horizontal distance of x = 3.1 m of the standard and high subplots 62

Figure 29 Contour maps of soil water content simulated in the homogeneous model at selected times during the simulation year of 1992 64
Figure 30 Contour maps of water content simulated in the heterogeneous model at selected times during the simulation year of 1992 66
Figure 31 Contour maps of pressure head simulated in the homogeneous model at selected times during the simulation year of 1992 68
Figure 32 Contour maps of pressure head simulated in the heterogeneous lithofacies model at selected times during the simulation year of 1992 69
Figure 33 Daily values of average water flux simulated at the bottom of the standard and high subplots (z = 15.8 m at the water table) during the period (1990 – 1996) in the homogeneous and heterogeneous lithofacies models 73
Figure 34 Contour maps of water flux simulated in the homogeneous model at selected times during the simulation period (1990 – 1996) 75
Figure 35 Contour maps of water flux simulated in the heterogeneous lithofacies model at selected times during the simulation period (1990 – 1996) 79
Figure 35 cont. Contour maps of water flux simulated in the heterogeneous lithofacies model at selected times during the simulation period (1990 – 1996) 80
Figure 36 Cumulative plant N uptake simulated at the standard and high subplots during the simulation period (1990 – 1996) in the homogeneous and heterogeneous lithofacies models 81
Figure 37 Average N concentration simulated in the root zone of the standard subplot during the period (1990 – 1996) in the homogeneous and heterogeneous lithofacies models 86
Figure 38 Average N concentration simulated in the root zone of the high subplot during the period (1990 – 1996) in the homogeneous and heterogeneous lithofacies models 86
Figure 39 Total N mass simulated in the root zone of the standard subplot during the period (1990 – 1996) in the homogeneous and heterogeneous lithofacies models 88
Figure 40 Total N mass simulated in the root zone of the high subplot during the period (1990 – 1996) in the homogeneous and heterogeneous lithofacies models 88
Figure 41 NO_3-N breakthrough curve simulated at the bottom of the root zone of the standard subplot (z = 1.8 m) during the period from 1990 to 1996 in the homogeneous and heterogeneous lithofacies models 91
Figure 42 NO_3-N breakthrough curve simulated at the root zone of the high subplot (z = 1.8 m) during the period from 1990 to 1996 in the homogeneous and heterogeneous lithofacies models 92
Figure 43 Average NO_3-N concentration simulated in the deep vadose zone of the standard and high subplots during the period from 1990 to 1996 in the homogeneous and heterogeneous lithofacies models 94
Figure 44 Total NO_3-N mass simulated in the deep vadose zone of the standard and high subplots during the period from 1990 to 1996 in the homogeneous and heterogeneous lithofacies models 95

Figure 45 Contour maps of NO_3-N concentrations in the homogeneous model at the standard subplot during the simulation period (1990 – 1996) 97
Figure 46 Contour maps of NO_3-N concentrations in the homogeneous model at the standard subplot during the simulation period (1990 – 1996) 99
Figure 47 Contour maps of NO_3-N concentrations in the heterogeneous model at the standard subplot during the simulation period (1990 – 1996).....103
Figure 48 Contour maps of NO_3-N concentrations in the heterogeneous model at the high subplot during the simulation period (1990 – 1996) 105
Figure 49 Breakthrough curves of NO_3-N concentration at seven observation points located at various depths of the standard subplot in the homogeneous and heterogeneous lithofacies models. SL1 at z = 2; Var1 at z = 3.05 m; HP1 at z = 4.3 m; S at z = 6.75 m; Var2 at 7.9 m; C-Si-L at z = 12.65 m; and SL2 at z = 15.2 m. All points are located at the same horizontal distance of x = 3.1 m.....109
Figure 50 Breakthrough curves of NO_3-N concentration at seven observation points located at various depths of the high subplot in the homogeneous and heterogeneous lithofacies models. SL1 at z = 2; Var1 at z = 3.05 m; HP1 at z = 4.3 m; S at z = 6.75 m; Var2 at 7.9 m; C-Si-L at z = 12.65 m; and SL2 at z = 15.2 m. All points are located at the same horizontal distance of x = 3.1 m.....110
Figure 51 Average NO_3-N concentration at the water table of the standard and high subplots during the simulation period (1990 – 1996) in the homogeneous and heterogeneous lithofacies models 111
Figure 52 Total NO_3-N flux at the water table of the standard and high subplots during the simulation period (1990 – 1996) in the homogeneous and heterogeneous lithofacies models 112
Figure 53 Cumulative NO_3-N flux at the water table of the standard and high subplots during the simulation period (1990 – 1996) in the homogeneous and heterogeneous lithofacies models 114

EXECUTIVE SUMMARY

The unsaturated zone acts as a critical buffer zone that protects groundwater from potentially harmful chemicals, which are spilled on the land surface or applied in agricultural areas as pesticides and fertilizers. Currently, the principal tool for evaluating nutrient management practices with respect to impact on groundwater quality is the root zone nutrient mass balance method. We still lack adequate understanding of fundamental processes interacting throughout the vadose zone, especially below the root zone. Better understanding of reactive transport processes in California's deep heterogeneous vadose zone is a key to assess both near- and long-term impact of agricultural management practices on groundwater quality. It requires intensive characterization of vadose zone properties and a quantitative linkage between multiscale observations, including precipitation, irrigation events, fertilizer applications, and soil and crop interactions.

The leading research objectives of this study were 1) to develop a modeling strategy to study effects of deep vadose zone heterogeneity on nitrate transport; and 2) to validate the modeling strategy to estimate nitrate transport to groundwater by utilizing the field site characterization of relatively deep highly heterogeneous alluvial sediments, and to investigate the uncertainty in predictions of solute flux to groundwater. Four research hypotheses lead our project design:

1. The deep unsaturated zone acts as a buffer zone that protects groundwater contaminant sources;
2. Field scale nitrogen transport is a nonlinear function of transport and reaction processes defined at the local scale (field scale measurement points), and controlled by physical and chemical heterogeneity in the vadose zone;
3. Denitrification below the root zone is significant;
4. Risk analysis of groundwater quality due to agrochemicals requires implementing effective modeling tools incorporating temporally and spatially varying processes (e.g., soil permeability, distribution of fines within the unsaturated zone) and boundary conditions (e.g., irrigation, precipitation, fertilizer application, evapotranspiration).

The project consisted of three key steps towards achieving the objectives:

1. evaluation of existing mass balance approaches for the assessment of field scale nitrate transport to groundwater,
2. development of a modeling strategy by combined use of stochastic and deterministic unsaturated flow and transport simulations that take into account the most relevant physical and biochemical processes involved in contaminant transport,
3. application of the modeling strategy to estimate nitrate transport to groundwater in deep highly heterogeneous alluvial sediments and validation of the modeling strategy by comparing the results with field measured nitrate distribution.

Previous annual and interim reports have focused on step 1. In this final report we summarize our findings from step 2 and 3.

The experimental results from a long-term (12 years, 1982-1995), well controlled, intensive field scale nitrogen applications on the alluvial fan of the Kings River (San Joaquin Valley, Kearney Agricultural Center) provided the basis for the validation of theoretical developments. Horizontal and vertical variability of the sediment stratigraphy of the research site is typical for many alluvial basins in California, and well characterized to the water table at a depth of about 16 m. The nitrate transport study at this specific site was used as an indicator of the effectiveness of the methodology in assessing the risk of groundwater contamination by agrochemicals in realistically

heterogeneous, unsaturated alluvial sediments as encountered in a majority of California's agricultural basins. The detailed description of local characterization was used to build a framework for vadose zone characterization in three-dimensions; thus, the field database in combination with the conceptual model development and validation can be used as basis to quantitatively evaluate nitrogen transport at other sites with similar field conditions.

Three modeling approaches, each representing a different subsurface scale of heterogeneity (field scale, lithofacies scale, and Darcy scale), provided three different levels of risk analyses of nitrate leaching to water table in response to the long-term site irrigation and nitrate management practices. None of the three models implemented herein is capable of sufficiently explaining the low nitrate levels observed at the site. The model-estimated deep vadose zone nitrate mass is at least four times larger than the measured deep vadose zone nitrate mass.

Our findings suggest that, given the highly variable soil texture, soil hydraulic properties and nitrate concentrations observed at the site, preferential flow paths at a scale even smaller than modeled here can lead to rapid, highly localized nitrate transport to water table. The significant degree of stratigraphic layering can enhance lateral flow and nitrate exchange among the adjacent subplots. Under the site conditions, denitrification in the deep vadose zone is limited, thus cannot account for the low nitrate levels observed at the site.

Model limitations, driven by the current state-of-the-art in computational resources, included the use of two-dimensional instead of three-dimensional simulation domains, the use of a linearized randomization of the significant spatial heterogeneity in the soil physical processes (using the scaling factor approach), a limited size of the simulation domain, and the use of a constant local scale dispersion coefficient. Future research work is needed to determine to which degree these limitations may have contributed to the modeling results, particularly with respect to the lack of significant preferential flow that is thought to occur in the deep vadose zone given the highly heterogeneous distribution of nitrate measured at the field site.

Regardless of these limitations, the implementation of the three modeling levels yields significant insight into the actual behavior of the highly transient flow and transport behavior in a deep alluvial vadose zone over a seven year period. It confirms and beautifully illustrates many of the findings of similar studies funded under the FREP program:

- The overall mass balance obtained by carefully monitoring the water and nitrogen budget of the root zone (top 1.8 m of the vadose zone) provides significant insight into the net water and nitrogen losses to groundwater.
- Denitrification does not explain the discrepancy between the (low) amount of nitrogen observed in the field and the (high) amount of nitrogen simulated in all three models. The field distribution of nitrogen and its isotopes is inconsistent with the concept of deep vadose zone denitrification
- The transient behavior of precipitation, irrigation, and evapotranspiration at the land surface affects not only the root zone, but rapidly affects moisture, suction, and water flux throughout a 16 m thick unsaturated zone. All of these are shown to be highly transient, even at the water table, under the irrigated, semi-arid conditions investigated here and typical for agricultural regions in semi-arid climates.
- Low irrigation efficiencies (on the order of 45% - 65%) contribute not only to significant leaching of fertilizer, but also to rapid transport of nitrate to groundwater. At the field site, irrigated at relatively low irrigation efficiencies, the travel time to groundwater through the 16 m thick vadose zone is predicted

(based on the three models) to be as short as 2 – 4 years. By the same token, higher irrigation efficiencies would result in significantly longer travel times. It remains to be seen to which degree preferential flow or fingering of flow through heterogeneous alluvial systems counteracts such increases in solute travel times through the vadose zone.

- Low irrigation efficiencies combined with fall application of fertilizer and high winter rainfall contribute significantly to the loss of nitrogen to groundwater. Precise timing of fertilizer applications with actual crop nitrogen uptake and improved irrigation efficiency can greatly alleviate this effect.
- Root zone and deep vadose zone monitoring, using traditional suction cup lysimeters, neutron probes, etc. is sufficient to monitor overall moisture conditions. More importantly, the significant spatial variability of nitrogen and moisture flux observed both, in the field and in the heterogeneous system modeling, leads us to conclude that current vadose zone monitoring techniques may be inadequate for monitoring field scale leaching rates of nitrogen to groundwater. A solid field scale root zone mass balance analysis, based on real field data and a cautious – conservatively low – estimate of denitrification and volatilization losses, currently remains the most reliable option to assess potential nitrogen losses to groundwater.

1. INTRODUCTION

Our findings based on the data analyses of the soil hydraulic and chemical properties of the site subsurface (Denton et al., 2004), in conjunction with the results of the traditional root zone N and water mass balance approach with uniform flow conditions (Appendix 1), lead to the conclusion that flux conditions in the deep vadose zone underlying the orchard may be highly heterogeneous in the presence of strongly heterogeneous geologic formations, highly variable hydraulic conductivity and water content, and strongly log-normally distributed nitrate concentrations.

The extensive deep vadose zone sampling campaign at the site provides the first extensive dataset for evaluating a model with a more refined characterization of the subsurface heterogeneity as opposed to the simplified root zone mass balance (MB) analysis. In an attempt to better simulate the subsurface geology and the corresponding soil hydraulic properties, two numerical models are developed to simulate transient, two-dimensional flow and nitrate transport through the 15.8 m thick vadose zone. A long-term 7 yr simulation is conducted both at the standard fertilizer subplot (110 kg N ha^{-1} yr^{-1}) and the high fertilizer subplot (365 kg N ha^{-1} yr^{-1}) with the modeling software HYDRUS-2D (Simunek et al., 1996). At the land surface boundary, the model is designed to handle temporally varying site flux boundary conditions corresponding to irrigation, precipitation, and evaporation for flow and nitrate fertilizer applications for transport. The model incorporates a sink term accounting for plant water and nitrate uptakes. Nitrate is simulated as a passive tracer in the deep vadose zone. This simplification is adopted based on the interpretation of the measured chemical properties such as nitrate, ^{15}N isotopes, soil pH, and soluble organic carbon. The subsurface is composed of eight *lithofacies* or *layers* (Denton et al., 2004) with vertically varying thicknesses over the simulation domain. The main emphasis of these two modeling approaches is to evaluate the impact of the spatial variability observed at the site at two scales, lithofacies (a few meters in thickness and tens of meters in lateral extent) and local scales (a few centimeters in thickness and a few decimeters in width), on water flow conditions, nitrate distribution, and N mass in the deep vadose zone. The first model conceptualizes each lithofacies as a homogenous unit with soil hydraulic parameters that are defined using the van Genuchten model and treated as constant *deterministic* values. While the homogeneous lithofacies approach is a simplification in accounting for the tremendous subsurface heterogeneity encountered at the site, strong, large scale subsurface heterogeneity is explicitly represented by varying soil properties according to lithofacies. Given the site database, which describes the spatial variability of soil hydraulic properties locally, the second numerical model is built upon the first model by accounting for the effects of local scale heterogeneity. The second model allows us to evaluate the impact of local heterogeneity on water flow and nitrate transport with heterogeneous lithofacies, each characterized by internally varying hydraulic properties.

2. OVERVIEW OF MULTI-DIMENSIONAL Vadose Zone Flow and Transport Modeling APPROACHES

This section provides a summary of methodologies used in existing deterministic and stochastic flow and transport models from a general point of view, along with the underlying principles of water flow and transport equations solved in our numerical simulations.

2.1 Governing Equations for Flow

Modeling flow and transport processes in porous media relies on a continuum approach which averages flux over a local volume of a porous medium, referred to as the *representative elementary volume* (REV) (as opposed to pore scale) (Yeh, 1998). This REV-averaged flux is then assigned to the center of the REV that serves as the mathematical definition of the spatial (point wise) location of the flux. Based on the continuum concept and the REV approach, water flow in variably saturated media at the laboratory scale is governed by the classical Richards equation (Richard, 1931), stated as below for two-dimensional flow:

$$\frac{\partial \theta}{\partial t} = \frac{\partial}{\partial x_i}\left[K(h)\left(K_{ij}\frac{\partial h}{\partial x_j} + K_{iz} \right)\right] - S \tag{1}$$

where θ is volumetric water content [L^3 L^{-3}], t is the time [T], h is the soil water pressure head [L], x_i (i=1,2) are the spatial coordinates [L], K_{ij} are components of a dimensionless hydraulic conductivity anisotropy tensor (i, j =1, 2); S is a sink term which represents the volume of water removed per unit time from a unit volume of soil due to plant water uptake [L^3 L^{-3} T^{-1}]. For a planar flow, $x_1 = x$ is the horizontal coordinate and $x_2 = z$ is the vertical coordinate (also elevation) that has its origin at the bottom of the domain and directed positively upward. In Eqn. (1), $K(h)$ is the unsaturated hydraulic conductivity [L T^{-1}], which is a function of pressure (or moisture content) under unsaturated conditions, given by

$$K(h,x,z) = K_s(x,z)K_r(h,x,z) \tag{2}$$

where K_r is the relative hydraulic conductivity and K_s is the saturated hydraulic conductivity. For isotropic medium, the diagonal entries of K_{ij} equal to one and off-diagonal entries of K_{ij} equal to zero (i.e., $K_{11} = K_{22} = K(h)$).

A simple model underlying flow through a porous media is Darcy's law. Obtained from empirical evidence, Darcy's law indicates that for an incompressible fluid flowing through a channel filled with a fixed, uniform and isotropic porous matrix, the Darcy's flux (scalar discharge per unit cross sectional area of the REV) in the horizontal direction q_x and vertical direction q_y can be expressed by

$$q_x = -K\frac{\partial H}{\partial x} = -K\frac{\partial h}{\partial x} \tag{3a}$$

$$q_z = -K\frac{\partial H}{\partial z} = -K\left(\frac{\partial h}{\partial z} + 1\right) \tag{3b}$$

where $\partial H / \partial x$ and $\partial H / \partial z$ are the total hydraulic gradient in the horizontal and vertical directions, respectively. Darcy's flux q can be then calculated by $q = \sqrt{q_x^2 + q_z^2}$. The total hydraulic gradient has two components: pressure head h and elevation head z. The elevation head gradient is zero for flow in the horizontal direction and is unity in the vertical direction. The proportionality constant K is the hydraulic conductivity dependent on both fluid properties and structure of the porous medium. Darcy's law defined for two dimensional flow is incorporated in Eqn. (1) in parentheses on the right side.

A number of closed-form formulas have been proposed to empirically describe the dependence of hydraulic functions $K(h)$ and $\theta(h)$ on pressure head (Brooks and Corey, 1964; Gardner, 1958; Haverkamp et al., 1977; van Genuchten, 1980; Russo, 1988). Among these relationships, Mualem (1976) and van Genuchten (1980) are widely used in modeling unsaturated flow.

2.2 Governing Equations for Solute Transport

The classic advection-dispersion equation for transport has been adopted to account for mixing and spreading of an inert solute during transient simulations (Bear, 1972):

$$\frac{\partial \theta c}{\partial t} = \frac{\partial}{\partial x_i}\left(\theta D_{ij}\frac{\partial c}{\partial x_j}\right) - \frac{\partial q_i c}{\partial x_i} - Sc_r \tag{4}$$

where c is the local concentration in the soil solution [M L^{-3}], θ is soil water content[L^3 L^{-3}], q_i is the i-th component of volumetric flux density [L T^{-1}], S is the sink term in the water flow equation (1), c_r is the concentration of the sink term [M L^{-3}], and D_{ij} is the hydrodynamic dispersion coefficient tensor [L^2 T^{-1}] (i, j = 1,2). Knowledge on water content and water flux q (i.e., Darcy's flux) are obtained from solutions of the Richard's equation (1). The second term on the right-hand side of Eqn. (4), $\partial q_i c / \partial x_i$, is referred to as the advection term that describes the transport of solute traveling at the same velocity as water. The first term on the right-hand side describes the spreading of solute that is caused by two mechanisms: 1) mechanical dispersion as a result of deviations of actual velocity on a microscale from the average velocity, and 2) molecular diffusion as a result of concentration variations. The hydrodynamic dispersion coefficient Dij tensor, which describes the combined effect of mechanical dispersion and molecular diffusion, is given by (Scheidegger, 1960)

$$D_{ij} = (\alpha_L - \alpha_T)\frac{v_i v_j}{v} + \alpha_T v \delta_{ij} + D_o \tag{5}$$

where α_L and α_T are longitudinal and transverse dispersivities, respectively, $v = \sqrt{v_i^2 + v_j^2}$, which is the magnitude of pore water velocity (sometimes referred to as specific discharge, given by $v = q/\theta$), δ_{ij} is the Kronecker delta (δ_{ij} = 1 if $i = j$, and δ_{ij} = 0 otherwise), and D_o is molecular diffusion.

2.3 Overview of Existing Deterministic Flow and Transport Models

Analytical solutions to the Richards' equation are possible only for special cases because of highly nonlinear dynamics of water flow in unsaturated media. Numerical models, as an alternative to physical experiments and analytical approaches, are used to analyze and predict flow motion. Deterministic numerical models are based on standard flow and dispersion equations (Eqn. (1) and (4)) and require a complete data description of input parameters (e.g., hydraulic conductivity and dispersion) at the same level of resolution as the grid spacing of a numerical code. Since such a complete dataset cannot be realistically obtained, spatial heterogeneity is often ignored below a certain scale threshold (above which characterization is available) and "effective" parameters are defined on the lower scales.

For the past several decades, we have seen considerable progress in the conceptual understanding of unsaturated water flow processes in general. A variety of numerical tools and

solution techniques, such as finite difference and finite element, for diverse purposes have been developed for simulating variably saturated flow problems. The mixed formulation of the Richards' equation, as given in Eqn. (1), is preferred over the alternative *h*-based (Rubin, 1968; Vauclin et al., 1979, Haverkamp et al., 1977; Haverkamp and Vauclin, 1979; Hills et al., 1989; Celia et al., 1990) and θ-based formulations (Haverkamp et al., 1977; Davis and Neuman, 1983; Hills et al., 1989; Kool and van Genuchten, 1991) since it maintains the mass conservative property inherent in the θ-based equation and combines benefits inherent in both θ-based and *h*-based forms of the equation while circumventing major drawbacks associated with each form (Celia et al., 1990).

Since the early 1980s, a number of numerical models have been developed for assessing risks from potential leaching of agrochemicals, in particular pesticides, to groundwater. Among the representative models is PRZM (Pesticide Root Zone Model), which was developed by Carsel et al. (1984). Further improvements resulted in the development of the updated PRZM-2 (Mullins et al., 1993), which links the PRZM and VADOFT (the Vadose Zone Flow and Transport Model, finite element model for one-dimensional flow and solute transport in the vadose zone), codes together, and the following version PRZM-3 (Carsel et al., 1998). RUSTIC model, developed by Dean et al. (1989), links three subordinate models: PRZM, VADOFT, and SAFTMOD (finite element model for two-dimensional flow and transport in the saturated zone developed by Huyakorn and Buckley, 1989). Other deterministic numerical models developed in the last two decades are CREAMS (Chemicals, Runoff, and Erosion from Agricultural Management Systems, Knisel, 1980), HSPF (Hydrological Simulation Program-FORTRAN, Johansen et al., 1984), GLEAMS (Groundwater Loading Effects of Agricultural management Systems, Leonard et al., 1987; Knisel et al., 1993), and LEACHM (Leaching Estimation and Chemistry Model, Wagenet and Hutson, 1989). These models have a range of complexities and have been extensively used under different circumstances (e.g., Smith et al., 1991; Laroche et al., 1996; Close et al., 1999; Malone et al., 1999; Dust et al., 2000; Rekolainen et al., 2000; Trevisan et al., 2000). These models can be used for simulating other solutes (e.g., nitrate) besides pesticides. Evaluation of these models is critical for the assessment of nitrate fate and transport, for instance, due to the limitations such as 1) only one-dimensional vertical simulation, thus neglecting realistic heterogeneity of the vadose zone in the horizontal directions, 2) predominant simulation in the root zone, consequently discontinuous treatment of subsurface (e.g., GLEAMS, PRZM, LEACHM), 3) simplified representations of physical phenomena, e.g., tipping bucket approach as opposed to solving Richard's equation for flow (GLEAMS, PRZM), or plug flow simplifications for transport, and 4) neglecting processes such as water and solute root uptake. Parrish et al. (1992) pointed out that the PRZM model is insufficient in the hydrologic components when tested against the field data. Spurlock (1998) evaluated PRZM, PRZM/VADOFT, LEACHM, and GLEAMS using experimental data in California and found that the applicability of PRZM and GLEAMS is questionable due their "tipping bucket" approach to describe downward water movement. Furthermore, most applications are not directly applicable in the presence of deep vadose zone due to simulation of root zone vadose zone processes only, consequently discontinuous treatment of subsurface (e.g., GLEAMS, PRZM, LEACHM).

More sophisticated, advanced numerical flow and solute transport models than those mentioned above are available to simulate one-, two-, or three-dimensional processes in variably saturated systems (VS2DT, Lappala et al., 1987 and Healy, 1990; VSAFT2, Yeh et al., 1993; SWMS-3D, Simunek et al., 1995; HYDRUS-1D, Simunek et al., 1998; HYDRUS-2D, Simunek et al., 1996. Both Hydrus-2D and VS2DT have been widely used in a number of agricultural and non-agricultural applications (McCord et al., 1997; Mailhol et al., 2001; Close et al., 2003). The VS2DT is a US Geographical Survey program that solves the Richard's equation for fluid flow and the advection-dispersion equation for solute transport by a finite difference approximation. In

addition to advection and dispersion, transport processes include first-order decay, adsorption, and ion exchange. The HYDRUS-2D is a finite element numerical model for simulating movement of water, solute and heat transport. The flow equation incorporates a sink term in the Richard's equation to account for water uptake by plant roots. The transport equations include, in addition transport processes (advection and dispersion), reactive transport processes, such as nonlinear and/or nonequilibrium reactions between the solid and liquid phases, linear equilibrium reactions between the liquid and gaseous phases, zero-order production, and two first-order decay reactions. Both the VS2DT and the HYDRUS-2D have undergone a series of upgrades and improvements and they are currently available with a graphical user interface.

2.4 Overview of Existing Stochastic Flow and Transport Models

Stochastic models are an attractive alternative to deterministic porous as they are commonly envisioned as a way to model both the uncertainty inherent in the nature and the lack of information about parameters at all points. Variability of parameters is treated as continuous random variables in space. For the justification of treating porous media properties as random variables, there is a distinction that needs to be drawn: randomness lies not in the physical nature of the porous media, which is deterministic, but in the limitation of our knowledge in estimating of heterogeneous properties (Harter, 1994). While the argument of whether the treatment of subsurface should be in a stochastic or deterministic framework has been long-lasting, field measurements of hydraulic properties that exhibit large scale spatial variability suggested that such parameters should be described in a stochastic context rather than in the traditional deterministic way (Freeze, 1975; Gelhar, 1986). Stochastic representation is maybe more realistic and useful than a zoned deterministic model.

Many researchers have attempted to study the effects of spatial variability on flow and transport in unsaturated zones (Dagan and Bresler, 1979; Jury, 1982; Jury et al., 1982; Simmons, 1982; Sposito et al., 1986; Russo and Dagan, 1991; Destouni, 1992). These simplified stochastic vadose zone transport models conceptualized the soil heterogeneity as though it was composed of a collection of hypothetical, isolated stream tubes (vertically homogeneous, statistically independent) with different velocities. Field studies (Ellsworth et al., 1991) and simulations (Russo, 1991) of transport in unsaturated, heterogenous porous formations suggest that the afromentioned transport models might be applicable to shallow depths.

Multi-dimensional numerical stochastic solute transport models, originally developed for the analysis of contaminant transport in groundwater, have been recently incorporated into the analysis of vadose zone transport processes (Russo, 1993; Harter and Yeh, 1996; Russo et al., 1998).

2.4.1 Upscaling of Solute Flux Predictions

Given the inherent variability of physical characteristics in the unsaturated zone, applications of flow and solute transport equations are faced with a major issue of *upscaling* that arises when models are used to study large-scale dynamic processes from small scale measurements. Sample sizes of measurements are generally much smaller than the scale of the problems in hand. In numerical modeling, spatial heterogeneity of the nature can be dealt with one of two ways. The existing spatial heterogeneity at the local scale is neglected and "effective" parameters are defined on the scale of interest. When choosing to represent a heterogeneous soil by its homogeneous equivalent, the subsequent question of estimating the effective properties arises. A straightforward approach is to use simple averaging (arithmetic or geometric) of the local soil hydraulic properties (Wildenschild and Jensen, 1999) to obtain effective parameters and

then to treat the medium with these parameters that are constant in space. Predictions based on the assumption of homogeneity can be expected to deviate from point measurements (Yeh, 1998). Then a measure of a difference between the prediction and point observations becomes imperative for making decisions (e.g., the spatial extent of contaminant).

In recent years, the stochastic approach has become increasingly popular for describing flow and transport in heterogeneous soils. Within the stochastic framework, parameters are treated as continuous random variables, and then used as input parameters for the well-established continuum description of flow and transport equations (Eqn. 1 and 4) to produce stochastic results (Polmann et al., 1991). Monte Carlo (MC) technique, briefly explained below, is ideally suited to dealing with upscaling.

2.4.2 Monte Carlo Approach

The Monte Carlo (MC) approach, combined with geostatistical simulation techniques, involves sequential generations of individual random realizations of input parameters (e.g., soil hydraulic properties) and subsequent deterministic solutions of flow and transport equations for each realization of input parameters. Each simulation is considered as a realization of a field. After multiple runs of the deterministic flow and transport model, statistics of water flux and solute concentration (mean and variance) are analyzed. The MC method, while offering advantages, has one major drawback: it is computationally intensive. This limitation is, however, is becoming less of a concern due to increase in the computer speed.

Former investigations of uncertainty in field scale solute flux have implemented the MC approach to saturated flow and transport problems (Smith and Schwartz, 1981; Dagan et al., 1992). Hopmans et al. (1988) and Ünlü et al. (1990) applied the MC technique to unsaturated flow problems for analyzing two–dimensional transient and one-dimensional steady unsaturated flow, respectively. Both studies indicated that heterogeneity in the direction of mean flow increases the variance of expected flux with increasing correlation scale. Harter (1994) applied the method for investigating expected steady state unsaturated flow in the framework of conditional stochastic analysis. The use of conditioned MC simulations is shown to reduce uncertainty in expected values (Harter and Yeh, 1996).

Previous modeling studies have considered a single realization of unsatured soil hydraulic properties to corroborate heterogeneous flow conditions under hypothetical (Russo, 1991; Russo et al., 1994) and realistic flow conditions (Russo et al., 1998). Although the single realization approach is not truly stochastic, it provides insight into the role of both intrinsic and extrinsic factors on solute migration to groundwater. From a three-dimensional flow and transport numerical model, Russo et al. (1998) brought two fundamental issues to our attention: 1) the transient nature of water flow under both natural and irrigated agricultural conditions in the vadose zone is affected by time-dependent processes which act on the soil surface; 2) relatively small variations in the soil hydraulic properties normal to the direction of flow can exert a significant influence on the spread of the solute plume.

To date, there is no work investigating the uncertainty in predictions of solute flux in a layered, highly heterogeneous deep vadose zone at a field scale using realistic, transient flow and transport boundary conditions for sufficiently long period of time (e.g., multi-year). The application of the homogeneous vadose zone approach and the single realization approach is the subject of this report.

3. MODEL DEVELOPMENT: WATER FLOW

Much research to date in subsurface fate and transport of nitrate has focused on the increased vulnerability of shallow water supply aquifers to nitrate contamination. The role of the deep vadose zone under intensively irrigated and fertilized areas such as orchards is still unknown. Identification of field-scale aquifer vulnerability to nitrate pollution in the Central Valley requires a quantitative linkage between multi-scale observations, including irrigation and precipitation events, soil and crop types, fertilizer applications, and subsurface aquifer properties. The primary objective of this report is to provide such a linkage using a long-term simulation model of flow and nitrate transport from the land surface to the water table at the standard and high subplots with homogeneous and heterogeneous soil hydraulic properties for individual lithofacies. Simulations of water flow and NO_3-N (as a tracer) start on January 1, 1990 and end on December 31, 1996 (a total of 2557 days). Simulated NO_3-N leaching beyond the root zone and accumulated NO_3-N mass in the deep vadose zone under the standard and high subplots are interpreted as N leaching risk.

The HYDRUS-2D model (Simunek et al., 1996) was used to numerically simulate the movement of water and NO_3-N. The program solves the Richards equation in Eqn. (1) using Galerkin-type linear finite element schemes with the mass conservative iterative scheme proposed by Celia et al. (1990). The HYDRUS-2D is presented here only in general terms. A detailed documentation of the software can be found elsewhere (Simunek et al., 1996; Rassam et al., 2003). As is usual practice in flow modeling, the simulation domain considered in this study is assumed to be isotropic; thus, the anisotropic hydraulic conductivity tensor reduces to a scalar, i.e., $K(h,x,z)$.

The HYDRUS-2D program was chosen to apply at our site for the following reasons: 1) the model has been intensively used in various applications, and its solution has been compared both with analytical and other published numerical results and its performance verified; 2) the flow model employs the mass-conserving formulation; 3) the soil domain can be differentiated into layers; 4) various types of initial and boundary conditions can be implemented; 5) it incorporates a sink term to simulate root water and nutrient uptake; and 6) long-term simulations can be achieved with a reasonable amount of computer time.

3.1 Unsaturated Soil Hydraulic Properties for Homogeneous Lithofacies

The unsaturated soil hydraulic properties in the HYDRUS-2D are described by a set of closed-form equations defined by van Genuchten (1980) who used the statistical pore size distribution model of Mualem (1976) to obtain a predictive equation for the unsaturated K function. The unsaturated hydraulic functions determined from the site data are defined by the van Genuchten equations (Mualem, 1976; van Genuchten, 1980). Note that in the HYDRUS-2D, the original van Genuchten equations were modified to add extra flexibility in the description of the soil hydraulic properties near saturation (Vogel and Cislerova, 1988). Without the modifications, the predicted hydraulic conductivity function $K(h)$ is extremely sensitive to small changes in the shape of the retention curve near saturation especially for fine textured soils due to the high non-linearity close to saturation. This can substantially impact the performance of numerical solutions of Eqn. (1) in terms of accuracy, stability, and rate of convergence of the numerical solution (Vogel et al., 2001). The extreme non-linearity occurs for values of the parameter n close to 1, representing fine textured soils and/or soils characterized by a relatively broad pore size distribution. As illustrated by Vogel et al. (2001), a modification to the van Genuchten model with a non-zero minimum capillary height (e.g., -2 cm) has no effect on the

retention function, yet leads to numerically more stable simulations. In our simulations the modified van Genuchten model is used.

3.1.1 Average Soil Hydraulic Properties

In heterogeneous soils, the translation of information about soil hydraulic properties measured on samples of a few cm in size (Darcy scale or local scale) to the scale that represents the typical resolution of flow and transport models (several meters) is referred to as the "upscaling" problem. It is considered a major challenge (Vogel and Roth, 2003). A major assumption is usually made to simplify the analysis: so called *effective hydraulic parameters* are chosen to represent average paramaters in an otherwise heterogeneous system. Despite the simplifying assumptions in the characterization of the spatial variability, this classic *deterministic* analysis of flow with average parameters in layered models have been used sometimes satisfactorily applied in laboratory and field scale problems (Hills et al., 1991; Wierenga et al., 1991; Schmalz et al., 2003). However, failures are more common, as pointed out in Glass et al. (1988) and Cushman et al. (2002).

Traditionally, effective hydraulic parameters are obtained by averaging (i.e., arithmetic, geometric, or harmonic averaging) properties that are determined from small-scale tests. These average properties are then used as input parameters for Eqn. (1). Previous numerical analyses concluded that, in general, neither the average moisture profile nor the average concentration profile in a heterogeneous field could be predicted by the concept of "equivalent soil" (i.e., a soil represented by the average of local scale data), if it is applied to entire domains. As suggested by (Jensen and Mantaglou, 1992), the stochastic approach can offer a rational framework for modeling the large scale heterogeneity in soils where soil formations are stratified. When the subsurface is composed of distinct layers, the assumption of relative homogeneity of soil hydraulic (and chemical) properties for each layer is a common practice to delineate different layers of soil texture, both in groundwater (Gego et al., 2001) and unsaturated flow and transport problems (Wierenga et al., 1991, Hills et al., 1991, Roth et al., 1991; Avanidou and Paleologos, 2002; Nimmo et al., 2002; Zhu and Mohanty, 2002b; Schmalz et al., 2003).

In the numerical model used here, the subsurface is characterized by eight layers (with spatially variable thickness) that reflect the boundaries of lithofacies at the field site. Boundaries of the layers are set to reflect the distribution of lithofacies in three boreholes along the tree-row (Figure 1a). These boreholes are chosen because they are representative of the primary features of the subsurface geology.

In the homogeneous lithofacies approach, each layer is conceptualized as a homogenous unit with average soil hydraulic parameters that are defined in the form of van Genuchten model and treated as constant deterministic values. While small scale subsurface heterogeneity is ignored, the larger-scale subsurface heterogeneity is well preserved by varying soil properties between facies and by using actual facies boundary distribution. This approach, applied in characterizing the subsurface of layered vadose zone systems (Wierenga et al., 1991, Hills et al., 1991), is computationally less time demanding than including all local scale heterogeneity into the model. Results will be used as the basis of comparison with the previous simple mass balance approach and with a truly heterogeneous model that incorporates a more refined characterization of lithofacies variability into modeling (see below).

3.1.2 Effective van Genuchten Parameters for Homogenous Lithofacies

A curve fitting procedure was applied to determine average van Genuchten parameters for eight layers that have vertically varying thicknesses over the simulation domain. Similar to the approach that is commonly applied in obtaining effective soil hydraulic properties, average curves of ln *K* and ln *h* were obtained by taking geometric average of the log transformed K and *h* data as a function of the saturation index ($K(\Theta)$ and h (Θ), respectively) (Wierenga et al., 1991; Russo and Bouton, 1992; Wildenschild and Jensen, 1999). Then van Genuchten parameters were fitted to both the average water retention and hydraulic conductivity data simultaneously by a least square optimization procedure. Table 1 shows the layers chosen for the simulation and corresponding average optimized soil hydraulic parameters. High values of the coefficient correlation (r^2) suggest good agreement between geometric average of ln *K* and ln *h* functions and those defined by the optimized parameters.

If the probability distribution of K is log-normal and if the flow is two-dimensional, the average *K* is exactly equal to the geometric mean of the local measurements of *K*, i.e., ln K = E (ln *K*) (de Marsily, 1986). As pointed out earlier in Yeh and Harvey (1990), who used different direct averaging techniques to derive the effective hydraulic conductivity of the layered sand, and later on in Wildenschild and Jensen (1999), geometric averaging fits the experimental layered data measured values of soil hydraulic properties better than arithmetic and harmonic averaging.

Table 1 Homogeneous soil hydraulic properties of the lithofacies given in the form of the van Genuchten parameters

Lithofacies	K_s (cm hr^{-1})	α (cm^{-1})	n	θ_r (cm^3 cm^{-3})	θ_s (cm^3 cm^{-3})	r^2 ln K	r^2 ln h
SL1	0.398	0.016	1.55	0.090	0.229	0.999	0.999
Var1	10.29	0.043	5.69	0.122	0.322	0.999	0.999
HP1	0.870	0.011	1.43	0.0001	0.263	0.999	0.999
S	10.92	0.030	5.05	0.122	0.331	0.999	0.999
Var2	0.560	0.011	1.74	0.170	0.229	0.999	0.999
C-Si-L	0.941	0.069	1.51	0.0001	0.245	0.999	0.999
SL2	0.398	0.006	2.32	0.150	0.348	0.999	0.999
HP2	0.394	0.009	1.83	0.172	0.275	0.999	0.999

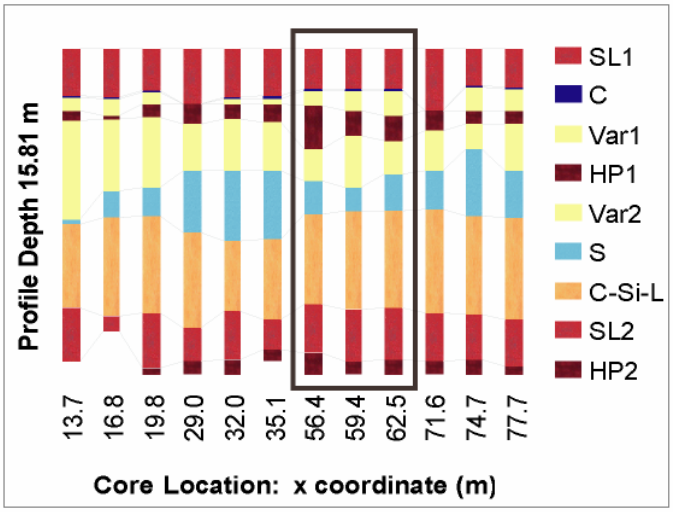

a)

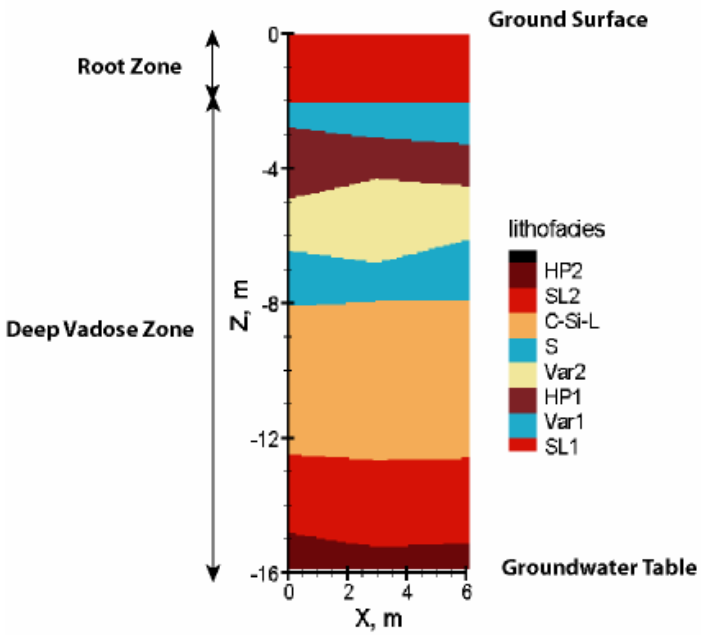

b)

Figure 1 a) East-west lithofacies cross section at y = 53.7 m (D-D' in Figure 2.1) identified at the fertilizer experimental site; b) boundaries of eight lithofacies identified from three boreholes shown inside the box in a) are used to characterize the site subsurface in the transient, variably saturated numerical model. Each layer is treated as a homogeneous unit with average soil hydraulic parameters that are defined in the form of the van Genuchten model.

3.2 Unsaturated Soil Hydraulic Properties for Heterogeneous Lithofacies

As an alternative to the homogeneous lithofacies model with homogenous soil hydraulic properties within the lithofacies, the heterogeneous lithofacies model was constructed with a single realization of scaling factors (Denton et al., 2004). By using the lithofacies means and variances, given in Table 2, the local scale heterogeneity both within and between lithofacies was taken into account in characterizing the subsurface heterogeneity. The lithofacies boundaries have a strong effect on the spatial variability of scaling factors.

Table 2 Basic statistics of scaling factors categorized by the lithofacies

		ln λ		
Lithofacies	# of Data	Mean	Variance	Standard Deviation
SL1	11	-0.916	0.966	0.983
Var1	7	0.728	0.339	0.582
HP1	8	-1.971	0.208	0.456
Var2	12	-1.535	0.232	0.482
S	8	0.272	0.830	0.911
C-Si-L	30	-1.999	0.300	0.548
SL2	11	-0.993	0.472	0.687
HP2	9	-1.651	0.289	0.538

Random Field of Scaling Factors within Lithofacies

Within the stochastic approach, the scaling factor is a so-called regionalized variable, $Z(xi)$, that is second order stationary and represents a realization of a random function distributed over the (two-dimensional) simulation domain. The expected value of scaling factor is constant in space, $E[Z(x_i)] = m$, and the covariance of the random function depends only the separation of the data points and independent of the position in space, $Cov[Z(x_i), Z(x_i + h)] = Cov(h)$.

Two principal assumptions associated with the heterogeneous lithofacies model are as follows:

- Because of difficulties in solving Richards' equation, only one simulated field of scaling factors was produced per lithofacies. Thus, the random field of scaling factors and results of the heterogeneous lithofacies simulations are not truly stochastic.
- A random field of scaling factors for each lithofacies was generated given that the correlation structure between the lithofacies is invariant

Eight, unconditional random fields of scaling factors, one for each lithofacies, was generated using the geostatistical sequential simulation algorithm **sgsim** in GSLIB (Deutsch and Journel, 1992) for the same domain size (x = 610 cm and z = 1580 cm) and the same grid discretization (Δx = 10 cm and Δz = 5 cm) as in the numerical model. This algorithm uses a Gaussian random field generator to generate a standard normal (Gaussian) function, which is completely characterized by a mean of zero and a variance of one, i.e., N (0,1). Given the information for the spatial correlation structure of the scaling factors (i.e., results of the variograms analysis, Appendix 3), the **sgsim** generates a value of scaling factor at each grid. Using the lithofacies mean and variances of scaling factors given in Table 2, a random field of

log-normal scaling factors, ln λ, was generated for each lithofacies separately by the following transformation:

$$\ln \lambda(x_i) = N(x_i) \cdot \sigma_{\ln \lambda} + \mu_{\ln \lambda} \tag{6}$$

where x denotes the spatial location and $N(x_i)$ is a normal random function N (0,1), distributed over the sampling of size k, for i=1,2,…,k, and $\mu_{\ln\lambda}$ and $\sigma^2_{\ln\lambda}$ are the mean and variance of scaling factors that vary as a function of lithofacies. The scaling factors obtained for the Kearney site are shown to be log-normally distributed (Appendix 3). Hence, the generated normal distribution, N (0.1), was used to obtain normally distributed log-transformed scaling factors ln λ. As a result, eight, randomly distributed log-normal scaling factors were generated for the entire simulation domain. From each random field of ln λ, only those values of scaling factors that fall within the lithofacies whose statistics (mean and variance) were used to generate the random field were extracted. A single realization of log-normal scaling factors was obtained when the extracted scaling factors corresponding to each lithofacies (Figure 1b) were combined all together.

The horizontal and vertical spherical semivariograms constructed for scaling factors were used to define the degree of spatial variability as required for the unconditional random field generation **sgsim** (Deutsch and Journel, 1992). The horizontal semivariogram shows a range (5.4 m) that extends over almost the entire horizontal dimension of the simulation domain. In the vertical direction, the range of 1.7 m is comparable to the average thickness of lithofacies. The sill of the horizontal semivariogram (0.77) is nearly half the sill in the vertical direction (1.49), suggesting a higher variability in the vertical direction than in the horizontal direction.

Two-Dimensional Distribution of Scaling Factors

A single realization of log-normally distributed scaling factors within the eight non-horizontal layers is shown in Figure 2. The range in the horizontal direction has a profound effect on the distribution of scaling factors. Scaling factors along the layering direction appear to be well correlated, showing a fairly smooth distribution. Consistent with the lithofacies means (Table 2), high values of scaling factors coincide within the Var1 and S, both having coarse-textured materials, whereas low values were generated within the HP1, Var2, and C-Si-L lithofacies that all have relatively small means. Due to highly contrasting mean values of scaling factors, scaling factors vary by two orders of magnitude across the lithofacies interfaces, particularly between the Var1 and HP1 and between the Var2 and S.

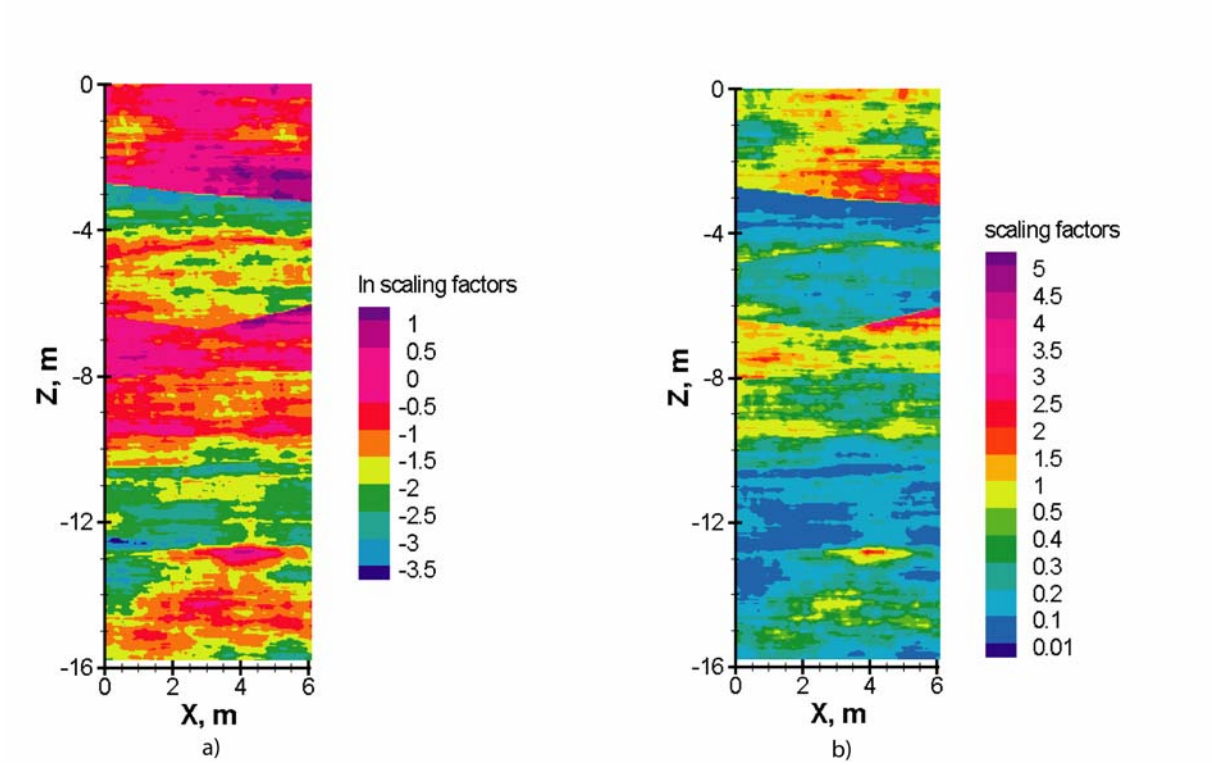

Figure 2 A single realization of scaling factors generated individually for each lithofacies, a) log-transformed scaling factors and b) scaling factors

The HYDRUS-2D, which can handle numerical calculations of flow with scaling factors, implements a linear type of scaling method both for pressure head *h* and hydraulic conductivity *K*, given by (Vogel et al., 1991):

$$h = \lambda_h \cdot h_r \tag{7a}$$

$$K = \lambda_K \cdot K_r \tag{7b}$$

in which soil water retention and hydraulic conductivity curves *h* and K at any location can be related to a reference h_r and K_r curves with two scaling factors, λ_h and λ_K. One-to-one transformation between λ_h and λ_K can be achieved by

$$\lambda_K = \left(\frac{1}{\lambda_h}\right)^2 \tag{8}$$

According to the Miller-Miller scaling technique which was used to produce the scaling factors for the Kearney site (Appendix 3), the same scaling factor is produced to relate soil water retention and hydraulic conductivity curves *h* and *K* at any location to a reference h_r and K_r curves. To transform the scaling factors generated based on the Miller-Miller approach, shown in

Figure 2b, to the linear model given in Eqn. (7a) and (7b), the following transformation was adopted:

$$\lambda_{h_L} = \frac{1}{\lambda_{M-M}} \tag{9a}$$

$$\lambda_{K_L} = \lambda_{M-M}{}^{2} \tag{9b}$$

where λ_{h_L} and λ_{K_L} refer to the scaling factors for the pressure head and hydraulic conductivity curves, respectively, in the linear model while $\lambda_{M\text{-}M}$ is the scaling factor in the Miller-Miller approach.

After the transformations, the random field of scaling factors, now defined based on the linear scaling mode, was entered into the HYRDUS-2D. The van Genuchten parameters of the reference curve used together with the scaling factors to describe the soil hydraulic properties of the eight-layered numerical model are as follows: K_s = 223.92 cm d^{-1}, α = 0.0239 cm^{-1}, n = 2.337, θ_r = 0.114, and θ_s = 0.307.

Keeping in mind again that our heterogeneous lithofacies model is a single realization approach and thus results will not be truly stochastic, our main focus is centered on the quantification of the spatial variability of N over sufficiently large area (meters) and sufficiently large time scale (years). Unlike previous modeling studies that have considered a single realization of soil hydraulic properties to corroborate heterogeneous flow conditions under hypothetical (Russo, 1991; Russo et al., 1994) and realistic flow conditions (Russo et al., 1998), our heterogeneous lithofacies approach accounts for lithofacies boundary effects and simulates realistic water and fertilizer practices for a long period of time (several years).

3.3 Plant Water Uptake

The modeling of water flow in unsaturated cropped soils requires the description of water uptake by plant roots. Root water uptake has typically been investigated at the microscopic and macroscopic levels. The microscopic approach requires details of root geometry as it describes flow of moisture into a single root within complex root-soil-water interactions (Gardner, 1960). When a whole rooting system is considered, it is impractical to construct a complete physical description of root water extraction. Therefore, the macroscopic approach is more suitable since it deals with the removal of moisture from the root zone without considering explicitly the effects of individual roots (Molz and Remson, 1970). At the macroscopic scale, a sink term, such as the S term in Eqn. (1), representing water extraction by the root system, is added to the dynamic water flow equation, e.g., the Richards equation (Nimah and Hanks, 1973; Molz, 1981; Clausnitzer and Hopmans, 1994). The sink term, as defined by Feddes et al. (1978), is

$$S(h) = a(h) \cdot S_p \tag{10}$$

where $a(h)$ is a dimensionless water stress response function (or root uptake reduction model) as a function of matric head h and S_p is the water uptake rate [T^{-1}] that defines the potential transpiration demand and is normalized over the root depth (i.e., $Sp = T$ [cm d^{-1}] /L_{RZ} [cm], where L_{RZ} = 180 cm is the depth of the root zone) (see below).

Several functional forms have been proposed for the S(h) function (Feddes et al., 1976, Molz, 1981, Hoffman and van Genuchten, 1983). HYDRUS-2D contains two alternative empirical functions for the water stress function a(h), each from a macroscopic viewpoint: one is linear and commonly known as Feddes function (Feddes et al., 1978) and the other is a nonlinear S-shaped function (van Genuchten, 1987). These models define how potential transpiration is reduced when the soil is no longer capable of supplying the amount of water demanded by the plant under given climate conditions. The concept of assigning critical soil water potential defining non-optimal conditions has been adopted in modeling plant uptake. For example, the S-shaped function proposed by van Genuchten (1987) is given in the form:

$$a(h) = \frac{1}{1 + \left(\frac{h}{h_{50}} \right)^3} \tag{11}$$

where h_{50} is the pressure head at which water extraction rate is reduced by 50% of the potential rate during dry soil conditions. Figure 3 shows a schematic plot of the S-shaped function used in our simulations for the parameters of h_{50} = -300 cm. If no water stress occurs in soil, a(h) = 1; thus, S_p in Eqn. (1) becomes equal to the potential transpiration rate.

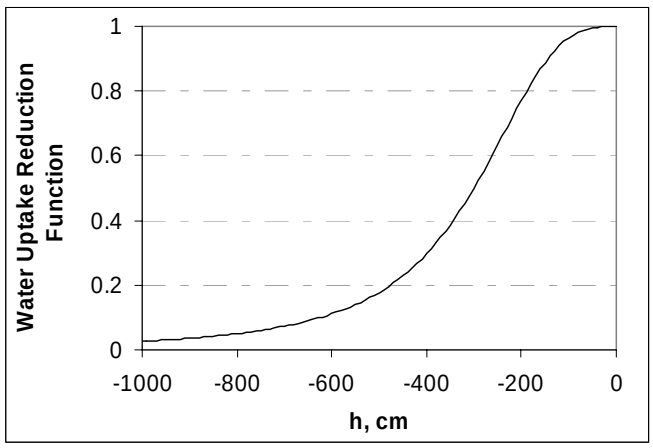

Figure 3 Schematic of the S-shaped plant water stress response function *a(h)* as defined by van Genuchten (1987)

3.3.1 Tree Root Distribution

The lateral extent as well as the depth of root penetration is an important feature of the tree system. In the numerical simulations considered here, the vadose zone is conceptually divided into two compartments: soil root zone and deep vadose zone (Figure 1b), similar to the way for the water and nitrate MB analysis (Appendix 1). An average of 1.8 m is used to represent the depth of the tree root zone where the most root activity is confined. The deep vadose zone is bounded by the soil root zone at the top and the water table at 15.8 m depth. Characteristically, for crops, new root growth starts near the soil surface in the spring and develops at deeper depths as the growing season progresses. For matured nectarine trees, activity of the root system and total root biomass is assumed to be invariant with time of growth stage. At the orchard, under flood irrigation and floor management system (no cover crop) at the orchard, it is anticipated that the root system of mature nectarine trees must have intermingled by intruding into empty space

available between trees and exploited soil over the root zone (Hughes et al., 1995). On the basis of experimental studies (Parker and Meyer, 1996) and in the interest of practicality, a homogenous root distribution was assumed over the entire root zone (1.8 m). S_p is defined according to

$$S_p = \frac{T_p}{L_z} \tag{12}$$

which distributes the potential transpiration rate T_p [L T^{-1}] uniformly over the root depth L_z [L] which is also assumed to be invariant of time for mature nectarine trees. Uniform root density may not be appropriate for localized irrigation systems such as drip irrigation, in particular, which causes a concentration of roots close to the tree rows (Tagliavini et al., 1996).

3.4 Initial Condition

For transient unsaturated flow simulations, the solution of Eqn. (1) requires the knowledge of the initial distribution of water content or pressure head data within the flow domain. Data for initial conditions at the site are not readily available, as is common in most studies. The section below describes how the initial condition is estimated.

3.4.1 Initial Pressure Profile: No Flow vs. Steady State Flow Conditions

When no data for initial conditions in a deep vadose zone are available, establishing initial conditions can be very challenging. Hydrostatic pressure equilibrium has been widely accepted as initial conditions within a homogeneous soil profile between the ground surface and water table (Nimmo et al., 2002; Zhu and Mohanty, 2002a) if no flow condition is applicable. Under such conditions, hydraulic head gradient between two vertical points is equal to the change in elevation (∇z) between the corresponding points. Even if the deep vadose zone is homogeneous, pressure developed at the ground surface under the hydrostatic equilibrium condition becomes much greater for a deeper water table than a shallow one, leading to numerical convergence problems due to the infinite tension at the surface. Besides, since water moves through the vadose zone in response to surface flux conditions such as precipitation, evaporation, or evapotranspiration no-flow condition is unlikely regardless of the depth of the vadose zone.

Alternatively, if one assumes that flux is constant and that steady state conditions are attained (Yeh, 1989; Harter and Yeh, 1998; Tartakovsky et al., 1999), then the pressure profile between the ground surface and the water table can be described by Darcy's equation, as given below for vertical flux conditions:

$$q = -K(h)\left(\frac{\partial h}{\partial z} - 1\right) \tag{13}$$

where z is the vertical distance, taken to be positive upward. Eqn. (10) leads to

$$z = \int_0^h \frac{K(h)dh}{K(h) - q} \tag{14}$$

Under a steady downward flux $q << K_s$ of the profile, the pressure profile in a homogenous soil closely follows the hydrostatic line. The pressure head is zero at the water table, becoming more

negative upward. At some depth, hydraulic conductivity begins to decrease, as a result of pressure drop and at some depth when K becomes numerically equal to the surface applied steady flux q, a critical singularity occurs, causing the denominator in the integrand of Eqn. (11) to become zero. This corresponds to a unit hydraulic gradient condition of unity and pressure head gradient of zero ($\partial h / \partial z = 0$); thus, gravity becomes the only force driving the downward flow above the capillary fringe of the water table (Rockhold et al., 1997; Nimmo et al., 2002; Zhu and Mohanty, 2002a)

In sufficiently deep vadose zones in arid regions (e.g., Mojave River basin, California), pressure head fluctuations may cease away with depth, creating a zone of steady state flux where the effects of atmospheric boundary conditions may become minimal and vertical flow is driven by gravity alone (Gardner, 1964). Then, the unsaturated hydraulic conductivity of the medium indicates downward flux q which is interpreted as a long-term average recharge rate, i.e., *quasi-steady state flux*, to the water table (Nimmo et al., 2002). Figure 4 illustrates a hypothetical pressure profile that can typically develop in a thick homogenous vadose zone under a quasi-steady state flux below the fluctuation zone.

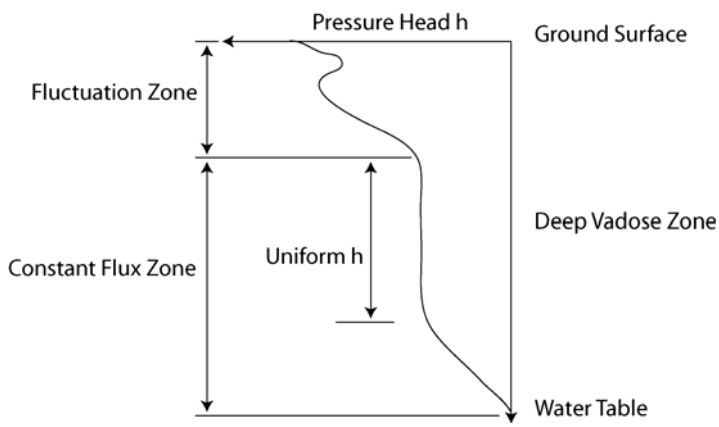

Figure 4 Hypothetical pressure head profile as a function of depth in deep vadose zones

On the contrary, if a substantial amount of transient infiltration occurs at the surface, leading to transient recharge to the water table, steady state flux q (i.e., average flux) in the constant flux zone of the deep vadose zone, as shown in Figure 4, may hardly exist. In addition to the transient surface fluxes, another complication plays a role in the development of an initial pressure profile for a layered deep vadose zone. As a result of substantial variations in hydraulic properties of texturally contrasting layers, pressure head in a layered system will not be uniform even with steady flow.

Rockhold et al. (1997) proposed an analytical method for solving Eqn. (11) for a layered system under a steady state flux condition. The solution includes integrating the equation segment by segment using a piece-wise approximation of ln K(h). They used the van Genuchten model (1980) and Mualem (1976) water retention and hydraulic conductivity models. In this study, their approach was implemented to generate the initial pressure profile for the two dimensional simulation domain. The approach is explained in Rockhold et al. (1997) and the FORTRAN code that solves Eqn. (11) was made available to us by the authors.

3.4.2 Pseudo Steady State Flux in the Kearney Site Deep Vadose Zone

In the case of transient flow conditions in the vadose zone, a *pseudo-steady state flux* at the bottom of the domain (or at the water table) can be achieved and then used to set up an initial pressure profile for an otherwise transient system. A simple, one-dimensional flow model was constructed at the site conditions to examine temporal and spatial variations in the downward flow through the 15.8 m profile with a domain discretization of Δz = 5 cm (i.e., 317 nodes). Similar to the two-dimensional model considered herein, this model has eight layers whose boundaries are defined by average thicknesses of major facies. Each facies was characterized by its average soil hydraulic properties obtained from the optimization process (Table 1). A long-term, 14-year simulation (1984 - 1997) was carried out with the modeling software HYDRUS-1D (Simunek et al., 1998). Data for daily precipitation and crop evapotranspiration and an average of 13 irrigations per year (at a rate of 13.4 cm ha^{-1} per irrigation) were prescribed at the surface boundary. For simplicity, an arbitrary initial pressure profile was set up: pressure is zero at the bottom (water table), and is linearly dropped to -200 cm at the surface. For such a long simulation time, the effect of arbitrary initial condition is expected to negligible; thus, has no significant impact on the long-term moisture profile.

Our simulation results suggest that, despite significant thickness of the deep vadose zone, changes in water flux across the land surface boundary produce temporal variations in the water flux even at the bottom of the 16 m thick vadose zone. The bottom flux fluctuates from approximately 0.05 to 1 cm d^{-1} in response to surface boundary conditions. The peak occurs during the middle of summer possibly due to the arrival of water from irrigation applications that occurred during spring time. The flux rapidly decreases as the effect of increasing evapotranspiration loss at the surface becomes more profound. With less water contributing from winter precipitation, it continues to gradually decrease until the middle of the following summer. These seasonal patterns in the flux recur every year (Figure 5). Since a hypothetical quasi-steady state flux does not develop at the Kearney site vadose zone, the minimum simulated flux of 0.05 cm d^{-1}, which occurs at the water table seasonally during winter, is chosen as an approximation to determine the initial condition of the two-dimensional simulation. Hereafter, this flux is referred to as *quasi- steady state flux*.

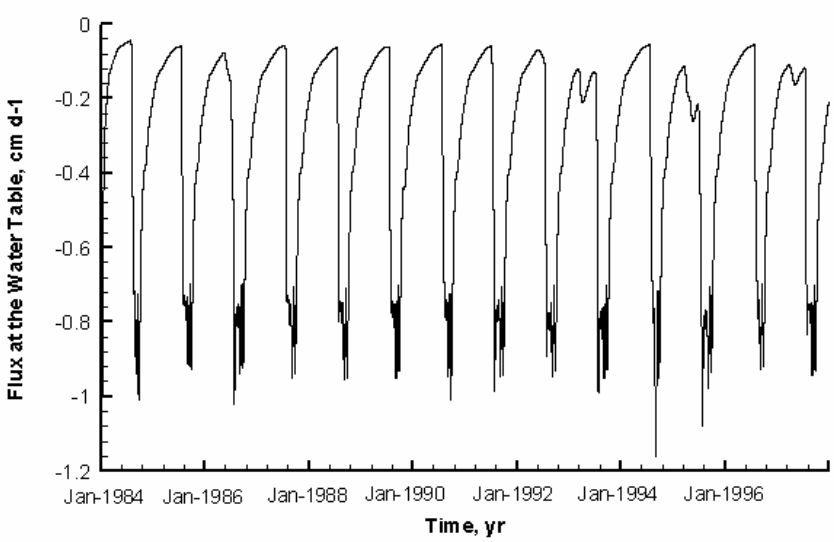

Figure 5 Temporal variations of water flux at the bottom (at z =15.8 m) during the period from 1984 to 1996 based on simulation results in the one-dimensional numerical simulation

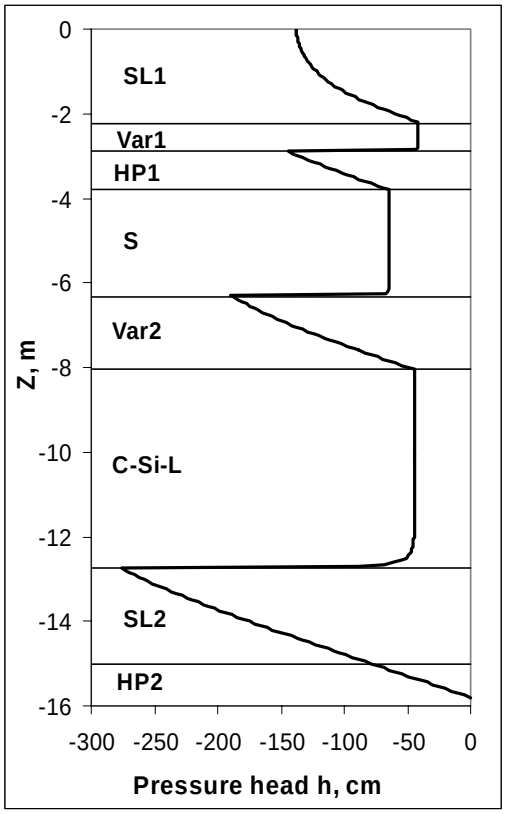

Figure 6 Initial condition pressure profile established for the eight-layered soil domain under a steady flux of 0.05 cm d^{-1}

3.4.3 Initial Pressure Profile for Two-Dimensional Layered Vadose Zone

To establish the initial condition of the two-dimensional layered models, Rockhold et al.'s (1997) analytical method was used with the quasi-steady state flux of 0.05 cm d^{-1} (~0.002 cm hr^{-1}) applied at the surface using the layer specific soil hydraulic parameters listed in Table 1. This method was designed for one-dimensional flows. Here, average layer thickness was used for the one-dimensional representation. As expected, the pressure profile varies within the layers as a function of the soil hydraulic properties of each layer. A typical steady state flux profile tends to form in the Var1, S, and C-Si-L lithofacies.

3.5 Boundary Conditions

The solution of Eqn. (1) requires the specification of boundary conditions imposed at the top, the bottom, and on the sides of the simulation domain shown in Figure 1.

3.5.1 Upper Boundary Condition

According to the sign convention used in the HYDRUS-2D, the vertical direction z is positively upward; that is, $z = 0$ m is the bottom of the model where the water table exists and $z = 15.8$ m is the ground surface. This convention is used exclusively to construct the numerical model and to describe the boundary conditions in the model. In the text, the ground surface is taken to be zero and the water table is located at -15.8 m consistently.

Daily values of water fluxes including precipitation, irrigation, and evapotranspiration are applied uniformly across the top surface. These prescribed fluxes occurring at the soil-air interface, referred to as atmospheric boundary conditions in the model, are defined by

$$q_w = q_0(t) \tag{15}$$

where q_o is the flux imposed at the surface [cm d^{-1}] for t > 0. Potential flux across the upper boundary is determined by the model as the difference between prescribed fluxes out of the system (evaporation) minus fluxes into the system (precipitation plus irrigation). Actual surface flux depends on the transient soil moisture conditions at the soil-air interfaces which are exposed to atmospheric boundary conditions and is calculated internally by the model. During the simulation, the model automatically shifts from a flux boundary condition (i.e., Neumann type) to a prescribed pressure head (i.e., Dirichlet type) according to two limiting values of surface pressure: hCritS and hCritA. hCritS is the maximum allowed pressure head at the surface and the latter specifies the minimum allowed surface pressure head. If surface pressure hCritS is reached, infiltration exceeds the conductive capacity of the surface soil. Since the model does not allow surface ponding, it reduces the surface flux rate to the saturated hydraulic conductivity of the medium. In a similar way, if soil becomes too dry to transmit water to the surface at the potential rate imposed by the climate conditions, evaporation flux is reduced to a rate which is determined by the minimum allowed surface pressure head of hCritA. In the present study, the maximum and minimum allowed pressure heads are set to 0 cm and -1000 cm, respectively, for the entire simulation period.

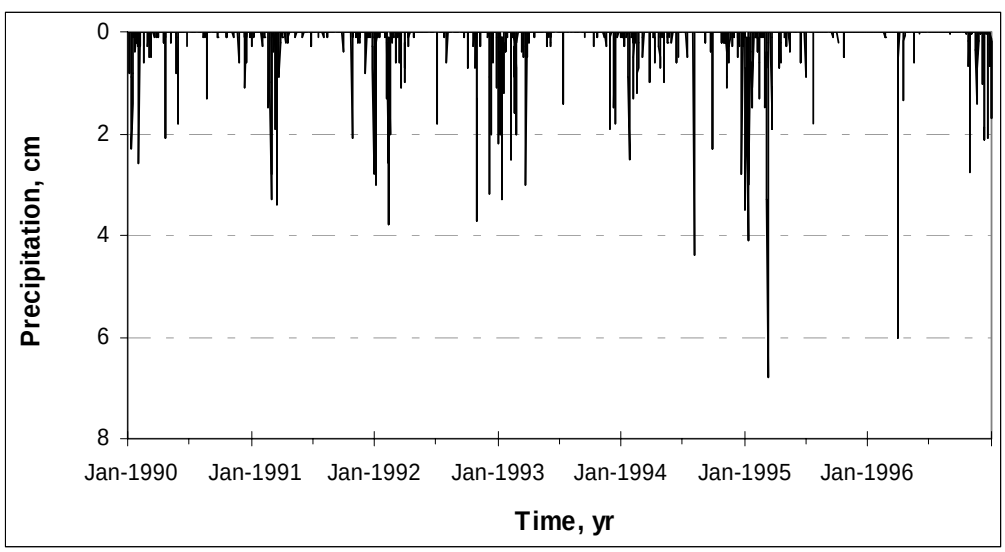

Figure 7 Daily values of precipitation from 1990 to 1996 as obtained from the Parlier CIMIS station in Fresno, California

Precipitation

Daily values of precipitation from 1990 to 1996, as obtained from the Parlier CIMIS station, are shown in Figure 7. Based on the 7 years of data, the annual precipitation averages to 37 cm (see below; Table 4). In most years, essentially no precipitation was recorded between May and early October. 1990 is the driest year with annual precipitation of 26 cm while 1995 is the wettest year having annual precipitation almost twice as much as that recorded in 1990 (49 cm).

Irrigation Inputs

Throughout the experiment, flood irrigation, as is common for many orchards in the project area, was performed at the orchard usually from April through September. The irrigation water was supplied by a pipe located at the east side of the orchard (Figure 8). A typical irrigation started at around 10 am at 300 gpm. The water was turned on to a lower flow rate of 150 gpm in the late afternoon (between 3 and 4 o'clock) and was left on overnight. The next day, in the morning around 7 am, the flow rate was increased to 300 gpm and the water was shut off that day around 10 am. Based on this site record, each irrigation applied an average of 13.44 cm water for roughly 24 hours (150 gpm for 15 hours and 300 gpm for 9 hours).

a) b)

Figure 8 A typical irrigation application at the orchard: a) irrigation pipe is located from north to south direction on the east side of the orchard; b) irrigation is almost complete.

Dates of irrigation events, which were obtained from the site records, are tabulated in Table 3 for the simulation duration of 1990 – 1996. The number of irrigations applied in a year at the orchard varies from 9 to 17. In the annual water mass balance analysis (Appendix 1), 13 irrigations per year with the average application of 13.44 cm of water (or 5.3 in) were considered to approximate the total water applied at the orchard. Herein, the exact number of irrigation applications is incorporated in the numerical model. Because of the absence of surface ponding in the HYDRUS-2D, any excess water on the surface is removed immediately from the system when the potential net flux exceeds the infiltration capacity of the surface soil that is exposed to the atmospheric conditions. At the orchard, losses of irrigation water at the surface due to surface runoff are negligible since the flood irrigation generates no surface water return flow. To avoid any artificial removal of water from the system, irrigation is distributed over two consecutive days at a lower application rate than 13.44 cm d^{-1}: at a rate of 9 cm d^{-1} in the first day and 44 cm d^{-1} in the second day. Note that we keep the total applied water the same while ensuring that the

application rates do not exceed the saturated hydraulic conductivity of the fist layer SL1 (Saturated K for the SL1 = 0.398 cm hr^{-1} = 9.55 cm d^{-1}, see Table 1).

Table 3 Records of irrigation applications at the fertilizer subplots from 1990 to 1996

	Years						
# of Irrigation	1990	1991	1992	1993	1994	1995	1996
1	29-Mar	7-Feb	22-Apr	19-Mar	21-Mar	1-May	1-May
2	17-Apr	3-May	29-Apr	16-Apr	14-Apr	10-May	9-May
3	8-May	22-May	7-May	3-May	10-May	22-May	21-May
4	4-Jun	3-Jun	18-May	18-May	23-May	31-May	3-Jun
5	14-Jun	20-Jun	28-May	1-Jun	1-Jun	8-Jun	25-Jun
6	21-Jun	1-Jul	3-Jun	9-Jun	9-Jun	20-Jun	2-Jul
7	27-Jun	15-Jul	9-Jun	18-Jun	16-Jun	3-Jul	30-Jul
8	3-Jul	30-Jul	18-Jun	24-Jun	23-Jun	10-Jul	11-Sep
9	10-Jul	8-Aug	25-Jun	1-Jul	30-Jun	25-Jul	3-Oct
10	24-Jul	6-Sep	1-Jul	9-Jul	16-Jul	7-Aug	
11	9-Aug		8-Jul	16-Jul	28-Jul	23-Aug	
12	5-Sep		23-Jul	30-Jul	8-Aug	6-Sep	
13	18-Sep		6-Aug	9-Aug	16-Sep	4-Oct	
14			20-Aug	24-Aug			
15			31-Aug	2-Sep			
16			10-Sep	14-Sep			
17			28-Sep				

Evapotranspiration

Evapotranspiration, abbreviated as *ET*, is one of the most difficult soil water balance parameters to measure. It defines a combination of two separate processes whereby water is lost from the soil surface by evaporation and from the root zone by crop transpiration. The amount of water available at the surface and the degree of shading affect evaporation process. Where the soil is able to supply water fast enough to satisfy evaporation demand, evaporation is determined by the potential evaporation. When soil is wetted, evaporation will be a large part of the total *ET* of the crop, especially at the beginning of the growth season. When water content in the topsoil drops, the limited availability of water exerts a controlling influence on soil evaporation. In the absence of water supply to the soil surface, evaporation decreases and may cease completely.

Reference and Potential Evapotranspiration

The most widely used techniques for *ET* estimates are referred as reference ET, commonly known as ET_o, in which potential *ET* for a grass (or an alfalfa) reference crop that fully shades the ground and does not suffer water stress is predicted using climatologic data (DWR, 2000). To be consistent with our terminology, the term "reference evapotranspiration" is used hereafter according to the definition given above and the terms "potential evapotranspiration", "potential evaporation" and "potential transpiration" refer to, respectively, the maximum possible rates of evapotranspiration, evaporation, and transpiration. In literature, crop evapotranspiration is synonymous to potential evapotranspiration.

Reference evapotranspiration is a climatic parameter and computed from weather data including solar radiation, air temperature, air humidity and wind speed. The Food and Agriculture Organization of the United Nations (FAO) modified version of the Penman-Monteith method, which has been recommended as the standard method for estimating ET_o, offers better results compared with other existing methods, such as Penman-Monteith (Jensen et al., 1990; Monteith, 1965), Blaney-Criddle (Blaney and Criddle, 1950), radiation, and pan evaporation. Detailed procedure on these methods is outlined elsewhere (Penman, 1948; Blaney, 1944; Ritchie, 1972; Doorenbos and Pruitt, 1977; Hanks, 1991). Daily ET_o data with grass as the reference crop are readily available from CIMIS meteorological stations located throughout California (www.dpla.water.ca.gov/cimis.html). CIMIS ET_o data are calculated on an hourly basis (summed over 24 hours to get daily values) using the Penman method.

Crop Coefficient

Crop evapotranspiration is dependent on factors such as crop characteristics, vegetative growth stage, canopy cover and height as well as soil surface properties, moisture content, and atmospheric variables. A preferable approach to relate reference evapotranspiration to crop *ET* is to use the standard definition of crop coefficients given as (Doorenbos and Pruit, 1977):

$$ET_c = K_c \cdot ET_o \tag{16}$$

where K_c is a crop coefficient, a dimensionless number that varies with crop type and crop growth stage. Actual evapotranspiration is equivalent to potential ET_c under non-stressed soil water conditions. The effects of characteristics that distinguish field crops from the reference grass are integrated into the crop coefficient K_c. Due to variations in the crop characteristics throughout the growing season, K_c for a given crop changes over time. A growing period can be divided into four distinct growth stages, resulting in four stages of crop coefficients: initial, crop development, mid-season, and late season. Generally, a small coefficient is expected in the early stages of the crop development and a large value when the crop is at full cover. K_c values have been developed for stone fruits, including nectarines and peaches, and are available in UC Cooperative Extension publications, Leaflet #21427 and #21428 (Synder et al., 1989a, Synder et al., 1989b). During non-growing periods K_c values are commonly assumed to be equal to those at the beginning of the growing season.

Partitioning of Potential Evapotranspiration

ET_o data combined with K_c values, while sufficient to determine water requirements and irrigation schedule guidelines, are not enough for numerical modeling of water movement in the root zone. One common difficulty encountered is the separation of *ET* into its two components: potential soil water evaporation *E* and plant transpiration *T*. The HYDRUS-2D requires potential evapotranspiration pre-partitioned into these two components, each separately entered into a single atmospheric input file. Evaporation is controlled by the water content and hydraulic gradient at the soil surface layer and it is essentially important in the early stages of crop development. Transpiration, on the other hand, is distributed over the root zone and can be limited to plant roots by soil water availability.

The leaf area index (LAI), defined as the ratio of vegetative area to soil surface area, has been used by several researchers to partition evapotranspiration into its components (Ritchie, 1972; Qui et al., 1999). Apart from the difficulty that LAI is not always measured for different crops at different growth stages, the main weakness of this method is that it tends to overestimate

transpiration in the early stages of plant growth although the crop coefficient is dominated by soil evaporation during that period (Brisson et al., 1992). Recently, a dual crop coefficient method (Allen et al., 1998) has been adopted to split K_c into two separate coefficients by

$$K_c = K_{cb} \cdot K_e \tag{17}$$

where K_{cb} is basal crop coefficient defining crop transpiration and K_e is soil water evaporation coefficient. The dual crop coefficient approach calculates the actual increases in K_c as a function of plant development and wetness of soil surface. The basal coefficient K_{cb} represents the baseline potential T in the absence of additional effects of soil wetting by irrigation or precipitation. The estimation of Ke requires a daily evaporating water balance computation in the upper topsoil.

At the site, as no direct measurement of evapotranspiration of nectarine trees is available, daily values of ET_o were obtained from a nearby weather station of CIMIS, Parlier. Published K_c values and associated growth stages for stone fruits including nectarines are readily available from the Consumptive Use Program (CUP) model developed by the collaborative effort of the California DWR and the UC Davis (http://www.waterplan.water.ca.gov) (Orang et al., 2003). Under the climate conditions of the San Joaquin Valley, the growing season of nectarines begins early March and trees are usually harvested throughout August. The growing season is anticipated to start on March 1 and to end on October 10. This suggests a total duration of 228 days for the growing season with the following growth stages: 114 days for the rapid growth season, 91 days for the mid-season, and 23 days for the late season (Orang et al., 2003). In this study, the dual crop coefficient approach was used based on the growth stages given above to partition potential evapotranspiration data from 1990 to 1996 into potential evaporative flux occurring through the soil surface and potential transpiration that is distributed over the root zone. Daily potential evaporation was calculated as a function of the fraction of soil surface wetted and the wetting frequency at the surface due to daily values of precipitation or irrigation. For mature trees, we estimated that 70% of the soil surface is exposed to wetting at the orchard and used the same value throughout each growth season. The procedure outlined in the FAO No:56 paper by Allen et al. (1998) is implemented herein and the results are discussed below.

Daily values of the crop coefficient curve K_{cb} corresponding to the growth stages of nectarines remain the same each year but the combined effect of the K_{cb} and K_e curves varies as a function of precipitation patterns and irrigation schedules. Figure 9 is an illustration of temporal variations both in K_c and K_e curves plotted for 1990. In general, the largest difference between K_{cb} and K_e curves occurs before and after the growth stages (January - March and October - December) when trees are essentially dormant. Spikes in the K_{cb} + K_e curve represent increased evaporation caused by soil surface wetting through precipitation or irrigation. Depending on the magnitude and frequency of wetting events, the K_e curve fluctuates between the base of the K_{cb} curve, which means no water being lost by evaporation, and a maximum value of about 1.3. Before the growth stage starts, the Ke curve increases in response to rainfall frequency. During the irrigation season, the K_e shows large fluctuations, temporarily reaching the maximum value following each irrigation event.

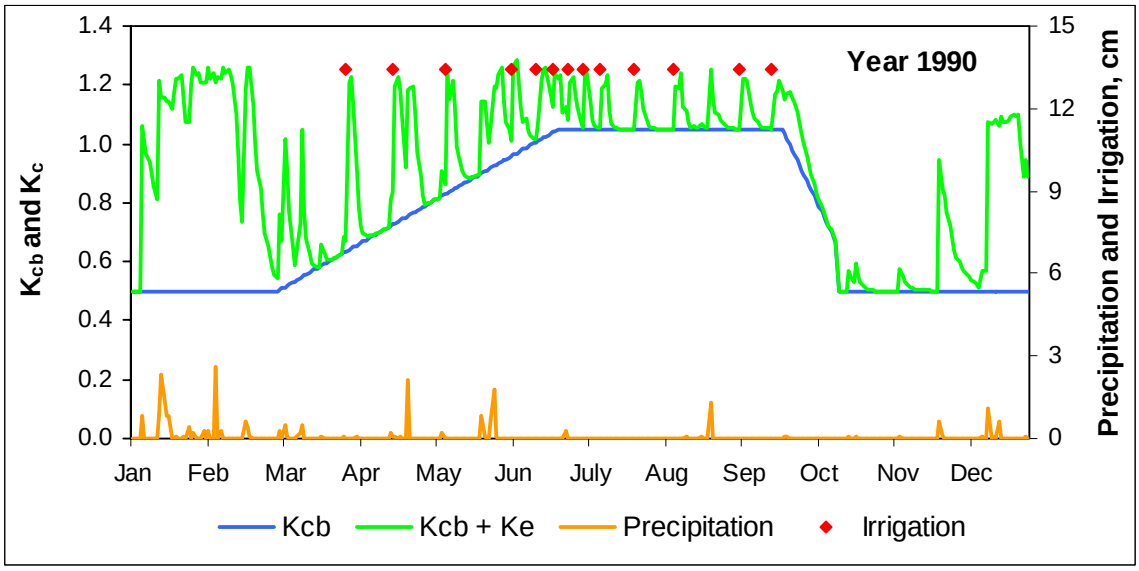

Figure 9 Crop coefficient curve for nectarine plotted together with precipitation and irrigation schedule for year 1990; K_{cb}: basal crop coefficient (solid blue line) varying as a function of the crop development stage, K_{cb} + K_e: combined effect of both transpiration coefficient K_{cb} and evaporation coefficient shown by solid green line

Figure 10 shows temporal variations in potential evaporatranspirative fluxes for 1990, partitioned into evaporation and transpiration. Also included are irrigation and precipitation data for the corresponding year. Annual potential evaporation averaged over 7 years is 17 cm, which is about 10 – 15% of the annual potential evapotranspiration and only a small fraction compared to the average annual potential transpiration of 111 cm (Table 4). Annual potential evaporation in 1995 is 16 cm, slightly smaller than that in 1995 (18 cm) although it may be expected to be larger for this year because of the larger K_e values estimated. This is a direct result of the smaller annual reference evapotranspiration recorded in 1995 than that in 1990 (Eqn. (5) and (6)) which is reflected also in the estimation of annual potential evapotranspiration. Figure 11 shows potential transpiration and evaporation throughout the simulation period.

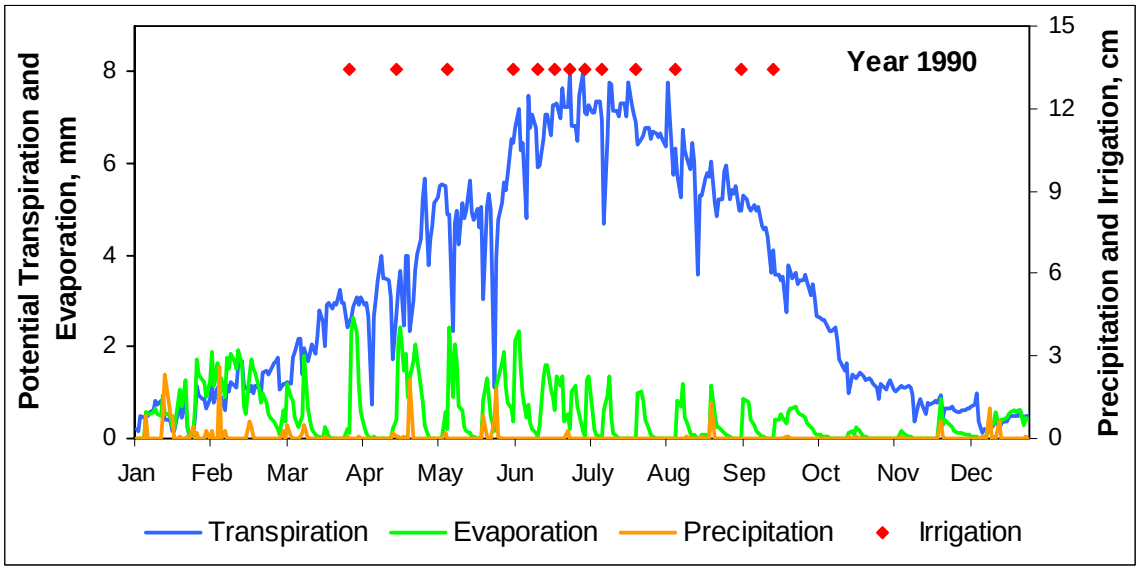

Figure 10 Daily values of potential transpiration and evaporation plotted with daily precipitation and irrigation data for 1990

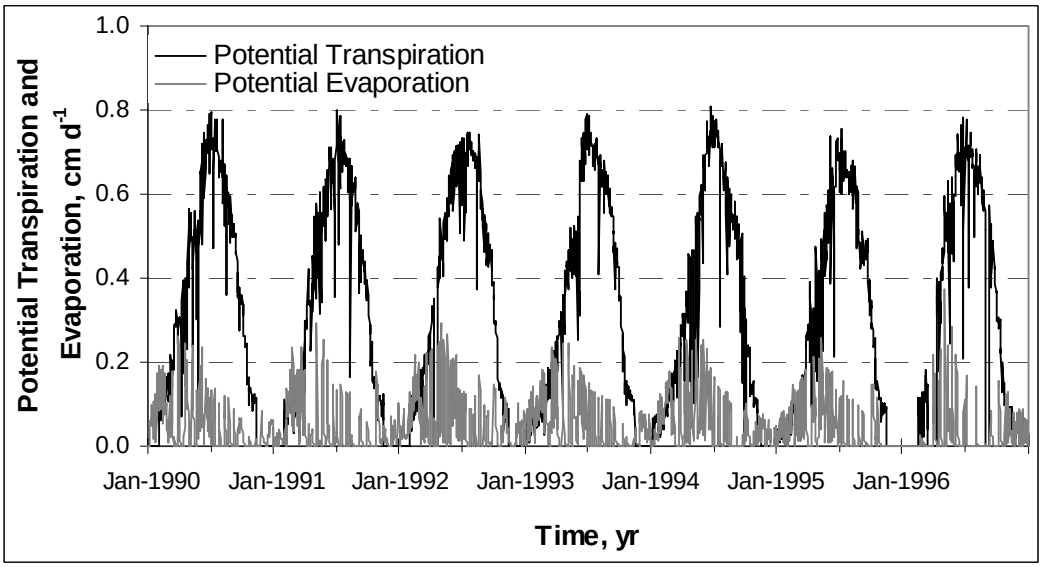

Figure 11 Daily potential transpiration and evaporation rates during the simulation period (1990 – 1996)

3.5.2 Lower and Vertical Boundary Conditions

At the bottom of the domain, a constant pressure of $h = 0$ cm is imposed, representing the water table position at 15.8 m depth. On the basis of the measured groundwater elevations at the end of the experiment in 1995, the bottom boundary condition reflects the site conditions. Vertical boundaries are assumed to be impermeable and simulated with zero flux boundary conditions.

According to the water level data downloaded from California Department of Water Resources Water Data Library (http://wdl.water.ca.gov/) at the nearest monitoring well (with the state well identification number 15S23E30B001M) to the site, groundwater levels during the experiment were usually within 14 – 20 m from the soil surface (Figure 12).

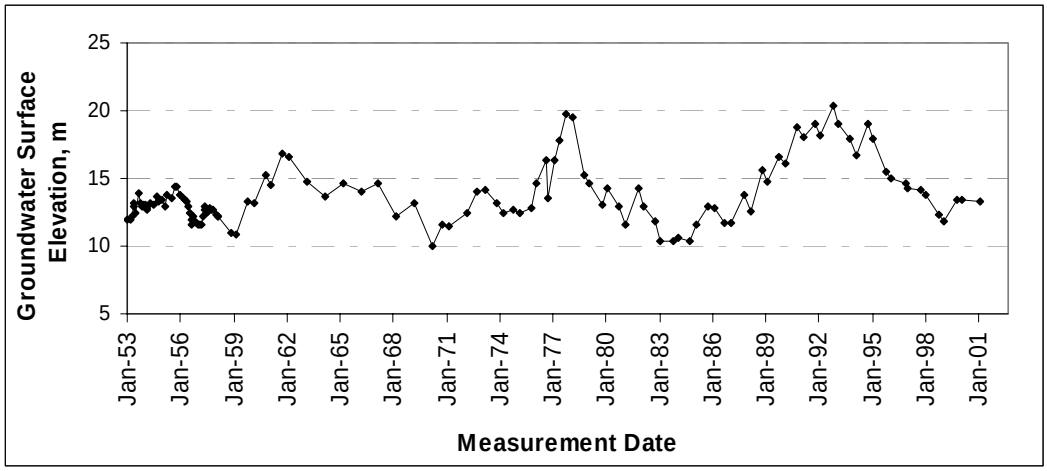

Figure 12 Hydrograph of a monitoring well (with the state well identification number 15S23E30B001M), located near the site

3.6 Time and Domain Discretization

The 7-yr simulation runs from January 1, 1990 through December 31, 1996. We use *days* for time units and *cm* for length units. During the simulation, time step size Δt is automatically controlled between the upper and lower limits of time step, given to be 1 day and 1×10^{-5} day (or ~ 1 sec), respectively, according to the convergence history (e.g., the maximum change in pressure head and water content during each time step).

The simulation domain size for both the subplots is x = 6.1 m and z = 15.8 m (20 and 52 ft, respectively). The domain is discretized into rectangular finite elements with Δx = 10 cm and Δz = 5 cm, resulting in 19654 grid points at each two dimensional domain. Space discretization is similar to those used in numerical modeling of flow processes in the root vadose zone (Vrugt et al., 2001).

4. NITROGEN TRANSPORT IN THE VADOSE ZONE

In studying solute transport, it is generally not feasible to obtain all four components of the dispersion tensor (for a two-dimensional problems). As a result, the usual practice in transport modeling is to assume a diagonalized dispersion coefficient, i.e., off diagonal terms of the D_{ij} tensor in Eqn. (5) being zero. Then, the two-dimensional transient transport equation in (4) simplifies to

$$\frac{\partial \theta c}{\partial t} = \frac{\partial}{\partial x}\left(\theta D_L \frac{\partial c}{\partial x}\right) + \frac{\partial}{\partial z}\left(\theta D_T \frac{\partial c}{\partial z}\right) - \frac{\partial q_x c}{\partial x} - \frac{\partial q_z c}{\partial z} - S c_r \tag{18}$$

where D_L and D_T are the longitudinal and transverse dispersion coefficients, respectively [L^{-1}], and x and z are the spatial coordinates in the horizontal and vertical directions, respectively. The molecular diffusion effect D_o in Eqn. (5) is generally secondary compared to the mechanical dispersion and assumed to be negligible in our study. For negligible D_o, the remaining (diagonal) terms of the diagonalized anisotropic dispersion tensor simplifies to:

$$D_L = (\alpha_L - \alpha_T)\frac{v_x^2}{v} + \alpha_T v \tag{19a}$$

$$D_T = (\alpha_L - \alpha_T)\frac{v_z^2}{v} + \alpha_T v \tag{19b}$$

in the horizontal and vertical directions, respectively. In this study, site-specific estimated values of longitudinal and transverse dispersivities, α_L and α_T, are not available; thus, they are inferred from the range of literature values used in numerical simulations of unsaturated flow under transient flow regimes (Roth and Hammel, 1996; Vogeler et al., 2001; Lafolie et al., 1997; Scotter and Tillman, 1991; Foussereau et al., 2000). The longitudinal dispersivity is taken to be 10 cm and the transverse dispersivity is set equal to one tenth of the longitudinal dispersivity, e.g., 1 cm (de Marsily, 1986). Consistent with our previous analysis, a constant bulk density value of 1.45 g cm^{-3} was used for all simulations. The uncertainty introduced by using constant transport parameter is expected to be smaller compared with the larger uncertainty associated with spatially variable soil hydraulic properties (Chen et al., 1994). Also, note that the central focus of this numerical simulation is to demonstrate the effect of non-horizontal layers with uniform soil hydraulic properties on water flow and nitrate transport.

4.1 Plant Nitrogen Nutrient Uptake

Several mechanisms are thought to operate on the processes by which plants obtain nutrients from the soil. Similar with the water uptake, root nitrogen uptake has been modeled both from a microscopic (Nye and Marriott, 1969) and macroscopic (Somma et al., 1998) viewpoint.

Nutrient movement toward the root surface occurs by diffusive transport and convective transport (Hopmans and Bristow, 2002). Diffusion is caused by nutrient concentration differences near the roots. Nutrients are also known to move against a concentration gradient through microscopic side growths known as root hairs. This process, referred to as *active root uptake*, occurs by a direct contact of roots with nutrients at the root-soil interface. Although not strictly proven, only a small fraction of nutrient uptake can occur by the active root uptake. The majority of nutrient uptake occurs as soil solution moves to root surfaces by convective transport whose magnitude is proportional to the plant water uptake (Dalton et al. (1975). This approach, known as macroscopic approach. or *passive uptake*, incorporates a sink term, such as S in the convection-dispersion equation (18) to describe the rate of nutrient uptake as a function of the rate of transpiration.

The HYDRUS-2D regards nitrogen uptake solely as a passive process, computing nitrate uptake from the product of local water uptake and nitrogen concentration. At high soil solution concentrations when the nutrient supply exceeds the plant demand, an exclusion mechanism can be invoked by an empirical parameter. As a result, solute uptake is reduced whenever the local concentration exceeds a certain critical threshold, *CRoot*, to match the predicted with observed

plant nutrient uptakes. This approach is applied in practice to account for plant uptake of nutrients in numerical models (Vogeler et al., 2001).

4.2 Initial Condition

In the absence of reliable estimates of background levels of naturally occurring nitrate concentrations, zero concentration [mg cm^{-3}] profile over the simulation domain was assumed as initial concentration for nitrate:

$$c(x, z, 0) = 0 \tag{20}$$

The N free soil domain used in the simulations introduces error in our analysis. The use of zero N levels allows us to trace nitrate transport in the entire vadose zone and witness the travel time in the entire domain. Besides, the long-term simulation results would eventually replace prescribed initial concentrations.

4.3 Upper Boundary Condition

At the upper boundary, the soil surface receives N from applied fertilizers and N from irrigation. A third type (Cauchy type) boundary condition was specified to define nitrate-nitrogen concentration into the domain along the upper boundary as follows:

$$-\theta D_T \frac{\partial c}{\partial z} + q_z c = q_o c_o \tag{21}$$

where c_o is the concentration of either fertilizer or irrigation N fluxes, which is determined from the fertilizer and irrigation application rates.

4.3.1 Fertilizer N Applications

Dates of fertilizer applications and applied N concentrations at the standard and high subplots are listed in Table 1. Total nitrogen pulse of given concentrations in Table 1 was applied as NO_3-N at the soil surface uniformly over the entire horizontal plane over a 1-day period. Similar to the practice at our orchard, in orchards of California and of other fruit-growing regions, fertilizer N during fall is traditionally applied when trees are dormant (Weinbaum et al., 1992). At the site conditions, the vast majority of ammonium-nitrate is expected to be nitrified and converted to nitrate rapidly. Supporting evidence from a nitrogen fertilizer leaching experiment, conducted by Ünlü et al. (1999), shows that under fertilized and irrigated systems, accumulated residual ammonium-nitrate is rapidly converted to nitrate following the harvest and leaches from the soil root zone before the following year begins. At the observation scale of months to years, such as ours, neglecting quick N transformation and its effect on root N uptake with increasing time scale may suffice.

Table 4 Records of fertilizer applications at the fertilizer subplots from 1990 to 1996. N concentrations are evaluated based on the amount of surface water flux (either irrigation, I, precipitation, P, or both, irrigation and precipitation, I+P) at the orchard.

Years	Dates of Fertilizer Applications		Subplot[1]	Days of Simulation	Applied N kg ha^{-1}	NO_3-N Concentration mg cm^{-3}	Irrigation+Rainfall[2] cm			
	28-Mar		H	88	85	0.0945	9			I
	7-May		H	128	85	0.0945	9			I
1990	4-Jun		H	155	85	0.0945	9			I
	17-Sep		S/H	261	110	0.1222	9			I
	22-Mar	23-Mar	H	448	85	0.47	0.71[3]	1	0.6[3]	R
	2-May		H	488	85	0.0945	9			I
1991	3-Jun		H	519	85	0.093	9			I+R
	5-Sep		S/H	614	85	0.0945	9			I
	20-Mar		H	810	85	0.770	1			R
	29-Apr		H	850	85	0.0945	9			I
1992	28-May		H	879	85	0.0945	9			I
	9-Sep		S/H	984	110	0.1222	9			I
	17-Mar		H	1174	85	0.0945	9			I
	3-May		H	1221	85	0.0945	9			I
1993	1-Jun		H	1278	85	0.0945	9			I
	13-Sep		S/H	1353	110	0.1222	9			I
	21-Mar		H	1541	85	0.0945	9			I
	10-May		H	1591	85	0.0945	9			I
1994	1-Jun		H	1613	85	0.0945	9			I
	16-Sep		S/H	1689	110	0.1222	9			I
1996	11-Sep		S/H	2446	110	0.1222	9			I

[1]S/H: Fertilizer applied both on the standard and high subplots; H: fertilizer applied on the high subplot.
[2] I: Fertilizer applied by irrigation water; R: fertilizer applied by rainfall; I+R: fertilizer by irrigation and rainfall.
[3] Fertilizer applied by rainfall in two consecutive days.

4.3.2 Irrigation N Applications

Irrigation N inputs were calculated from the quantity of irrigation water applied and its N concentration. Consistent with the root zone MB approach (Appendix 1), average NO_3-N concentration in irrigation water is taken to be 4 g m^{-3}. Each irrigation applied at an average of 13.44 cm day^{-1} supplies 5.4 kg N ha^{-1}. Based on the irrigation site records for 1990 – 1996, as listed in Table 4, annual N from irrigation ranges from 48 kg ha^{-1} in 1996 with 9 irrigations to 91 kg ha^{-1} in 1992 with 17 irrigations.

4.4 Lower and Side Boundary Conditions

When water is directed out of the domain at the water table at the bottom, a second type (Neumann type) boundary condition was prescribed to define a concentration gradient across the boundary:

$$-\theta D_T \frac{\partial c}{\partial z} = 0 \tag{22}$$

which is a simplified version of (6) without the advective flux component.

On the left and right sides of the domain, both dispersive and advective fluxes are zero, thus, $q_o\ c_o = 0$. The bottom and side boundary conditions, like these adopted here, have been

successfully applied in numerical modeling to represent field scale solute transport under unsaturated flow conditions (Foussereau et al., 2000).

5. RESULTS AND DISCUSSION OF NUMERICAL SIMULATIONS

5.1 Numerical Mass Balances for Water Flow

The error criterion of the flow and transport problem studied herein is chosen such that a global mass balance error below 1% is achieved. Figure 13 shows daily values of relative water mass balance error for the homogeneous lithofacies and heterogeneous lithofacies models. In general, trends in both curves suggest that the percent water mass balance error stabilizes within the first year of the simulation. It becomes nearly constant three years after the simulation starts and is further reduced to a relatively constant value of 0.12% for homogenous lithofacies model and 0.09% for the heterogeneous lithofacies model. Contrary to what is expected, the homogenous lithofacies model produces slightly higher mass balance errors throughout the simulation, particularly in the first year, than the heterogeneous lithofacies model. When changes in soil hydraulic properties across lithofacies boundaries occur sharply over the entire horizontal domain, as in the case for the homogeneous lithofacies model (see Figure 1), numerical simulations seem to be computationally more expensive. In the heterogeneous lithofacies model, while larger contrasts in soil hydraulic properties are apparent near the layer boundaries (Figure 2), non-uniform distribution of soil hydraulic properties seems to expedite numerical computations, contrary to our initial expectations.

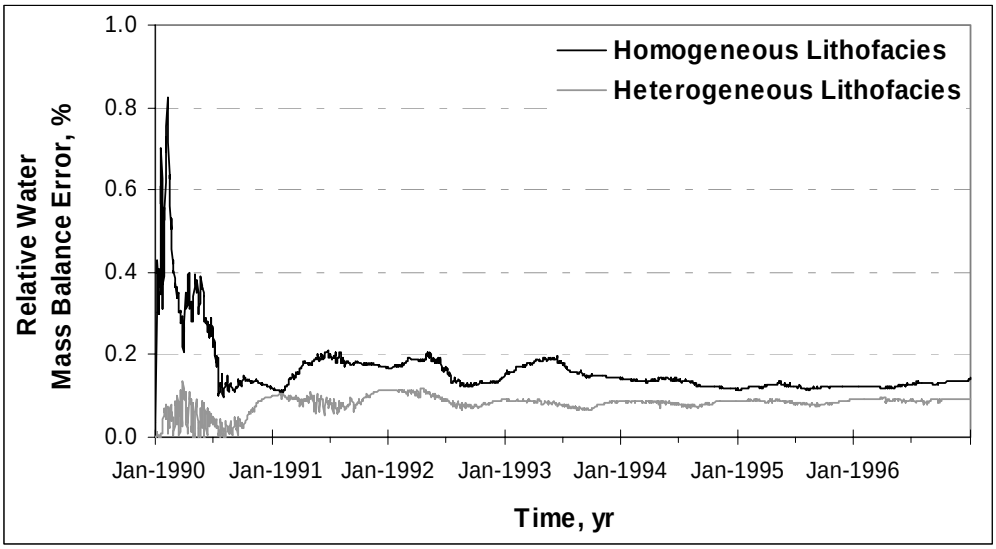

Figure 13 Variations of relative water mass balance (in percentages) during the period from 1990 to 1996 based on simulation results in the homogeneous and heterogeneous lithofacies models

As far as the computational time involved in the two models, while the design of the heterogeneous lithofacies model takes longer and the model requires more data to characterize the flow properties compared to the homogeneous lithofacies model, contrasting soil hydraulic properties at the local scale (heterogeneous lithofacies model) seems to improve mass balance. Numerical computations seem to be very sensitive to how soil hydraulic properties are defined. The runtime of the numerical simulations (both simulated subplots together) in the homogeneous lithofacies model is approximately 193 hours. In the heterogeneous lithofacie model, runtime is reduced substantially to 23 hours 31 min (using a PC with Pentium IV CPU, 1.8 GHz, 500 MB memory). Our finding underscores that contrasting soil hydraulic properties present across the entire horizontal domain (homogeneous lithofacies model) may be acting as a barrier to flow. Contrasting local scale heterogeneity (heterogeneous lithofacies model) may be offsetting the barrier effect and easing numerical computations.

5.2 Numerical Mass Balances for Nitrogen Transport

Figure 14 shows variations of relative N mass balance error at the standard subplot over the simulation period from 1990 to 1996 both in the homogeneous and heterogeneous lithofacies models. For the homogenous lithofacies model, N mass balance errors at the standard subplot fluctuate from near zero to 0.6% during the first four years (1990 – 1992) and then reaches a relatively stable condition around 0.2%. The heterogeneous lithofacies model produces higher N mass balance errors than the homogeneous lithofacies model in the first two years, reaching near 1% soon after N is applied to soil and 0.6% in the second year. Throughout the remaining of the simulation, N mass balance in the heterogeneous model is near 0.1%, about half the N mass balance in the homogenous lithofacies model during this period.

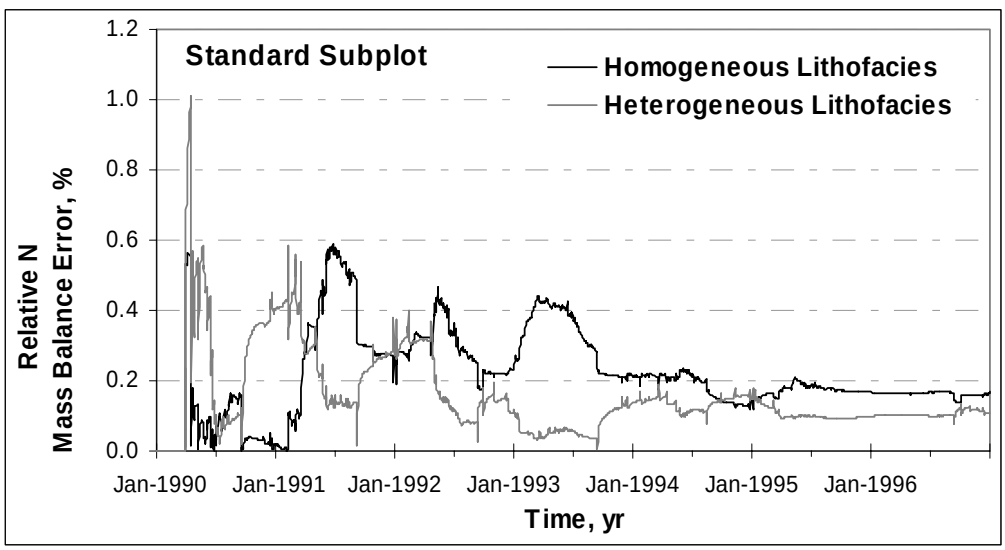

Figure 14 Variations of relative N mass balance (in percentages) at the standard subplot during the period from 1990 to 1996 based on simulation results in the homogeneous and heterogeneous lithofacies models

Figure 15 shows variations of relative N mass balance errors at the high subplot. The homogeneous model application at the high subplot tends to produce higher mass balance than at the standard subplot. Similar to the homogeneous lithofacies model at the standard subplot, a

stable N mass balance error of around 0.3% is attained towards to the end of 1994. From mid-1991 to mid-1992, the mass balance error is the highest around 0.6%. In the case of heterogeneous model, N mass balance at the high subplot is higher in the first year compared to the mass balance in the homogeneous lithofacies model. After 1994, N mass balance becomes less than 1% and gradually drops to 0.03%.

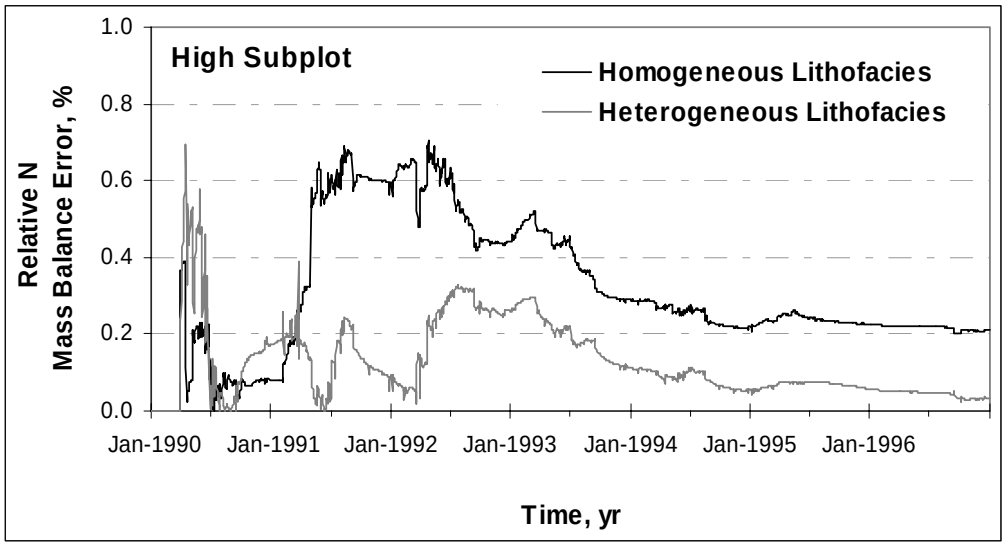

Figure 15 Variations of relative N mass balance (in percentages) at the high subplot during the period from 1990 to 1996 based on simulation results in the homogeneous and heterogeneous lithofacies models

Figure 16 shows variations of the automatically computed time step, Δt, over the simulation period for the two models. For the homogeneous model, Δt tends to stay in the lower range of specified limits of time step (~ seconds to minutes) from 1990 to 1994 (Figure 16a). Afterwards, there is an apparent increase in the time step, in particular during winter months when the system is subject to small surface fluxes from precipitation. Since time discretization is automatically adjusted by the model according to the numerical convergence, higher Δt observed after 1994 is expected and is the result of combined smaller water and N mass balance errors attained. In the heterogeneous lithofacies model, during winter times, Δt reaches the highest specified time step in the simulation (i.e., 1 day) and drops to near zero during irrigation seasons. While this trend in Δt is similar to those seen in the homogeneous lithofacies model, in general, the heterogeneous model is computed with larger time steps than the homogeneous model. This further supports our observation that the homogeneous layered model with contrasting soil hydraulic properties across the lithofacies interface is computationally more demanding. Thus, numerical solutions are not as simple as commonly thought.

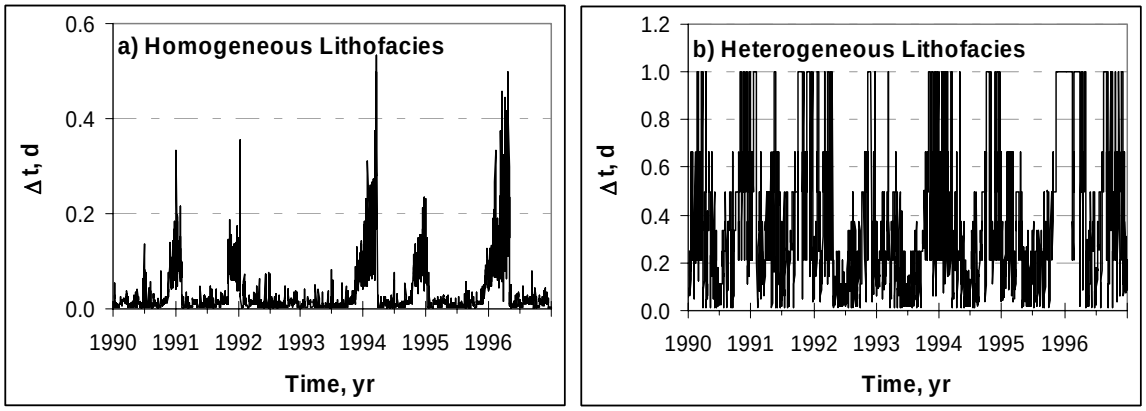

Figure 16 Variations of time step during the period from 1990 to 1996 based on simulation results in the a) homogeneous and b) heterogeneous lithofacies models

5.2.1 Numerical Stability of Nitrogen Transport Model

Numerical solutions of solute transport equation may exhibit non-physical oscillatory behavior and/or excessive dispersion near sharp concentration fronts, in particular for convection-dominated problems. Two dimensionless numbers, the Peclet number (*Pe*) and the Courant number (*Cr*), can be used as a measure of model capability in solving (4) and to control the extent of numerical oscillations. The Peclet number, when locally defined, is the ratio of convective fluxes to dispersive fluxes. It is defined by $Pe = \ell \,|\, v \,|\, / D$, where is *l* is a characteristic length of local scale (i.e., the domain discretization Δx). While acceptable small oscillations may be obtained with a local Pe as high as 10 (Huyakorn and Pinder, 1983), Pe should not exceed about 5 to eliminate numerical oscillations. The Courant number is associated with the time discretization and defined by $Cr = \Delta t \,|\, v \,|\, / R\Delta x$, where *R* is the retardation factor (equal to unity for tracers). To stabilize the numerical solution and avoid oscillations in the Galerkin finite element result, the stability criterion of $Pe \cdot Cr \leq 2$ is fulfilled during the simulation.

In Figure 17 and 18, daily values of *Pe* and *Cr* throughout the simulation period are shown, respectively, for the two models. *Pe* values vary with a narrow range from 1.61 to 1.67 for the homogeneous lithofacies model. In the heterogeneous lithofacies model, the range becomes even smaller (1.666 to 1.667). In the homogeneous lithofacies model, *Cr* varies only slightly between near zero to 0.81 while in the heterogeneous lithofacies model it reaches as high as near 0.99. Given the ranges of *Pe* and *Cr* values from both models, $Pe \cdot Cr$ takes the highest value of about 1.36 in the homogeneous lithofacies model and 1.65 in the heterogeneous lithofacies model. This confirms that the stability criterion of less than 2 is always satisfied throughout the simulations period. These results, combined with the relative N mass balance error of less than 1%, show evidence that our long-term numerical simulation of N transport meets the desired numerical solution criterion typically used in unsaturated media (Roth and Hammel, 1996).

5.3 Surface Water Flux

Potential flux across the soil surface is determined by the difference between potential evaporation and precipitation (flux positive out of the domain). Actual surface flux is *a priori* unknown. It is determined internally by the model from the rate of prescribed potential flux

depending on the prevailing soil water availability at the soil-air interface. When pressure at the surface becomes smaller than the maximum allowed pressure head of hCritA = -1000 cm, potential evaporation capacity is exceeded.

During the simulations of both models, the maximum potential flux (e.g., irrigation at the applied rate of 9 cm d^{-1}) was maintained slightly smaller than the saturated hydraulic conductivity of the top layer SL1 to avoid surface ponding. In other words, the soil infiltration capacity of the SL1 is never exceeded even when the soil becomes fully saturated, i.e., when hCritA = 0 is reached at the top boundary.

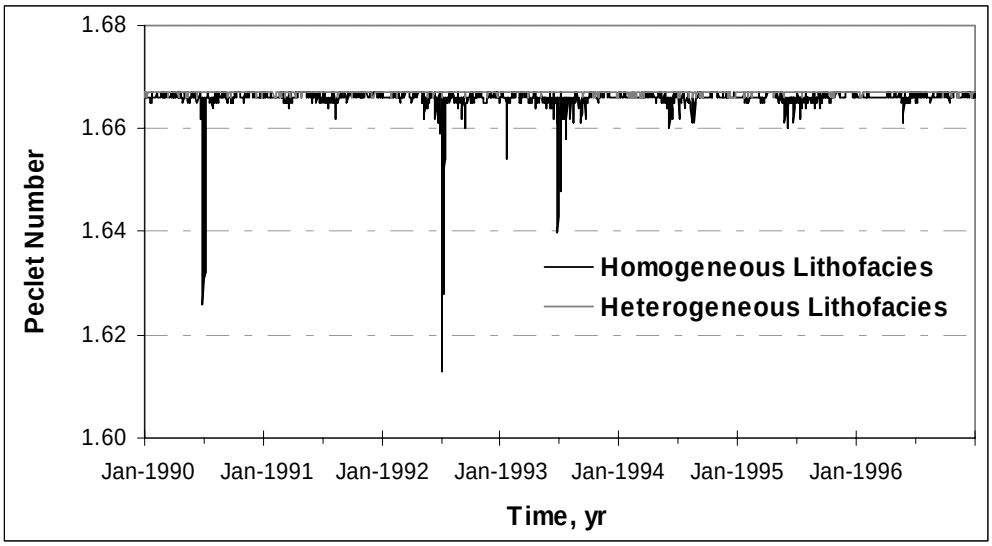

Figure 17 Variations of Peclet number during the period from 1990 to 1996 based on simulation results in the homogeneous and heterogeneous lithofacies models

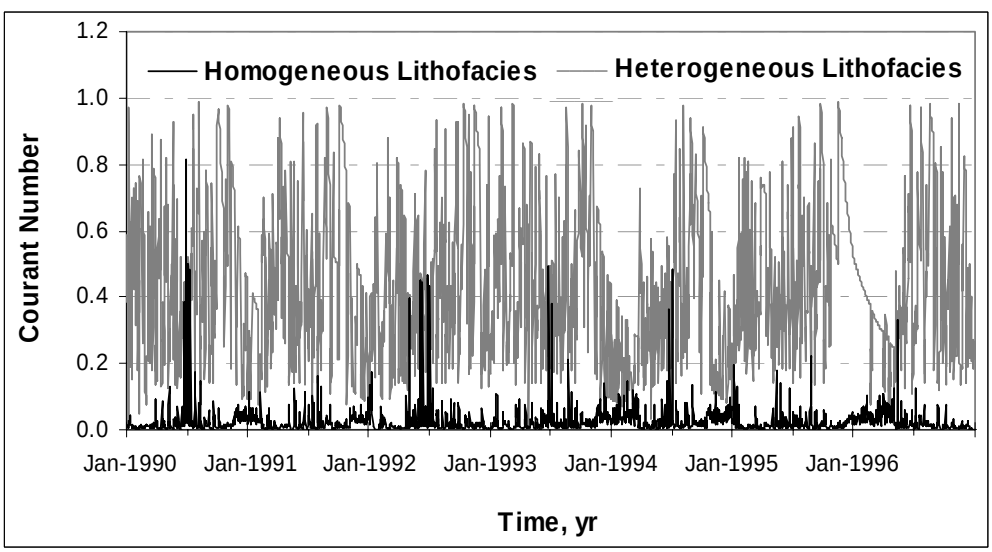

Figure 18 Variations of Courant number during the period from 1990 to 1996 based on simulation results in the homogeneous and heterogeneous lithofacies models

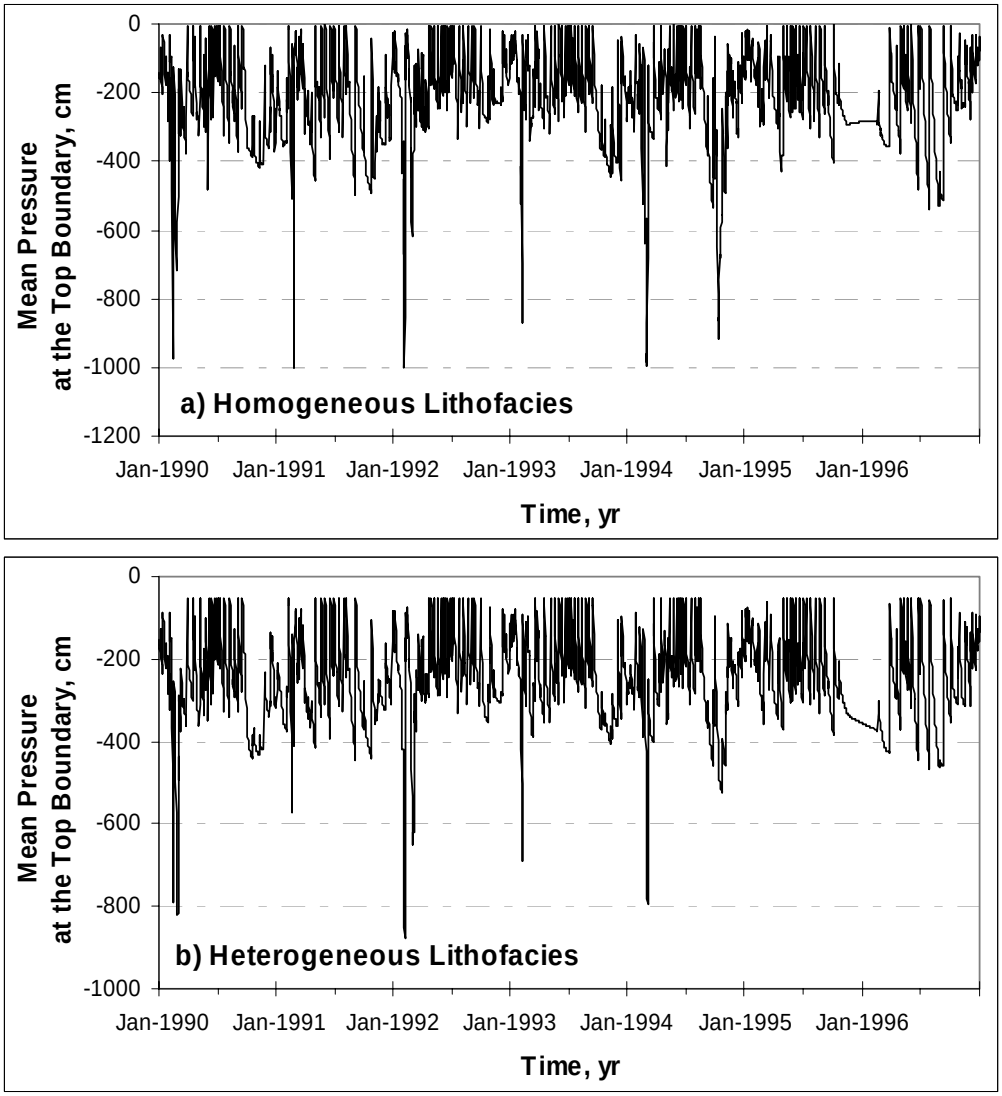

Figure 19 Variations of mean pressure head at the top boundary (ground surface, z = 0 m) during the period from 1990 to 1996 based on simulation results in the a) homogeneous and b) heterogeneous lithofacies models

Figure 19 shows variations of mean pressure head (the term *mean* refers to the arithmetic mean unless stated otherwise) across the top boundary as a function of surface fluxes at the atmospheric boundary for the homogeneous lithofacies and heterogeneous lithofacies models. In the homogeneous lithofacies model, pressure head at each node across the boundary is the same since surface flux is applied uniformly. During irrigations, it becomes nearly zero, showing conditions close to saturation, since the applied irrigation rate is slightly smaller than the saturated hydraulic conductivity of SL1 lithofacies. In the heterogeneous lithofacies model, due to changes in soil hydraulic properties across the boundary, mean pressure is reduced to nearly -

54 cm during irrigation seasons. During winter times, mean pressure from both models is comparable, generally varying from -400 cm to -200 cm. As a result of similar mean pressure estimated from both models, estimated actual surface fluxes from both models are almost identical, as seen in Figure 20a **(**fluxes into the system are shown negative). In the homogeneous lithofacies model, mean pressure at the surface drops to the minimum allowed surface pressure head of hCritS = -1000 cm occasionally. Comparison of potential and actual surface fluxes for the homogeneous lithofacies model, as shown for the in Figure 20b, suggests that a short period of extreme dry conditions at the atmospheric boundary seems have a negligible effect on the ability of surface soil to transmit the prescribed potential evaporation rate since potential surface fluxes are equal to actual fluxes.

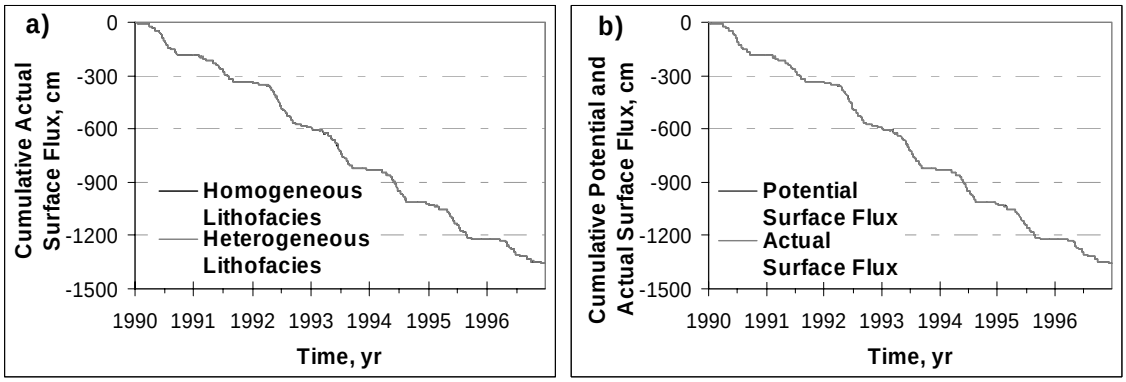

Figure 20 Variations of cumulative actual and potential surface fluxes during the period from 1990 to 1996 based on simulation results in the homogeneous and heterogeneous lithofacies models. a) Actual cumulative surface flux in the homogeneous and heterogeneous lithofacies models and b) potential and actual cumulative surface fluxes in the homogeneous lithofacies model.

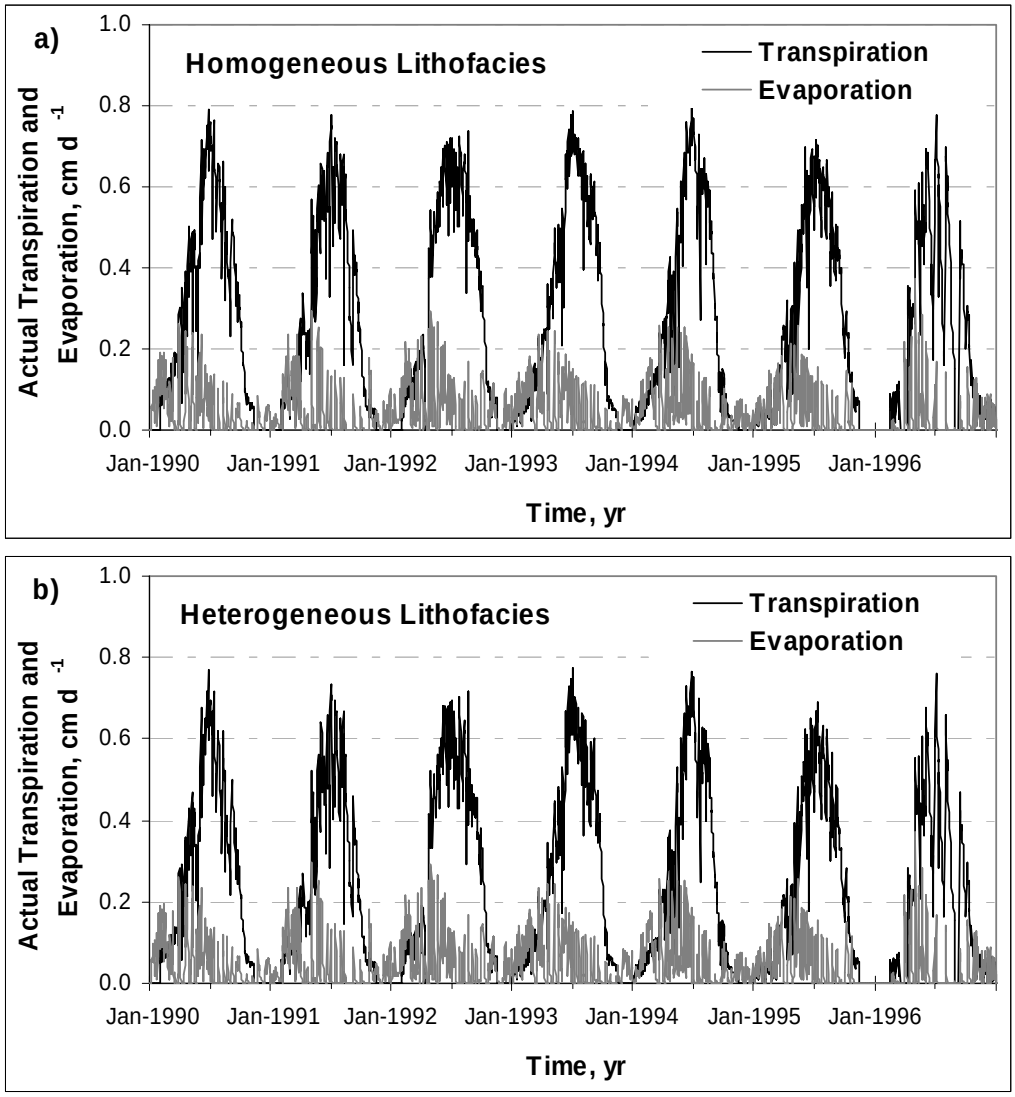

Figure 21 Daily values of model simulated (actual) transpiration and evaporation during the period simulation period (1990 – 1996) in the a) homogeneous and b) heterogeneous lithofacies models

5.3.1 Soil Evaporation

Figure 21 shows daily values of model estimated evaporation and transpiration during the simulation period (1990 – 1996) in the homogeneous and heterogeneous lithofacies models. Actual evaporation (also equal to potential evapotranspiration) is the same and shows similar seasonal patterns from year to year. At the beginning of each growth period, water is predominantly lost by soil evaporation. When the development stage begins, soil evaporation has less effect on total crop evapotranspiration because of tree canopies covering the ground. Year to year variations of cumulative evaporation are summarized in Table 5 and will be discussed furthermore in the context of annual water mass balance and annual recharge to the deep vadose zone.

5.4 Plant Water Uptake

Figure 22 compares daily values of prescribed potential and model calculated transpiration (actual) over the 7-yr simulation period for the homogeneous lithofacies and heterogeneous lithofacies models. Year to year variations of transpiration between the two models are similar. In both models, at the beginning of each growth period, water uptake by transpiration is low while evaporation is high (Figure 21). During the development period, transpiration increases rapidly and becomes the dominant process. Average peak transpiration rate of 0.8 cm d^{-1} is reached during the mid-season, during the months of either June or July of every year. Transpiration stops rising at the beginning of the mid-season and then starts to fall off at the end of each growth season. Potential transpiration outside of the growth season (January 1 – March 1 and October 10 – December 31) is essentially at minimum as characterized by the flat basal crop coefficient curve (Figure 9). Unlike many existing numerical studies that focused on plant uptake processes (either water, nutrient, or both) only for a short period (~ days to months) that covers only the duration of plant growth season, our numerical study is a long-term simulation with a time scale of years. To provide an uninterrupted long-term flow simulation at a reasonable computational cost, the minimum potential transpiration was set to zero during extreme dry conditions, January 1 – 31 and November 15 – December 31. During these periods of every year, the root zone may not have enough water to supply prescribed transpiration.

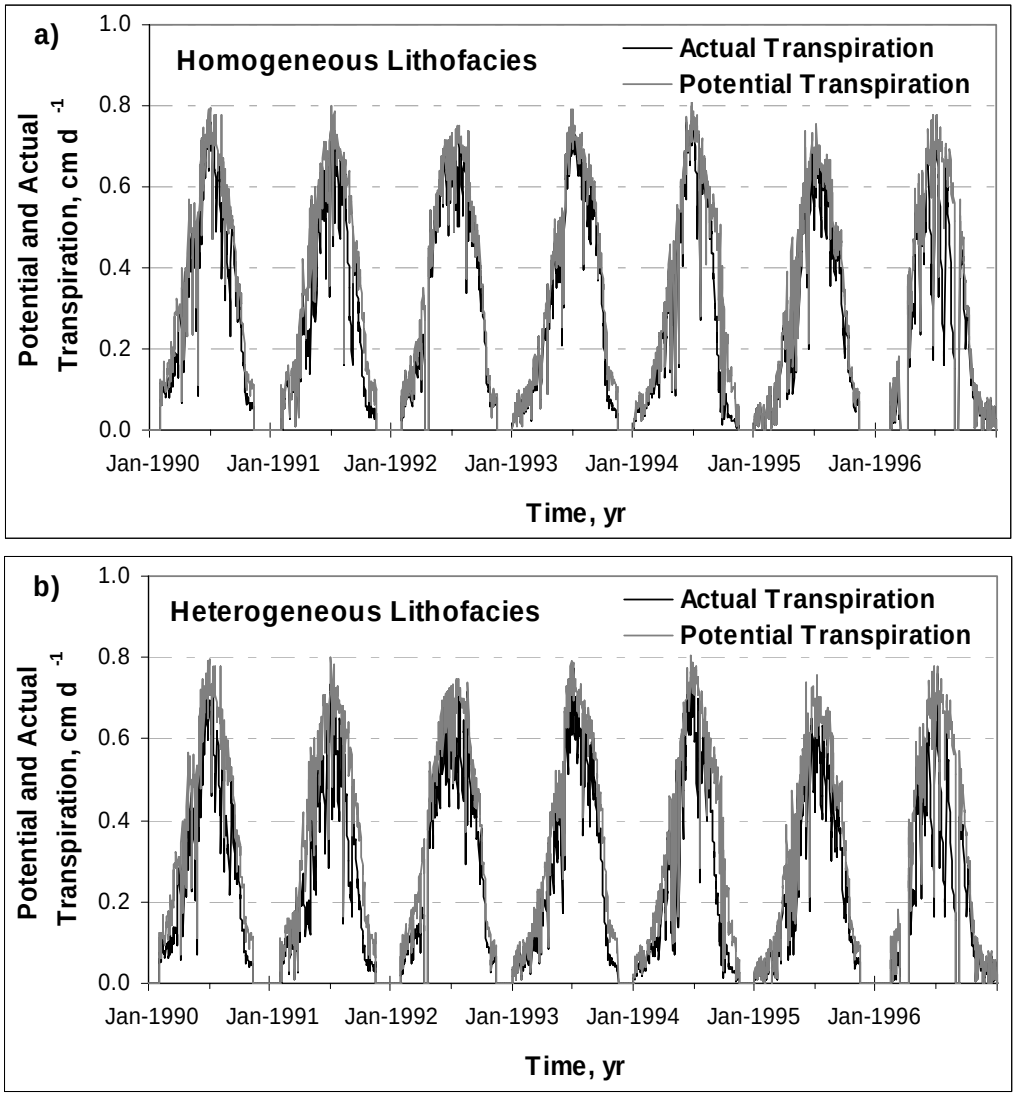

Figure 22 Comparison of daily values of potential and model simulated (actual) transpiration during the simulation period (1990 – 1996) in the a) homogeneous and b) heterogeneous lithofacies models

The difference between potential and actual transpiration is the degree of reduction in water uptake that occurs according to the S-shaped water reduction function in Eqn. (10). Since the water reduction function is defined based on the distribution of pressure head in the root zone, smaller pressure head at the surface (Figure 19) and in the root zone (see below, Figure 24) during the growth season is indicative of drier soil conditions that produce more reduction in transpiration or equivalently in plant water uptake.

Comparison of daily transpiration values between the two models shows larger differences between potential and actual transpiration rates for the heterogeneous lithofacies model than the homogeneous lithofacies model. Figure 23 shows that total reduction over the 7 years is 106 cm for the homogeneous lithofacies model and 178 cm for the heterogeneous

lithofacies model. In the homogeneous lithofacies model, potential transpiration is reduced by 8 to 21% annually (equivalent to about 9 to 21 cm), depending on the climate conditions and irrigation patterns over the 7 years. In the heterogeneous lithofacies model under the same climate and irrigation patterns, reduction in potential transpiration varies between 17 to 31% (equivalent to 20 and 32 cm). Local variations in pressure as a result of local heterogeneity in the spatial hydraulic properties reduces wetting within the root zone (see Figure 24a). This seems to reduce the water available for plant uptake, as expected under heterogeneous soils (Selker et al., 1996). In both the models the degree of reduction during the late growth seasons of 1991 and 1994, and during the mid-season of 1996 is noticeably higher than the reduction in other years. This is potentially caused by either insufficient irrigation at the orchard during these periods or irregular irrigation schedule or a combination of both. A substantial amount of reduction in 1996 with 9 irrigations may reflect the driest soil conditions over the 7-year period in the root zone.

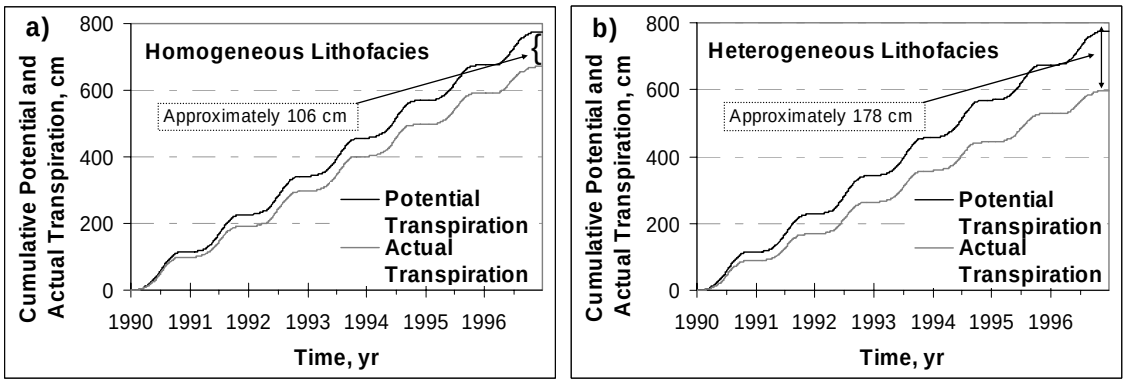

Figure 23 Cumulative potential and model simulated (actual) transpiration during the simulation period (1990 – 1996) in the homogeneous and b) heterogeneous lithofacies models

5.5 Pressure Head and Soil Water Content in the Vadose Zone

In this section, mean pressure variations in the root zone and the deep vadose are compared. The effects of lithofacies on pressure and water content variations throughout the vadose zone are discussed.

5.5.1 Mean Pressure Head in the Root Zone and in the Deep Vadose Zone

Results from both models suggest that temporal changes in the mean pressure head are primarily controlled by irrigation applications both in the root zone (Figure 24) and in the deep vadose zone (Figure 25). For the homogenous lithofacies model, during irrigation seasons, the mean pressure in the root zone varies widely from near full saturation to about -200 cm. During winter months, pressure head usually remains below -200 cm with less fluctuation occurring typically between -200 cm and -400 cm. The longest period of dry condition is observed in 1994 during winter months. Starting in August, the mean pressure sharply drops below -400 cm and remains below -200 cm till the beginning of 1995. According to annual precipitation and irrigation records, the model estimated net annual recharge to the deep vadose zone during 1994 is smaller than the model estimated long-term average recharge (7-yr avg., Table 5). During the growth period (March to October) in 1996, the root zone experiences the driest soil condition where the mean pressure fluctuates between about -100 cm to -400 cm. On the basis of precipitation and irrigation records, 1996 is the driest year with the minimum recharge to the deep vadose zone.

For the heterogeneous lithofacies numerical model, seasonal and annual trends in the mean pressure in the root zone are similar to those trends seen for the homogeneous lithofacies model, but the mean pressure throughout the simulation period is shifted down by approximately -80 cm during irrigation seasons and -50 cm during winter months. The timing of low points and associated mean pressure heads, however, correlates well with the corresponding results from the homogeneous model.

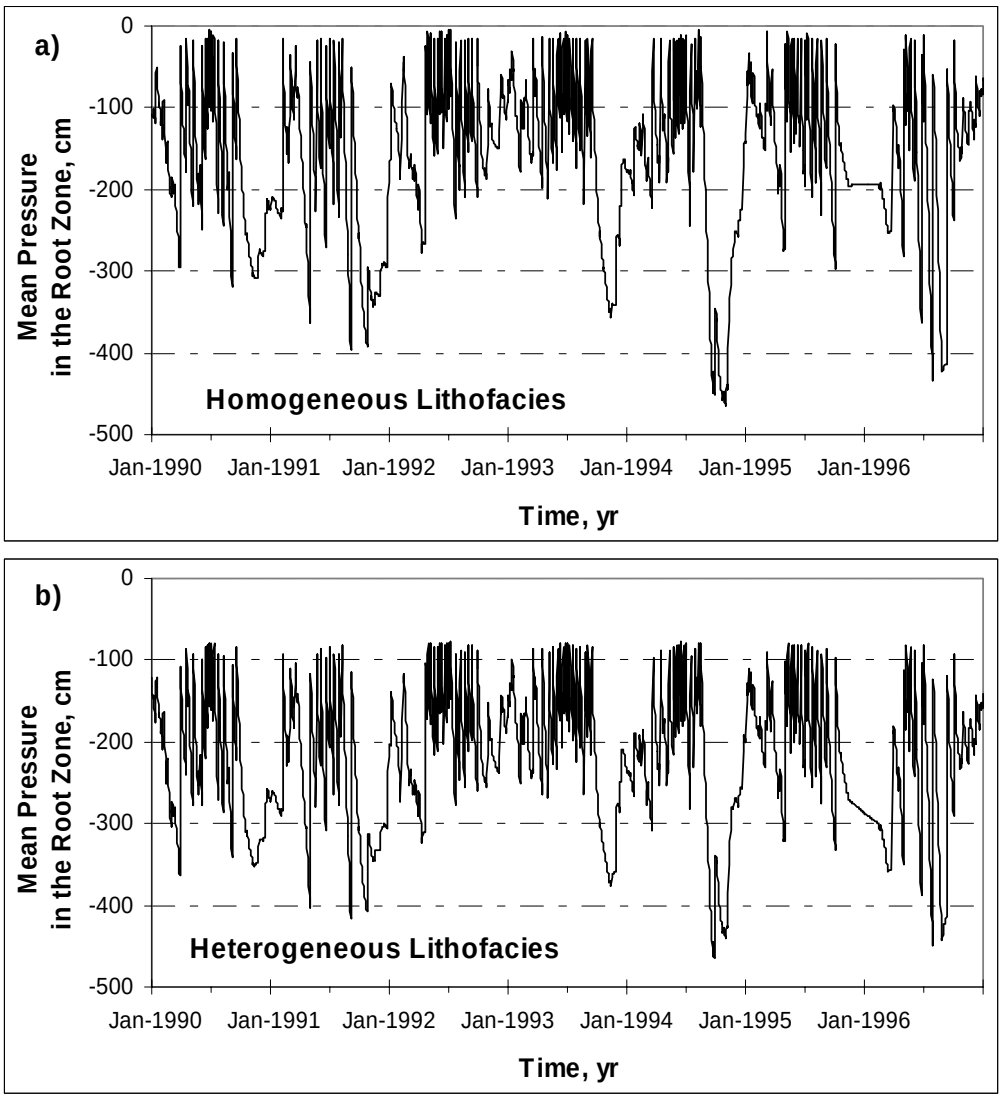

Figure 24 Variations of mean pressure head simulated in the root zone ($0 \le z \le 1.8$ m) during the simulation period (1990 – 1996) in the a) the homogeneous and b) heterogeneous lithofacies models

The mean pressure in the deep vadose zone estimated from the homogeneous lithofacies model shows a smaller range of variations between and within seasons. During irrigation events, the mean head pressure usually varies between -60 cm and -90 cm (Figure 25). During winter months, pressure head typically fluctuates between -90 cm and -120 cm. Exception to this occurs

during the months of October through December in 1992 and January through March in 1993 where the mean pressure head remains above -90 cm. The root zone water mass balance analysis, which will be presented in a later section, suggests that annual precipitation and irrigation during 1992 and 1993 are much higher than the long-term average quantities (37 cm and 175 cm, respectively), resulting in relatively high recharge to the deep vadose zone (see Table 5).

For the heterogeneous lithofacies model, timing of high and low points of mean pressure head correspond well with those from the homogeneous lithofacies model. However, the mean pressure in the deep vadose zone in the heterogeneous lithofacies model is smaller than that in the homogeneous lithofacies model, ranging usually between -150 cm and -300 cm.

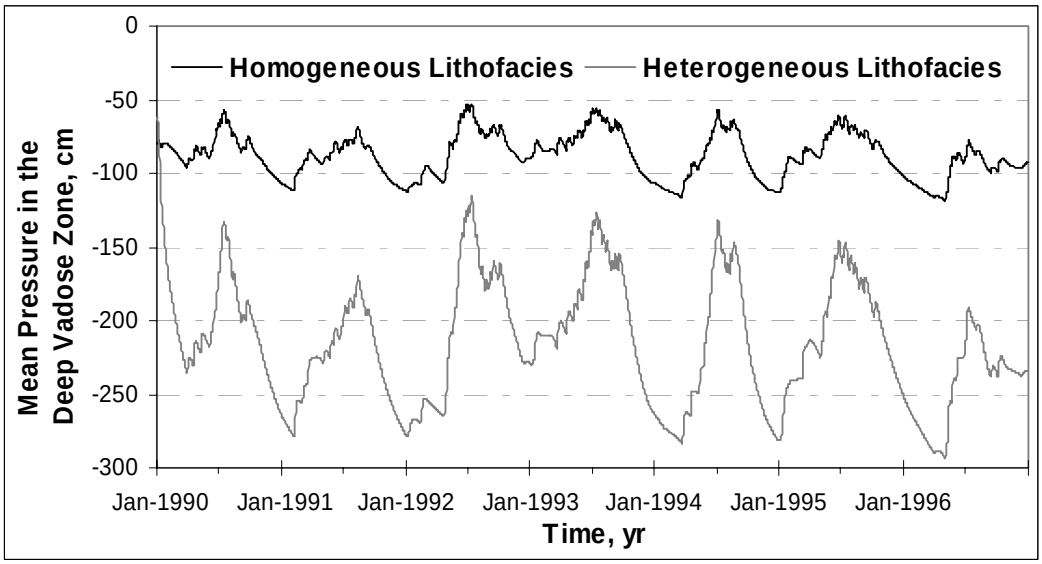

Figure 25 Variations of mean pressure head in the deep vadose zone of the standard and high subplots (1.8 m < z ≤ 15.8 m) during the simulation period (1990 – 1996) in the homogeneous and heterogeneous lithofacies models

5.5.2 Effect of Lithofacies on Soil Water Content and Pressure Head

To monitor temporal variations of water content and pressure head throughout the profile, eight observation points are placed at various depths in the domain at the standard and high subplots. One of the observations points, referred to as "Root Zone", is suitably located at z = 1.8 m to monitor the change in these quantities at the bottom of the root zone. The other seven points are positioned along the textural interface of lithofacies at the vertical distances of z = 2, 3.05, 4.3, 6.75, 7.9, 12.65, 15.2 m from the ground surface. These vertical locations correspond to the bottom of each lithofacies from the upper most SL1 through SL2. Each point is placed at the same horizontal distance of x = 3.1 m to represent conditions at the center of the simulation domain. No observation point is assigned at the bottom of the HP1 at z = 15.8 cm as it describes the water table (i.e., saturated condition with pressure head of 0 cm and soil water content of 0.275 cm^3 cm^{-3}, Table 1). Variations of water content and pressure head at the observation locations are shown for both the homogeneous and heterogeneous models. However, comparisons between the two models cannot be made since these quantities at the selected locations from the heterogeneous lithofacies model may not correspond to the characteristics of each lithofacies due to randomness in the distribution of soil hydraulic parameters (i.e., scaling factors).

5.6 Soil Water Content

Temporal changes of water content at the eight observations points are shown in Figures 26a and 26b for the homogeneous and heterogeneous lithofacies models, respectively. The estimated ranges within the lithofacies can be explained by a combined effect of three factors: i) the magnitude of surface fluxes, ii) the proximity to the boundary, and iii) the soil hydraulic properties of lithofacies. Both models show a profound repetitive sequence of water content throughout the profile in response to seasonally varying surface fluxes. Surface boundary fluxes have a stronger effect on temporal fluctuations of soil water content in the upper layers than in deeper parts of the domain. At the root zone, transient surface fluxes create largest seasonal fluctuations in soil water content (Figures 26a and b**)**.

In the homogeneous lithofacies model, soil moisture at the root zone during the irrigation seasons usually reaches an average of value of 0.221 cm^3 cm^{-3} while outside of the irrigation season it drops to near 0.15 cm^3 cm^{-3}. Based on the soil hydraulic properties of the lithofacies SL1, which represents the root zone, the former value corresponds to near saturation (saturated water content = 0.229 cm^3 cm^{-3}) and the latter represents a relatively dry condition of near zero saturation (residual water content = 0.09 cm^3 cm^{-3}). Observation points at the root zone and at the SL1 are 20 cm apart. Variations of water content at the SL1 are almost identical to those observed at the root zone. Although the SL1 and HP1 show different soil characteristics, the upper layers SL1 and HP1 responds to any water input, either of irrigation or precipitation, more rapidly than other underlying layers such as the C-Si-L, and SL2. Between the end of irrigation season in 1992 and the beginning of irrigation season in 1993, water content at the bottom of the SL1 and 0.23 cm^3 cm^{-3} at the bottom of HP1 is relatively constant around 0.2 cm3 cm^{-3}. This is consistent with higher recharge to the root zone from precipitation (Table 5) and in turn, higher mean pressure head estimated both in the root zone and in the deep vadose zone during this period of time (Figures 24 and 25).

Changes in water content at the bottom of the Var1 and S in response to surface fluxes are nearly identical regardless of their proximity to the surface although the Var1 and S, which are composed of coarse textured deposits (e.g., high hydraulic conductivity, Table 1), are separated by the HP1 that has predominantly fine textured depositions. During irrigation seasons, both the Var1 and S drain rapidly following irrigations, without experiencing high variations in water content. During winter months of dry conditions, water content at the bottom of both Var1 and S reaches to the average residual water content (0.122 cm^3 cm^{-3}, Table 1). Similarly, the HP1 and Var2 experience similar ranges of water content regardless of their proximity to the surface. During winter months where surface fluxes are minimal, both the layers stay at a relatively saturated condition, which is opposite of what is seen for the Var1 and S. It is anticipated that the HP1 and Var2 with fine textural materials retain water (e.g., small hydraulic conductivity, Table 1). The least amount of variations during irrigation periods is observed at the bottom of the SL2 layer where the soil remains nearly saturated throughout the simulation period without a significant effect of boundary fluxes

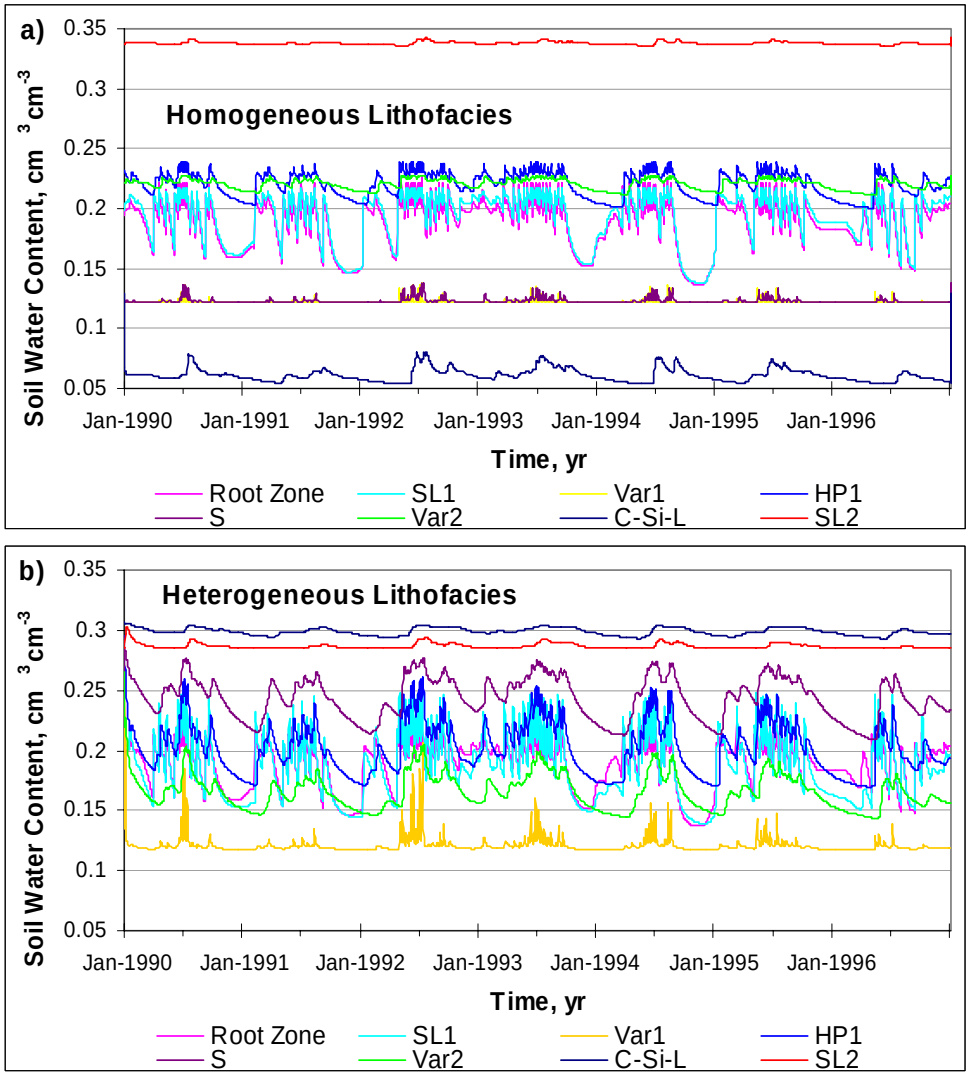

Figure 26 Variations of pressure head at eight observation points located at various depths of the standard and high subplots based on simulation results in the a) the homogeneous and b) heterogeneous lithofacies models. Root Zone at z = 1.8 m; SL1 at z = 2 m; Var1 at z = 3.05 m; HP1 at z = 4.3 m; S at z = 6.75 m; Var2 at 7.9 m; C-Si-L at z = 12.65 m; and SL2 at z = 15.2 m. All points are located at the same horizontal distance of x = 3.1 m.

As compared to the homogeneous lithofacies model, in the heterogeneous lithofacies model, much higher variations of water content, both within and between seasons, are seen at the observation points. Exceptions to this occur at the bottom of the C-Si-L and SL2 where water content shows only slight seasonal variations.

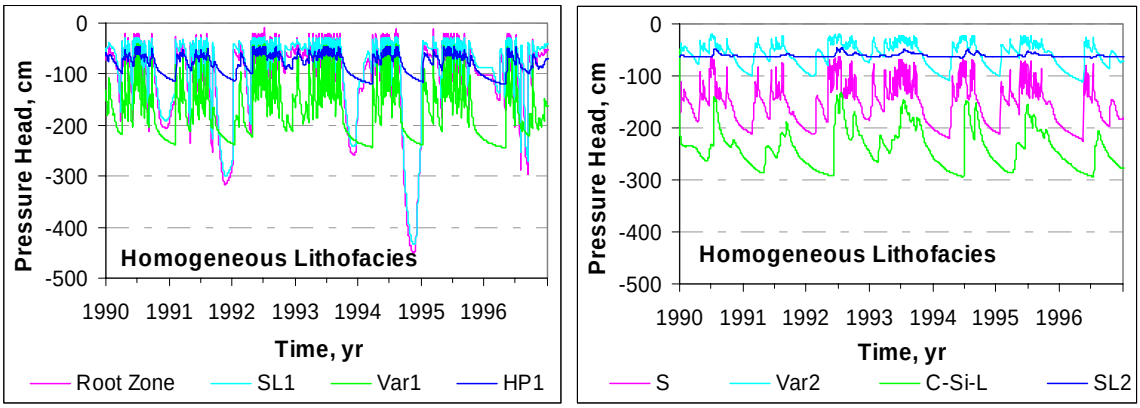

Figure 27 Variations of pressure head at eight observation points located at various depths based on simulation results in the homogeneous lithofacies model. Root Zone at z = 1.8 m; SL1 at z = 2 m; Var1 at z = 3.05 m; HP1 at z = 4.3 m; S at z = 6.75 m; Var2 at 7.9 m; C-Si-L at z = 12.65 m; and SL2 at z = 15.2 m. All points are located at the same horizontal distance of x = 3.1 m of the standard and high subplots

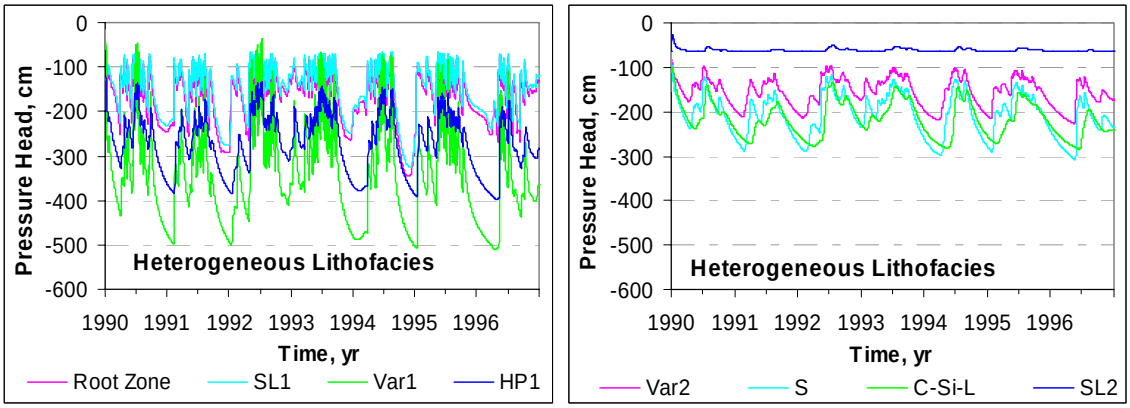

Figure 28 Variations of pressure head at eight observation points located at various depths based on simulation results in the heterogeneous lithofacies model. Root Zone at z = 1.8 m; SL1 at z = 2; Var1 at z = 3.05 m; HP1 at z = 4.3 m; S at z = 6.75 m; Var2 at 7.9 m; C-Si-L at z = 12.65 m; and SL2 at z = 15.2 m. All points are located at the same horizontal distance of x = 3.1 m of the standard and high subplots

5.7 Pressure Head

The three aforementioned factors, namely i) the magnitude of surface fluxes, ii) the proximity to the boundary, and iii) the soil hydraulic properties of lithofacies, that control water content variations between lithofacies act in the same way controlling pressure head variations between lithofacies. In both the homogeneous and heterogeneous lithofacies models, seasonally varying surface fluxes create large variations in pressure head throughout the profile (Figures 27 and 28**).**

In the homogeneous lithofacies model, the trends of pressure head at the root zone are similar to those at the bottom of the SL1, both typically ranging from -30 cm to -90 cm during

irrigation seasons and dropping near -130 cm during winter. Within lithofacies from the SL1 to Var2, soil pressure head follows irrigation events closely, increasing when water is added and decreasing rapidly upon soil moisture depletion by drainage and root uptake. During irrigations seasons, when irrigation water is applied frequently, such as in 1993 and 1994 (with 17 and 16 irrigations, respectively), pressure head still fluctuates widely yet does not drop below approximately -200 cm. On the contrary, during 1991 and 1996 (with 10 and 9 irrigations, respectively), pressure head fluctuates and goes below -200 cm. The impact of surface flux on pressure head near the bottom of the domain within the SL2 lithofacies is negligible, shown by a relatively constant pressure head of about -50 cm. Soil hydraulic properties seem to play a predominant role than the proximity to surface when pressure head variations for Var1 and S are compared. Both Var1 and S response to varying surface fluxes rapidly and experience large pressure head variations ranging from -50 cm to -250 cm, as expected on the basis of their coarse-grained sand deposits. Similarly, within the HP1 and Var2 soil hydraulic properties seem to be more effective in controlling pressure head variations. Both having fine soil textures, the HP1 and Var2 response to changes in surface fluxes rather slowly and experience pressure head variations only between approximately –50 cm and –100 cm.

In the heterogeneous lithofacies model, the ranges of pressure head, especially within the SL1, Var1, and HP1, are greater than those estimated in the homogeneous lithofacies. At the bottom of SL2, the pressure head shows only slight seasonal variations, which is similar to the homogeneous lithofacies model. Higher variations in pressure head in the heterogeneous lithofacies model, both within and between seasons, are consistent with higher variations the mean pressure head in the root zone and in the deep vadose zone as estimated by this model (Figures 24 and 25).

5.8 Two-Dimensional Spatial Distribution of Soil Water Content

The homogeneous and heterogeneous lithofacies numerical simulations generate output data for variables of interests, such as soil water content, pressure head, flux, and N concentrations, at each node at pre-selected print times. The space discretization used produces 62 data points over the horizontal dimension at a given depth interval of 5 cm. For the entire depth of 15.8 m, each model contains 19654 data points at each print time. In this section, two-dimensional spatial distributions of water content data simulated by the homogeneous and heterogeneous lithofacies models are analyzed and discussed for selected days of the simulations (abbreviated as DOS hereafter).

5.8.1 Homogeneous Lithofacies Model

Several daily outputs from the homogeneous lithofacies model simulations are shown in Figure 29. Data corresponds to 9 selected times for the wettest year 1992 between two consecutive irrigations events (1st and 2nd irrigations). Despite the uniform water application at the surface and homogenous soil properties assigned in each layer, the inclined layers create spatially uneven, irregular shapes of soil moisture distribution During pre-irrigation conditions (DOS = 842, i.e., April 22, Table 3), the root zone is relatively dry. Following the first day of the irrigation (DOS = 843), the root zone (SL1 layer) exhibits large changes in water content, most of which becomes fully saturated. As the soil moisture pulse in the root zone travels downward, it dampens out via root water uptake. The Var1 layer below the SL1 layer also exhibits rapid changes of water content due to its proximity to the surface and its coarse textural depositions. In contrast to the Var1, the HP1 layer having fine texture materials tends to transmit water slower and thus is subjected to minor water content changes. In the deeper portions of the vadose zone below the C-Si-L, no apparent changes in water content are seen in response to the 1st irrigation.

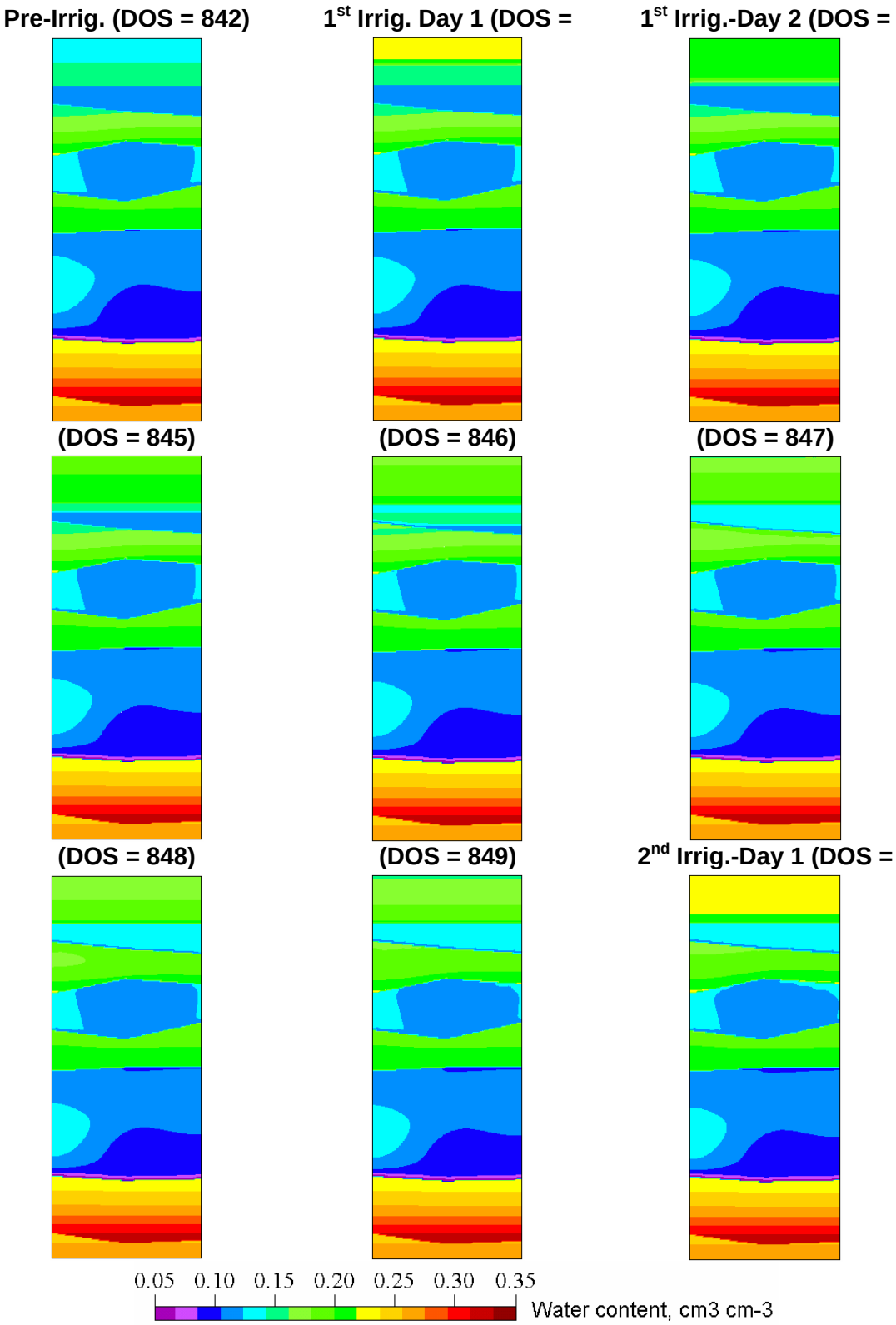

Figure 29 Contour maps of soil water content simulated in the homogeneous model at selected times during the simulation year of 1992

All contour maps show that the layered structure causes discontinuities in water content across the boundaries, as also reported by Schamalz et al. (2003) who simulated unsaturated flow through a two-dimensional layered vertical cross section that depicts the shape of a large multi-layered sand tank (approximately 5 m x 3 m at the base and 6 m x 5.6 m at the top) using the HYRUS-2D code and in situ and laboratory measured parameters of the van Genuchten –Mualem model. The driest areas are produced at the interface between the C-Si-L and SL2 layers. Under natural, layered vadose zone systems, the interface between a highly conductive layer and a less conductive layer is shown to form a strong capillary barrier restricting the vertical movement of flow and solute transport across the interface (Iqbal, 2000). If lateral flow is dominant within a highly conductive layer, capillary barrier seems to be even more effective. In our simulations, as a result of contrasting soil hydraulic properties, the interface between the C-Si-L and SL2 seems to be acting as an effective capillary barrier, delaying drainage from the fine-textured C-Si-L layer to the SL2 layer. Similarly, across the interface between the SL2 and HP2, water is being held in the SL2 against gravity causing the soil moisture of the SL2 layer to reach to saturation.

5.8.2 Heterogeneous Lithofacies Model

Water content contour maps generated from the heterogeneous lithofacies model simulations are shown in Figure 30. These maps provide a better visual demonstration of the advancing wetting fronts between the 1st and 2nd irrigation in 1992. Due to small-scale heterogeneity in the soil hydraulic properties, the heterogeneous lithofacies model creates more irregular water content patterns compared to the homogeneous lithofacies model. As a result of local heterogeneity, these simulations generate a random distribution of water content with much less discontinuity in water content across the boundaries compared to the homogeneous lithofacies model. Consistent with the correlation scale of scaling factors, the horizontal layering observed at the site tends to create pronounced anisotropy with a scale of horizontal correlations larger than the vertical one. Thus, soil moisture pulses are more connected and thus less variable

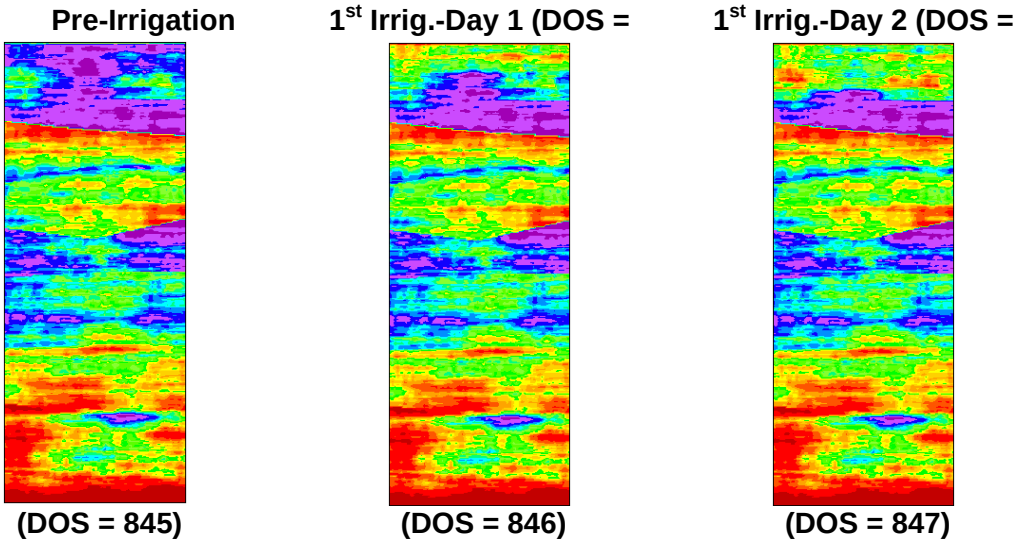

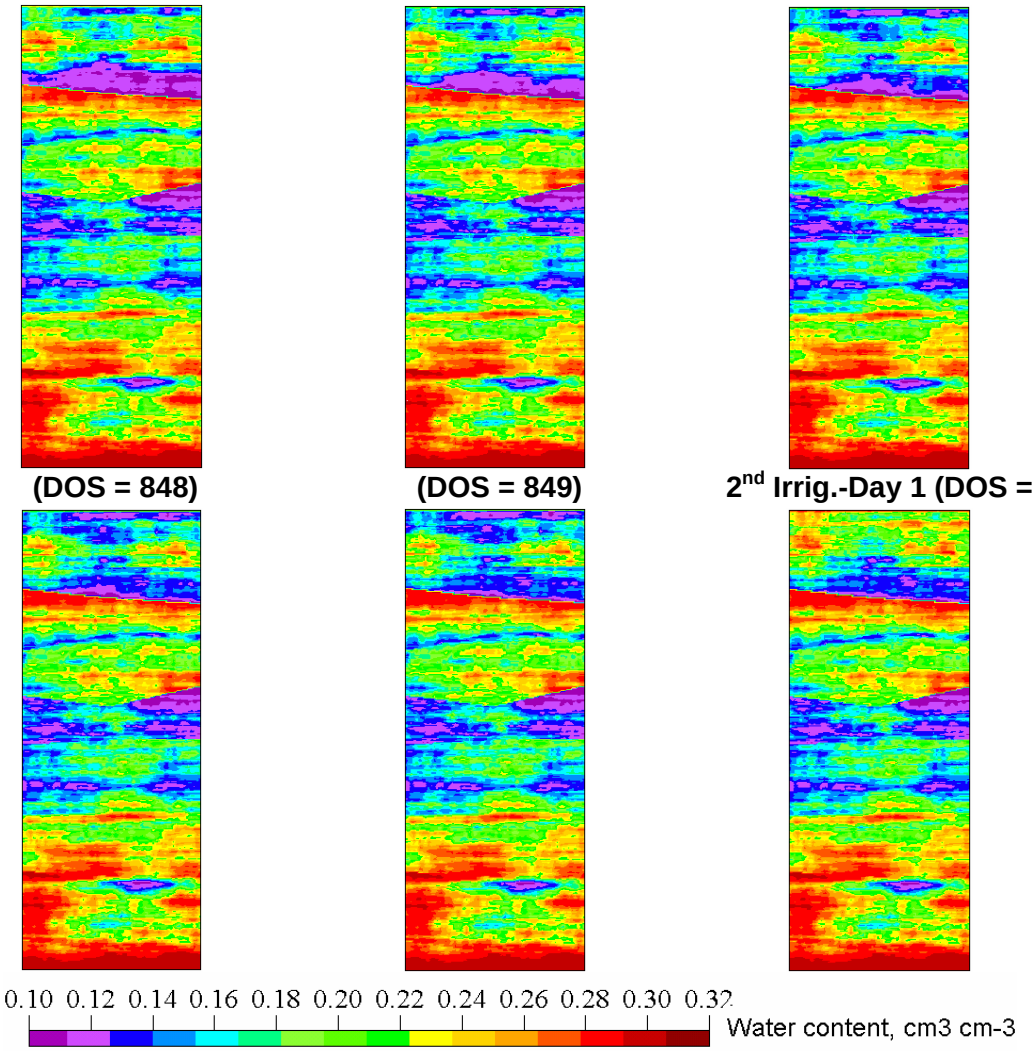

Figure 30 Contour maps of water content simulated in the heterogeneous model at selected times during the simulation year of 1992

in the horizontal direction than in the vertical direction. Similar to the results from the homogeneous lithofacies model, the 1st irrigation event (during DOS = 843 and 844) results in increased water content to a depth of 1.8 m. Drying starts rapidly in the root zone within a day after the irrigation (e.g., DOS = 845) and the advancing wetting front moves downward in the layer Var1 underlying the root zone. Despite a significant drying within the zones of coarse textured materials, zones of fine textured materials, both within and below the root zone remain well saturated even prior to irrigations where the soil exhibits dry conditions (e.g., DOS = 842 and 849). The HP1 lithofacies underneath Var1, a rather coarse-textured lithofacies, particularly in the vicinity of the interface, retains more water than the Var 1 layer. The S layer located on top of a rather fine-textured layer the Var2 seems to act as a capillary barrier, minimizing water leaching into the lower layer. Comparison of contour maps of these daily water content distributions between two consecutive irrigations suggests that patterns of wetting do not change over time between infiltration events (e.g., DOS = 844 and 850). Every new event recreates the same paths for soil moisture pulses.

The overall appearance of water content distribution is in qualitative agreement with those of Russo (1991) who studied the transport of a tracer through a hypothetical, vertical cross section of unsaturated media using a single realization of scaling factors, similar to the approach taken in this study, to define the variability of soil hydraulic properties.

5.9 Two-Dimensional Spatial Distribution of Pressure Head

Two-dimensional spatial distributions of pressure head data simulated by the homogeneous and heterogeneous lithofacies models are presented below to complement the water content maps presented above. Similar to the water content data from the heterogeneous lithofacies model, pressure head remains correlated over the correlation scale of soil hydraulic properties. However, pressure head distributions appear to show horizontally more continuous patterns across the lithofacies than water content maps (Figure 32**)**. This is in qualitative agreement with the previous theoretical studies that examined the stochastic nature of two-dimensional, pressure head and flux variations for heterogeneous unsaturated media under steady flow conditions in a Monte Carlo framework (Hopmans et al., 1988; Khaleel et al., 2002). Patterns of pressure head are in good agreement with those of water content (Figure 32). Layers of larger pressure head (matric head) coincide with layers of lower soil moisture.

5.10 Recharge from the Root Zone

Annual soil root zone water budget for the entire simulation period is presented in Table 5 for the homogeneous and heterogeneous lithofacies models. Annual net percolating water R (actual recharge in units of cm yr^{-1}) from the root zone to the deep vadose zone is calculated based on the simulated annual fluxes at the atmospheric boundary and in the root zone by

$$R = I + P - E - T \tag{23}$$

where I and P are annual irrigation and precipitation, E is annual actual evaporation and T is annual actual transpiration, each defined in cm yr^{-1}. While the root zone water budget analysis presented here is conceptually the same as the conventional mass balance analysis applied in Appendix 1, the present analysis i) accounts for inter-annual variations and ii) partitions evapotranspiration into the model calculated values of evaporation and transpiration.

Annual recharge values in both the homogeneous and heterogeneous models are highly correlated with the amount of applied irrigation water (r^2 = 0.96 and 0.97, respectively). The minimum recharge to the deep vadose zone is simulated in 1996 with 9 irrigations. During this period, the recharge is 57 cm yr^{-1} in the homogeneous lithofacies model and 67 cm in the heterogeneous lithofacies model. The maximum recharge, on the other hand, is simulated in 1992 when 17 irrigations are applied. During this period, the recharge reaches 145 cm in the homogeneous model and 156 cm in the heterogeneous model. When 13 irrigations are considered in the model, the homogeneous lithofacies model simulates recharge to the deep vadose zone from 83 cm to 113 cm which is comparable to the annual recharge of 110 cm yr^{-1} estimated from the long-term water mass balance analysis (Appendix 1). In the heterogeneous model, annual recharge during years with 13 irrigations is larger, ranging from 94 cm in 1990 to 123 cm in 1995. Higher fluctuations in pressure head in the root zone of the heterogeneous lithofacies model, as a result of local variations in soil hydraulic properties, result in less plant water uptake, and in turn, more recharge to the deep vadose zone. On the basis of the 7-yr average data, the annual net recharge is 10 cm more in the heterogeneous model than the homogeneous model.

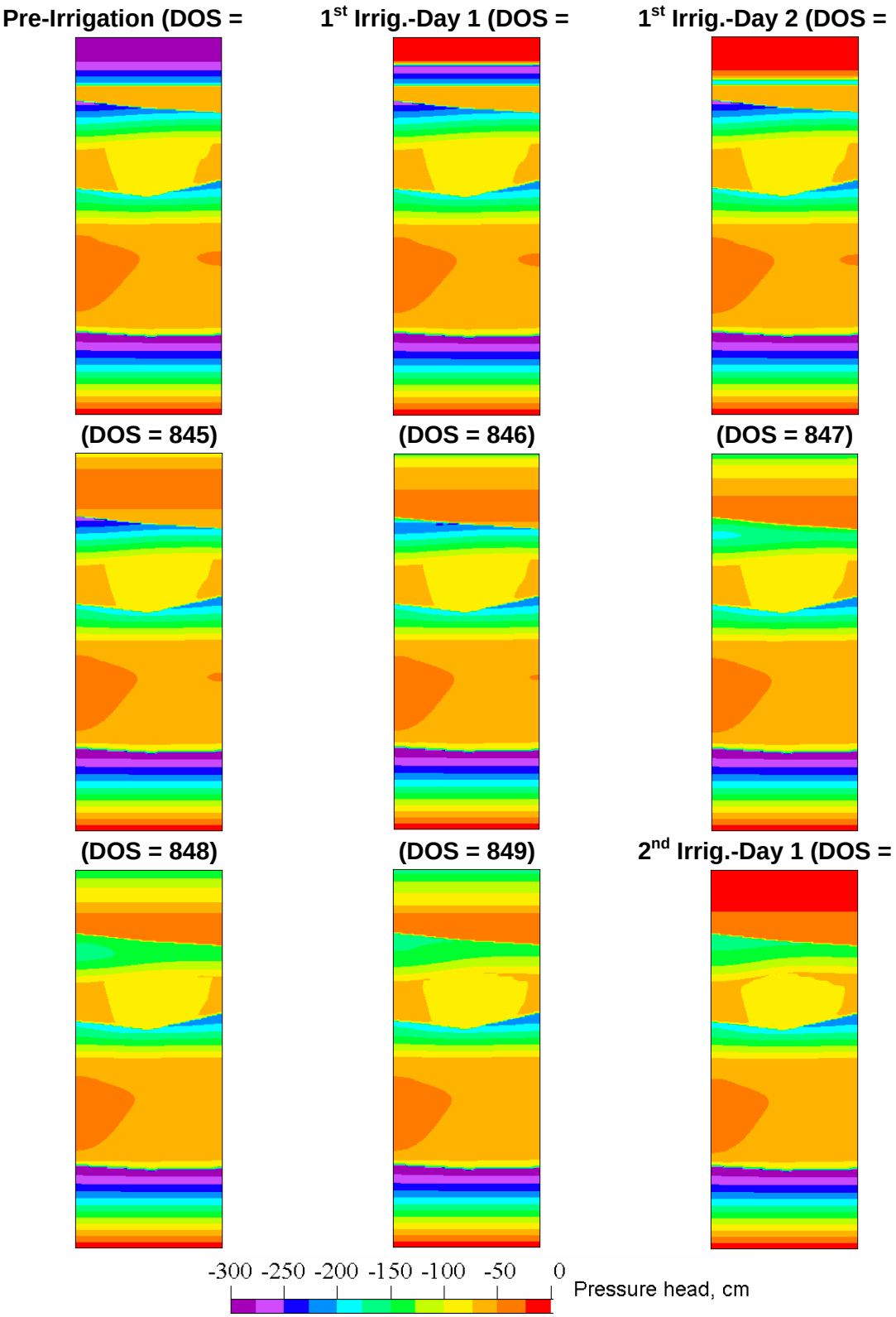

Figure 31 Contour maps of pressure head simulated in the homogeneous model at selected times during the simulation year of 1992

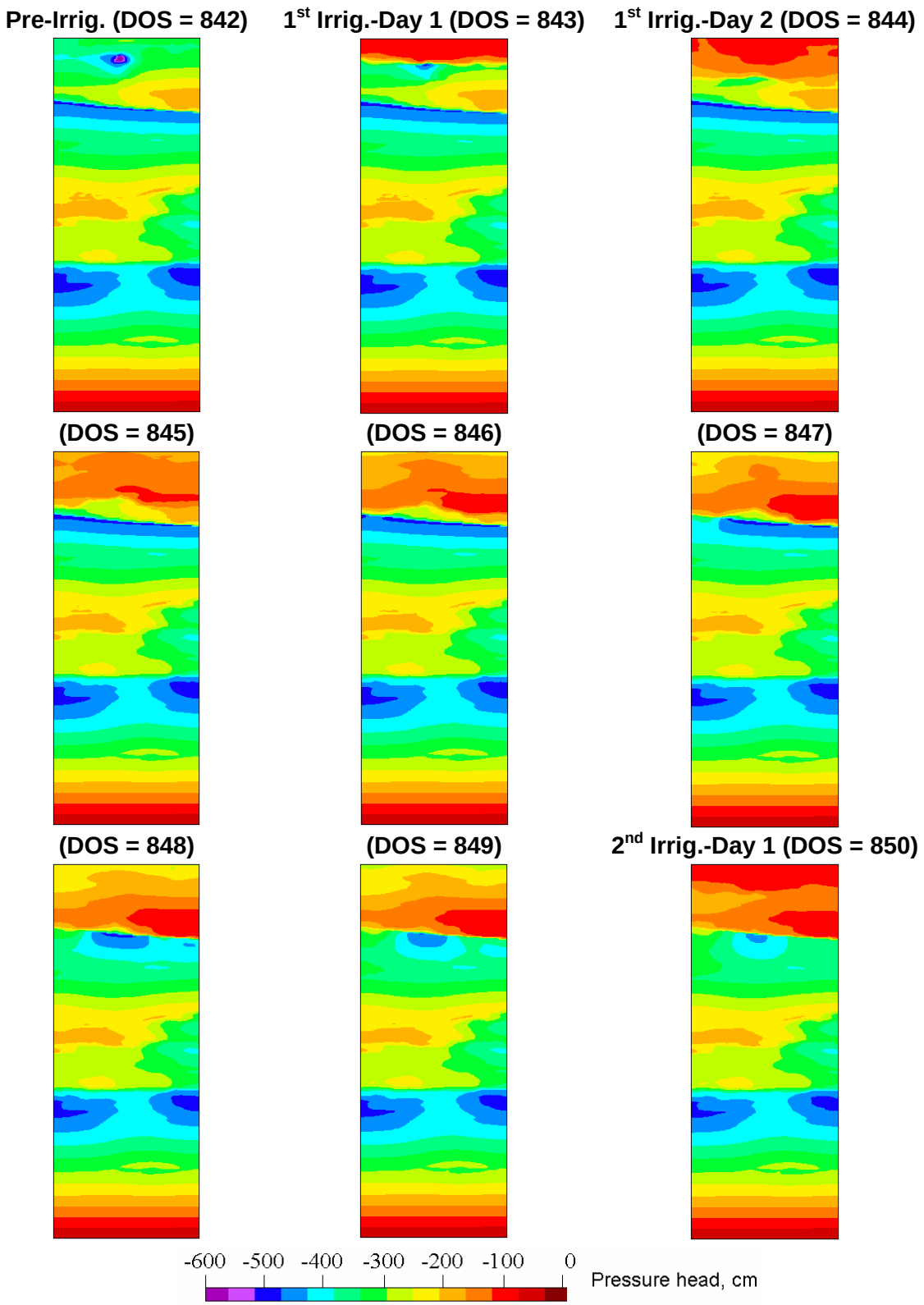

Figure 32 Contour maps of pressure head simulated in the heterogeneous lithofacies model at selected times during the simulation year of 1992

5.11 Irrigation Efficiency

Irrigation efficiency is a common practice for estimating the excess amount of water that is applied to account for water losses due to non-uniformity, evaporation, and runoff as well as deep percolation. A suggested amount of irrigation for a well-managed nectarine orchard is 114 cm under furrow irrigation systems (Day et al., 2000). At the site conditions, annual applied irrigation water varies from 121 cm to 228 cm over the 7 years. The 7-yr long-term average applied water is 175 cm under 13 irrigations per year. These values are well above the typically applied water (Day et al., 2000).

At the orchard conditions, annual irrigation efficiency values are estimated based on the ratio of the applied irrigation to the amount of water used by transpiration. Values for the homogeneous lithofacies model varies between 49% and 68% over the 7 years. In the case of the heterogeneous lithofacies model, irrigation efficiency is even lower, ranging from 41% to 60%. These values are negatively correlated with the number of irrigation applications (r^2 = -0.97 for both the models). The ranges of irrigation efficiency we estimate are within the application efficienties typically encountered in surface irrigation applications (Martin et al., 1991).

Key conclusions drawn from the numerical water mass balance analysis of the two models are as follows:

- Annual recharge to the deep vadose zone simulated by the two models varies considerably from year to year, regardless of the model used.
- Variations in the annual recharge to the deep vadose zone between the homogeneous and heterogeneous lithofacies model are small.
- Simulation results suggest that irrigation schedules that did not closely synchronize the timing of crop water requirements lead to substantial reductions in plant water uptake even during years where a large amount of irrigation was applied (e.g., 1992 and 1993).

Simulation results suggest that the site irrigation management practices did not properly account for the site climate conditions. During wet years (1992 through 1995), the amount of irrigation applied was at least the same or even more than the amount applied during the dry years (e.g., 1990, 1991, and 1996). This inconsistency can be seen, even without the simulation results, if the raw site records of climate and irrigation data (Table 5) are compared.

5.11.1 Role of Plant Water Uptake in the Root Zone Water Budget Analysis

In Table 5**,** potential recharge to the deep vadose zone is evaluated using the model prescribed values of potential transpiration and evaporation while actual recharge is based on the model calculated values. The difference between annual potential recharge and actual recharge as denoted by "ΔRecharge" in Table 5 shows annual reduction of potential transpiration to actual transpiration. The conventional water MB analysis (Appendix 1), if applied again to evaluate annual water mass balance, would provide values of deep vadose zone recharge equivalent to potential recharge values shown in Table 5 because the method assumes potential evapotranspiration is completely consumed in the root zone. As a result of this assumption, plant water uptake is systematically overestimated and consequently net annual percolation to the deep vadose zone is underestimated. Based on the 7-yr averaged simulated data, if the conventional method was used instead of the homogeneous lithofacies, annual deep percolation would be underestimated by 15 cm. While this miscalculation associated with the aforementioned assumption may be considered small given the simplicity of the approach, the 7-yr cumulative reduction reaching to 106 cm in the homogeneous lithofacies model and to 178 cm in the heterogeneous lithofacies model is not small to be negligible (Figure 23). This reduction

representing the amount of water that would otherwise leach below the root zone is artificially lost in the root zone system. This is higher than the long-term annual recharge to the deep vadose zone (99 cm, Table 5). In the case of the heterogeneous lithofacies model, the difference between annual potential and actual recharge rates are even higher. If the traditional root zone water MB were applied, instead of the numerical heterogeneous lithofacies model, actual recharge to the deep vadose zone over the 7 years would be underestimated by 178 cm (Figure 23b).

The simulation results suggest that a proper investigation of actual transpiration is an essential means of estimating the long-term water mass balance. The traditional root zone water MB analysis can systematically underestimate the long-term recharge to the deep vadose zone.

Table 5 Annual root zone water mass balance from 1990 to 1996 based on simulation results in the a) homogeneous and b) heterogeneous lithofacies models

a) Homogeneous Lithofacies		Precipitation	Irrigation	Potential Transpiration	Actual Transpiration	Evaporation	Potential Recharge	Actual Recharge	ΔRecharge	Irrigation Efficiency
Year	# of Irrigation				cm					%
1990	13	26	175	115	100	18	67	83	16	57
1991	10	37	134	112	91	15	44	65	21	68
1992	17	43	228	114	105	21	136	145	9	46
1993	16	41	215	115	105	19	122	132	10	49
1994	13	35	175	113	94	20	78	96	19	54
1995	13	49	175	106	95	16	102	113	11	54
1996	9	28	121	102	80	11	36	57	21	66
7-yr avg.	13	37	175	111	96	17	84	99	15	55

b) Heterogeneous Lithofacies		Precipitation	Irrigation	Potential Transpiration	Actual Transpiration	Evaporation	Potential Recharge	Actual Recharge	ΔRecharge	Irrigation Efficiency
Year	# of Irrigation				cm					%
1990	13	26	175	115	88	18	67	94	27	50
1991	10	37	134	112	80	15	44	76	32	60
1992	17	43	228	114	95	21	136	156	20	41
1993	16	41	215	115	94	19	122	142	21	44
1994	13	35	175	113	85	20	78	105	28	49
1995	13	49	175	106	85	16	102	123	21	48
1996	9	28	121	102	70	11	36	67	31	58
7-yr avg.	13	37	175	111	85	17	84	109	26	49

5.12 Long-term Water Recharge to Groundwater

Figure 33 compares average daily water flux simulated at the lower boundary of the domain in both the homogeneous and heterogeneous lithofacies models. Despite the variations in water content, pressure head, and plant water uptake, close agreement exists between the results of the tow models with respect tot the amount of deep percolating water. The heterogeneous lithofacies model tends to estimate slightly higher water recharge rates throughout the simulation, except during the first half of 1990 where water flux rate is approximately an order of magnitude higher in the heterogeneous lithofacies model.

Results from the two models suggest that inter- and intra-annual variations of water flux to groundwater are dependent on atmospheric boundary conditions despite the presence of the 15.8 m deep vadose zone. There is a clear seasonal pattern in the flux recurring every year. A periodic minimum recharge of approximately 0.05 cm d^{-1} coincides with winter and early spring percolation seasons during which recharge rates at the surface are the minimal. Higher water flux occurs during irrigation seasons than winter times, as expected. After a rapid increase during April to May, water flux reaches to the peak during the middle of summer (July through August). It starts decreasing as the increasing water loss at the surface from evapotranspiration becomes effective. Annual peak fluxes depend on the amount of annual irrigation. The peak water flux in 1992 with 17 irrigations occurs at a rate of 1.5 cm d^{-1} while the peak water flux in 1996 with 9 irrigations is reduced to 0.36 cm d^{-1}.

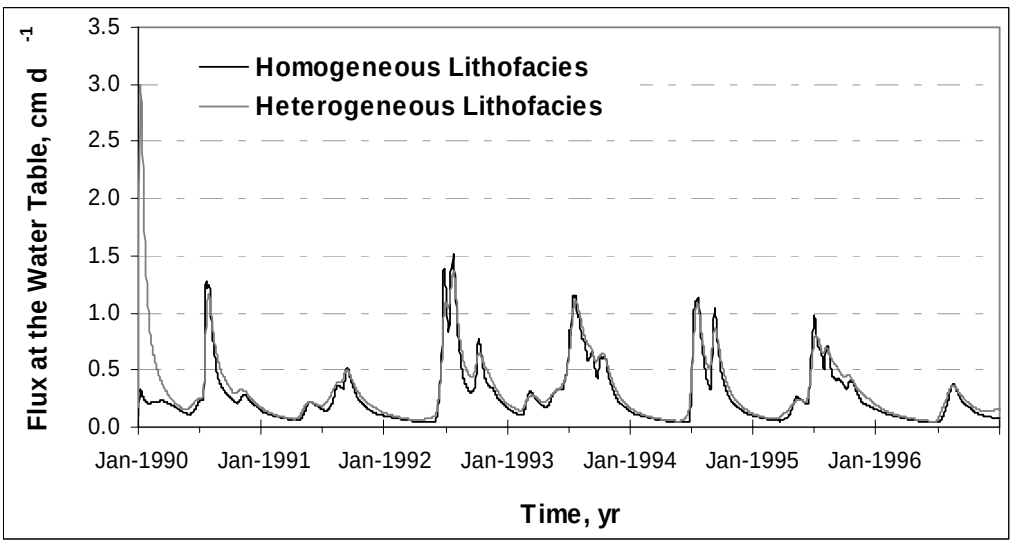

Figure 33 Daily values of average water flux simulated at the bottom of the standard and high subplots (z = 15.8 m at the water table) during the period (1990 – 1996) in the homogeneous and heterogeneous lithofacies models

The simulation results for water flux at the water table highlight that the capillary barrier effect is more controlling than local variations in the soil hydraulic properties. As discussed earlier (Section 4.6 and 4.7), the interface between the C-Si-L and SL2 is apparently acting as a controlling feature consistently in the two models. On the basis of our results, another key finding is that irrigation wetting regime is the major source of the long-term deep percolation. Field studies, conducted to determine the relationship between the amount of recharge water and

irrigation water applied, confirms that increasing levels of added water produces corresponding increases in the rate of percolating water (Troiano et al., 1993). Therefore, in areas vulnerable to leaching, irrigation water should be managed to minimize loss of water to deep percolation in much of California's irrigated areas, especially in orchards where a substantial amount of water is being applied.

5.13 Two-dimensional Spatial Distribution of Water Flux

Contour maps of daily water flux rates are prepared at 18 selected times using simulated output data from the homogeneous and heterogeneous lithofacies models. For each year from 1990 to 1994, three contour maps are displayed (a total of 15 contour maps) to show the distribution of flux 1) on the day of the first spring N fertilizer application, 2) on the day of the fall N application, and 3) at the end of each year. The contour map at DOS = 2191 represent the data at the end of 1995. The remaining two contour maps demonstrate water flux distributions on the day of the fall N fertilizer and at the end of the simulation period in 1996. The selected outputs are provided to describe both intra- and inter-annual variations in flux.

5.13.1 Homogeneous Lithofacies Model

Figure 34 shows contour maps of water flux simulated in the homogeneous model at 18 selected times over the simulation period. In general, flux rates simulated during fall seasons (i.e., contours on the day of fall N application, DOS = 88 in 1990 and 810 in 1992) are much greater, several orders of magnitude, than those during spring (i.e., contours on the day of spring N application, DOS = 261 in 1990 and 984 in 1992, respectively). Due to large seasonal fluctuations, data shown in the contour maps are log-transformed flux rates. Comparison of flux rates during winter (i.e., contours at the end of a simulation year) and the early stages of irrigation seasons (i.e., spring season) suggests that year to year flux rates below the root zone vary significantly depending on winter wetting patterns. Some years (e.g., 1990, 1991, and 1993) the entire vadose zone exhibits drier conditions and smaller flux rates during spring than winter. For other years, the situation is reversed. At the end of each simulation year, patterns of fluxes tend to be the same (e.g., DOS = 365, 731, 1461, 1826, and 2191).

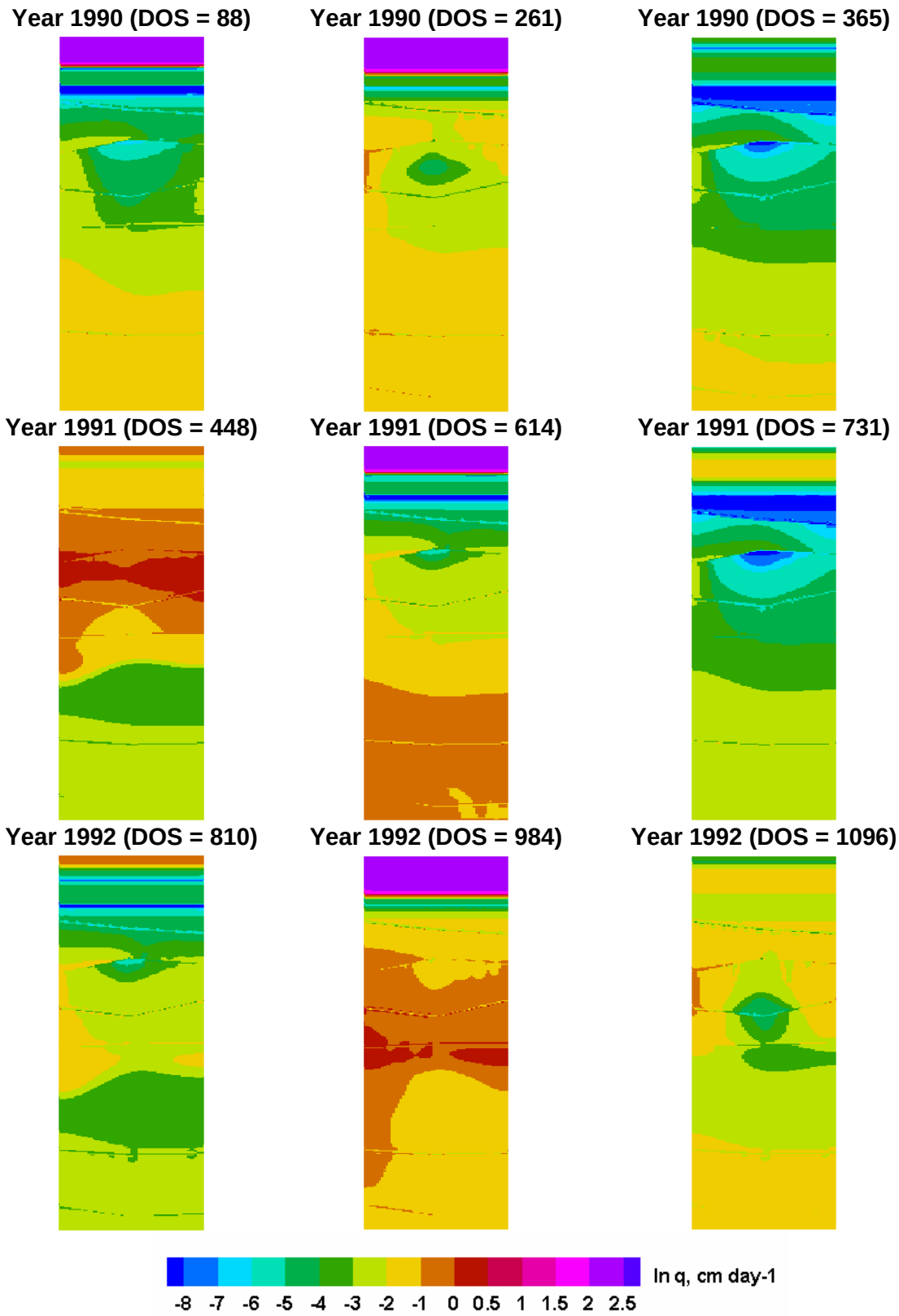

Figure 34 Contour maps of water flux simulated in the homogeneous model at selected times during the simulation period (1990 – 1996)

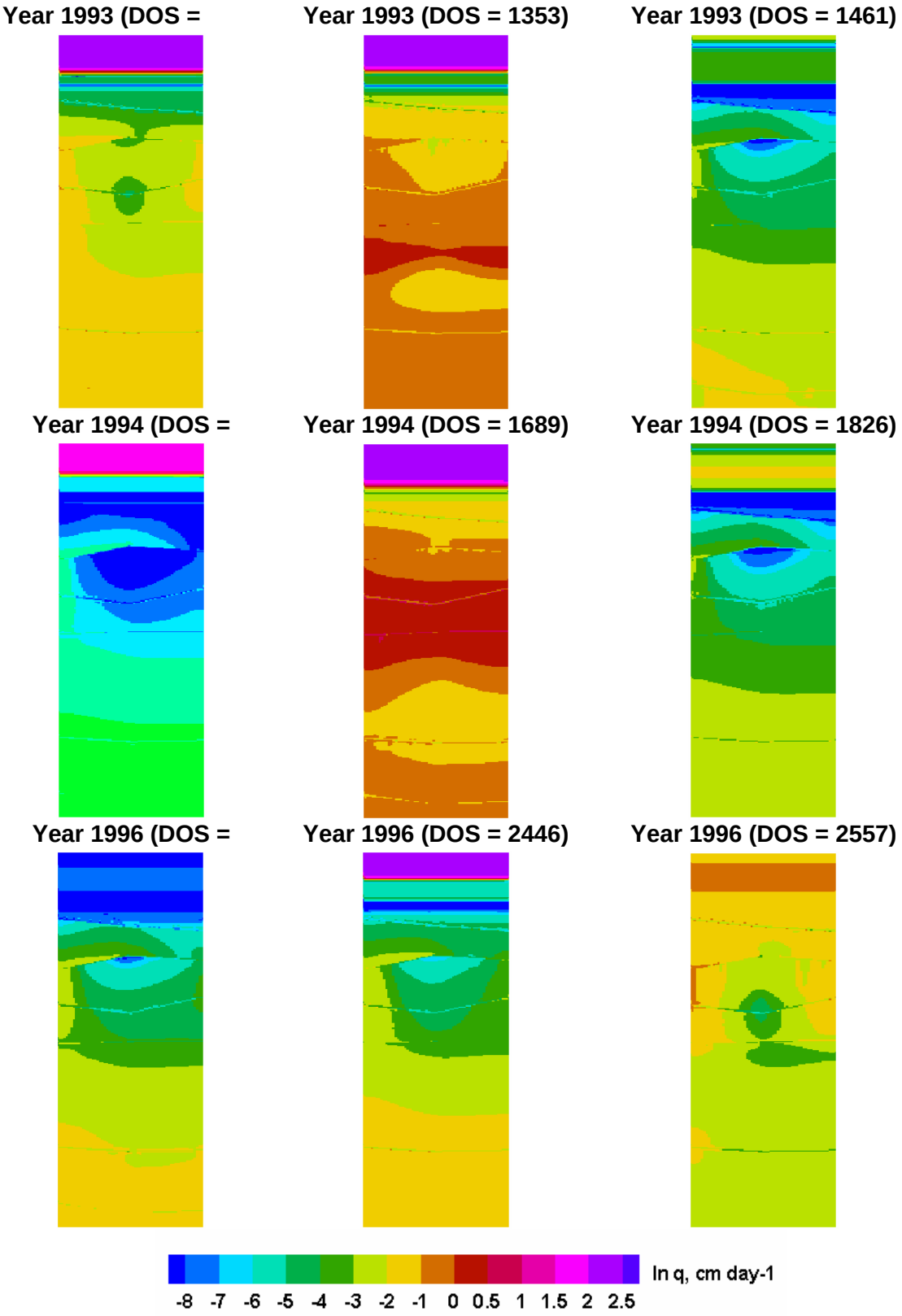

Figure 34 cont. Contour maps of water flux simulated in the homogeneous model at selected times during the simulation period (1990 – 1996)

Every irrigation event creates flux rates in the root zone that are equivalent to the saturated hydraulic conductivity of the SL1 layer (Table 1). Thus, the root zone becomes saturated temporarly. Since the spring of 1991 and 1992 contour maps represent soil moisture condition with rainfall events (Table 4, rainfall of 0.9 cm in 1991 and 1.1. cm in 1992), the root zone does not reach to a full saturation. Also the wetting front tends to progress deeper in the root zone during fall irrigations than during the spring irrigations (e.g., DOS = 88 vs. 261 in 1990 and 1174 vs. 1353 in 1994), suggesting that repeated irrigations progressively increase the root zone saturation.

Similar to the water content distribution from the homogeneous lithofacies model, the layered structure produces a sharp change in water flux rates across the layer boundaries. The effect of the inclined boundaries seems to overcome the uniformity of surface fluxes, creating irregular patterns of flux rates below the root zone. Because of differences in their soil hydraulic properties, lithofacies show different rates of fluxes under the prevailing moisture conditions. During dry conditions, the Var1 layer, located between two layers of predominantly fine-textured materials (i.e., SL1 and HP1), have smaller flux rates than the layers above and below the Var1. Slower movement of flux consistently appears within the layer Var2 along the interface between the Var2 and the overlying layer HP1. This is consistent with the water content distributions shown earlier (Figure 33) and suggests that this interface seems to act as a capillary barrier that minimizes water leaching into the underlying layer.

In general, patterns of flux throughout the profile and the magnitude of flux to the water table are mainly controlled by the surface boundary conditions. As discussed earlier, water fluxes at the bottom of the domain experience both intra- and inter-annual fluctuations despite the deep vadose zone. Another key observation is that patterns of flux rates reoccur in the same places during the same time of a given simulation year.

5.13.2 Heterogeneous Lithofacies Model

In the heterogeneous lithofacies model, flux rates exhibit local variations due to the randomly distributed soil hydraulic properties (i.e., scaling factors). However, comparison of the contour maps from the heterogeneous lithofacies model with the homogeneous lithofacies model indicates that zones of higher flux rates in the two models correlate well. This implies that the local heterogeneity within the lithofacies has only a limited impact on the magnitude of flux rates. This observation further suggests that the laterally extensive hardpans such as the HP1 at the site, when intercalated between highly permeable sediments such as the Var1 and S layers, represent confining layers that are known to reduce the vertical permeability. It is likely that in our modeling, the lithofacies boundary effect overcomes the local heterogeneity effect on flux rates, and in turn on nitrate transport to the water table.

Several similarities between the results of the two models exist with respect to the flux rates, as described below. Flux rates simulated during irrigation seasons are several orders of magnitude greater than those estimated during spring and winter seasons (Figure 35), consistent with the results of the homogeneous lithofacies model. Consecutive irrigation events increase the flux rates both in the root zone and in the deep vadose zone substantially. Small scale irregularities at the wetting front average to yield a lithofacies scale smooth, nearly flat wetting front. The effect of lithofacies boundaries is most pronounced between the Var1 and HP1 and between the Var2 and S layers. Based on the distribution of scaling factors (Figure 2), the highest contrast in soil hydraulic properties occurs along the interfaces between the Var1 and HP1 and

between the Var2 and S. Thus, these interfaces are expected to create capillary barriers to flow and nitrate transport. Note that most of both the Var1 and S layers coincide with areas of the highest scaling factors (Figure 2) and have the smallest flux rates under the prevailing moisture conditions, consistent with their coarse-textured media. The most pronounced finger-like patterns are consistently seen around the mid-way of the interface between the Var2 and S layers. Flow becomes fingered immediately below the interface and is primarily gravity-driven. During successive irrigation events, fingers recur in the same places, as reported previously in the laboratory (Wang et al., 2003) and in field experiments (Ritsema et al., 1998). This observation is similar to the most widely studied and documented occurrence of the phenomenon, so called "unstable flow", that takes place during infiltration from a fine-textured layer into a coarse one occurs (Glass et al., 1988; Wang et al., 1998).

As recognized by a number of researchers, the assumption of uniform flow velocity, similar to the one made in the MB method (Appendix 1), may result in erroneous travel time estimations of chemicals. In reality, solute moves faster as a result of preferential flow that is caused by flow through macropores and zones of higher local conductivity and the wetting front instability (Ghodrati and Jury, 1990). The latter becomes important in sandy soils where fine sand is overlain by coarse (Glass et al., 1988). Unstable wetting fronts and fingering have been documented widely both in homogenous and heterogeneous media, not only in sandy soils (Glass et al., 1988; Selker et al., 1992; Ritsema et al., 1993) but also in loam and clay soils (Flury et al., 1994). Wang et al. (1998) have confirmed that during infiltration into a layered fine-over-coarse system under laboratory settings, the wetting front in the loam is retarded at the interface and flow becomes unstable and fingered immediately below the interface.

Given the highly heterogeneous soil texture, strong layering, and large seasonal fluctuations in surface fluxes at the site, we believe that the results of our heterogeneous lithofacies model are likely to oversimplify the extent of fingering and preferential flow paths that are commonly encountered under field and laboratory settings (Glass et al., 1991; Wang et al., 1998; Wang et al., 2003a; Wang et al., 2004). This is primarily attributed to the scaling approach whose weakness lies in its smoothing effect of soil hydraulic properties.

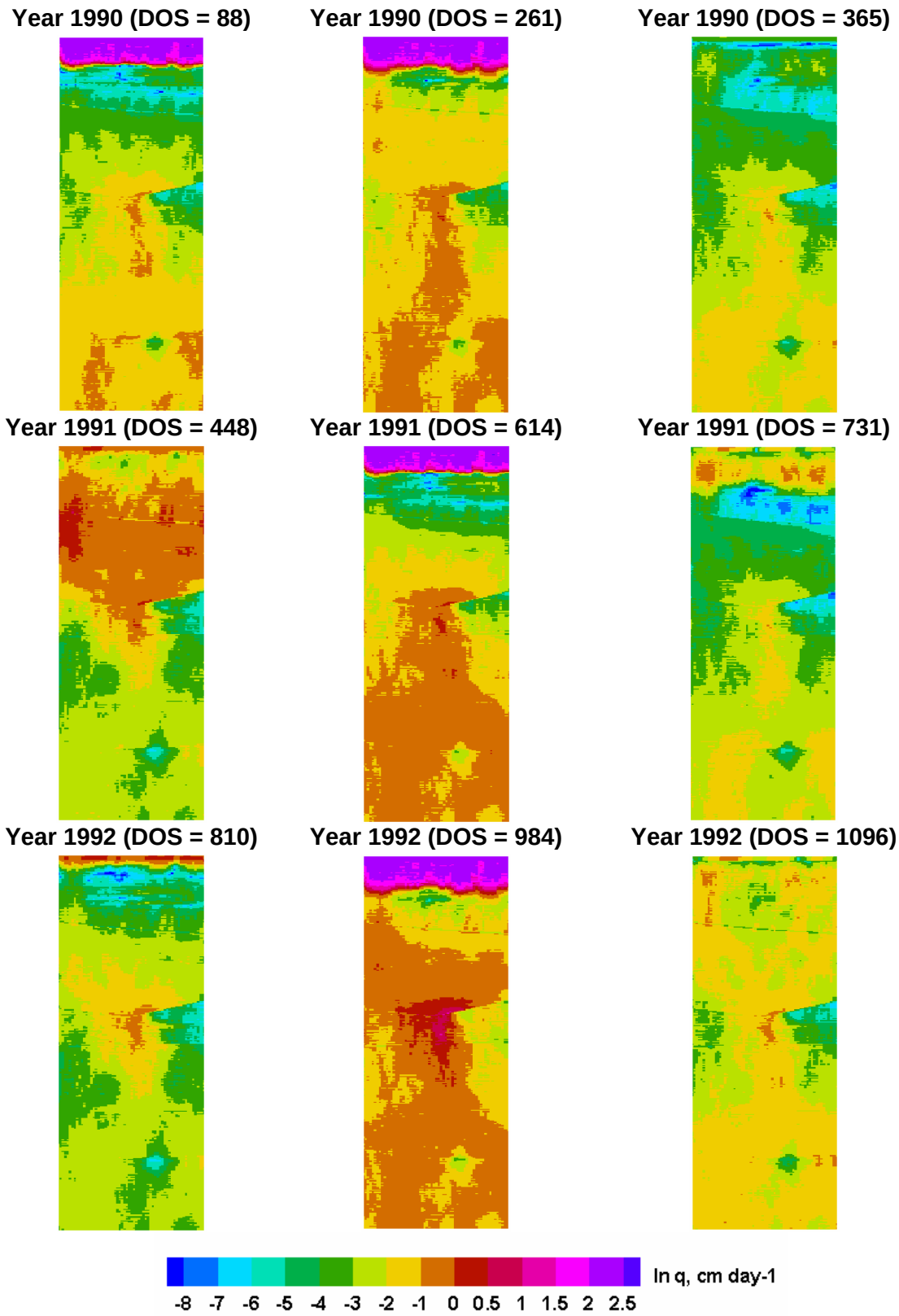

Figure 35 Contour maps of water flux simulated in the heterogeneous lithofacies model at selected times during the simulation period (1990 – 1996)

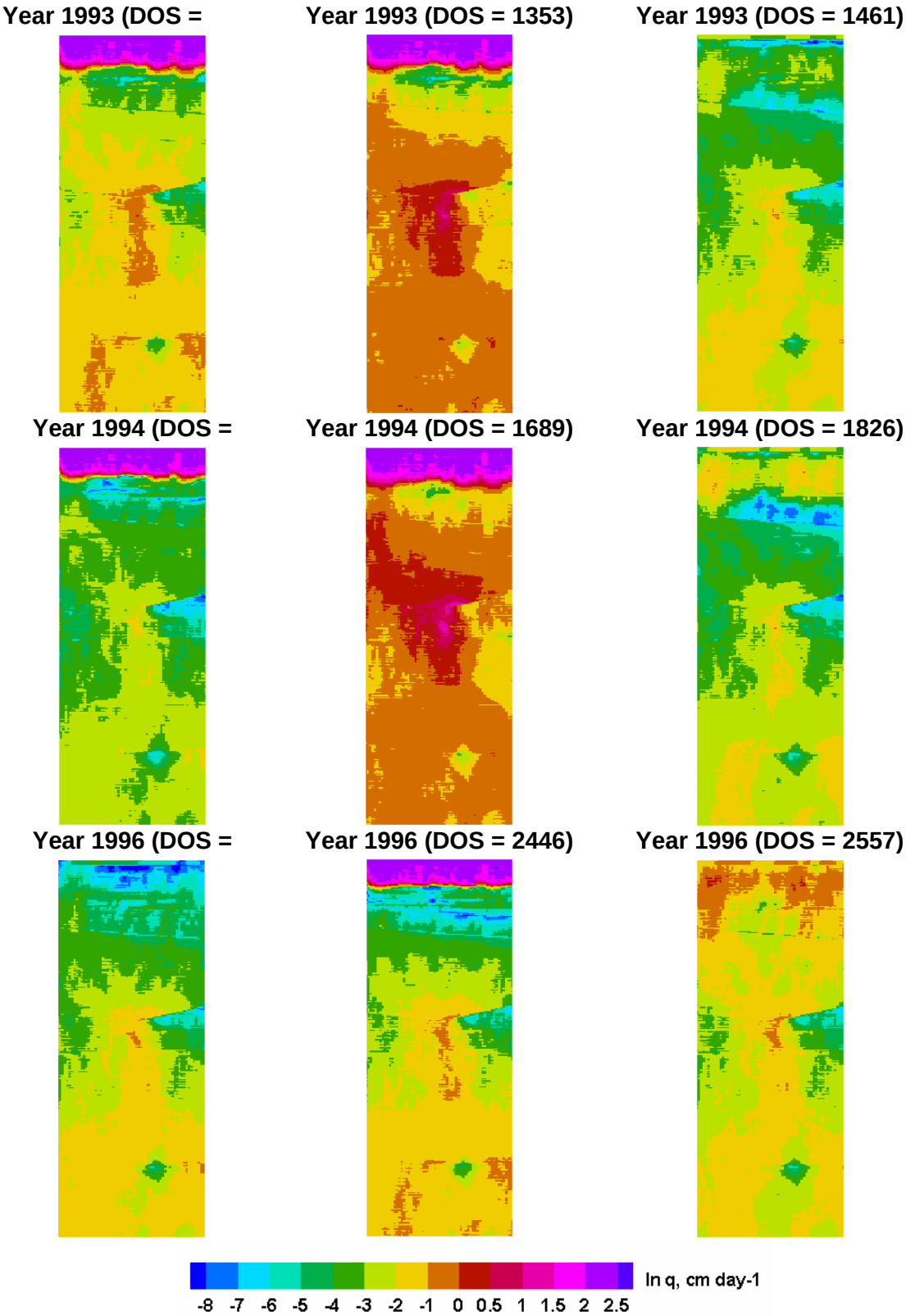

Figure 35 cont. Contour maps of water flux simulated in the heterogeneous lithofacies model at selected times during the simulation period (1990 – 1996)

5.14 Plant Nitrogen Uptake

Temporal variations of cumulative N uptake data at the standard and high subplots during the 7 years are presented in Figure 36 for both the homogeneous and heterogeneous lithofacies model. The results are based on the maximum concentration threshold *CRoot* = 0.02 mg cm^{-3} which remains the same at each subplot and each model. In the heterogeneous model, plant N uptake is reduced as a result of higher reduction in potential transpiration. In the two models, most N uptake occurs after mid-June when trees enter its rapid growth phase. A small spike that appears in each year's cumulative N uptake curve, except in 1995, is a response of N uptake to fall fertilizer application. Annual and cumulative N uptake in each successive yearly simulation is listed in Tables 6 and 7 for the standard subplot and the high subplot, respectively, for each model. Because of the zero initial N condition, the total annual N uptake both at the standard and high subplots are smaller in the first year than those observed in other years.

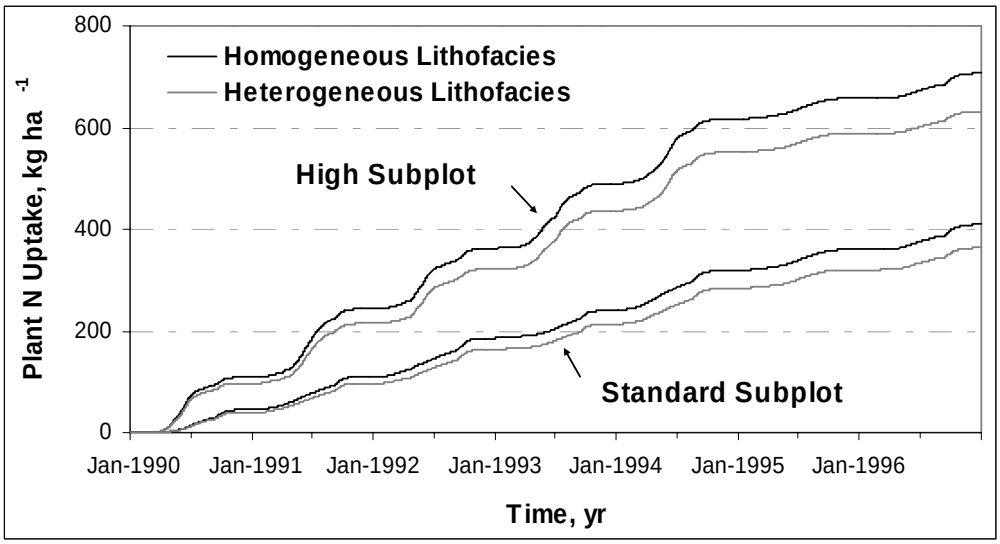

Figure 36 Cumulative plant N uptake simulated at the standard and high subplots during the simulation period (1990 – 1996) in the homogeneous and heterogeneous lithofacies models

In Tables 6 and 7, annual N uptake is partitioned into two periods: N uptake after fall application in the same year and before fall application in the subsequent year. The zero initial concentration reduces N uptake both before and after fall application in 1990. For the following years, N uptake after fall application at both subplots are comparable. The model produces comparable N uptake values at both standard and high subplots for 1995 and 1996 because of the irrigation and fertilization practices imposed consistently at both sites (i.e., no application in 1995 and one application of 110 kg N ha^{-1} in 1996). In the homogeneous lithofacies model, the simulated N plant uptake of 41 kg ha^{-1} in 1995 is mainly the contribution of N applied from the previous year and N from irrigation during the growth season of 1995. In the heterogeneous lithofacies model, the simulated N plant uptake in 1995 reduces to 37 kg ha^{-1}. According to the model results, the majority of N plant uptake at the high subplot occurs before fall N applications,

as shown by higher plant N uptakes before fall applications compared to N uptake after fall applications (Tables 6 and 7).

5.14.1 Effects of Applied Irrigation on Plant Nitrogen Uptake

The interpretation of the simulated annual N uptake relative to applied irrigation is not straightforward because of the lack of information on the background levels of naturally occurring nitrate concentrations at the site. Additionally, the absence of fertilizer application in 1995 makes the interpretation of data for 1995 and 1996 with data from other years harder. In an attempt to exclude the impact of the initial condition and no N application on the annual N uptake, N uptake simulated between 1991 and 1994 are considered for an exclusive analysis of the relation between the amount of irrigation and plant N uptake.

Table 6 Annual and cumulative *NO_3-N* uptake values at the standard subplot based on simulation results in the a) homogeneous and b) heterogeneous lithofacies models

Standard Subplot

Homogeneous Lithofacies

a)		Annual NO_3-N Uptake	NO_3-N Uptake Before Fall Application	NO_3-N Uptake After Fall Application	Cumulative NO_3-N Uptake
Year	# of Irrigation			kg ha^{-1}	
1990	13	44	31	14	44
1991	10	66	48	18	110
1992	17	75	52	23	186
1993	16	54	38	16	240
1994	13	79	57	22	319
1995	13	41	NA	NA	360
1996	9	50	26	24	410
4-yr avg.	(1991 - 1994)	69	49	20	
7-yr avg.	(1990 - 1996)	59	42	20	

Heterogeneous Lithofacies

		Annual NO_3-N Uptake	NO_3-N Uptake Before Fall Application	NO_3-N Uptake After Fall Application	Cumulative NO_3-N Uptake
Year	# of Irrigation			kg ha^{-1}	
1990	13	40	28	12	40
1991	10	58	41	16	97
1992	17	66	46	21	163
1993	16	49	35	15	213
1994	13	71	49	21	283
1995	13	37	NA	NA	320
1996	9	44	23	21	364
4-yr avg.	(1991 - 1994)	61	43	18	
7-yr avg.	(1990 - 1996)	52	37	18	

A frequent application of irrigation is expected to enhance plant N uptake by supplying additional N for plants and by promoting actual transpiration. However, according to the simulation results, it counteracts by accelerating water leaching below the root zone and thus removing available N via deep percolation. For instance, the maximum annual N uptake at the standard subplot is estimated to be 79 kg ha^{-1} and 71 kg ha^{-1} in the homogeneous and heterogeneous lithofacies model, respectively, for 1994 that has a moderate irrigation application (13 irrigations) and moderate winter precipitation (35 cm yr^{-1}). The minimum annual N uptake is estimated to be 54 kg ha^{-1} and 49 kg ha^{-1} in the homogeneous and heterogeneous lithofacies model, respectively, in 1993 with 16 irrigations.

In the case of the high subplot, the effect of irrigation on plant N uptake is similar. Both in the homogeneous and heterogeneous lithofacies models, the maximum annual plant N uptakes, 121 kg ha^{-1} and 105 kg ha^{-1}, respectively, are simulated in 1991 with 10 irrigations. The minimum annual plant N uptakes, 106 kg ha^{-1} and 95 kg ha^{-1} are obtained for 1992 with the highest number of irrigation applications (17 irrigations).

Table 7 Annual and cumulative *NO_3-N* uptake values at the high subplot based on simulation results in the a) homogeneous and b) heterogeneous lithofacies models

High Subplot

Homogeneous Lithofacies

Year	# of Irrigation	Annual NO_3-N Uptake	NO_3-N Uptake Before Fall Application	NO_3-N Uptake After Fall Application	Cumulative NO_3-N Uptake
		kg ha^{-1}			
1990	13	97	84	12	97
1991	10	121	102	18	217
1992	17	106	85	21	323
1993	16	113	98	15	436
1994	13	114	94	20	550
1995	13	37	NA	NA	586
1996	9	45	24	21	631
4-yr avg.	(1991 - 1994)	113	95	18	
7-yr avg.	(1990 - 1996)	90	81	18	

Heterogeneous Lithofacies

Year		Annual NO_3-N Uptake	NO_3-N Uptake Before Fall Application	NO_3-N Uptake After Fall Application	Cumulative NO_3-N Uptake
		kg ha^{-1}			
1990	13	87	76	11	87
1991	10	105	89	16	192
1992	17	95	77	18	287
1993	16	102	89	13	389
1994	13	103	84	19	492
1995	13	33	NA	NA	525
1996	9	39	21	18	564
4-yr avg.	(1991 - 1994)	101	85	17	
7-yr avg.	(1990 - 1996)	81	73	16	

5.14.2 Model Estimated versus Measured Plant Nitrogen Uptake

It is difficult to facilitate one to one comparison between the measured and model estimated plant N uptake values because the time period of the measured values (1983 – 1985 and 1991 – 1994) do not completely coincide with the simulation period (1990 – 1996). More importantly, the simplification of zero initial condition and no N application in 1995 in the models makes this comparison even more complicated. Nevertheless, long-term average quantities can be used, instead of annual values, to infer if the passive N uptake approach adopted in the models may suffice to handle the plant N uptake process in particular and to predict long-term trends of potential plant N uptake. In an attempt to eliminate the effect of the initial condition and no N application on the simulated annual plant N uptakes, only the data between 1991 and 1994 are considered.

At the standard subplot, in the homogeneous lithofacies model, the estimated plant N uptakes range from 54 kg ha^{-1} to 79 kg ha^{-1} with an average of 69 kg ha^{-1} based on the 4 years of simulated data (1991 – 1994). For the same time period, the heterogeneous lithofacies model simulates plant N uptakes ranging from 49 kg ha^{-1} to 71 kg ha^{-1} with an average of 61 kg ha^{-1}. Compared with the measured 7-yr average value of 83 kg ha^{-1} listed in Table 7, the average simulated values are underestimated by 14 kg ha^{-1} and 22 kg ha^{-1} and outside of the margin of the error (95% confidence intervals) estimated for the measured data (Table 7) based on the standard, linear error analysis (Berthouex and Brown, 1994) at the lower and upper 95% confidence intervals.

In the case of the high subplot, the situation is reversed: the model estimated 4-yr average values of 113 and 101 kg N ha^{-1} in the homogeneous and heterogeneous lithofacies models, respectively, are only slightly different than the 7-yr average value of 105 kg N ha^{-1} (Table 7). Both values are within the error of margins estimated for the measured data at the high subplot.

Table 8 Plant NO_3-N uptake measured at the standard and high subplots during the period from 1983 to 1985 and from 1991 to 1994

	Measured Annual N Uptake	
	Standard	High
Year	kg ha^{-1}	
1983	88	120
1984	85	113
1985	89	101
1991	90	118
1992	89	112
1993	70	79
1994	68	95
7-yr avg (1983 - 1994)	83	105
Variance	29	104
Standard Deviation	5	10
Upper	90	120
Lower	68	79
95% Confidence Interval	72/93	85/126

In the view of field scale, long-term averaged quantities, the difference between the measured and the model estimated plant N uptake at the high subplot is of minor importance. Although the corresponding difference for the standard subplot seems to be significant, a further adjustment of CRoot value (increasing the parameter > 0.02 mg cm^{-3}) at the standard subplot alone should be avoided since it would lead to an inconsistent treatment of the same process at both sites. Overall, the numerically simulated plant N uptake values demonstrate some partial evidence that the macroscopic, passive N uptake approach may suffice to provide a representative range of plant N uptake values if the approach is used as part of a long-term groundwater quality risk assessment plan.

5.15 Temporal Variations of Nitrogen in the Root Zone

In this section, temporal variations of N in the root zone are compared between the two fertilizer applications and between the two numerical models. Comparisons include average N concentration within the root zone, total N mass that is stored within the root zone, and root zone N mass budget. Nitrogen concentrations are defined in aqueous phase in units of g m^{-3}.

5.15.1 Average Nitrogen Concentration

Figures 37 and 38 show variations of average N concentration simulated by the homogeneous and heterogeneous lithofacies models from 1990 to 1996 in the root zone of the standard subplot and high subplot, respectively. Average N concentration in the root zone provides an overall representation of the occurrence of N in the root zone. It is evaluated by arithmetically averaging point concentrations over the entire vertical plane from the surface to the depth of z = 1.8 m.

The root zone average N concentration simulated in the two models is remarkably similar both at the standard and high subplot. As N moves at the same rate as water, temporal changes of average root zone N concentration both under the standard and high subplots depend largely on the water fluxes from the surface. At the standard subplot, the average peak concentration is elevated rapidly to about 40 g m^{-3} immediately after the fall application in each year, except in 1995 (Figure 37). The peak concentration remains relatively stable throughout winter months (between October and December) unless there is considerable amount of water that carries N out of the root zone such as in 1992 and 1996. The portion of the breakthrough curve associated with the 1992 and 1996 fall applications look alike with a smaller area underneath the curve. The amount of net annual recharge during 1992 and 1996 cannot be solely responsible for more rapid loss of N from the root zone since overall soil conditions observed during these years are opposite of each other. The simulated net recharge from the root zone to the deep vadose zone in 1992 is 145 cm and 156 cm in the homogeneous and heterogeneous lithofacies models, respectively. The net water recharge to the deep vadose zone simulated in 1996 is the minimum with a value of 57 cm and 67 cm in the homogeneous and heterogeneous lithofacies models, respectively.

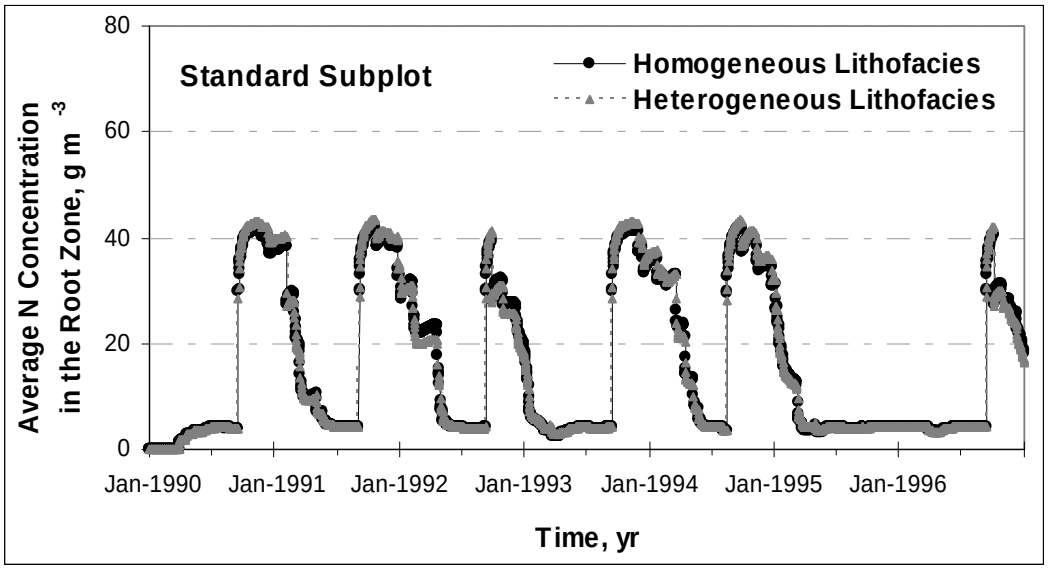

Figure 37 Average N concentration simulated in the root zone of the standard subplot during the period (1990 – 1996) in the homogeneous and heterogeneous lithofacies models

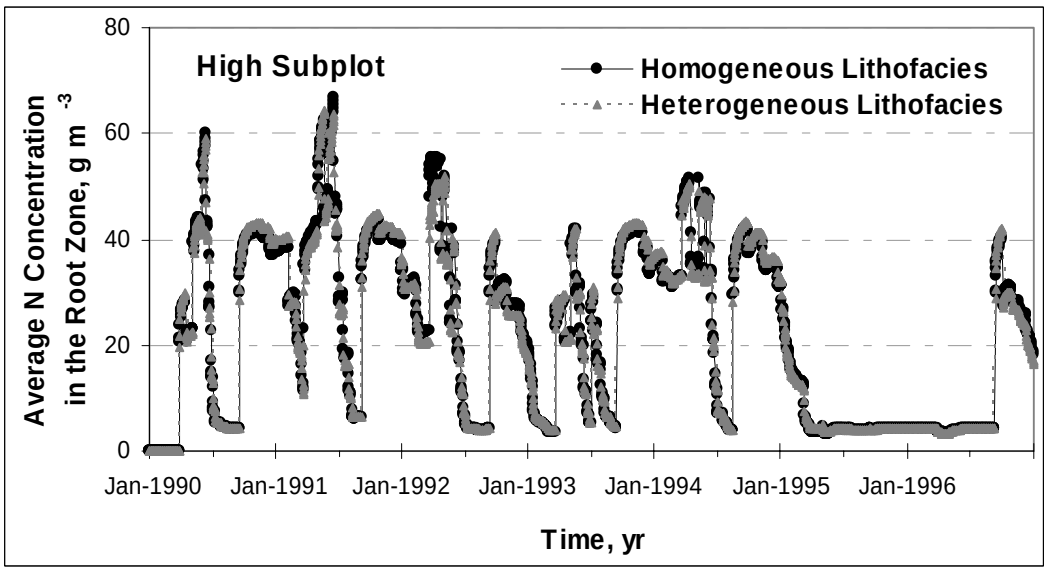

Figure 38 Average N concentration simulated in the root zone of the high subplot during the period (1990 – 1996) in the homogeneous and heterogeneous lithofacies models

A close look at the site irrigation records reveals that in both 1992 and 1996, a one-time irrigation application occurs after the fertilizer application. This clearly demonstrates that, irrigation following the fall fertilizer application has a more profound impact on N loss from the root zone than the magnitude of the annual net water recharge to the deep vadose zone. This observation also explains the reduced plant N uptake during 1993 since a substantial amount of N might has already left the root zone before the next growth season starts. Annual N uptake for 1993 is

estimated to be 54 kg ha^{-1} and 49 kg ha^{-1} in the homogeneous and heterogeneous lithofacies models, respectively. These values are less than the 4-yr averaged value of 69 kg N ha^{-1} and 61 kg N ha^{-1} (based on 1991 – 1994 data). It is noted that the difference between the plant N uptake estimated for 1993 and the plant uptake estimated based on the 4-yr average data is greater during the growth season than after the growth season. In 1993, plant N uptake is 38 kg ha^{-1} and 35 kg ha^{-1} for the corresponding models during the growth season as apposed to the 4-yr average of 49 kg N ha^{-1} and 43 kg N ha^{-1} (based on 1991 – 1994 data) (Tables 7).

At the high subplot, the breakthrough curve contains typically two peaks per year, one associated with the 100 kg ha^{-1} fall application and the other associated with the spring N application (three times at the rate of 85 kg N ha^{-1} each year except in 1995 and 1996). The overall appearance of the average N concentration curve in response to fall applications is similar to that seen at the standard subplot (Figure 38). Both the timing and the magnitude of the peak concentrations from fall applications at the high subplot correlate well with the corresponding results at the standard subplot. The highest average peak concentration is observed in 1991 at the rate of about 67 g m^{-3} in the homogeneous lithofacies model and 64 g m^{-3} in the heterogeneous lithofacies model. This can be a result of the first spring fertilizer applied with precipitation, instead of irrigation, resulting in a higher N application rate (i.e., less diluted N concentration). The peak is reduced in other years when the timing of irrigation and fertilizer applications coincides (e.g., in 1990, 1993 - 1995).

Comparison of the average peak concentrations between the standard and high subplots suggests that peaks do not vary directly as a function of the total applied fertilizer N. The applied amount during spring is about 2.5 times the fall application, yet the average peak concentration corresponding to spring fertilizer applications is approximately 1.5 times the average peak concentration resulting from fall applications.

5.15.2 Total Nitrogen Mass

In Figures 39 and 40 temporal variations of model simulated total N mass storage in the root zone under the standard and high subplots, respectively, are shown from 1990 to 1996. The characteristics of the curve are similar to those of the average N concentration seen in Figures 37 and 38. Both at the standard and high subplots, results from the homogeneous lithofacies model are the same as those from results from the heterogeneous lithofacies. At the standard subplot, a small mass of 13 kg ha^{-1} that accumulates in the root zone before the first fertilizer applications in 1990 is the contribution from irrigation. Total N mass storage raises to a peak of approximately 120 kg ha^{-1} each year immediately after the fall fertilization. Nitrate mass is lost gradually during winter months after the fertilizer application. Since transpiration, and in turn plant N uptake, during winter is limited, the root zone N mass declines only slightly under moderate winter precipitation. Heavy precipitation (e.g., January through March in 1992 and 1995) expedites the loss of N from the root zone. Once the growing season starts at the beginning of spring next year, N uptake resumes, causing N mass in the root zone to sharply decrease (e.g., 1991 and 1994). Consistent with the observations for average N concentration in the root zone, a substantial amount of nitrate is carried below the root zone primarily by irrigation applications that take place after the fall fertilizer application (e.g., 1992 and 1996).

At the high subplot, total N mass reaches the amount of 120 kg ha^{-1} following fall applications each year in the same way as at the standard subplot (Figure 40). Total N mass peaks associated with spring applications vary from 150 kg ha^{-1} in 1993 and 240 kg ha^{-1} in 1991. Variations in irrigation schedule during spring N applications have a strong impact on the amount of N storage in the root zone as shown by different shapes of curves and different peaks in each

year. In 1992 and 1994, the mass from fall applications is combined with that resulting from spring applications. The timing of high and low N mass in the root zone coincides with the timing of high and low average concentrations in the root zone (Figures 37 and 38).

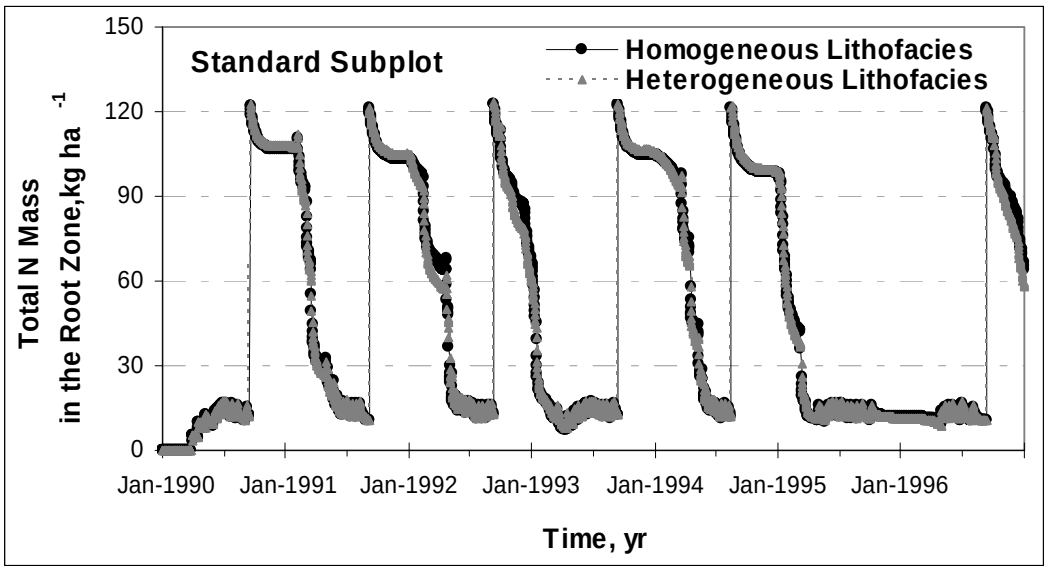

Figure 39 Total N mass simulated in the root zone of the standard subplot during the period (1990 – 1996) in the homogeneous and heterogeneous lithofacies models

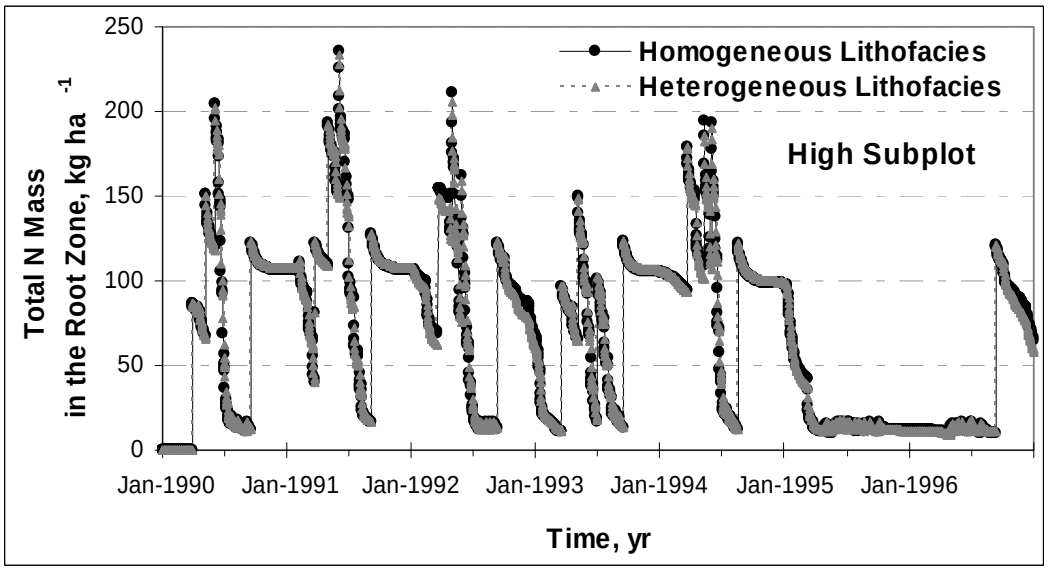

Figure 40 Total N mass simulated in the root zone of the high subplot during the period (1990 – 1996) in the homogeneous and heterogeneous lithofacies models

5.15.3 Annual Root Zone Nitrogen Budget

Annual root zone N budget, presented in Tables 9 and 10 for the standard and high subplots, respectively, is performed based on the simulated results of the homogeneous and heterogeneous lithofacies models. Total N in the vadose zone at the end of each simulation year is conceptually divided into two compartments: N in the root zone N_{RZ} and N in the deep vadose zone N_{DVZ} (Figure 3.1). End of year N mass in the vadose zone varies as a function of N from fertilizer and irrigation (N inputs in the root zone) and N plant uptake (see Tables 11 and 12) within the year. The root zone N mass varies widely as a function of irrigation schedule. Neither the fertilizer treatment nor the model used has a strong effect on the amount of N mass in the root zone at the end of each year. The minimum N mass of 12 kg ha^{-1} occurs in 1995, regardless of the fertilizer applications and the model used, in response to no N application during that year. The maximum N mass is obtained in 1990 at both the subplots and varies from 107 kg N ha^{-1} in the homogeneous lithofacies model to 108 kg N ha^{-1} in the heterogeneous lithofacies model (Tables 9 and 10).

5.16 Nitrogen Concentration at the Root Zone

Temporal variations of nitrogen concentration are monitored at the bottom of the root zone (x = 3.1 m and z = 1.8 m) during the entire simulation period for quantifying N loss from the root zone underneath the standard and high subplots. Similar to the simulation results for average N concentration and N mass storage in the root zone, monitored N concentrations at each subplot, which are shown in Figures 41 and 42, are only slightly different between the homogeneous and heterogeneous models. Variations of N concentrations depend largely on surface water fluxes. The arrival time of peak concentrations at both subplots vary significantly corresponding to the time of irrigation after fertilizer applications and winter precipitation patterns. A base nitrogen concentration of about 4 g m^{-3} (4 mg L^{-1}) detected at both subplots is equivalent to N concentration coming from the irrigation water.

Table 9 Annual root zone NO_3-N mass balance at the standard subplot based on simulation results in the a) homogeneous and b) heterogeneous lithofacies models

Standard Subplot

Homogeneous Lithofacies

a)		Vadose Zone		Root Zone	Deep Vadose Zone
		Beginning of Year	End of Year	End of Year	
Year	# of Irrigation	NM_0	NM_T	N_{RZ}	N_{DVZ}
1990	13	0	132	107	25
1991	10	132	225	103	122
1992	17	225	334	67	267
1993	16	334	304	105	199
1994	13	304	308	98	210
1995	13	308	243	12	231
1996	9	243	301	64	237

Heterogeneous Lithofacies

b)		Vadose Zone		Root Zone	Deep Vadose Zone
		Beginning of Year	End of Year	End of Year	
Year	# of Irrigation	NM_0	NM_T	N_{RZ}	N_{DVZ}
1990	13	0	138	108	30
1991	10	138	240	105	136
1992	17	240	361	60	301
1993	16	361	359	106	253
1994	13	359	361	99	262
1995	13	361	284	12	273
1996	9	284	342	58	284

NM_o: NO_3-N mass in the vadose zone at the beginning of a simulation year [kg ha^{-1}]
NM_T: NO_3-N mass in the vadose zone at the end of a simulation year [kg ha^{-1}]
NM_{RZ}: NO_3-N mass in the root zone at the end of a simulation year [kg ha^{-1}]
NM_{DVZ}: NO_3-N mass in the deep vadose zone at the end of a simulation year [kg ha^{-1}]

Table 10 Annual root zone *NO_3-N* mass balance at the high subplot based on simulation results in the a) homogeneous and b) heterogeneous lithofacies models

High Subplot

Homogeneous Lithofacies

a)		Vadose Zone		Root Zone	Deep Vadose Zone
		Beginning of Year	End of Year	End of Year	
Year	# of Irrigation	NM_0	NM_T	N_{RZ}	N_{DVZ}
1990	13	0	312	107	205
1991	10	312	579	107	472
1992	17	579	801	67	734
1993	16	801	620	105	515
1994	13	620	678	98	580
1995	13	678	482	12	470
1996	9	482	466	64	401

Heterogeneous Lithofacies

b)		Vadose Zone		Root Zone	Deep Vadose Zone
		Beginning of Year	End of Year	End of Year	
Year	# of Irrigation	NM_0	NM_T	N_{RZ}	N_{DVZ}
1990	13	0	324	108	216
1991	10	324	613	108	505
1992	17	613	856	60	796
1993	16	856	756	106	650
1994	13	756	785	99	686
1995	13	785	566	12	554
1996	9	566	544	58	486

NM_o: NO_3-N mass in the vadose zone at the beginning of a simulation year [kg ha^{-1}]
NM_T: NO_3-N mass in the vadose zone at the end of a simulation year [kg ha^{-1}]

NM_{RZ}: NO_3-N mass in the root zone at the end of a simulation year [kg ha^{-1}]
NM_{DVZ}: NO_3-N mass in the deep vadose zone at the end of a simulation year [kg ha^{-1}]

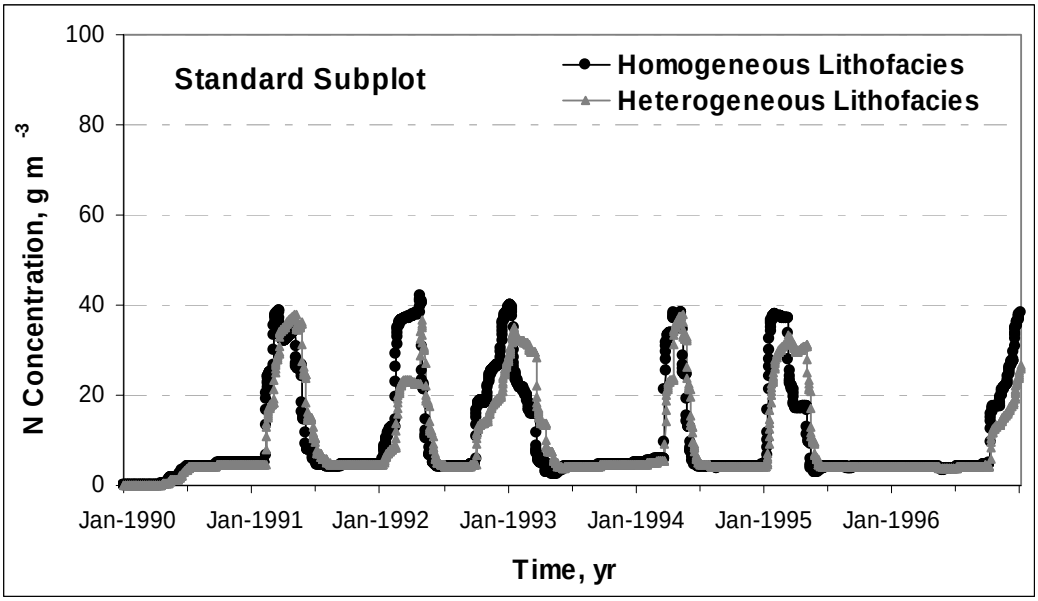

Figure 41 *NO_3-N* breakthrough curve simulated at the bottom of the root zone of the standard subplot (z = 1.8 m) during the period from 1990 to 1996 in the homogeneous and heterogeneous lithofacies models

5.16.1 Standard Subplot

At the standard subplot, the homogeneous lithofacies model produces a breakthrough curve with a consistent peak concentration of approximately 42 g m^{-3} in each year in response to N fertilizer application in the preceding year (Figure 41). Detectable nitrogen concentration (>0.04 g m^{-3}) is first observed at the root zone at DOS = 108 day from the homogeneous lithofacies model and at DOS = 109 day from the heterogeneous lithofacies model. The first detected N results from the earliest irrigation that is applied at DOS = 88 day. This points out that regardless of the model used, the travel time of N through the 1.8 m root zone following an irrigation event is about 20 days. This further suggests that an transfer rate is 9 cm d^{-1} (= 180 cm / 20 day). Nitrogen concentration that results from 1990 and 1993 fall applications, respectively, at the root zone rises instantly after the first spring irrigation in 1991 and 1994. A rapid increase in the concentration implies that average winter precipitation that occurs after the fall N fertilizations and before the irrigation seasons during these years is sufficient enough to carry a significant amount of N to near the bottom of the root zone. The peak concentration in 1991 is reached 87 days after the first irrigation while the arrival time of the peak concentration in 1994 is reduced by half compared to the year 1991 (50 days) due to the more frequent spring irrigation applications in 1994.

The time of first arrivals of N from 1991 and 1994 fall applications are noticeably shifted to the left, indicating earlier arrivals compared to 1990 and 1993 fall applications. This indicates that above average precipitation that occurred soon after the fall N application during 1991 and 1995 (37 and 41 cm yr^{-1}, respectively) causes N to reach the bottom of the root zone and furthermore to leave the root zone before the irrigation season starts. The impact of winter precipitation during 1995 (January through March) on N leaching is more pronounced than that during 1991, resulting in much earlier arrival of the peak at the root zone.

Temporal variations of N concentration at the bottom of the root zone after the 1992 fall application is significantly different from those discussed above. Onetime irrigation following the fertilizer application in 1992 accelerates N leaching, causing a substantial amount of N loss from the root zone. The time elapsed between fall N fertilizer application and the peak concentrations appearing at the root zone ranges from 206 days to 238 days when no irrigation follows N fall application (e.g., 1990, 1991, 1993, 1994). While the peak concentration in the late 1992 remains unaffected (~ 40 g m^{-3}), the peak arrival to the bottom of the root zone is highly accelerated, almost twice as much as those observed in other years (~ 100 days). A similar phenomenon is expected for 1996 due to a onetime irrigation after the fall N application. In the heterogeneous lithofacies model, the arrival time of peak concentrations is shifted to the right and the peak concentrations are somewhat lower.

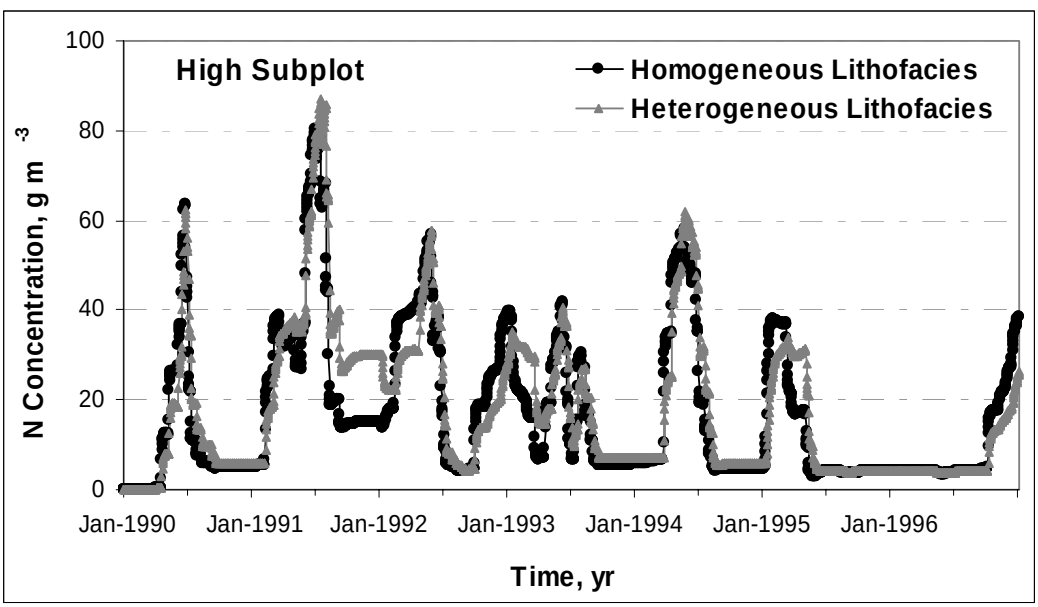

Figure 42 NO_3-N breakthrough curve simulated at the root zone of the high subplot (z = 1.8 m) during the period from 1990 to 1996 in the homogeneous and heterogeneous lithofacies models

5.16.2 High Subplot

At the high subplot, using the heterogeneous model over the homogeneous model does not change the shape of the N breakthrough curve at the root zone notably (Figures 41 vs. 42).

Peak concentrations are slightly higher and delayed in the heterogeneous model than in the homogeenous lithofacies model.

The first appearance of detectable N concentration at the root zone of the high subplot coincides with that of the standard subplot, which is expected since N results from the first irrigation that is applied at both the subplots at the same way. More similarities between the N concentration curves at the high and standard subplots are observed during 1995 and 1996 because both receive the same rate of water and N fluxes during these two years. Much earlier arrival of the first peak in 1990 at the high subplot compared to the standard subplot is a direct contribution of the spring fertilizer applications (three times at the rate of 85 kg ha^{-1}). Consistent with the previous findings, the highest peak concentration of 80 g m^{-3} and 87 g m^{-3}, in the homogeneous and heterogeneous lithofacies models, respectively, occurs in 1991. Even though the total N applied at the high subplot is more than twice the amount of one fall application, the maximum concentration is only increased by half when compared with that observed at the standard subplot (40 g m^{-3}). In 1992 and 1994 where the time of fertilizer applications coincide with the time of irrigations, the peak concentrations are reduced to two third the peak in 1991 (60 g m^{-3}). If spring fertilizer applications are a month apart, such as in 1991, 1992 and 1994, fall and spring applications have a combined effect at the root zone, resulting in one peak concentration and uninterrupted mass of N leaching to the deep vadose zone. The changes in N concentration at the root zone throughout 1993 are notably different from those observed in other years possibly due to the combined effect of two mechanisms: 1) above average precipitation that occurs after N fertilization in 1992 creates the first peak which is similar to that observed at the standard subplot and 2) spring N applications in 1993, which are separated by a period that is longer than a month, appear to form two peaks at the rate of about 40 g m^{-3}, instead of one at the rate of 60 g m^{-3} when the effect of fall and spring applications is combined (e.g., 1992 and 1994). The results for 1993, in particular, illustrate the counteracting effect of irrigation on the availability of N in the root zone. During 1993, higher N uptake before fall application (Table 7) and smaller irrigation efficiency (Table 5) support the possibility that irrigation promotes transpirative fluxes and N uptake, thus increases N use efficiency while simultaneously enhancing deep percolation which increases N loss from the root zone.

5.17 Temporal Variations of Nitrogen in the Deep Vadose Zone

In this section, temporal variations of N in the deep vadose zone are compared between the two fertilizer applications and between the two numerical models. Simulated N data analyzed here include average N concentration and N mass storage in the deep vadose zone.

5.17.1 Average Nitrogen Concentration

Figure 43 compares temporal variations of average N concentration (defined in g m^{-3} in aqueous in the deep vadose zone of the standard and high subplots between the homogeneous and heterogeneous lithofacies models. From 1990 to 1993 during which N concentration continues to increase, resulting a net accumulation of N, the heterogeneous lithofacies model produces lower N concentration in the deep vadose zone at both subplots than the homogeneous lithofacies model. During this period, higher differences between the two models are seen at the high subplot than the standard subplot.

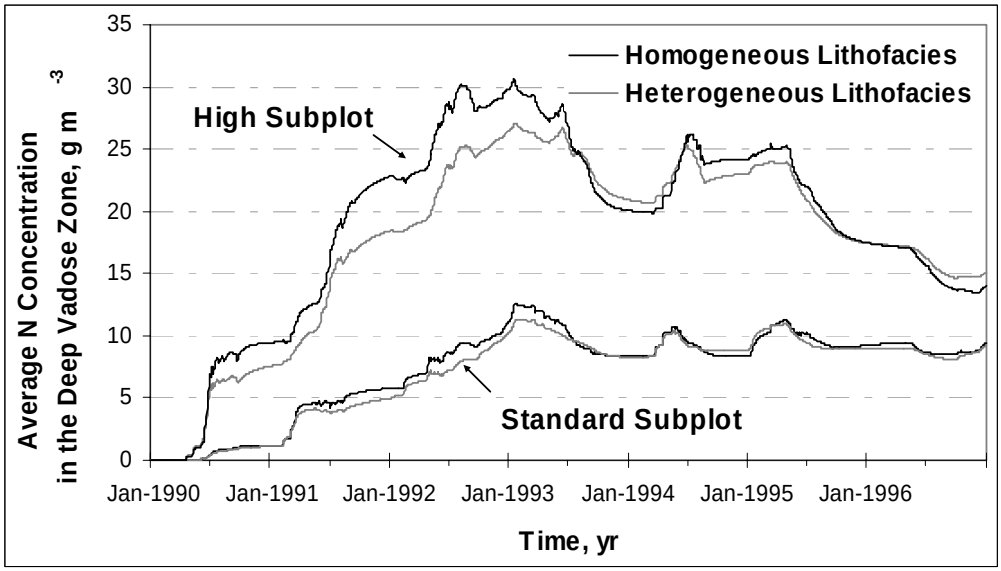

Figure 43 Average *NO_3-N* concentration simulated in the deep vadose zone of the standard and high subplots during the period from 1990 to 1996 in the homogeneous and heterogeneous lithofacies models

At the standard subplot, the peak average concentration of approximately 12 g m^{-3} is observed in 1993. In 1993 and afterwards, both models yield an average N concentration that remains steady with seasonal fluctuations between 8 g m^{-3} and 11 g m^{-3}. The absence of fertilizer application in 1995 does not cause a significant N depletion in the deep vadose zone. While the average peak concentrations vary from year to year at the standard subplot, annual trends in the data from 1993 to 1995 appear to be similar and can be qualitatively divided into two stages. During the first stage, average concentration continues to increase and reaches a maximum value during spring of each year due to N leaving the root zone by winter precipitation followed by spring irrigations. The second stage is a sharp decrease in the concentration possibly caused by two mechanisms acting simultaneously: increasing root N uptake in the root zone, thus diminishing N leaching below the root zone, and increasing drainage and in turn N loading at the water table due to successive irrigation events. Average N concentration continues to drop rapidly if onetime irrigation occurs after fall N application (e.g., 1992 and 1996). During the second half of 1994, the situation is slightly reversed, shown by an increase in the average concentration rather than a decrease. This is attributed to a stronger impact of 1994 winter precipitation (41 cm yr^{-1}) that is above the average on the magnitude of N loss from the root zone. With respect to the maximum contamination level (MCL) for drinking water (10 g m^{-3}), the standard subplot (receiving 100 kg ha^{-1} yr^{-1}) represents a moderate risk for groundwater pollution with average N concentration in the deep vadose zone occasionally exceeding the MCL during irrigation seasons.

Similar to the standard subplot, average N concentration under the high subplot increases continuously during the first 3 years of the simulation from 1990 to 1992. The average peak concentration of 30 g m^{-3} that is simulated during spring 1992 is about three times higher than the value simulated at the standard subplot for the corresponding year (12 g m^{-3}). No fertilizer application in 1995 has a stronger effect on the high subplot, causing N to deplete rapidly until N from fall 1996 application is carried to the deep vadose zone by irrigation water. Under the high

subplot that received 365 kg N ha^{-1} yr^{-1}, average N concentration never goes below the MCL, posing a potentially high risk of groundwater pollution.

5.17.2 Total Nitrogen Mass

The overall appearance of the N mass curve in the deep vadose zone, shown in Figure 44, is like that of average N concentration (Figure 43). A net accumulation of N below the root zone occurs until spring 1992 where N storage starts to decrease rapidly. Tables 9 and 10 summarize annual deep vadose zone N storage at the end of each simulation year under the standard and high subplots, respectively. Smaller values obtained for the first year reflect the influence of the initial condition of zero concentration. When the results between the two models are compared at each subplot, trends seen for the average N concentration are reversed: the heterogeneous model produces higher total N mass than the homogeneous lithofacies model both at the standard and high subplots and variations between the models are higher between 1993 and 1996 than the previous years.

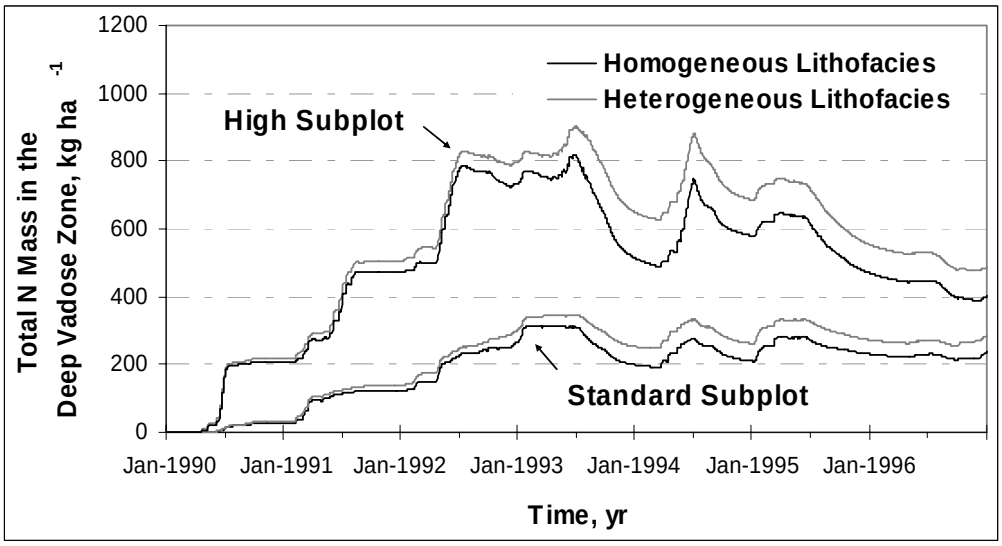

Figure 44 Total NO_3-N mass simulated in the deep vadose zone of the standard and high subplots during the period from 1990 to 1996 in the homogeneous and heterogeneous lithofacies models

5.17.3 Annual Deep Vadose Zone Nitrogen Budget

Based on the simulated results of the homogeneous and heterogeneous lithofacies models, annual deep vadose zone N budget at the standard and high subplots is analyzed (Tables 9 and 10). Contrary to what is observed in the root zone N mass budget, the deep vadose zone N mass is affected largely by the fertilizer applications and to a lesser extend by the type of model used. The high subplot, when compared to the standard subplot, has 12% to 59% more N mass in the homogenous lithofacies model and 14% to 58% in the heterogeneous lithofacies subplot. The heterogeneous lithofacies model, when compared to the homogeneous lithofacies model, produces 11% to 21% more N mass in the deep vadose zone of the standard subplot and from 5% to 21% in the deep vadose zone of the high subplot. In all cases, the deep vadose zone N mass increases as the root zone N mass decreases (r^2 = -0.57 for the standard subplot (same for each model) and r2 = -0.19 and -0.23 at the high subplot in the heterogeneous and homogeneous lithofacies model, respectively). Depending on the transience behavior of water fluxes between

1991 and 1994, the deep vadose zone N storage at the standard subplot estimated by the models varies from 122 to 262 kg ha^{-1} (~ 1.1 to 2.4 times the application rate). During this period, the deep vadose zone N at the high subplot from both models varies widely from 472 to 686 kg ha^{-1} (~1.3 to 1.9 times the application rate). The deep vadose zone at the end of the simulation reflects the effect of no fertilizer application in 1995 and a standard application in 1996. The heterogeneous model yields 284 kg ha^{-1} under the standard subplot and 486 kg ha^{-1} under the high subplot. These are approximately 17% higher than those values estimated by the homogeneous lithofacies model (Tables 9b and 10b).

5.18 Two-Dimensional Spatial Distribution of Nitrogen in the Vadose Zone

In this section, two dimensional contour maps of N concentrations simulated in the homogeneous and heterogeneous lithofacies models are shown at selected times to analyze the movement and spreading of N in the vadose zone over the 7 year simulation.

5.18.1 Homogeneous Lithofacies Model

Figure 45 demonstrates contour maps of N concentrations simulated in the homogeneous lithofacies model at the standard subplot. Twelve contour maps are presented between the first N fertilizer application in 1990 (DOS = 261) and the final day of the simulation in 1996 (DOS = 2557). For each year, two contour maps are prepared, showing the distribution of N concentrations on the day of the fall N application and at the end of the simulation year. Simulated data for 1995 during which no N fertilizer is applied are skipped.

One common observation in all contour maps is that N plumes are smooth and spatially connected both in the vertical and horizontal directions. This is expected on the basis of uniform surface application of N, homogeneous soil hydraulic properties within layers. N plumes are not subject to any vertical spreading as they move through the SL1 and Var1 as a result of the horizontal boundary between the SL1 and Var1. As time progresses and N passes through the interface between the Var1 and HP1, it begins spreading in the longitudinal direction. Spreading along the side boundaries is greater than along the center of the domain. The enhanced N spreading along the sides, the flow appears to be essentially gravity dominated, which in the vicinity of the vertical sides of the domain. As N moves downward below the HP1, the shape of N plumes follows the shape of the interface between the Var1 and HP1 layers. The downward movement and spreading of N is subject to significant changes as N moves across the inclined interface between the coarse-textured layer Var1 to the fine-textured layer HP1. Since the shape of N plumes below the HP1 does not change significantly, interfaces between other layers below the HP1 does not seem to play a big role in N movements and spreading.

Comparison of the two N contour maps given for each year demonstrates the downward movement of N after the fall N application and before the following year. Since this period is outside of the growing season, the applied N mass is not consumed by trees. Note that the fall applied N during 1992 and 1996 travels beyond the root zone by the end of the simulation year 1992 and 1996 (DOS = 1096 and 2557, respectively), mainly due to the one-time fall irrigation applied after the N fertilizer application during these years. The fall applied N in other simulation years travels only within the SL1 mainly in response to winter rainfall (e.g., DOS = 365, 731, 1461, and 1826.

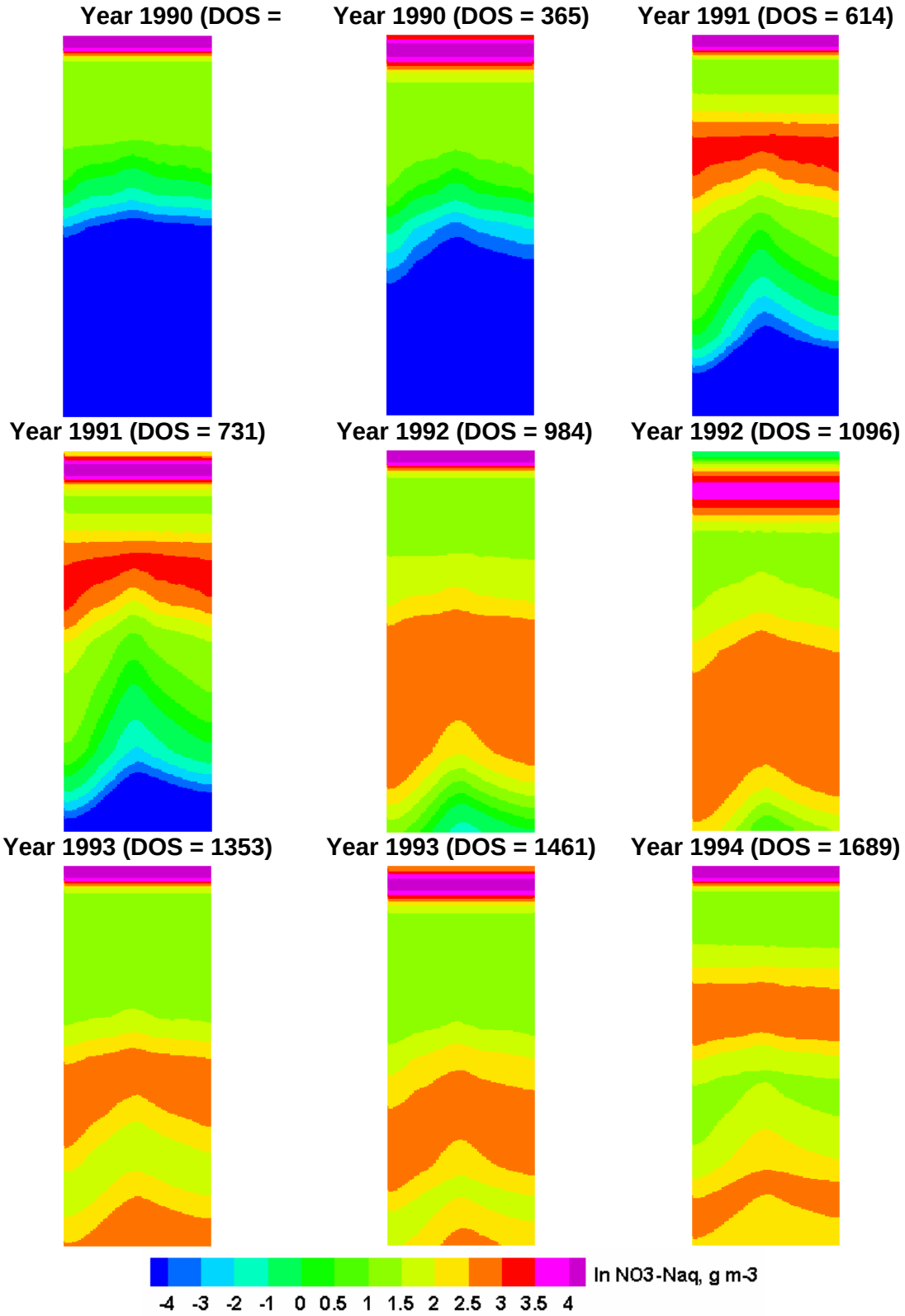

Figure 45 Contour maps of NO_3-N concentrations in the homogeneous model at the standard subplot during the simulation period (1990 – 1996)

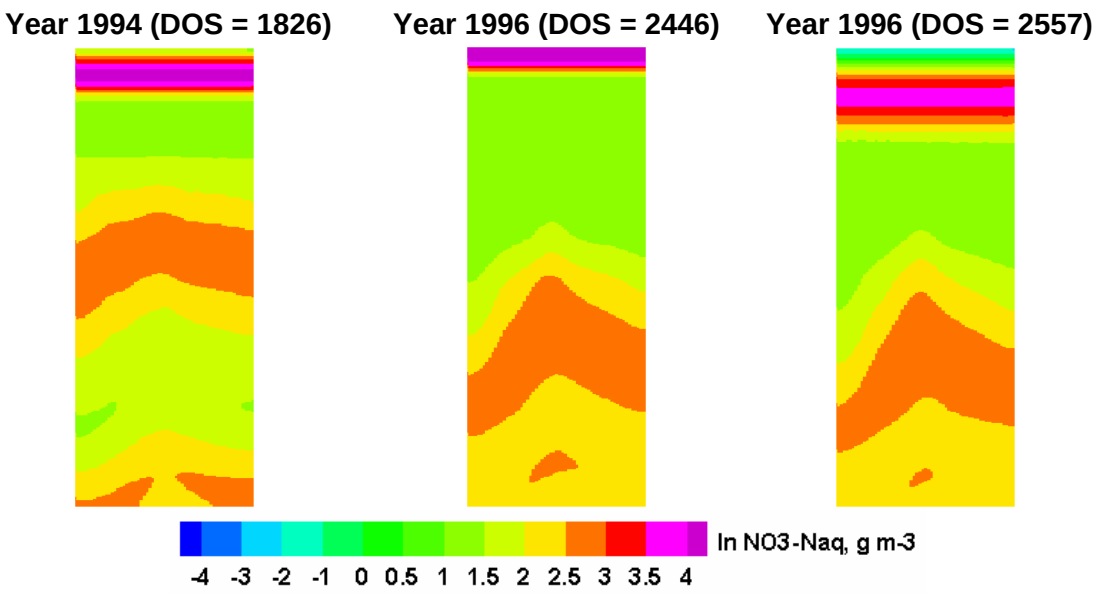

Figure 45 cont. Contour maps of NO_3-N concentrations in the homogeneous model at the standard subplot during the simulation period (1990 – 1996)

The first arrival of N plume at the water table during 1992 corresponds to N from irrigation applied during the growing season in 1990, implying that average travel time to groundwater table is less than 3 years. At the end of the simulation (DOS = 2557), the water table receives two large N plumes associated with the 1990 and 1991 fall applications. In the vadose zone, N plume associated with the 1992 application travels approximately two third of the vertical domain. Another large N plume is located near the bottom of the root zone.

Simulation results of the homogeneous lithofacies model for N concentrations at the high subplot are shown in Figure 46. Contour maps are prepared using daily outputs of the N concentrations on selected days between DOS = 88 (the day of the first N fertilizer application) and DOS = 2557. From 1990 to 1994, five maps for each year are shown: four maps, each showing N distribution on the day of fertilizer applications (three maps during spring and one during fall N applications) and one map at the end of the simulation year. Since no N is applied in 1995, simulated data for this year are skipped. For 1996, two contour maps of N distribution are shown, one on the day of the fall application and the other at the end of the year.

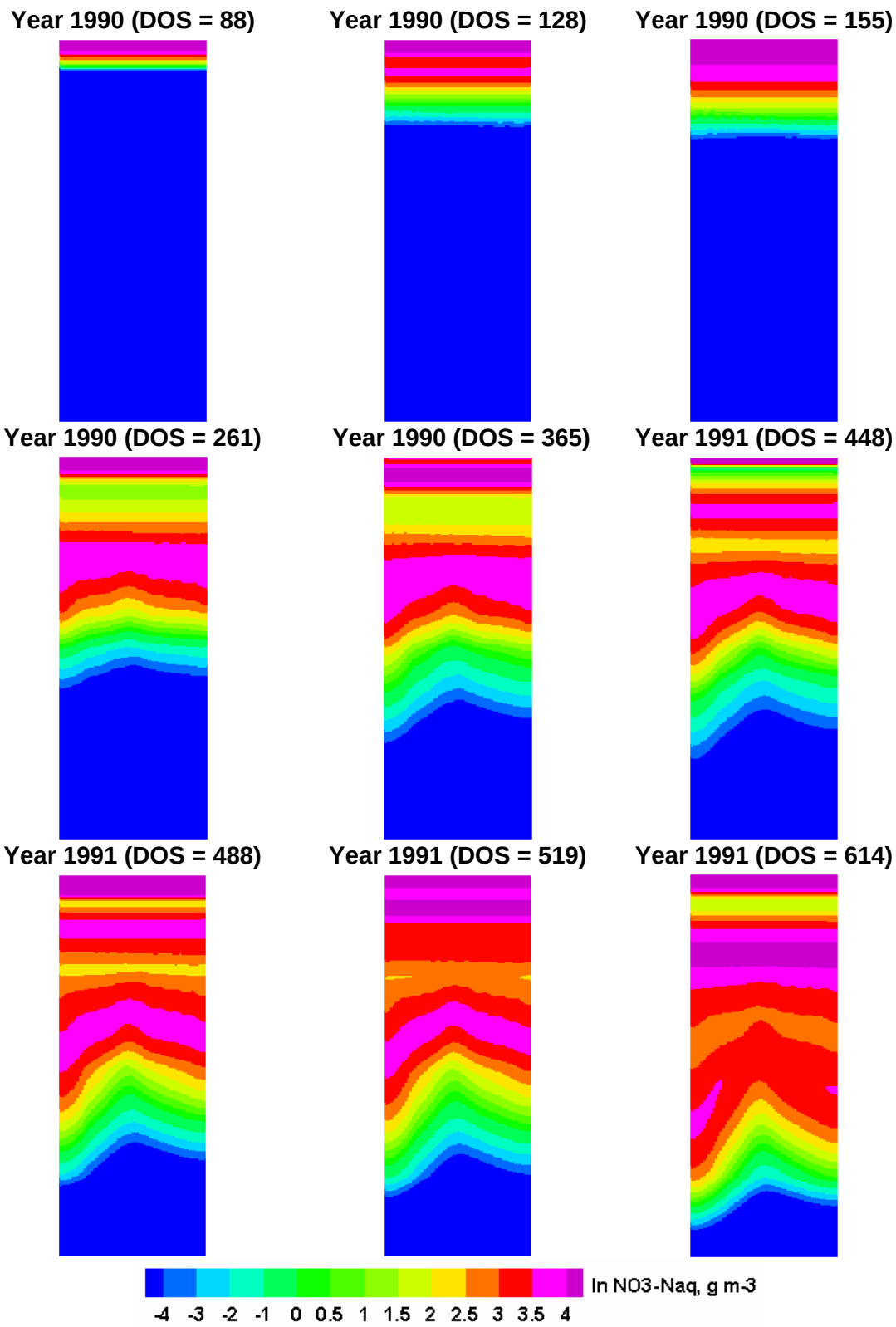

Figure 46 Contour maps of NO_3-N concentrations in the homogeneous model at the standard subplot during the simulation period (1990 – 1996)

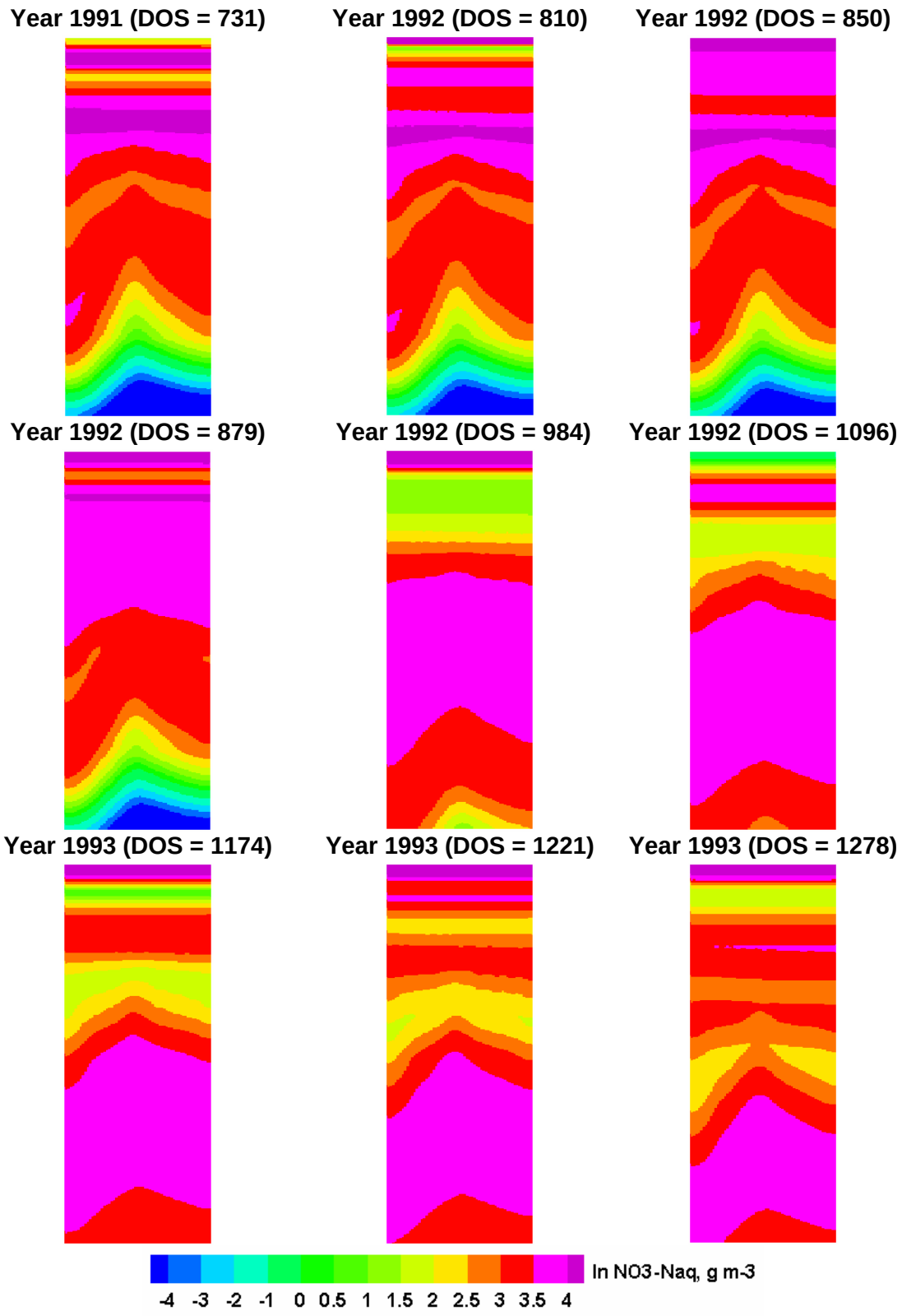

Figure 46 cont. Contour maps of NO_3-N concentrations in the homogeneous model at the high subplot during the simulation period (1990 – 1996)

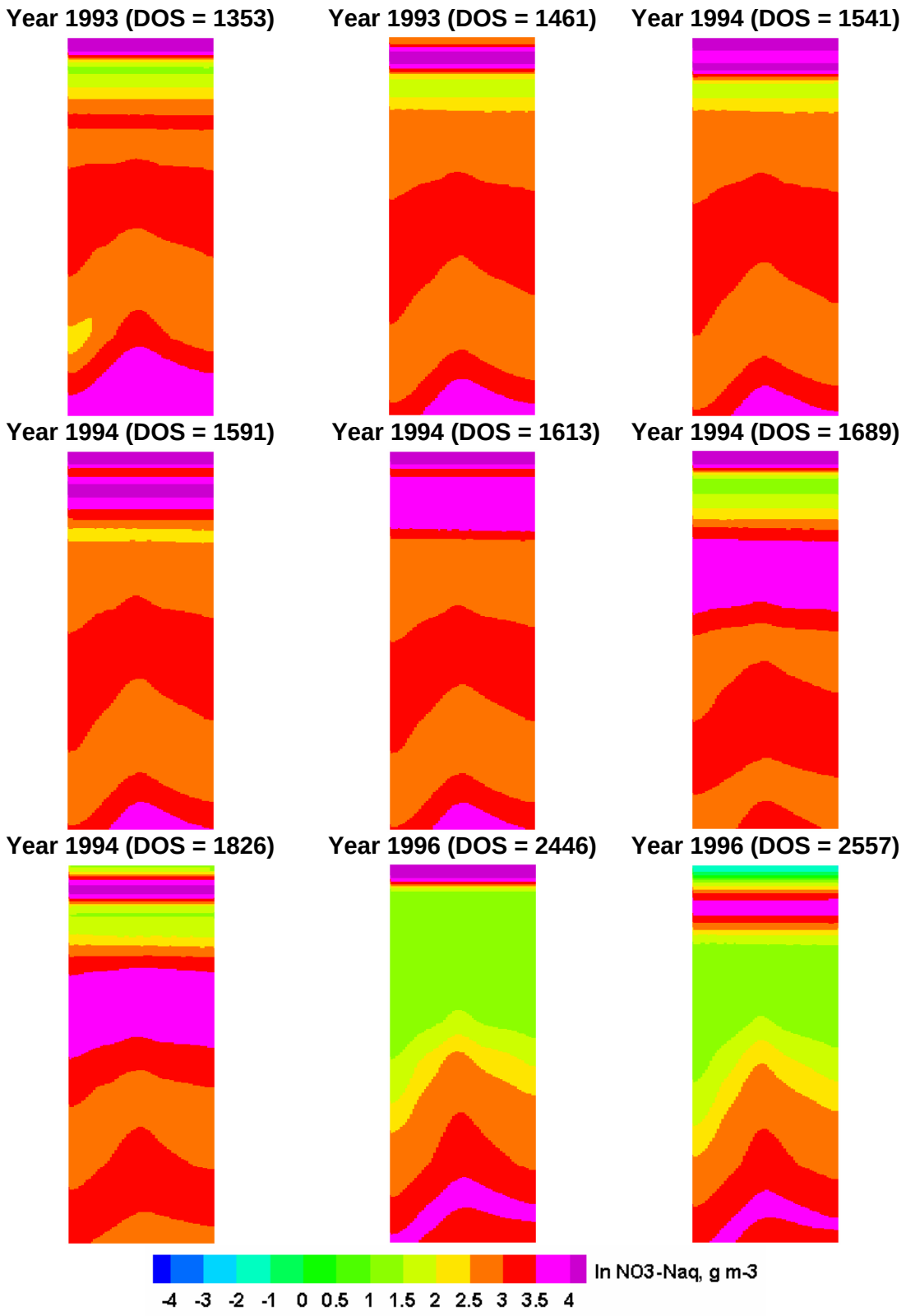

Figure 46 cont. Contour maps of NO_3-N concentrations in the homogeneous model at the high subplot during the simulation period (1990 – 1996)

In general, as a result of higher N application rates, the vadose zone under the high subplot contains larger size of N plumes and the water table receives higher N concentrations more frequently than the standard subplot.

Overall, the simulation results at the high subplot show that N leaching to the water table is driven primarily by irrigation events and to a lesser degree by winter precipitation. Similar to the standard subplot, N plumes are smooth and spatially connected both horizontally and vertically. Below the HP1, more longitudinal spreading occurs along the sides of the domain than the center. In general, N plumes resulted from the spring applications move separately at early times during the irrigation season (e.g., DOS = 128 and 155). Towards the end of the season, plumes are united as a result of frequent irrigation applications and move downward as one large plume (e.g., DOS = 261 and 365). Similarly, N plumes from fall applications tend to merge with N plumes from spring applications that are applied previously during the growing season. Examples of such behavior are seen in 1992 (DOS = 519) and in 1992 (DOS = 850). The large plume that extends vertically over the half the domain at the end of 1992 is in fact a combination of all prior spring and fall N applications. Comparison of contour maps at the end of year 1994 (DOS = 1826) and on the day of the fall N application in 1996 (DOS = 2446) suggest that the majority of the N applied during 1994 travels throughout the profile in less than two years. This further suggests that the travel time of N to the water table varies significantly as a function of surface fluxes.

5.18.2 Heterogeneous Lithofacies Model

Figures 47 and 48 demonstrate examples of contour maps of N concentrations in the heterogeneous lithofacies model at the standard and high subplots, respectively. Contour maps are prepared between the first N fertilizer application in 1990 (DOS = 88 for the standard subplot and DOS = 261 for the high subplot) and the final day of the simulation in 1996 (DOS = 2557) at the same days as the homogeneous lithofacies model discussed above.

Local scale heterogeneity of scaling factors seems to produce considerable variability and vertical spreading in N concentrations. The local scale dispersivity incorporated into both the homogeneous and heterogeneous lithofacies models is expected to create smooth N distributions (Russo, 1991; Hills et al., 1994). However, in the case of the heterogeneous lithofacies model, the local variability of soil hydraulic properties seems to suppress the smoothing effect of the local dispersivity, creating finger-like patterns. Similar to the homogenous lithofacies model results, N plumes at shallow depths are initially nearly flat with a limited longitudinal spreading both at the standard and high sybplots (Figures 47 and 48). As time progresses, N concentrations exhibit more longitudinal spreading and the leading edge of N plumes is less smooth compared to the results from the homogeneous lithofacies model. Also note that N plumes tend to be spatially more continuous in the vertical direction than in the horizontal direction. Contrary to the homogeneous lithofacies model results, longitudinal spreading is more enhanced along the horizontal center of the domain.

At the high subplot, similar to the homogeneous lithofacies model, N plumes from spring applications merge with N plume resulting from fall applications (Figure 48). However, they become progressively more irregular over time compared to the heterogeneous model results at the standard subplot and the homogeneous model results both at the standard and high subplots. The heterogeneous lithofacies model leads to N plumes that split into several paths, something that would be expected under highly heterogeneous field soil. Finger-like patterns seem to cease away with depth below the C-Si-L layer. It is likely that the layering effect may smooth out the leading edge.

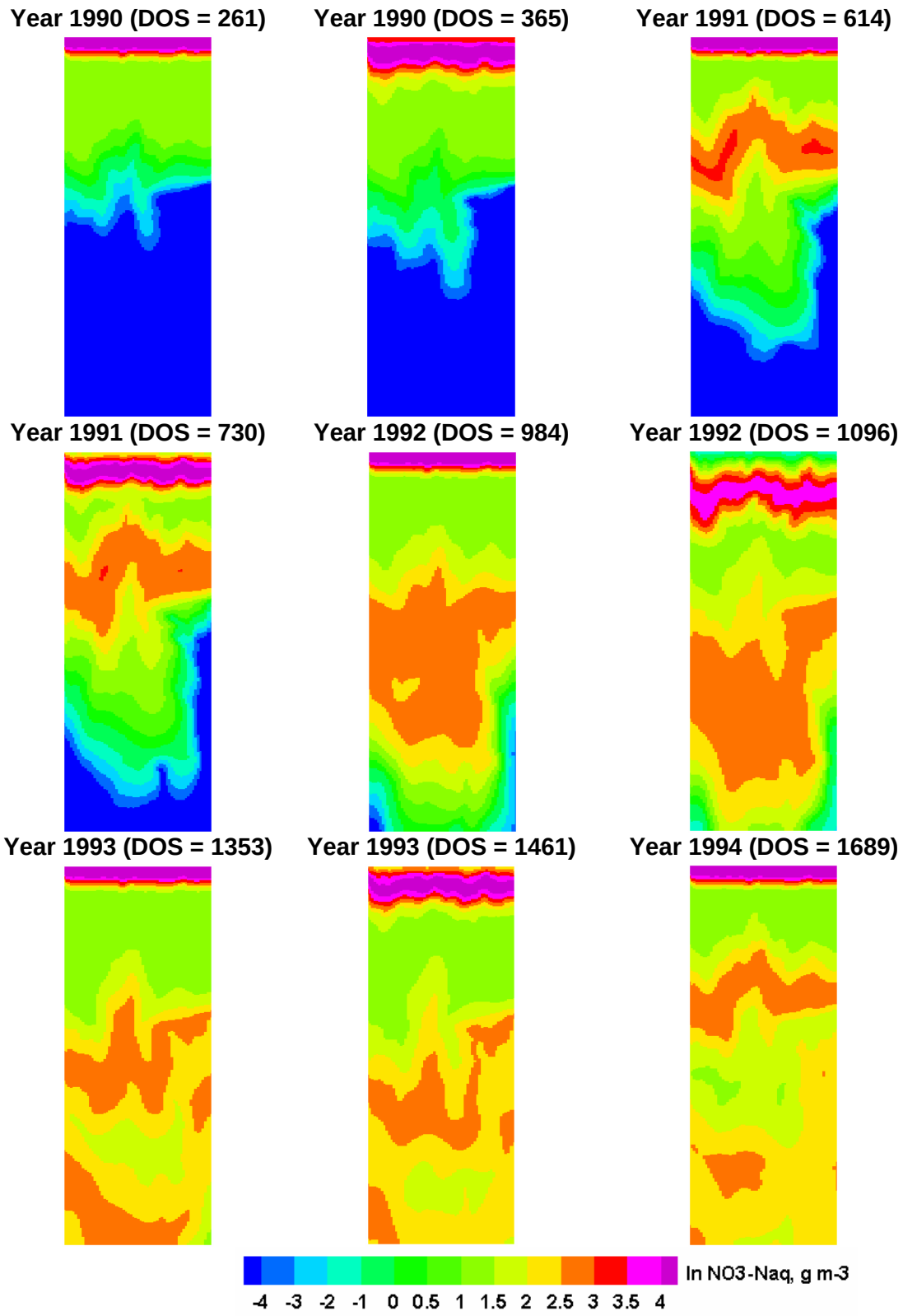

Figure 47 Contour maps of NO_3-N concentrations in the heterogeneous model at the standard subplot during the simulation period (1990 – 1996)

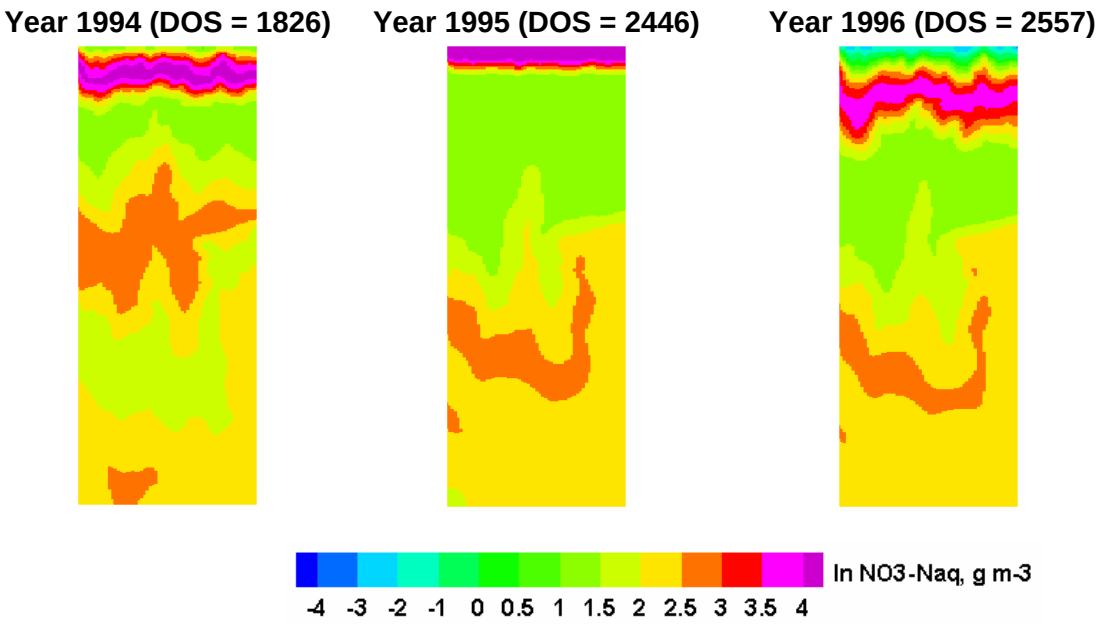

Figure 47 cont. Contour maps of NO_3-N concentrations in the heterogeneous model at the standard subplot during the simulation period (1990 – 1996)

Simulated distributions of N concentration in the heterogeneous lithofacies models are similar to the distributions of solute concentration observed from field experiments under unstable preferential flow conditions (Rudolph et al., 1996; Wang et al., 2003a) and numerical studies applied through a heterogeneous soil using field observations for the hydraulic parameters (Hills et al., 1994). Similarities also exist between our results and those of Khaleel et al. (2002) who applied a single realization of hypothetical heterogeneous unsaturated media to study flow and tracer transport perpendicular to a perfectly stratified system. Their study has shown that bedding perpendicular to flow direction, similar to our case, enhances lateral mixing and prevents rapid growth of preferential flow paths under unsaturated flow conditions.

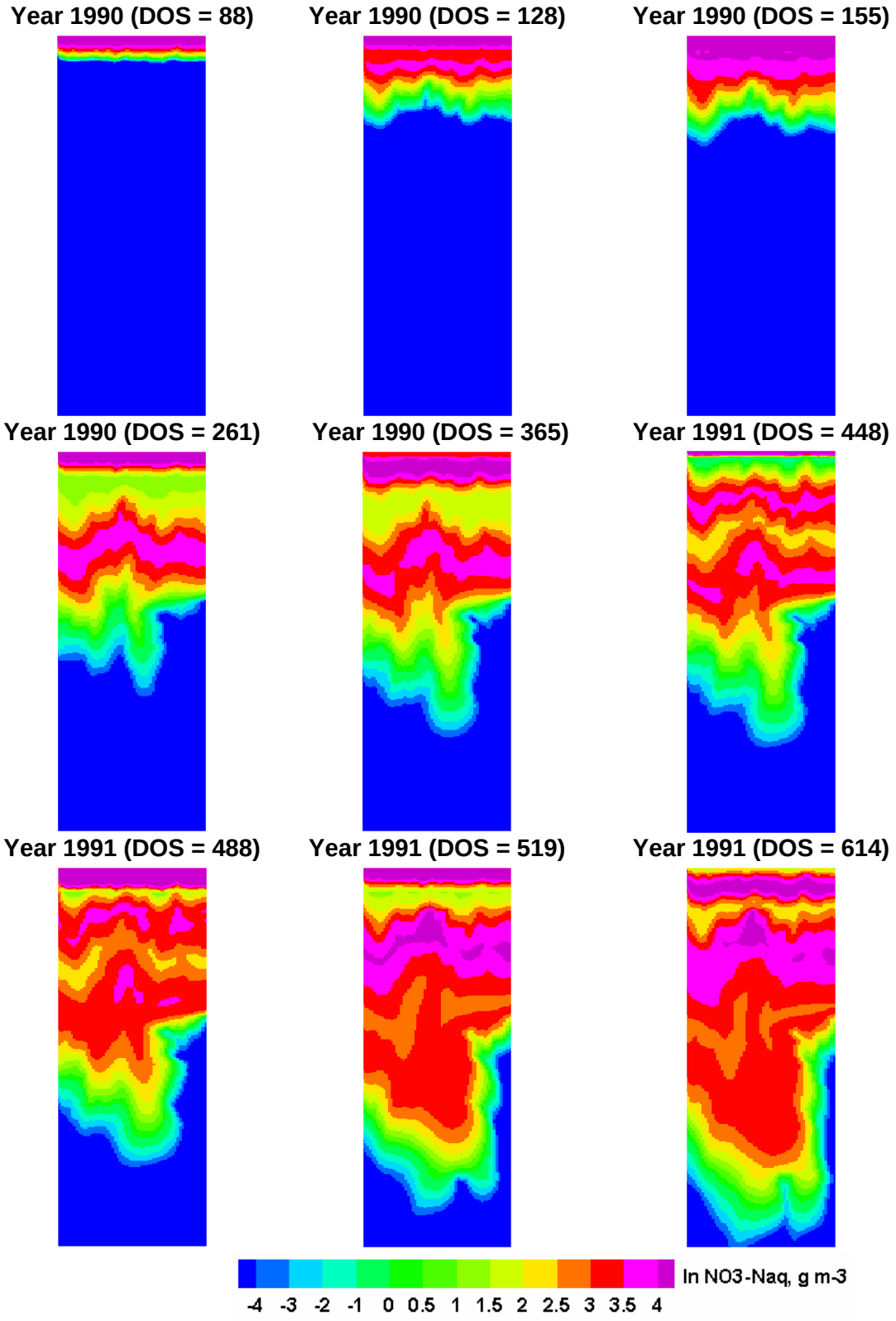

Figure 48 Contour maps of NO_3-N concentrations in the heterogeneous model at the high subplot during the simulation period (1990 – 1996)

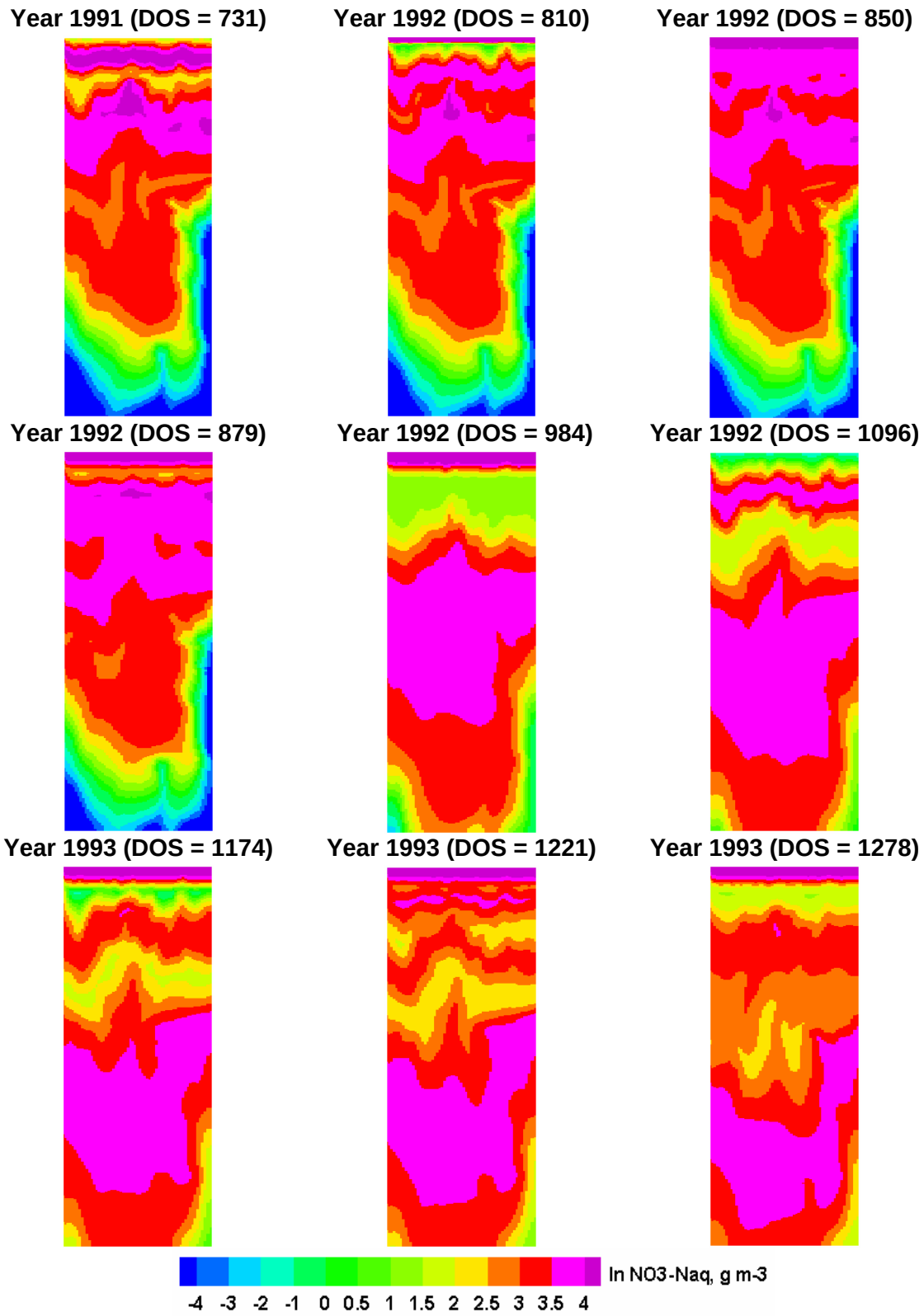

Figure 48 cont. Contour maps of NO_3-N concentrations in the heterogeneous model at the high subplot during the simulation period (1990 – 1996)

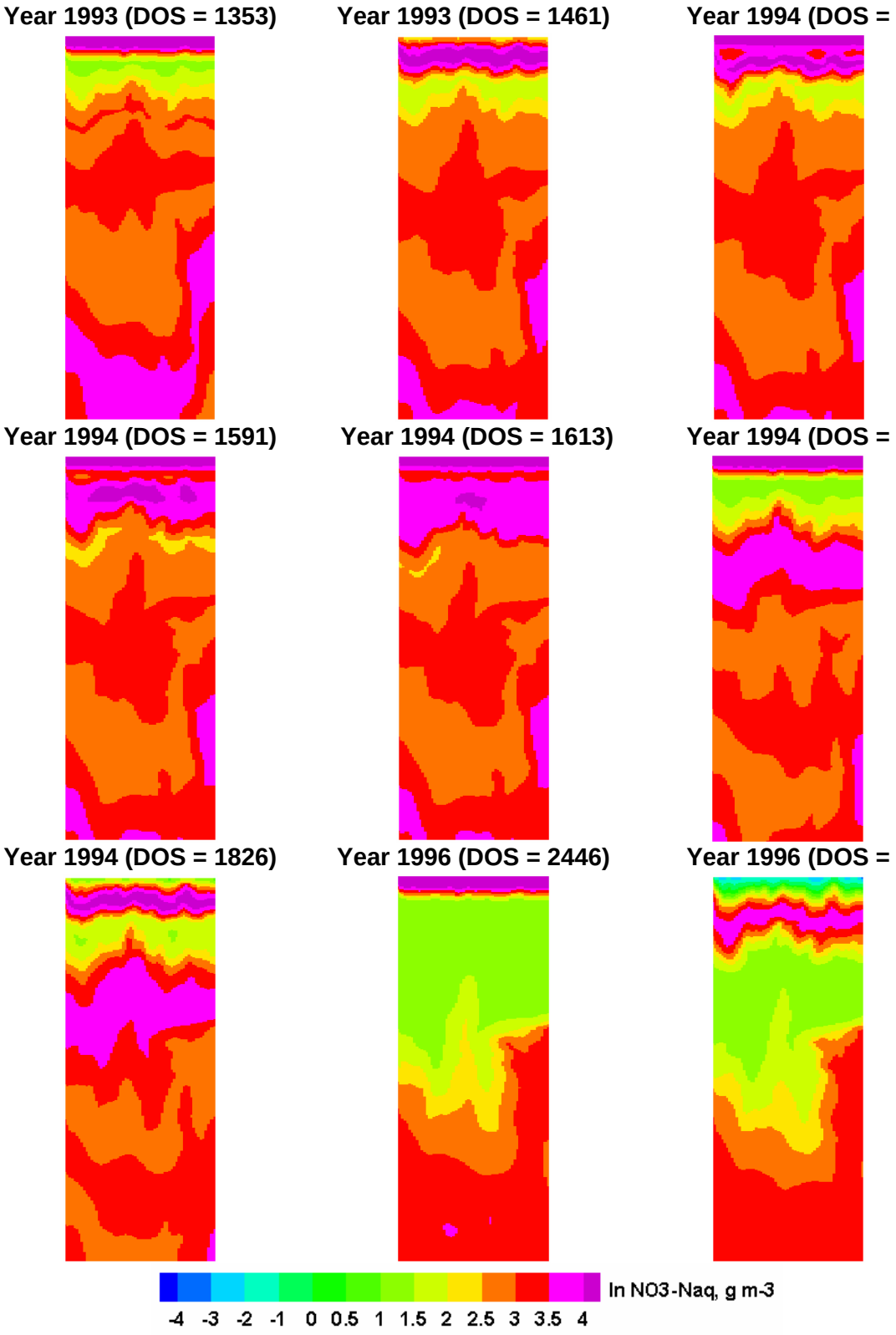

Figure 48 cont. Contour maps of NO_3-N concentrations in the heterogeneous model at the high subplot during the simulation period (1990 – 1996)

From their experimental study, Steenhuis et al. (1998) assessed the movement of nitrate in a sandy layered system and found a clear evidence of preferential flow in layered system where a coarse sand layer located between two fine sand layers. The study found that plumes become increasingly irregular with time and both water and nitrate are funneled into fingers by passing most of the soil matrix, and recharging groundwater much faster than if solute moved evenly through the vadose zone.

5.19 Nitrogen Concentration and Travel Time in the Lithofacies

Breakthrough curves of N concentration monitored at the seven observations points corresponding to the bottom of each lithofacies (except the HP1) are shown in Figure 49 for the standard subplot and in Figure 50 for the high subplot. At each observation point, the breakthrough curves estimated by the homogeneous and heterogeneous lithofacies models are compared.

Both the standard and high subplots, only minor differences are seen between the breakthrough curves of N from the two models. At both subplots, as N moves from one layer to another, peak concentrations and first time N arrivals at the top of each layer shifts to right. Breakthrough curves become smoother and the peak concentrations lessen with travel distance. The first arrival time of detectable N concentration at each layer varies as a function of both the thickness and soil hydraulic properties of the lithofacies. Nitrogen arrives at the bottom of the Var1 shortly after reaching the bottom of the SL1. Similarly, N is first detected at the bottom of the Var1 soon after it is observed at the bottom of the Var2. In both the models, coarser textured deposits and associated higher water flux rates of the Var1 and S layers expedite N travel and cause greater risk of N leaching to groundwater. On the contrary, late arrival of N from the bottom of the S to the bottom of the SL2 clearly reflects the role of heavier-textured soils of the C-Si-L and SL2 in slowing down the rate of N flux to water table.

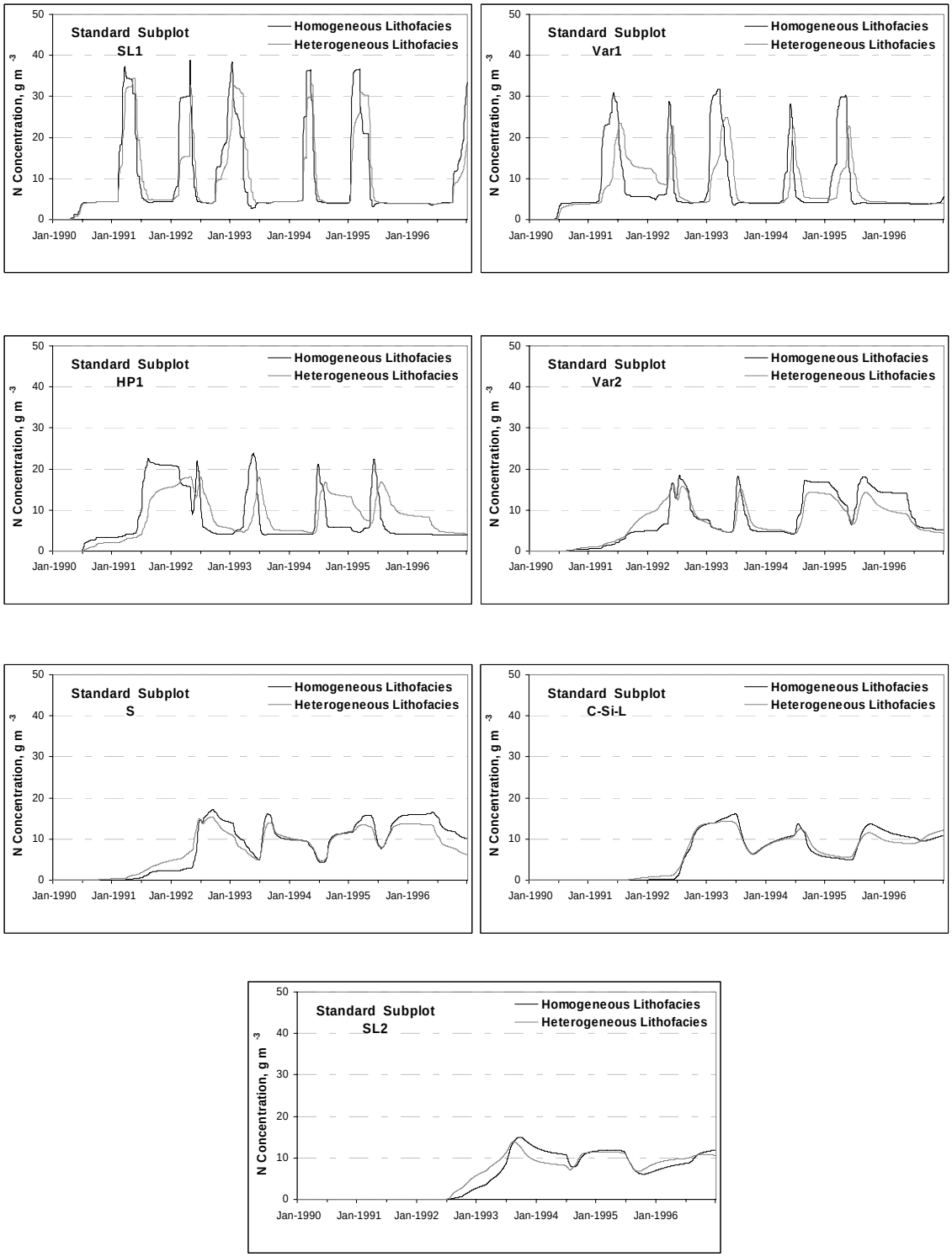

Figure 49 Breakthrough curves of NO_3-N concentration at seven observation points located at various depths of the standard subplot in the homogeneous and heterogeneous lithofacies models. SL1 at z = 2; Var1 at z = 3.05 m; HP1 at z = 4.3 m; S at z = 6.75 m; Var2 at 7.9 m; C-Si-L at z = 12.65 m; and SL2 at z = 15.2 m. All points are located at the same horizontal distance of x = 3.1 m.

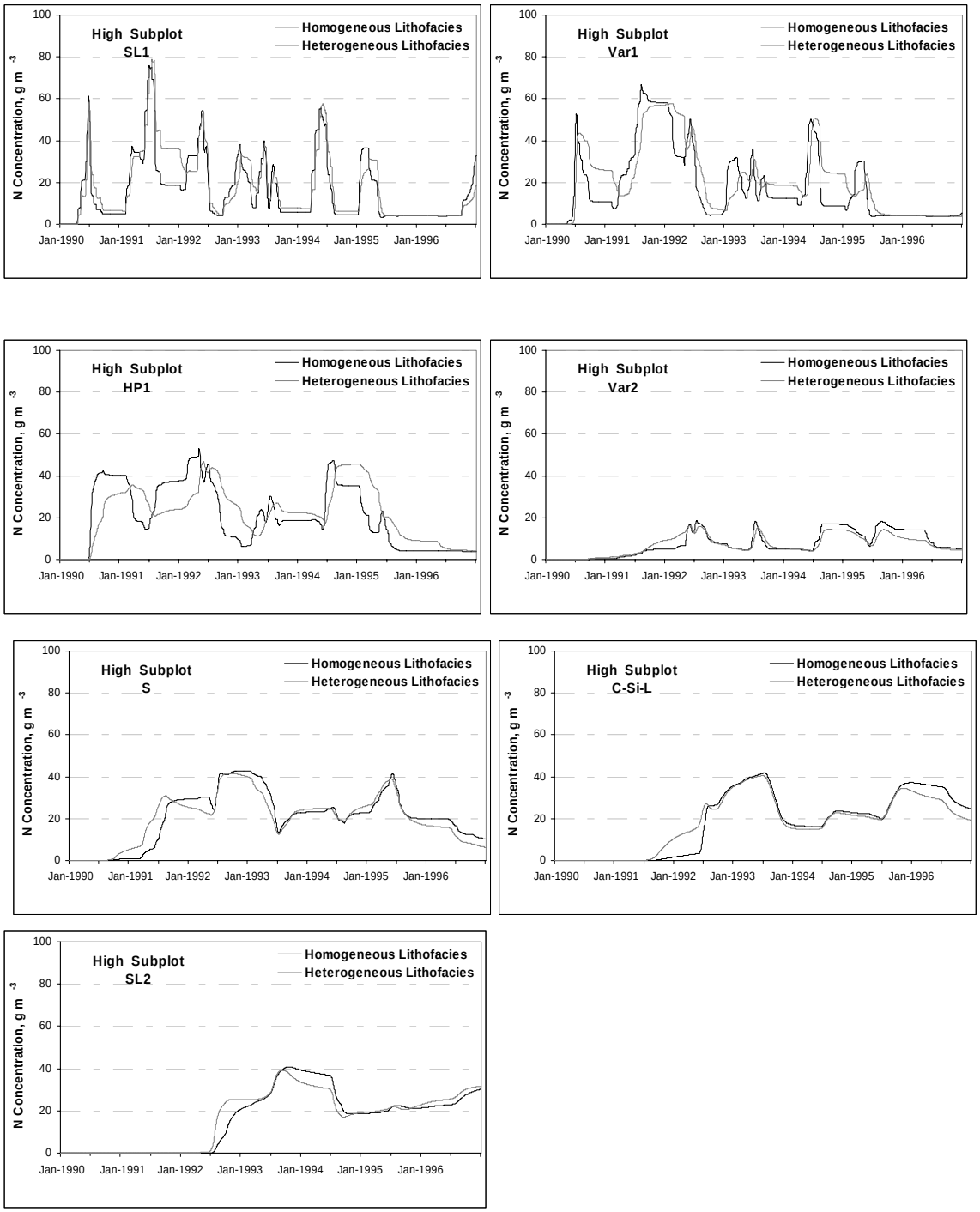

Figure 50 Breakthrough curves of NO_3-N concentration at seven observation points located at various depths of the high subplot in the homogeneous and heterogeneous lithofacies models. SL1 at z = 2; Var1 at z = 3.05 m; HP1 at z = 4.3 m; S at z = 6.75 m; Var2 at 7.9 m; C-Si-L at z = 12.65 m; and SL2 at z = 15.2 m. All points are located at the same horizontal distance of x = 3.1 m.

5.20 Average Nitrogen Concentration at Water Table

Figure 51 shows variations of nitrogen concentrations in the leachate at the water table as simulated by the homogeneous and heterogeneous lithofacies models under the standard and high fertilizer applications. Average N concentration, which is obtained by averaging the N concentration across the bottom of the domain, increases as the fertilizer application rate increases. Comparison of the model results at each subplot suggests that during 1992 and 1993, the homogeneous lithofacies model produces higher N concentrations at the water table than the heterogeneous lithofacies model. Thereafter, only small differences between the two model results are observed.

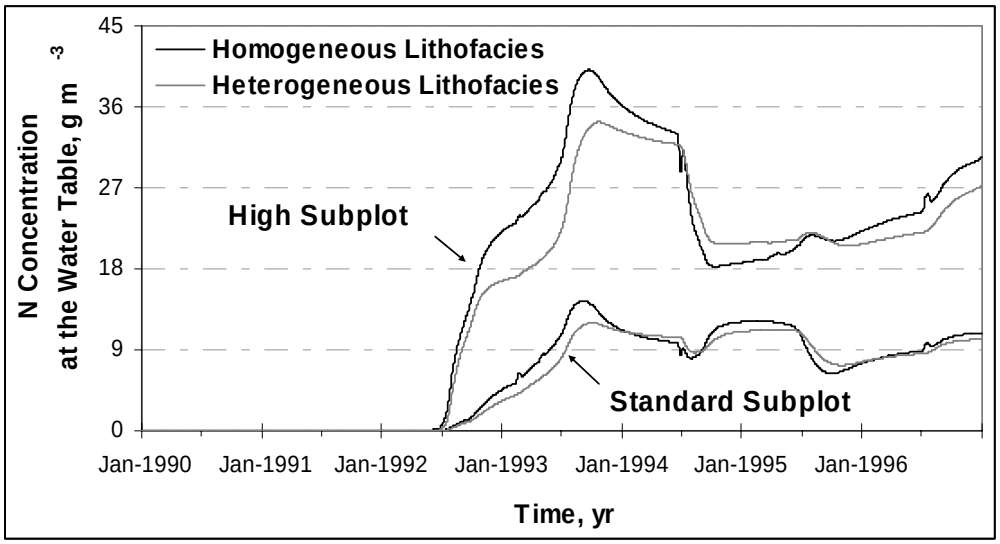

Figure 51 Average NO_3-N concentration at the water table of the standard and high subplots during the simulation period (1990 – 1996) in the homogeneous and heterogeneous lithofacies models

Nitrogen concentration under the high subplot is approximately three times larger than that under the standard subplot. For instance, the average peak concentration that occurs in 1993 both under the standard and high subplots varies from 34 to 40 g m^{-3} at the high subplot and from 12 to 14 g m^{-3} at the standard subplot, depending on the model used. Starting mid-1994, N concentration at the water table under the high subplot tends to remain between 18 g m^{-3} to 30 g m^{-3}, highly exceeding the MCL drinking standard for nitrate (10 g m^{-3}). For the most part of the simulation, the corresponding N concentration at the standard subplot is either slightly below or exceeding the MCL.

5.21 Nitrogen Travel Time to Groundwater

The residence time of nitrate in the vadose zone, following fertilizer applications, is of particular concern from groundwater quality point of view. Neither the fertilizer applications (standard or high) nor the type of model applied (homogeneous or heterogeneous) has a strong effect on the first breakthrough of nitrate at the water table. Under the water management schedules at the orchard and the site climate conditions during 1990-1996, the estimated first arrival of N to water table is approximately 2.5 yr after the simulation starts at both subplots. At

the standard subplot, the first arriving N in 1992 results from the first irrigation application while at the high subplot it is a contribution of both the irrigation and the first spring N application (on March 28 or at DOS = 88). The time that it takes for the first arrival of N at the water table should be reduced to 2.3 years if the time of surface N application is accounted for. Besides, if the first time of nitrate appearance at the bottom of the root zone is taken into account (about 20 days following an irrigation event), the travel time of nitrate fluxes to the water table is further reduced to approximately 2.2 years.

5.22 Nitrogen Flux to Groundwater

Figure 52 shows variations of daily total N flux (per unit width) at the water table corresponding to the standard and high fertilizer applications. Values of total N flux from the homogeneous and heterogeneous lithofacies model are presented together in Figure 58. Values are computed based on daily local N concentrations and water fluxes along the boundary nodes of each model. Also shown in Figure 52 on the right axis are the daily values of average water flux simulated by the homogeneous lithofacies model (discussed earlier in Section 4.8). Consistent with the previous observations for water flow and N transport, temporal variations seen in the total N flux at the bottom simulated by the homogeneous lithofacies model are comparable to those simulated by the heterogeneous lithofacies model. In 1993, the rate of N flux in the homogeneous lithofacies model is slightly higher. During 1994 and thereafter the situation is reversed as shown by higher rates of N flux at the water table estimated by the heterogeneous lithofacies model.

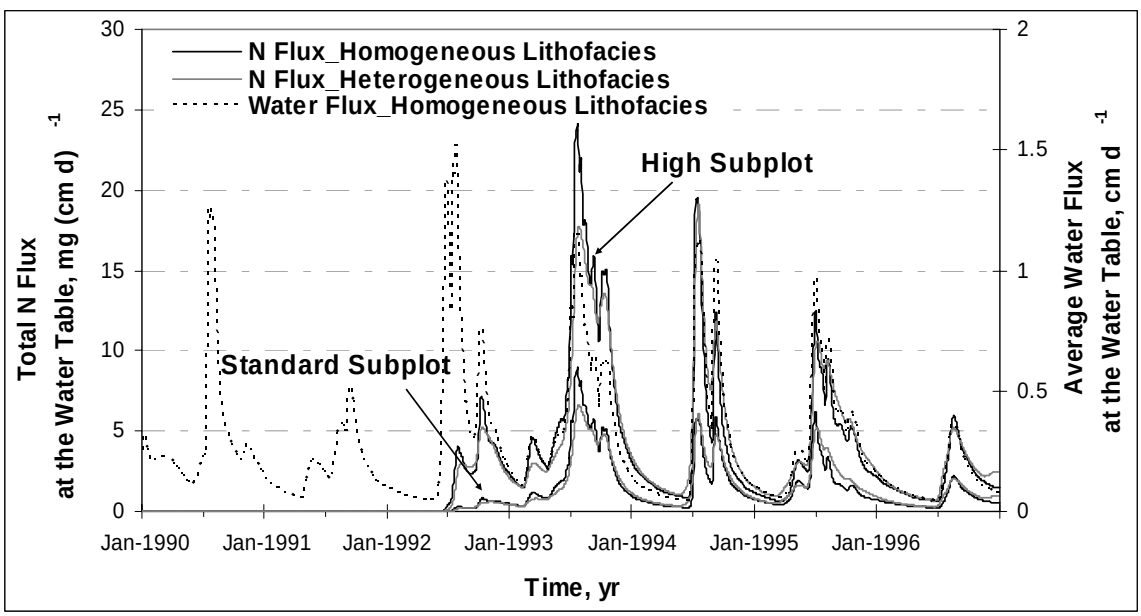

Figure 52 Total NO_3-N flux at the water table of the standard and high subplots during the simulation period (1990 – 1996) in the homogeneous and heterogeneous lithofacies models

The numerical results for water flow show that under highly transient surface fluxes, water fluxes to water table experience seasonal and annual variations despite the presence of the deep vadose zone. Comparison of the overall appearance of average water flux curve (a dotted

line in Figure 52) and total N flux curves (solid lines) reveals that the rate of movement of water and N are in good agreement, as shown by high rates of N fluxes corresponding to high percolation rates. Percolating water and N leaching at the bottom are quantitatively related to each other and they are both mainly driven by the magnitude of irrigation fluxes prescribed at the surface. This finding, which has been also confirmed by field experiments conducted to determine the relationship between the amount of water by irrigations and the amount of fertilizer and pesticides leaching (Biggar and Nielsen, 1978; Wagenet and Hutson, 1986; Troiano et al., 1993), underscores the importance of budgeting irrigation water in irrigated agriculture to mitigate downward movement of surface applied agrochemicals through decreasing deep percolation.

N flux curves at the standard and high subplots, while they are different in their magnitudes yet similar in their shapes, imply that split N applications during spring at the high subplot do not tend to cause higher fluctuations in N fluxes to water table. This may further suggest that the magnitude of N fluxes to water table is potentially controlled by annual total fertilizer application rates while inter- and intra-annual variations in N fluxes are driven by surface water fluxes. Comparison of peak N fluxes between the standard and high subplots indicates that N flux at the high subplot is expected to be about three times higher than that at the standard subplot during 1993 and 1994. During this period, daily total N flux varies approximately from 6 mg (cm d)$^{-1}$ to 9 mg (cm d)$^{-1}$ at the standard subplot and from 18 mg (cm d)$^{-1}$ to 26 mg (cm d)$^{-1}$ at the high subplot.

5.22.1 Cumulative Nitrogen Flux to Groundwater

Cumulative N fluxes at the water table over the 7-yr simulation period are shown in Figure 53 as simulated in the homogeneous and heterogeneous lithofacies models at the standard and high subplots. At the end of the simulation, cumulative N flux at the water table of the standard subplot varies from 250 g m^{-1} in the homogeneous lithofacies model to 257 g m^{-1} in the heterogeneous lithofacies model. For the corresponding models, cumulative N flux at the high subplot varies from 714 g m^{-1} to 717 g m^{-1}. While the shapes of cumulative N flux curves for the two subplots are alike, the magnitude of the cumulative N flux to groundwater at the high subplot is approximately three times higher than that at the standard subplot. This is only slightly smaller than the ratio of the annual fertilizer application rates between the two subplots (365/110 = 3.3). A sharp slope change in the first rising curve is the rapid effect of fall N application from 1990. The third rising curve smoothly grows without a change in slope. This is attributed to the mixing of fall N application in 1992 with spring N applications in 1993. The late irrigation that occurs in 1992 after the fall N application expedites the mixing of fall and spring N applciaitons.

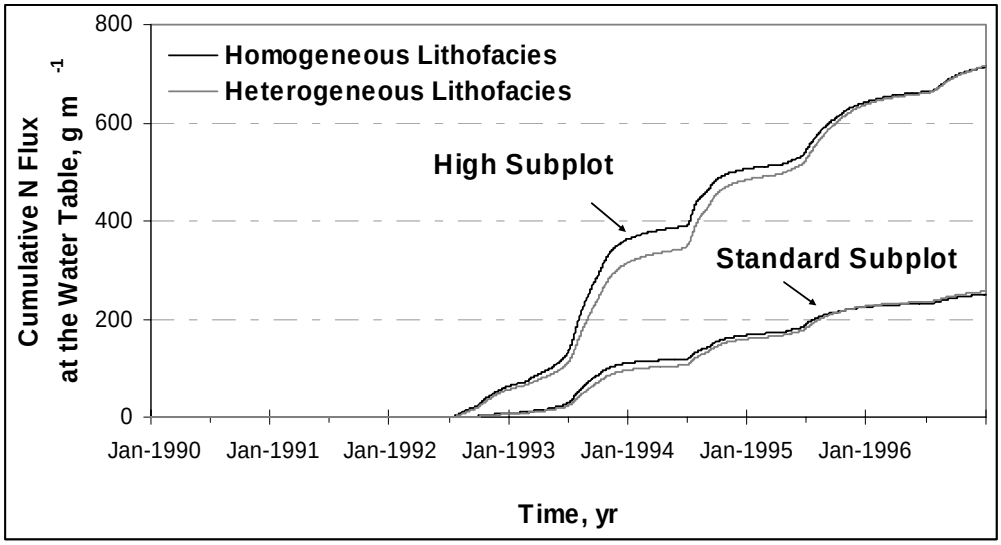

Figure 53 Cumulative NO_3-N flux at the water table of the standard and high subplots during the simulation period (1990 – 1996) in the homogeneous and heterogeneous lithofacies models

5.23 Annual Vadose Zone Nitrogen Budget

Annual vadose zone N mass balance analysis during the 7 yr simulation period is completed based on the simulation results of the homogeneous and heterogeneous lithofacies models at the standard and high subplots. Results of the analysis are shown in Table 11 for the standard subplot and in Table 12 for the high subplot. The difference between annual N inputs that are applied at the surface from fertilizer and irrigation applications (i.e., N_F+N_I) and annual outputs including plant N uptake within the root zone and N leaching at the water table (i.e., N_P+N_L) defines annual N storage in the vadose zone. In the calculation of absolute MB error, the model prescribed annual N inputs and outputs are summed (i.e., N_F+N_I -N_P-N_L), and then compared with the rate of change of N mass in the vadose zone N between the beginning and the end of a simulation year (i.e., NM_T –NM_0). In comparing the model results for the both subplots, the absolute MB error ranges from -8 to 0 kg N ha^{-1} at the standard subplot and from 0 to -17 kg N ha^{-1} at the high subplot. This suggests that both the models tend to underestimate N mass and the error associated with this underestimation is anticipated to be higher by increasing fertilizer rate. In terms of comparing the model results with each other, the heterogeneous lithofacies model seems to offer advantages over the homogeneous lithofacies model by providing smaller MB error (Table 11b and 12b).

In comparing the 7-year simulation results at the subplots, annual N leaching at the water table of the high subplot is much greater than that found under the standard subplot. This indicates that a substantial portion of the additional N applications during spring (85 kg N ha^{-1} applied three times totaling to 255 kg N ha^{-1}) at the high subplot appears as excess N that ultimately contributes to water table.

N leaching estimated by the heterogeneous lithofacies model at the standard and high subplots is of the same order as that estimated by the homogeneous lithofacies model at the corresponding subplots. This is contrary to what is expected given the fact that the heterogeneous lithofacies models accounts for spatial variability within the lithofacies, unlike the homogeneous lithofacies model. While the results look similar, an apparent trend suggests that during 1992 and

1993 the homogeneous lithofacies model results in greater N leaching at each subplot than the heterogeneous lithofacies model. Afterwards, the situation is reversed with N leaching estimated by the heterogeneous lithofacies model being greater than the homogeneous lithofacies model.

Table 11 Annual root zone and vadose zone *NO_3-N* mass balance at the standard subplot based on simulation results in the a) homogeneous and b) the heterogeneous lithofacies models

Standard Subplot

Homogeneous Lithofacies

a)	Inputs		Outputs				
	Fertilizer	Irrigation	NO_3-N Plant Uptake	NO_3-N Leaching			Absolute
Year	N_F	N_I	N_P	N_L	$N_F+N_I-N_P-N_L$	NM_T-NM_0	MB Error
1990	110	70	44	0	135	132	-4
1991	110	54	66	0	98	93	-5
1992	110	91	76	13	113	109	-4
1993	110	86	54	167	-26	-30	-4
1994	110	70	79	94	7	4	-3
1995	0	70	41	93	-64	-65	-1
1996	110	48	50	43	66	58	-8

Heterogeneous Lithofacies

b)	Inputs		Outputs				
	Fertilizer	Irrigation	NO_3-N Plant Uptake	NO_3-N Leaching			Absolute
Year	N_F	N_I	N_P	N_L	$N_F+N_I-N_P-N_L$	NM_T-NM_0	MB Error
1990	110	70	40	0	140	138	-3
1991	110	54	58	0	106	103	-3
1992	110	91	66	11	124	120	-4
1993	110	86	49	146	1	-2	-3
1994	110	70	71	104	5	2	-3
1995	0	70	37	109	-76	-76	0
1996	110	48	44	50	64	58	-7

N_F : Annual NO3-N applied with fertilizer at the standard subplot [kg ha^{-1}]
N_I : Annual NO3-N applied with irrigation [kg ha^{-1}]
N_P : Annual NO3-N plant N uptake [kg ha^{-1}]
N_L : Annual NO3-N leaching at the water table [kg ha^{-1}]
NM_O : NO3-N mass in the vadose zone at the beginning of a simulation year [kg ha^{-1}]
NM_T : NO3-N mass in the vadose zone at the end of a simulation year [kg ha^{-1}]
Absolute MB error: $(NN_T – NM_O) – (NG + NI – NP – NL)$ [kg ha^{-1}]

Table 12 Annual root zone and vadose zone *NO_3-N* mass balance at the high subplot based on simulation results in the a) homogeneous and b) the heterogeneous lithofacies models

High Subplot

Homogeneous Lithofacies

a)	Inputs		Outputs				
	Fertilizer	Irrigation	NO_3-N Plant Uptake	NO_3-N Leaching			Absolute
Year	N_F	N_I	N_P	N_L	$N_F+N_I-N_P-N_L$	NM_T-NM_0	MB Error
1990	365	70	108	0	326	312	-15
1991	365	54	135	0	284	267	-17
1992	365	91	119	103	234	222	-12
1993	365	86	127	491	-166	-181	-15
1994	365	70	127	235	72	58	-14
1995	0	70	41	224	-195	-196	-1
1996	110	48	50	118	-9	-16	-7

Heterogeneous Lithofacies

b)	Inputs		Outputs				
	Fertilizer	Irrigation	NO_3-N Plant Uptake	NO_3-N Leaching			Absolute
Year	N_F	N_I	N_P	N_L	$N_F+N_I-N_P-N_L$	NM_T-NM_0	MB Error
1990	365	70	97	0	338	324	-13
1991	365	54	118	0	301	288	-13
1992	365	91	107	92	258	243	-14
1993	365	86	114	424	-87	-100	-13
1994	365	70	115	278	42	29	-13
1995	0	70	37	252	-219	-219	0
1996	110	48	44	131	-16	-22	-6

N_F : Annual NO3-N applied with fertilizer at the high subplot [kg ha^{-1}]
N_I : Annual NO3-N applied with irrigation [kg ha^{-1}]
N_P : Annual NO3-N plant N uptake [kg ha^{-1}]
N_L : Annual NO3-N leaching at the water table [kg ha^{-1}]
NM_O : NO3-N mass in the vadose zone at the beginning of a simulation year [kg ha^{-1}]
NM_T : NO3-N mass in the vadose zone at the end of a simulation year [kg ha^{-1}]
Absolute MB error: (NNT – NMO) – (NG + NI – NP – NL) [kg ha^{-1}]

As far as the annual variations of N leaching are concerned, the water table starts receiving N during mid-1992. The first arriving N plumes are attributed to the irrigation applied N at the standard subplot and the irrigation and fertilizer applied N at the high subplot during 1990 (on March 28 or at DOS = 88). As the simulation time elapses beyond 1992, N surplus of the previous growing seasons leaching down to the deep vadose zone displaces N that is already traveled downward near the water table. Therefore, N leaching diverges significantly after 1992. The maximum N leaching is estimated in 1993 at the rate of 167 and 146 kg N ha^{-1} at the standard subplot as estimated by the homogeneous and heterogeneous lithofacies models, respectively. The maximum N leaching occurs in 1993 at the high subplot, at the rate of 491 and 424 kg N ha^{-1} at the high subplot as estimated by the corresponding models. It is approximately three times (2.9 times to be exact) higher compared to that occurring at the standard subplot. Nitrogen leaching during 1996, which is nearly half the N leaching estimated in the previous year, has more to do with the contribution of N applied during 1993 than during 1992 since the final irrigation in 1992 followed by the fertilizer application causes N to leave the root zone much faster than in other years.

6. SYNTHESIS OF MODELING APPROACHES: METHODS, RESULTS, AND DISCUSSION

Three modeling approaches are developed in an attempt to evaluate the long-term impacts of various fertilizer applications on groundwater quality through a 15.8 m deep alluvial vadose zone underlying a former nectarine orhard located at the Kearney research Center, Fresno, California. The models applied include:

- A root zone water and N mass balance method with uniform soil properties and flow conditions in the vadose zone
- A transient, two-dimensional numerical flow and nitrate transport model with 8 layers, each represented by homogeneous average soil hydraulic properties (referred to as *homogeneous lithofacies model*)
- A transient, two-dimensional numerical flow and nitrate transport model with 8 layers, each represented by heterogeneous, randomly distributed soil hydraulic properties (referred to as *heterogeneous lithofacies model*)

The orchard was subject to a long-term, 12 year fertilizer experiment (1984-1995) with various N fertilizer treatments ranging from 0 to 365 kg N ha^{-1}. Sixty continuous boreholes were drilled to a depth of 15.8 m in the vadose zone underneath three fertilizer subplots with annual applications of 0, 110, and 365 kg N per ha^{-1} (referred to as "control", "standard", and "high" subplot, respectively). The entire vadose zone was characterized extensively for soil texture, soil hydraulic and chemical properties based on field and laboratory analysis of over 1000 soil samples extracted from the boreholes. Ten major lithofacies (or layers) identified based on a visual inspection of soil cores for color, texture, and cementation range in thickness and are laterally continuous across the site. Our findings based on advanced statistical and geostatistical analyses as applied to soil core data reveal the presence of strongly heterogeneous geologic formations at the site, highly variable water content data, and strongly log-normal hydraulic conductivity and nitrate data, all leading to the hypothesis that highly heterogeneous, skewed or log-normally distributed flux conditions and, in coarse facies, fingering-like flow can dominate the vadose zone hydrology in these alluvial sediments.

The modeling strategy progresses in a phased approach from a simple to an increasingly complex characterization of the subsurface heterogeneity to determine whether the models applied can quantify the N mass observed at the site at the end of the experiment. Each model demonstrates a different level of risk analysis by representing the site subsurface by a different scale of heterogeneity (e.g., field, lithofacies, and Darcy's scale) to predict the loss of nitrate from the root zone, nitrate storage in the deep vadose zone, and potential nitrate leaching to groundwater in response to the long-term site irrigation and N management practices. Results from three models represent three different levels of risk analysis for assessing the long-term impact of various nitrate fertilizer management practices on groundwater quality, with an emphasis on the role of heterogeneity at three scales.

The root zone N mass balance (MB) analysis coupled with a root zone water MB was applied to estimate annual water and N fluxes out of the root zone beneath each subplot by utilizing the site database for irrigation, climate (e.g., precipitation and evapotranspiration), fertilization, and plant uptake data and literature reference values, where needed. This model with uniform soil hydraulic properties and uniform water flow conditions at the field scale provides the *first level risk assessment* for the amount of nitrate in the deep vadose zone and nitrate travel time to groundwater from the three subplots. The homogeneous lithofacies model includes numerical simulations carried out for 7 years (1990 – 1996) at the standard and high subplots with realistic, temporally varying site boundary conditions for flow and nitrate transport

utilizing the site database. The subsurface in this model is composed of eight non-horizontal layers, representing the boundaries of major lithofacies that were identified at the field. Each lithofacies is conceptualized as a homogenous unit with average (*effective*) soil hydraulic parameters that are defined in the form of the van Genuchten model. The model vertical domain is 15.8 m, covering the entire vadose zone. The horizontal simulation domain is 6.1 m representing the individual subplots of the original field experiment. This model with homogeneous lithofacies explores soil heterogeneity at the lithofacies scale and provides the *second level risk assessment* for the amount of nitrate in the deep vadose zone and nitrate travel time to groundwater from the two subplots. The soil hydraulic database generated for the site and spatial variability of soil hydraulic properties observed at the site provides a framework for a modeling strategy to substantiate the applicability of highly heterogeneous flow conditions in the deep vadose zone. The heterogeneous lithofacies model is also constructed both at the standard and high subplot in an attempt to account for the effects Darcy's scale heterogeneity on flow and to asses the long-term impact of various nitrate fertilizer management practices on groundwater quality. This model is the same as the previous numerical model in terms of the simulation period (7 years from 1990 –1996), boundary and initial conditions. Each lithofacies is now characterized as a heterogeneous unit using randomly distributed scaling factors. This model with the highest possible resolution presents the *third level risk assessment* for potential nitrate leaching to groundwater under the two subplots. In all three models, nitrate moves as a non-reacting solute (tracer) in the deep vadose zone. This is a simplification adopted based on the interpretation of the measured chemical properties such as nitrate, ^{15}N isotopes, soil pH, and soluble organic carbon.

As an alternative approach to the three N modeling exercises, kriging interpolation of the measured nitrate and water content data, with the product giving the nitrate mass, was applied as a robust quantitative model to estimate total nitrate mass storage based on point measurements underneath the three fertilizer subplots.

The key findings from the modeling results, which are reviwed briefly below, provide not only an important resource for further research in characterizing highly heterogeneous field soils but also an educational component for growers, farm advisors, and irrigation districts on the potential leaching rates of agricultural chemicals.

6.1 Homogeneous vs. Heterogeneous Lithofacies

Regardless of whether the homogeneous or the heterogeneous lithofacies model is used, transient surface fluxes, particularly from irrigation events, have a strong impact on soil moisture content and pressure head data, creating large seasonal fluctuations both in the in the root zone and in the deep vadose zone. Temporal changes of soil water content and pressure head in each lithofacies seem to vary by various factors such as the magnitude of surface boundary fluxes, the proximity to the surface boundary, and the soil hydraulic properties of individual lithofacies. The range of pressure head variations between irrigation events is higher in the shallow than in the deeper portion of the profile. The upper layers respond to any water input, either of irrigation or precipitation, more rapidly than the deeper layers regardless of variations in their soil texture characteristics. Water fluxes throughout the deep vadose zone and at the water table simulated in the homogeneous and heterogeneous lithofacies models are in good agreement. Both the models simulate water fluxes that are in direct relation to irrigation applications.

As far as the model estimates, such as N fluxes, the deep vadose zone N mass and N leaching to the water table, are concerned, the two numerical models, as presented as the second and third risk assessment tools, provide indistinguishable results. The ultimate conclusion drawn

in light of this finding is that the local heterogeneity defined in the heterogeneous model makes little to no difference in the results. In other words, the refinement of the subsurface characterization does not affect model estimates.

Three factors, namely i) the correlation scale of soil hydraulic properties, ii) the scaling technique, and iii) the lack of the third dimension, can explain why close similarities are found between the latter two model results. These factors may work collectively to produce a potential smoothing effect within the lithofacies in the heterogeneous model.

6.1.2 Effect of Correlation of Soil Hydraulic Properties on Model Results

Variogram analysis of our data for the scaling factors produces pronounced anisotropy, with a horizontal range of 5.4 m and a smaller vertical range of 1.7 m. The horizontal range extends much of the horizontal domain of the heterogeneous lithofacies while the vertical range is approximately equal to the average thickness of most of the lithofacies used in the model (average thickness of SL1, Var1, HP1, Var2, S, and HP1 is near or less than 2.5 m). The large sampling distance in the horizontal did not allow resolution of spatial variability at a scale relevant to the horizontal size of the simulation domain. Similarly, because of insufficient vertical sampling within the lithofacies, the range estimated may not characterize the local correlation scale within the lithofacies. Eventually, larger ranges in both directions generates well correlated, rather smooth distribution of scaling factors within the lithofacies. As a result, the local spatial variation of scaling factors, which is hypothesized in delineating the site heterogeneity, seems to be overcome by the lithofacies boundary effects.

Based on stochastic analysis of unsaturated flow, Hopmans et al. (1988) used MC simulations for analyzing two-dimensional steady state flow using randomly distributed scaling factors that vary only in the horizontal direction (perpendicular to the mean flow direction) and found the variability of pressure head and flux decreases with an increase in the correlation length. This is also consistent with Ünlü et al.'s (1990) findings based on a MC application of one-dimensional transient unsaturated flow: increasing the variability of soil hydraulic properties increases the variability of pressure head and water flux.

6.1.3 Effect of Scaling Analysis on Model Results

Despite its widespread use, scaling technique and using scaling factors as random variables may be a less realistic representation of the extent of heterogeneity observed at the Kearney site. The fundamental theories of Miller and Miller similitude scaling technique have been essentially derived based on the principle that microscopic soil-particle structures are geometrically identical but variant in sizes.

The soil hydraulic properties of the Kearney site vadose zone, in particular hydraulic conductivity, exhibit high degrees of spatial variability, varying several orders of magnitude over the vertical sampling domain (~ 16 m). Variation in soil textures is the major source of heterogeneity at the core scale. The stratification, or layering formation, is the dominant heterogeneity at a larger scale. The Miller and Miller scaling technique, which may not be valid in natural field soil heterogeneity where soil properties vary significantly, seem to produce potential smoothing of local heterogeneity. With the combined effect of the smoothing due to the scaling analysis and the relatively large correlation scales for the scaling factors, the heterogeneous lithofacies model may still represent the heterogeneity more at the lithofacies scale than at the local scale. Therefore, the layering becomes the dominant effect on flow and transport results in both the models. As also reported by Abbasi et al. (2004), who studied a two

dimensional flow and transport using the HYDRUS-2D model and the linear scaling method to quantify spatial variability of soil hydraulic properties from 38 soil samples, our study provides eveidence that the unsaturated soil hydraulic properties estimated from small soil cores in the laboratory may not adequately describe field-scale soil water status in view of considerable variability and uncertainity in the defined parameters.

6.1.4 Effect of Lack of Third Dimension on Model Results

The occurrence of highly variable nitrate concentrations in all the three subplots is convincing evidence for significant three-dimensional flow and nitrate transport under the site conditions. The better evidence for the occurance of a three dimensional processes is perhaps the presence of relatively higher N concentrations and greater N mass under the control subplot than the adjacent standard subplot. The phenomenon that the average N concentration and N mass under the control subplot, which can be explained as a result of possible movement of N from a neighboring subplot, has been encountered in other field studies that took place in a layered vadose zone system (Steenhuie et al., 1998). From our data analysis of soil texture, soil water content and nitrate, a strong impact of layering on flow and N transport is evident. The homogeneous and heterogeneous lithofacies models, both of which delineate each lithofacies as a distinct hydrologic unit, are limited by the lack of the third dimension. Therefore, the impact of a three-dimensional layering on the flow and nitrate processes cannot be truly demonstrated by the two-dimensional numerical models.

6.2 Root Zone Mass Balance Approach vs. Numerical Modeling

The most commonly applied root zone nitrogen MB approach is used to estimate water percolation rate and travel time to water table and N mass storage in the deep vadose zone, based on the assumption of uniform flow conditions through the deep vadose zone. The simple root zone MB approach, which is considered as the first level risk assessment tool, yields the deep vadose zone mass of 218 (130/334) kg N ha^{-1} for the control subplot, 261 (147/427) kg N ha^{-1} for the standard subplot and 478 (271/784) kg N ha^{-1} for the high subplot at the time of drilling in 1997. Values in parentheses are the margin of errors given to reflect potential errors in both water and N fluxes. The numerical models predict 237 and 284 kg N ha^{-1} at the standard subplot and 401 and 486 kg N ha^{-1} at the high subplot (the homogeneous and heterogeneous lithofacies models, respectively). Surprisingly, the ranges of deep vadose zone values simulated by the numerical models for both the standard and high subplots are in good agreement with those predicted by the simple MB approach (Table 13**)**.

With respect to the average concentration at the water table, the numerical models estimate a value of approximately 10 g m^{-3} under the standard subplot at the end of the simulation. This is in close agreement with that estimated from the root zone MB approach in the corresponding subplot (9 g m^{-3}). In the case of the high subplot, as a result of increasing N leaching through the profile, higher potential for nitrate accumulation in groundwater exists. Estimated values from the numerical models vary between 27 - 30 g m^{-3}, nearly three times higher than the value estimated under the standard subplot. These values are only slightly higher than the value of 25 g m^{-3} estimated from the root zone MB method. These results point out that elaborate efforts to construct a numerical flow model with increasingly refined spatial definitions of the hydraulic properties may not always be justified. Therefore, on the basis of the N mass storage estimates, all the three models providing comparable deep vadose zone N mass estimates for 1997 is maybe insensitive to the spatial variability of soil hydraulic properties.

However, it is noteworthy to point out that the above direct comparison of the numerical models with the root zone MB model should be also viewed within the context of model components. For instance, the secondary N inputs, such as dry and wet N depositions and non-symbiotic N fixing, and secondary N outputs, including denitrification and ammonification, are taken into account only in the root zone MB approach with their margins of errors (Table 3.1). In the numerical models, since N is treated as a tracer, the amount of N mass is solely driven by the magnitude of water fluxes. The implementation of these secondary processes in the numerical models would make the model construction more difficult and would require more computational time, but could not alter the estimates of the numerical models considerably.

While close agreement between the three models is found with respect to the deep vadose zone N mass and average leachate N concentration, significant discrepancies between the root zone MB approach and the numerical models exist for the estimates of travel time to water table. Based on the long-term average annual net water and N fluxes below the root zone as applied in the root zone MB method, the travel time through the deep vadose zone is estimated to be approximately 3.2 years. The numerical models, on the other hand, estimate a travel time of 2.2 years for the first nitrate plume arrival at the water table. The discrepancy in the travel time and the similarity in the the deep vadose zone N mass between the models points out that in the numerical models water moves much faster yet carries greater amount of N mass with it. On the basis of our comparison in relation to the travel time estimates, the numerical models seem to offer more conservative perspective than the simple root zone MB approach for the risk assessment of groundwater quality.

Table 13 Comparison of the measured and model predicted deep vadose zone NO_3-N mass at the control, standard, and high subplots

	Deep vadose zone N storage					
	Control		Standard		High	
Deep Vadose Zone N Mass			kg ha^{-1}			
Measured	48	(42/62)	36	(33/47)	87	(79/107)
Predicted for 1997						
Root Zone MB	218	(130/334)	261	(147/427)	478	(271/784)
Homogeneous Lithofacies Model			237		401	
Heterogeneous Lithofacies Model			284		486	

6.3 Measured vs. Model Predicted Deep Vadose Zone N Mass

Both the root zone MB method and the numerical models severely overestimate the measured N mass in the deep vadose zone (Table 13). The total N mass in the vadose zone obtained from kriging interpolation of water content and nitrate concentration is 52 (±10), 40 (±7), and 93 (±14) kg N ha^{-1} for the control, standard, and high subplots, respectively. Values given in parentheses represent the confidence intervals of the average kriging error variance. The deep vadose N mass (without the root zone) is 48, 36, and 87 kg N ha^{-1}, respectively. These values are less than one-quarter of the deep vadose zone total N mass estimated from the three modeling approaches adopted herein.

The discrepancy between the kriged (measured) and the root zone MB analysis cannot be explained by estimation errors in the MB method and in the geostatistical analysis of vadose zone N mass. At the site conditions denitrification may locally occur throughout the deep vadose zone, but could not account for the relatively low nitrogen mass measured in the deep vadose zone

(Appendix 2). Instead, non-uniform flow conditions in the vadose zone are believed to be the reason. Apparently, in alluvial sediments, the commonly used assumption of uniform flow in the deep vadose zone, as implemented in the MB analysis, is inadequate to predict nitrate levels in the deep vadose zone below the root zone. In conclusion, none of the three models is adequate for explaining the observed fate of nitrate in the 16-m deep vadose zone under the highly heterogeneous geology of the alluvial sediments observed at the orchard site, coupled with the associated heterogeneity of the soil hydraulic properties. Why such low N mass has been encountered in the vadose zone at the site still remains an unanswered question.

Despite the high discrepancies between the model N estimates and the measured N at the site, we gain useful insight through these modeling practices and our key findings based on data analysis of the site records and the results from the three modeling exercises can be considered significant for the implications of fertilizer management practices. The modeling results provide interested parties with a comprehensive view of groundwater vulnerability under fertilizer and irrigation practices and climate conditions that are typical of those found in orchards of California. The efficiency of N utilization decreases and in-season N losses increase rapidly as N rate increases. Underscoring field study findings that have focused on N leaching from the root zone (Bonilla et al., 1999), our results show that residual nitrate is often susceptible to leaching by off season precipitation and most importantly by late fall or excessive early spring irrigations. Although fall application of ammonium based fertilizer is often recommend in Central and Northern California to avoid the rapid conversion of ammonium to nitrate (Smith and Cassel, 1991), the soil at the orchard has adequate moisture and warm temperature (above 50° F) to complete the conversion before the physiological activities of the trees start in the subsequent year. Contrary to the common belief among farmers that fall applied N would be readily available for uptake by trees during spring, our model results suggest that appreciable amount of N could leach below the root zone by moderate to heavy rainfall during winter. The site records and the model results suggest that irrigation is the main driving factor controlling leaching of nitrate from the root zone. Thus, N loss from the root zone during irrigation season is expected to be highest. Irrigation events following fall N applications could result in a substantial amount of N loss from the root zone. As a result, N becomes unrecoverable before the next growing season begins. Nitrate leaching appears to be affected not only by the amount of irrigation,but also by the irrigation patterns. Historical irrigation records and climate data at the Kearney site do not appear to follow a particular irrigation pattern in relation to annual climate changes. Irrigation events that are not distributed uniformly over time, cause either a substantial deep percolation or cause trees to suffer stress. The average annual water application estimated to be 175 cm under average 13 irrigations is higher than an application rate recommended (e.g., 114 cm yr^{-1}) for a well managed nectarine orchard under furrow irrigation.

Overall, the synthesis of flow modeling results indicates that the downward movement of water and N to groundwater can be substantially reduced by proper water management practices during irrigation seasons. We recommend that irrigation management practices (both timing and quantity) should be well integrated with crop water requirements and should properly account for site climate conditions. As far as N management practices are concern, the synchronization of N application with the time of most rapid N uptake should be practiced to assure the best crop use of N and least N loss from the root zone. Instead of fall N application, inorganic fertilizers could be conveniently delayed until early spring.

6.3.1 Effect of Denitrification on Deep Vadose Zone N Mass

Denitrification decreases nitrate-nitrogen concentrations, but increases the relative amount of isotopically heavy NO_3- $\delta^{15}N$. Traditionally, such low nitrate-nitrogen concentrations

in the deep vadose zone and total nitrogen mass have been attributed to denitrification. At the site conditions, a weak vertical trend found in the nitrate concentration does not support that theory. Similarly, no significant difference in the levels of $\delta^{15}N$ data was found with depth or with lithofacies distributions. Given the lack of a significant vertical trend in NO_3-N and $\delta^{15}N$ data and very low amounts of organic matter and organic carbon measured throughout the profile at each subplot, we believe that favorable conditions for natural attenuation of nitrate at the site do not exist. Even after accounting for partial denitrification (10 – 20%), groundwater may be receiving much more nitrate than what would be under natural conditions. This finding, suggests that under the site conditions, it is unlikely for the deep vadose zone to act as a buffer zone that protects groundwater pollution from surface applied nitrate (see Hypothesis 2 in the Executive Summary).

6.3.2 Effect of Preferential Flow on Deep Vadose Zone N Mass

Denitrification is indeed a good indicator of the state of nitrate transport to groundwater. If the observed fate of nitrate in the deep vadose zone cannot be explained by denitrification, why was the total nitrogen storage in the deep vadose zone so low?

Our detailed geologic, hydraulic and geochemical analysis of a typical deep vadose zone in the eastern San Joaquin Valley demonstrates that alluvial vadose zones are subject to significant geologic variability, which in turn causes hydraulic properties and water flow in the vadose zone to exhibit strong spatial variability. While such variability is expressed to only a limited degree in the variability of the observed moisture content, it leads to highly variable concentrations of chemicals, such as nitrate. Significant scatter in nitrate data is similar to that postulated in other experimental (Hills et al. 1991; Roth et al. 1991) and numerical (Harter and Yeh 1996; Ünlü et al. 1990; Tompson and Gelhar 1990) studies in highly heterogeneous vadose zones. Thus, the proposed conceptual framework of preferential flow in the deep vadose zone may provide the answer: preferential flow paths would be responsible for most of the water and nitrate transport from the root zone to the water table, quickly flushing nitrate to deeper portions of the vadose zone, allowing for little or no denitrification. This would also explain the occurrence of high nitrate-nitrogen concentrations with low $\delta^{15}N$ levels throughout the vadose zone profile. In line of this theory, outside preferential flow paths, lower nitrate-nitrogen would occur in stagnant water zones. Due to their longer residence time, nitrate in these zones would be subject to a small amount of denitrification. This would explain the higher levels of $\delta^{15}N$ that were also found scattered throughout most of the profile. Since much of the annual recharge occurs through the preferential flow paths, the actual downward flow rate is locally much higher than that estimated by the models. Hence, as a result of shorter nitrate travel, N storage in the deep vadose zone should be significantly lower than our estimates. Overall, if this conceptual preferential flow is confirmed, Hypothesis 3 is proven to be valid (see Executive Summary). Both the simple MB model and the numerical models used in this study are limited in their ability to diagnose the preferential flow that we believe exists at the Kearney site. The importance of this finding is that while limited denitrification took place in the stagnant water areas of the vadose zone, the majority of the nitrate-nitrogen transport occurred in preferential flow paths, where no significant denitrification appears to have taken place. Hence, the low average nitrate-nitrogen concentration in the vadose zone pore water should not be interpreted as an indicator for high denitrification and low nitrate impact on groundwater. Rather it may be the result of swift, unattenuated nitrate-nitrogen transport to the water table, leaving less nitrate-nitrogen stored in the deep vadose zone and more nitrogen pollution in groundwater.

Besides macropores in the root zone, other conditions trigger and support preferential flow paths. These conditions include “funneling” due to flow through or above embedded clay or

sand lenses, which also occurs if soil layers are inclined, and "fingering" as a result of a sharp textural interface between a fine soil overlying a coarse soil and "wetting front instability". In a more recent review, de Rooij (2000) has listed the followings as possible causes of wetting front instability: an increase of K with depth, water repellency, redistribution of infiltration after the end of a rain or irrigation, air entrapment, and non-ponding rainfall. Based on our close examination of the site subsurface textures, it is evident that these conditions may be present at the site and have been shown by other field studies to create unstable, preferential flows in a variety of settings in both uniform (Glass et al., 1991; Wang et al., 1998, Wang et al., 2003a) and layered soil systems (Flury et al., 1994; Steenhuis et al., 1998; Wang and Feyen, 1998; Wang et al., 2003b). Furthermore, extrinsic factors such as irrigation management and fertilizer applications contribute large variability in water fluxes and nitrate concentrations (Böhlke, 2002; Wang et al., 2004). Sometimes, more than 80% of the infiltrating water is transported in preferential flow paths to the deep subsoil during single rain events (Ritsema et al., 1998). Field evidence also supports the existence of preferential flow due to repeated infiltration cycles (Glass et al., 1989) and the occurrence of fingers recurring on the same places during successive irrigation events in a water repellent sandy field soil (Ritsema et al., 1998). However, the two-dimensional representation of local scale heterogeneity via the scaling factor approach, and the modeling of nitrate transport using the advection-dispersion equation does not adequately address such phenomena (see Hypothesis 4, Executive Summary).

In light of worldwide vulnerability of shallow groundwater resources to nitrate contamination, our conclusions underscore the need for a rigorous examination of current agricultural practices in an attempt to increase irrigation and N uptake efficiency and decrease adverse effect of N contamination on groundwater. The traditional interpretation of deep vadose zone measurements should be reconsidered. The common practice of compositing soil samples taken from immediately below the root zone provides an estimate of the average nitrate-nitrogen concentration at that depth. But our work indicates that recharge water may constitute only a minor portion of that vadose zone water and is not effectively represented by composite soil samples. It appears that taking average concentrations a closure term in the N mass balance is also not appropriate for estimating the amount of denitrification.

6.3.3 Effect of Layered Lithofacies on Deep vadose Zone N Mass

As reported previously (Russo, 1991; Sudicky, 1986), the horizontal layering at the site creates a pronounced anisotropy of soil hydraulic properties with a scale of horizontal correlations larger than the vertical one. This can imply that transverse fluxes and lateral mixing at the site is maybe present. The detection of higher N concentrations under the control subplot is not unique to our site as it has been encountered in other field studies that took place in a sandy, layered floodplain soil (Steenhuis et al., 1998). From their experimental study, Steenhuis et al. (1998) assessed the movement of water and nitrate over in a sandy layered system where a coarse sand layer located between two fine sand layers. Their key findings are described below to present empirical evidence for why greater N mass under the control subplot was observed at our site. They detected nitrate earlier at a high concentration at a deeper soil profile than upper parts, which is a clear evidence of preferential flow in their sandy layered system. They also showed that water and nitrate were funneled into fingers by passing most of the soil matrix and recharging groundwater much faster than if solute moved evenly through the vadose zone. Similar to our observation, they found high nitrate concentrations unexpectedly under a control plot. Consistent with their speculation, this phenomenon can be explained as a consequence of possible horizontal movement of nitrate from a neighboring N treated subplot.

Evidence for three-dimensional flow is inferred based on the potential layering effect on water flow and nitrate transport. At low water content, hydraulic conductivity of coarse textured layer, such as the Var1 layer, becomes extremenly low and the infiltrating water front may encounter a significant resistant to flow. As a result, most of water and nitrate in the overlying finer sediments, e.g., the SL1 layer, would move laterally around the coarse-textured layer. Higher water content observed in the fine-grained sediments, such as the C-Si-L and SL2, supports this hypothesis (Figure 2.10). This phenomenon is indeed observed in a series of tracer experiments conducted in unsaturated sand and gravel deposits on Cape Cod, Massachusetts (Rudolph et al., 1996).

7. FUTURE WORK

This study offers a rich database for detailed geologic, hydraulic, and chemical characterization of the deep vadose zone stratigraphy that is typical for alluvial sediments in the eastern San Joaquin Valley, California. Although the fundamental findings of this study, namely the highly heterogeneous nitrate and soil hydraulic properties, strong control of the heterogeneous flow conditions on the nitrate transport, are site-specific, they can provide general insight into the role of vadose zone on pollution migration to groundwater, using nitrate as an example, in other areas where the water table is deeper than the root zone and where significant layering and spatial variability occur. Besides, the site database provides a foundation for the development and validation of modeling tools different than used herein to assess the potential for nitrate leaching to groundwater in the presence of a deep, heterogeneous vadose zone at the site. While keeping the model limitations in mind, our study serves for the subsequent development of field-scale N transport model and suggests some directions for future work on how to account for the tremendous heterogeneity observed at the site.

- Mainly due to computational requirements, we focus on a domain that extends over several meters, noting that a flow domain of this size might be relevant to the transport of a single N plume associated with a fertilizer treatment subplot. As common in many field studies, relatively large sampling distance of soil hydraulic properties at the site did not allow resolution of the spatial variability at the simulation scale. Future work should consider a scale of simulation domain that is larger than the horizontal extent of an individual subplot and also larger than the horizontal correlation scale of soil hydraulic properties.
- Modeling heterogeneous flow conditions becomes increasingly important in environmental assessment and will considerably benefit protection of vulnerable groundwater resources. The heterogeneous lithofacies model is based on a single realization of soil hydraulic properties; thus, they are not truly stochastic. The application of MC method under realistic site conditions is probably an effort in the right direction. Uncertainties associated with predictions of flow and nitrate transport can be assessed with alternative realizations. Continuous advances in numerical techniques and computer hardware are making it increasingly possible to carry out comprehensive simulations of preferential flow processes in the vadose zone using the MC approach.
- A three-dimensional model can be built to accommodate at least two subplots. Future model should include an alternative method for describing soil properties (e.g., multi-Gaussian flow field) to better characterize the impact of heterogeneous flow conditions in the deep vadose zone on nitrate leaching to the water table. The construction of lithofacies scale variability of soil hydraulic properties is important in the view of the systematic assessment of the leaching potential of nitrate. To encompass most significant heterogeneity, the size of the three-dimensional domain should be larger than the correlation scale of the heterogeneity.
- As we have no evidence on the spatial variations of dispersivities, we used constant parameters to keep the study focused on the effect of heterogeneity of soil hydraulic properties on

nitrate flow. Our assumption of using constant dispersivity values relies on previous studies that concluded that solute spread due to heterogeneity is much higher than spread caused by the conventional pore-scale hydrodynamic dispersion (Bresler and Dagan, 1979). Solute front is shown to be less uniform with sharper concentration fronts when dispersion coefficient is set to zero (Hills et al., 1994). Follow up studies should address the impact of smaller or zero dispersion on the deep vadose zone N mass.

- Vertical boundaries are assumed to be impermeable and simulated with zero flux boundary conditions. The effects of side boundary conditions can be dealt with a domain of interest being much larger than the domain simulated.
- If a long period of simulation (~ years) is considered, it is anticipated that background levels of N in the soil profile can be still assumed to be insignificant.

If confirmed, the presence of highly heterogeneous flow conditions will help us design more informative field investigations and more frequent monitoring and measurement of agricultural chemicals to groundwater. The extension of this work with the above recommendations can make it possible to honor the natural spatial variability of hydraulic properties as well as preferential flow.

Extension Activities related to this project:

- Harter, T., "Nitrate in the deep alluvial unsaturated zone: Linking agriculture with groundwater quality?", Monterey County Water Resources Management Agency, Nitrate Technical Advisory Committee Meeting, 6/27/02.
- Harter, T., "Dairy Monitoring and Monitoring Options", Groundwater Nitrate Conference, Fresno, California Groundwater Resources Association, 11/13/2002.
- Harter, T., "Hydrology and the Management of Dairies and other Confined Animal Facilites" (including role of vadose zone monitoring), "Science for Everyone" Series, Vacaville Public Library, 3/31/2004.
- Harter, T., *Member*, Monterey County Nitrate Technical Advisory Committee, 1997-current.
- Harter, T., *Member*, UC ANR Workgroup on Farm Water Quality Assessment, 2001-current
- Harter, T., *Member*, Subcommittee on denitrification, USDA-NRCS Technical Committee for developing the Comprehensive Nutrient Management Plans for confined animal farming operations, 2002-current.
- Harter, T., *Member*, CALFED Panel on Appropriate Water Measurement in Agriculture, 2001-2004.

Technical/Scientific Conference Presentations:

- Harter, T., "Nitrate in California Groundwater: Current Issues", California Groundwater Resources Asssociation Annual Meeting, Orange, CA, 9/18/2002.
- Harter, T., "Nitrate in California Groundwater: Current Issues", Lawrence Livermore National Laboratory, Seminar Series, 10/2/2002.
- Harter, T., "Multiscale Assessment of Nonpoint Source Pollution in Groundwater: The Dairy Case", USGS Menlo Park Seminar Series, 10/24/2002.
- Harter, T., Moderator, "Nitrogen Cycling and Chemistry", California Groundwater Resources Association, Groundwater Nitrate Conference, 11/13/2002.
- Harter, T., Y. S. Onsoy, "Geostatistical Interpolation of Field Data in Three-dimensions to Assess Nitrate Leaching to Groundwater", European Geophysical Society Annual Meeting, Nice, France, 4/10/2003.
- Harter, T., "Multi-scale Assessment and Monitoring of Nonpoint Source Pollution in Groundwater", Advanced International Workshop on Strategies for Controlling and Predicting Transport of Contaminants to Groundwater from the Unsaturated Zone, Ravello, Italy, 4/14/2003.
- Harter, T., J. W. Hopmans, "Role of Vadose zone flow processes in regional scale hydrology", Conference on Unsaturated Zone Modeling: Progress, Challenges and Applications, Wagening, The Netherlands, 10/5/2004.
- Harter, T., "Dairies and Groundwater Quality: Monitoring and Assessment", Department of Environmental Sciences, University of California, Riverside, 11/2004.
- Onsoy, S. Y., et al., "Assessment of long-term nitrate transport to groundwater in a deep alluvial unsaturated zone", American Geophysical Union Annual Meeting, San Francisco, 12/14/2004.
- Harter, T., S. Y. Onsoy, "Agricultural Nitrogen Leaching: Fate and Transport in Deep Alluvial Unsaturated Zones", Symposium on Nitrogen Eutrophication in Xeric Wildland

and Agricultural Systems, 23rd Plant Biology Symposium, University of California, Riverside, January 19-20, 2005.

- Harter, T., "Vadose zone flow processes in regional scale hydrology", Workshop on Upscaling in Porous Media, Utrecht, The Netherlands, July 11-13, 2005.

REFERENCES

Allen, R. G., L. S. Pereira, D. Raes, and M. Smith, 1998. FAO Irrigation and Drainage Paper. No. 56. Crop evapotranspiration. FAO of the United Nations, 300 pp.

Avanidou, T., and E. K. Paleologos, 2002. Infiltration in stratified, heterogeneous soils: Relative importance of parameters and model variations. *Water Resour. Res.*, 38(11): 14-1 - 14-15.

Bear, J., 1972. Dynamics of Fluid in Porous Media. Elsevier, New York, 764 pp.

Biggar, J. W., and D. R. Nielsen, 1978. Field monitoring of soil water constituents in the unsaturated zone. *In*: L. G. Everett and K. D. Schmidt (eds.) Establishment of Water Quality and Monitoring Programs. Proc. Am. Water Resources Assoc., San Francisco, Ca. 12-14 June 1978. Tech. Publ. Ser. No. TPS79-1. Am. Water Resour. Assoc., Minneapolis, MN, p. 106-121.

Berthouex, P. M., and L. C. Brown, 1994. *Statistics for Environmental Engineers*. CRS Press Inc., 335 pp.

Blaney, H. F., 1944. Evapo-transpiration. Presented at the Soil Conversation Meeting, Pasadena, California.

Blaney, H. F., and W. D. Criddle, 1950. Determining consumptive use and irrigation water requirements, Agr. Research Service, U.S. Dept. of Agr., Technical Bull. No. 1275.

Bresler, E. G., and G. Dagan, 1979. Solute transport in unsaturated heterogeneous soil at field scale 2. Applications. *Soil. Sci. Soc. Am. J.*, 43: 467-472.

Böhlke, J. -K., 2002. Groundwater recharge and agricultural contamination. *Hyrogeology J.*, 10: 153-179.

Bonilla, C. A., J. F. Munoz, and M. Vauclin, 1999. Opus simulation of water dynamics and nitrate transport in a field plot. *Ecol. Model.*, 122: 69-80.

Brisson, N. B. Seguin, and P. Bertuzzi, 1992. Agrometeorological soil water mass balance for crop simulation model. *Agric. For. Meteorol.*, 59: 267-287.

Brooks, R. H., and A. T. Corey, 1964. Hydraulic properties of porous media. Hydrol. Pap. 3. Colo. State Univ., Fort Collins, 27 pp.

Carsel, R.F., J.C. Imhoff, P.R. Hummel, J.M. Cheplick, and A.S. Jr. Donigian, 1998. PRZM-3: A Model for Predicting Pesticide and Nitrogen Fate in the Crop Root and Unsaturated Soil Zones: Users Manual for Release 3.0.

Chen, Z., R. S. Govindaraju, and M. L. Kavvas, 1994. Spatial averaging of unsaturated flow equations under infiltration conditions over areally heterogeneous fields 2. Numerical simulations. *Water Resour. Res.*, 30(2): 535-548.

Celia, M. A., E. T. Bouloutas, and R. L. Zarba, 1990. A general mass-conservative numerical solution for the unsaturated flow equation. *Water Resour. Res.*, 26(7): 1483-1496.

Clausnitzer V., J. W. Hopmans, and D. R. Nielsen, 1992. Simultaneous scaling of soil-water retention and hydraulic curves. *Water Resour. Res.*, 28(1): 19-31.

Clausnitzer, V., and J. W. Hopmans, 1994. Simultaneous modeling of transient three-dimensional root-growth and soil-water flow. *Plant Soil*, 164(2): 299-314.

Close, M. E., J. P. C. Watt, and K. W. Vincent, 1999. Simulation of picloram, atrazine, and simazine transport through two new zealand soils using LEACHM. *Aust. J. Soil Res*., 37: 53-74.

Close, M. E., L. Pang, G. N. Magesan, R. Lee, and S. R. Green, 2003. Field study of pesticide leaching in an allophanic soil in New Zealand. 2: Comparison of simulations from four leaching models. *Aust. J. Soil Res*., 41(5): 825-846.

Cushman, J. H., L. S. Bennethum, and B. X. Hu, 2002. A primer on upscaling methods for porous media. *Adv. Water Resour*., 25: 1043-1067.

Dagan, G., V. Cvetkovic, and A. Shapiro, 1992. A solute flux approach to transport in heterogeneous formations 1. Theoretical general framework. *Water Resour. Res.*, 28(4): 369-1376.

Dalton, F. N., P. A. C. Raats, and W. R. Gardner, 1975. Simultaneous uptake of water and solutes by plant roots. *Agron. J*., 67: 334-339.

Davis, L. A., and P. S. Neuman, 1983. Documentation and user's guide: UNSAT2 - Variably saturated flow model, Final Report, WWWL / TM - 1791 -1, Water, Waste & Land, Inc., Ft. Collins, Colorado.

Day, K. R., H. L. Andris, R. H. Beede, K. M. Klonsky, R. L. De Moura, and P. Livingston, 2000. Sample Costs to Establish A Peach/Nectarine Orchard and Produce. UC Cooperative Extension.

Dean, J. D., P. S. Huyakorn, A. S. Donigian, K. A. Jr. Voos, R. W. Schanz, J. Meeks, and R. F. Carsel, 1989. Risk of unsaturated/saturated transport and transformation of chemical concentrations (RUSTIC) Volume I: Theory and code verification. EPA/600/3-89/048a. U.S. EPA, Environmental Research Laboratory, Athens, GA.

De Marsily, G., 1986. Quantitative Hydrogeology. Academic Press, San Diego, 440 pp.

Denton, M. A., 2004. Hydraulic Characterization of a Heterogeneous, Deep vadose Zone Beneath an Orchard in the Eastern San Joaquin Valley. M.S. Thesis. University of California, Davis.

Deutsch, C. V., and A. G. Journel, 1992. *GSLIB: Geostatistical Software Library and User's Guide*. Oxford University Press, New York, 340 pp.

De Rooij, G. H., 2000. Modeling fingered flow of water in soils owing to wetting front stability: a review.*J. Hydrol.*, 231-232: 277-294.

Destouni, G., 1992. Prediction uncertainty in solute flux through heterogeneous soil. *Water Resour. Res.*, 28(3): 793-801.

Doorenbos, J. and W. O. Pruitt, 1977. Crop water requirements. Rev. 1977. FAO Irrig. And Drain. Paper 24, FAO of the United Nations, Rome, 144 pp.

Dust, M., N. Baran, G. Errera, J. L. Hutson, C. Mouvet, H. Schafer, H. Vereecken, A. Walker, 2000. Simulation of water and solute transport in field soils with the LEACHP model. *Agric. Water Manag*., 44: 225-245.

Ellsworth, T. R., W.A. Jury, F. F. Ernst, and P. J. Shouse, 1991. A three-dimensional field study of solute transport through unsaturated layered porous media, 1. Methodology, mass recovery and mean transport. *Water Resour. Res.*, 27(5): 951-965.

Feddes, R. A., P. J. Kowalik, K. K. Malinka, and H. Zaradny, 1976. Simulation of field water uptake by plants using a soil water dependent root extraction function.*J. Hydrol.*, 31(1-2): 13-26.

Feddes, R. A., P. J. Kowalik, and H. Zaradny, 1978. Simulation of Field Water Use and Crop Yield. Simulation Monographs, Pudoc, Wageningen, The Netherlands, 188 pp.

Foussereau, X., W. D. Graham, G. A. Akpoji, G. Destouni, and P. S. C. Rao, 2000. Stochastic analysis of transport in unsaturated heterogeneous soils under transient flow regimes. *Water Resour. Res.*, 36(4): 911-921.

Freeze, R. A., 1975. A stochastic-conceptual analysis of one-dimensional groundwater flow in nonuniform homogeneous media. *Water Resour. Res.*, 11(5): 725-741.

Flury, M., H. Flühler, W. A. Jury, and J. Leuenberger, 1994. Susceptibility of soils to preferential flow of water: A field study. *Water Resour. Res.*, 30(7): 1945-1954.

Gardner, W. R., 1958. Some steady state solutions of unsaturated moisture flow equations with application to evaporation froma water table. *Soil Sci*., 85(4): 228-232.

Gardner, W. R., 1960. Dynamic aspects of water availability to plants. *Soil Sci*., 89: 63-73.

Gardner, W. R., 1964. Water movement below the root zone, paper presented at the 8th International Congress on Soil Science. Int. Soc. of Soil Sci., Bucharest, Romania.

Gelhar, L. W., 1986. Stochastic Subsurface Hydrology: from theory to applications. *Water Resour. Res.*, 22(9): 135S-145S.

Gego, E. L., G. S. Johnson, and M. Hankins, 2001. An evaluation of methodologies for the generation of stochastic hydraulic conductivity fields in highly heterogeneous aquifers. *Stochastic Environ. Res. Risk Assessment*, 15(1): 47-64.

Ghodrati, M., W. A. Jury, 1990. A field-study using dyes to characterize preferential flow of water. *Soil Sci. Soc. Am. J*., 54: 1558-1563.

Glass, R. J., T. S. Steenhuis, and J. -Y. Parlange, 1988. Wetting front instability as a rapid and far-reaching hydrologic process in the vadose zone. *J. Contam. Hydrol*., 3: 207-226.

Glass, R. J., T. S. Steenhuis, and J. -Y. Parlange, 1989. Mechanism for finger persistence in homogeneous, unsaturated, porous media: theory and verification. *Soil Sci*., 148: 60-70.

Glass, R. J., J. -Y. Parlange, and T. S. Steenhuis, 1991. Immesible displacement in pororus media: stability analysis of three-dimensional, axisymmetric disturbances with application to gravity-drven wetting front instability. *Water Resour. Res.*, 27(8): 1947-1956.

Hanks, R. J., 1991. Soil Evaporation and transpiration. *In* R.J. Hanks and J.T. Ritchie (Eds.) *Modeling Plant and Soil Systems*, p. 245-260.

Harter, T., 1994. Unconditional and Conditional Simulation of Flow and Transport in Heterogeneous, Variably Saturated Porous Media. Ph.D. Dissertation. University of Arizona.

Harter, T., and T. -C. J. Yeh, 1996. Stochastic analysis of solute transport in heterogeneous, variably saturated soils. *Water Resour. Res.*, 32(6): 1585-1595.

Harter, T., and T. -C. J. Yeh. 1998. Flow in vadose random porous media nonlinear numerical analysis and comparison to analytical stochastic models. *Adv. Water Resour*., 22(2): 257-272.

Haverkamp R, M. Vaclin, J. Touma, P. J. Wierenga, and G. Vachaud, 1977. A comparison of numerical simulation models for one-dimensional infiltration. *Soil Sci. Soc. Am. J*., 41: 285-294.

Haverkamp, R., and M. Vauclin, 1979. A note on estimating finite difference interblock hydraulic conductivity values for transient unsaturated flow problems. *Water Resour. Res.*, 15(1): 181-187.

Healy, R. W., 1990, Simulation of solute transport in variably saturated porous media with supplemental information on modifications to the U.S. Geological Survey's Computer Program VS2D: U.S. Geological Survey Water-Resources Investigations Report 90-4025, 125 pp.

Hills, R. G., D. B. Hudson, I. Porro, and P. J. Wierenga, 1989. Modeling one-dimensional infiltration into very dry soils. 2. Estimation of soil water parameters and model predictions. *Water Resour. Res.*, 25(6): 1271-1282.

Hills, R. G., P. J. Wierenga, D. B. Hudson, and M. R. Kirkland, 1991. The second Las Cruces trench experiment: Experimental results and two-dimensional flow predictions. *Water Resour. Res.*, 27(10): 2707-2718.

Hills, R. G., K. A. Fisher, M. R. Kirkland, and P. J. Wierenga, 1994. Application of flux-corrected transport to the Las Cruces Trench site. *Water Resour. Res.*, 30(8): 2377-2385.

Hoffman, G. J., and M. Th.van Genuchten, 1983. Soil properties and efficient water use: water management for salinity control. *In*: H.M. Taylor, H.M., W.A. Jordan, and T.R. Sinclair (eds.) Limitations to Efficient Water Use in Crop Production. American Society of Agronomy, Madison, Wisconsin, p. 73-85.

Hopmans, J. W., H. Schukking, P. J. J. F. Torfs, 1988. Two-dimensional steady state unsaturated water flow in heterogeneous soils with autocorrelated soil hydraulic properties. *Water Resour. Res.*, 24(4): 2005-2017.

Hopmans, J. W., and K. L. Bristow, 2002. Current capabilities and future needs of root water and nutrient uptake modeling. *In*: D.L. Sparks (ed.) Advances in Agronomy, Vol. 77, Academic Press, p. 105-183.

Hughes, K. A., P. W. Gandar, and H. N. de Silva, 1995. Exploration and exploitation of soil by apple, kiwifruit, peach, Asian pear, and grape roots. *Plant and Soil*, 175: 301-309.

Huyakorn, P.S., and G.F. Pinder, 1983. Computational Methods in Subsurface Flow. Academic Press, London, United Kingdom

Huyakorn, P.S. and J.E. Buckley, 1989. SAFTMOD: Saturated zone flow and transport two-dimensional finite element model. HydroGeoLogic, Inc., Herndon, VA.

Jensen, K. H., and A. Mantaglou, 1992. Application of stochastic unsaturated flow theory, numerical simulations, and comparisons to field observations. *Water Resour. Res.*, 28(1): 269-284.

Jensen, M. E., R. D. Burman, and R. G. Allen, 1990. Evapotranspiration and irrigation requirements. Manuals and reports on engineering practice. No. 70. Am. Soc. Civil Eng., New York.

Johansen N. B., J. C. Imhoff, J. L. Jr. Kittle, and A. S. Donigian, 1984. Hydrological Simulation Program-Fortran (HPSF): User's Manual for Release 8. EPA-600/3-84-066, US Environmental Protection Agency, GA.

Jury, W. A., 1982. Simulation of solute transport using a transfer-function model. *Water Resour. Res.*, 18(2): 363-368.

Khaleel, R., T. -C. J. Yeh, Z. Lu, 2002. Upscaled flow and transport properties for heterogeneous unsaturated media. *Water Resour. Res.*, 38(5): 1053, doi:10.1029/2000WR000072.

Kool, J. B., J. C. Parker, and M. TH.van Genuchten, 1985. Determining soil hydraulic properties from one-step outflow experiments by parameter estimation. I. Theory and numerical study. *Soil Sci. Soc Am. J.*, 49: 1348-1354.

Lafolie, F., L. Bruckler, and A. M. de Corkborne, 1997. Modeling the water transport and nitrogen dynamics in irrigated salad crops. *Irrig. Sci.*, 17: 95-104.

Laroche, A. M., J. Gallichand, R. Lagace, and A. Pesant, 1996. Simulating atrazine transport With HSPF in an agricultural watershed. *J. Environ. Eng. ASCE*, 122: 622-630.

Lappala, E. G., R. W. Healy, and E. P. Weeks, 1987. Documentation of computer program VS2D to solve the equations of fluid flow in variably saturated porous media: US Geological Survey Water-Resources Investigations Report 83-4099, 184 pp.

Mailhol, J. C., P. Ruelle, and I. Nemeth, 2001. Impact of fertilization practices on nitrogen leaching under irrigation. *Irrig. Sci.*, 20(3): 139-147.

Malone, R. W., R. C. Warner, S. R. Workman, and M. E. Byers, 1999. Modeling surface and subsurface pesticide transport under three field conditions Using PRZM-3 and GLEAMS. *Trans. ASAE*, 42: 1275-1287.

McCord, J. T., C. A. Gotway, and S. H. Conrad, 1997. Impact of geologic heterogeneity on recharge estimation using environmental tracers: Numerical modeling investigation. *Water Resour. Res.*, 33(6): 1229-1240.

Molz, F. J., and I. Remson, 1970. Extraction term models of soil moisture use by transpiring plants. *Water Resour. Res.*, 6: 1346-1356.

Molz, F.J., 1981. Models of water transport in the soil-plant system: A review. *Water Resour. Res.*, 17(5): 1245-1260.

Monteith, J. L., 1965. Evaporation and environment. *In*: G.E. Fogg (ed.) The Sate and Movement of Water in Living Organisms. Academic Press, New York, N.Y., p. 205-234.

Mualem, Y., 1976. A new model for predicting the hydraulic conductivity of unsaturated porous media. *Water Resour. Res.*, 12(3): 513-522.

Mullins, J. A., R. F. Carsel, J. E. Scarbrough, A. M. Ivery, 1993. PRZM-2, A Model for Predicting Pesticide Fate in the Crop Root and Unsaturated Soil Zones: User Manual for Release 2.0. U.S. EPA, Environmental Research Laboratory, Athens, GA. EPA/600/R-93/046, 379 pp.

Nimah, M. N., and R. J. Hanks, 1973. Model for estimating soil water, plant, and atmospheric interrelations. I. Description and sensitivity. *Soil Sci. Soc Am. J.*, 37: 522-527.

Nimmo, J.R., J.A. Deason, J.A. Izbicki, and Peter Martin, 2002. Evaluation of unsaturated zone water fluxes in heterogeneous alluvium at a Mojave Basin Site. Water Resour. Res., 38(10), 1215, doi:10.1029/2001WR000735.

Nye, P. H., and F. H. Marriott, 1969. Theoretical study of the distribution of substances around roots resulting from simultaneous diffusion and mass flow. *Plant Soil*, 3: 459-472.

Parker, M. L., and J. R. Meyer, 1996. Peach tree vegetative and root growth respond to orchard floor management. *Hortscience*, 31(3): 330-333.

Penman, H.L., 1948. Natural evaporation from open water, bare oil, and grass. Proc. Roy. Soc. London England, A193, 120-146.

Polmann, D. J., D. Mckaughlin, S. Luis, L. W. Gelhar, and R. Ababou, 1991. Stochastic modeling of large-scale flow in heterogeneous unsaturated soils. *Water Resour. Res.*, 27(7): 1447-1458.

Rassam, D., J. Simunek, and M.Th. van Genuchten, 2003. *Modeling Variably Saturated Flow with HYDRUS-2D*. 1st edition. ND Consult, Brisbane, Australia.

Rekolainen, S., V. Gouy, R. Francaviglia, O. -M. Eklo, I. Barlund, 2000. Simulation of soil water, bromide and pesticide behavior in soil with the GLEAMS model. *Agric. Water Manag*., 44: 201-226.

Ritchie, J. T., 1972. A model for predicting evaporation from row crop with incomplete cover. *Water Resour. Res.*, 8(5): 1204-1213.

Ritsema, C. J., L. W. Dekker, J. M. H. Hendrickx, and W. Hamminga, 1993. Preferential flow mechanism in a water repellent sandy soil. *Water Resour. Res.*, 29(7): 2183-2194.

Ritsema, C. J., L. W. Dekker, J. L. Nieber, T. S. Steenhuis, 1998. Modeling and field evidence of finger formation and finger recurrence in a water repellent sandy soil. *Water Resour. Res.*, 34(4): 555-567.

Rockhold, M. L., C. S. Simmons, and M. J. Fayer, 1997. An analytical solution technique for one-dimensional, steady vertical water flow in layered soils. *Water Resour. Res.*, 33(4): 892-902.

Roth, K., W. A. Jury, H. Fluhler, and W. Attinger, 1991. Transport of chloride through a vadose field soil. *Water Resour. Res.*, 27(10): 2533-2541.

Roth, K., and K. Hammel, 1996. Transport of conservative chemical though an unsaturated two-dimensional Miller-similar medium with steady state flow. *Water Resour. Res.*, 32(6): 1653-1663.

Rubin, J., 1968. Theoretical analysis of two-dimensional, transient flow of water in unsaturated and partly unsaturated soils. *Soil Sci. Soc Am. J.*, 32: 607-615.

Rudolph, D. L., R. G. Kachanoski, M. A. Celia, D. R. LeBlanc, and J. H. Stevens, 1996. Infiltration and solute transport experiments in unsaturated sand and gravel, Cape Cod, Massachusetts: Experimental design and overview of results. *Water Resour. Res.*, 32(3): 519-532.

Russo, D., 1988. Determining soil hydraulic properties by parameter estimation: On the selection of a model for the hydraulic properties. *Water Resour. Res.*, 24: 453-459.

Russo, D., 1991. Stochastic analysis of simulated vadose zone solute transport in a vertical cross section of heterogeneous soil during nonsteady water flow. *Water Resour. Res.*, 27(3): 267-283.

Russo, D., 1993. Stochastic modeling of macrodispersion for solute transport in a heterogeneous unsaturated porous formation. *Water Resour. Res.*, 29(2): 383-397.

Russo, D., and G. Dagan, 1991. On solute transport in a heterogeneous porous formation under saturated and unsaturated water flows. *Water Resour. Res.*, 27(3): 285-292.

Russo, D., E. Bresler, U. Shani, and J. C. Parker, 1991. Analyses of infiltration events in relation to determining soil hydraulic-properties by inverse problem methodology. *Water Resour. Res.*, 27(6): 1361-1373.

Russo, D., and M. Bouton, 1992. Statistical analysis of spatial variability in unsaturated flow parameters. *Water Resour. Res.*, 28(7): 1911-1925.

Russo, D., J. Zaidel, and A. Laufer, 1994. Stochastic analysis of solute transport in partially saturated heterogeneous soil 1. Numerical experiments. *Water Resour. Res.*, 30(3): 769-779.

Russo, D., J. Zaidel., and A. Laufer, 1998. Numerical analysis of flow and transport in a three-dimensional partially saturated heterogeneous soil. *Water Resour. Res.*, 34(6): 1451-1468.

Qui, G.Y., K. Momii, T. Yano, and R. J. Lascano, 1999. Experimental verification of a mechanistic model to partition evapotranspiration into soil water and plant evaporation. *Agric. For. Meteorol*., 93: 79-93.

Schmalz, B., B. Lennartz, M. Th.van genuchten, 2003. Analysis of unsaturated water flow in a large sand tank. *Soil Sci*., 168(1): 3-14.

Scheidegger, A.L., 1960. The Physics of Flow through Porous Media. University of Toronto Press. Toronto.

Scotter, D. R., and R. W. Tillman, 1991. Movement of solutes associated with intermittent soil-water flow 1. Tritium and bromide. *Aust. J. Soil Res*., 29(2): 175-183.

Selker, J. S., T. S. Steenhuis, and J. Y. Parlange, 1992. Wetting front instability in homogeneous sandy soils under continuous infiltration. *Soil Sci. Soc Am. J.*, 56: 1346-350.

Selker, J. S., T. S. Steenhuis, and J. Y. Parlange, 1996. An engineering approach to fingered vadose zone pollutant transport. *Geoderma*, 70: 197-206.

Simunek, J., K. Huang, and M. Th.van Genuchten, 1995. The SWMS_3D Code for Simulating Water Flow and Solute Transport in Three-Dimensional Variably-Saturated Media. Version 1.0. Research Report No. 139, US Salinity Laboratory, USDA, ARS, Riverside, California.

Simunek, J., T. Vogel, and M. Th.van Genuchten, 1996. HYDRUS-2D Code for Simulating Water Flow and Solute Transport in Two-Dimensional Variably Saturated Media. Version 1.0. US Salinity Laboratory USDA/ARS, Riverside, CA. and IGWMC-TPS 53. Golden, Colorado School of Mines

Simunek, J., M. Sejna, and M. TH.van Genuchten, 1998. HYRDUS-1D Software Package for Simulating the One-Dimensional Movement of Water, Heat, and Multiple Solutes in Variably-Saturated Media. Version 2.0. US Salinity Laboratory Agricultural Research Service, US Department of Agriculture Riverside, California.

Simmons, C. S., 1982. A stochastic-convective transport representation of dispersion in one-dimensional porous-media systems. *Water Resour. Res.*, 18(4): 1193-1214.

Smith, S. J., and D. K. Cassel, 1991. Estimate nitrate leaching in soil materials. *In* R.F. Follett, D.R. Keeney, and R.M. Cruse (eds.) Managing Nitrogen for Groundwater Quality and Farm Profitability. Soil Sci. Soc. Am. Madison, Wisconsin.

Smith, L., and F. W. Schwartz, 1981. Mass transport 2. Analysis of uncertainty in prediction. *Water Resour. Res.*, 17(2): 351-369.

Somma, F., V. Clausnitzer, and J. W. Hopmans, 1998. Modeling of transient three-dimensional soil water and solute transport with root growth and water and nutrient uptake. *Plant Soil*, 202: 281-293.

Sposito, G., W. A. Jury, V. K., Gupta, 1986. Fundamental problems in the stochastic convection-dispersion model of solute transport in aquifers and field soils. *Water Resour. Res.*, 22(1): 77-88.

Spurlock, F., 1998. Evaluation of Current Simulation Models to Predict Pesticide Movement to Ground and Surface Water Under California Conditions. Environmental Hazards assessment Program. Department of Pesticide Regulation, Sacramento, California.

Steenhuis, T., K. Vandelheuvel, K.W. Weiler, J. Boll, J. Daliparthy, S. Herbert, and K. -J. S. Kung, 1998. Mapping and interpreting soil textural layers to assess agri-chemical movement at several scales along the eastern seabord (USA). Nutrient Cycling in Agroecosystems, 50: 91-97.

Sudicky, E. A., 1986. A natural gradient experiment on solute transport in a sand aquifer: Saptial variability of hydraulic conductivity and its role in the dispersion process. *Water Resour. Res.*, 22: 2069-2082.

Synder, R. L., B. J. Lanini, D. A. Shaw, and W. O. Pruitt, 1989a. Using reference evapotranspiration (ET_o) and crop coefficients to estimate crop evapotranspiration (ET_c) for agronomic crops, grasses, and vegetable crops. Cooperative Extension, University of California, Berkeley, Leaflet No. 21427, 12 pp.

Synder, R.L., B.J. Lanini, D.A. Shaw, and W.O. Pruitt, 1989b. Using reference evapotranspiration (ET_o) and crop coefficients to estimate crop evapotranspiration (ET_c) for trees and vines. Cooperative Extension, University of California, Berkeley, Leaflet No. 21428, 8 pp.

Tartakovsky, D. M., S. P. Neuman, and Z. Lu, 1999. Conditional stochastic averaging of steady-state unsaturated flow by means of Kirchhoff transformation. *Water Resour. Res.*, 35(3): 731-745.

Tagliavini, M., D. Scdellazi, B. Marangoni, and M. Toselli, 1996. Nitrogen fertilization management in orchards to reconcile productivity and environemtnal aspects. Fert. Res., 43: 93-102.

Tompson, A. F. B. and L. W. Gelhar, 1990. Numerical simulation of solute transport in three-dimensional randomly heterogeneous porous media. *Water Resour. Res.*, 26(10): 2541-2562.

Trevisan, M., G. Errera, G. Goerlitz, B. Remy,and P. Sweeney, 2000. Modelling ethoprophos and bentazone fate in a sandy humic soil with primary pesticide fate model PRZM-2. Agric. Water Manag., 44: 317-335.

Troiano, J., C. Garretson, C. Krauter, J. Brownell, and J. Huston, 1993. Influence of amount and method of irrigation water application on leaching of atrazine. *J. Environ. Qual*., 22(2): 290-298.

Ünlü K., D. R. Nielsen, and J. W. Biggar, 1990. Stochastic analysis of vadose flow: One-dimensional Monte Carlo simulations and comparisons with spectral perturbation analysis and field observations. *Water Resour. Res.*, 26(9): 2207-2218.

Ünlü, K., G. Ozenirler, and C. Yurteri, 1999. Nitrogen fertilizer leaching from cropped and irrigated sady soil in Central Turkey. *Eur. J. Soil Sci*., 50: 609-620.

van Genuchten, M. T., 1980. A closed form of equation for predicting the hydraulic conductivity of unsaturated soils. *Soil Sci. Soc Am. J.*, 44: 892-898.

van Genuchten, M. T., 1987. A numerical model for water and solute movement in and below the root zone. Research Report. No 121. US Salinity Lab, ASR USDA, Riverside. CA.

Vauclin, M., J. Khanji, G. Vachaud, 1979. Experimental and numerical study of a transient, two dimensional unsaturated-saturated water table recharge problem. *Water Resour. Res.*, 15(5): 1089-1101.

Vrugt, J.A., M. T. van Wijk, J. W. Hopmans, and J. Simunek, 2001. One-, two-, and three-dimensional root water uptake functions for transient modeling. *Water Resour. Res.*, 37(10): 2457-2470.

Vogel, T., Cislerova, M., 1988. On the reliability of unsaturated hydraulic conductivity calculated from the moisture retention curve. *Trans. Porous Media*, 3: 1-15.

Vogel, T. and M. Cislerova, 1988. On the reliability of unsaturated hydraulic conductivity calculated from the retention curve. *Trans. Porous Media*, 3: 1-15.

Vogel , T., M. Cislerova, and J. W. Hopmans, 1991. Porous media with linearly variable hydraulic properties. *Water Resour. Res.* 27(10): 2735-2741.

Vogel , T., M. Th.van Genuchten, and M. Cislerova, 2001. Effect of the shape of the soil hydraulic functions near saturation on variably-saturated flow predictions. *Adv. Water Resour*., 24: 133-144.

Vogel, H. J., and K. Roth, 2003. Moving through scales of flow and transport in soil. *J. Hydrol*., 272(1-4): 95-106.

Vogeler, I., S. R. Green, D. R. Scotter, and B. E. Clothier, 2001. Measuring and modeling the transport and root uptake of chemicals in the unsaturated zone. *Plant Soil*, 231: 161-174.

Yeh, T. -C., and D. J. Harvey, 1990. Effective unsaturated hydraulic conductivity of layered sands. *Water Resour. Res.*, 26(6): 1271-1279.

Yeh, T. -C. J., R. Srivastava, A. Guzman, and T. Harter, 1993. A numerical model for water flow and chemical transport in variably saturated porous media. *Ground Water*, 31(4): 634-644.

Yeh, T. -C. J., 1998. Scale Issues of Heterogeneity in Vadose Zone Hydrology. *In:* G. Sposito (ed.) Scale Dependence and Scale invariance in Hydrology. Cambridge University Press, p. 224-265.

Wagenet, R. J., and J. L. Hutson, 1989. LEACHM: A process-based Model for Water and Solute Movements, Transformations, Plant Uptake and Chemical Reactions in the Unsaturated Zone, Version 2.0., Vol. 2., New York State Water Resources Institute, Cornell University, Ithaca, NY.

Wang, Z., J. Feyen, and C. J. Ritsema, 1998. Susceptibility and predictability of conditions for preferential flow. *Water Resour. Res.*, 34(9): 2169-2182.

Wang, Z., A. Tuli, and W. A. Jury, 2003a. Unstable flow during distribution in homogeneous soil. *Vadose Zone J.*, 2: 52-60.

Wang, Z., L. Wu, T. Harter, J. Lu, and W. A. Jury, 2003b. A field study of unstable preferential flow during soil water redistribution. *Water Resour. Res.*, 39(4), 1-1 – 1-11.

Wang, Z., W.A. Jury, A. Tuli, and D. Kim, 2004. Unstable flow during redistribution: Controlling factors and practical implications. *Soil Sci. Soc Am. J.*, 3: 549-559.

Weinbaum, S. A., R. S. Johnson, and T. M. DeJong, 1992. Causes and consequences of overfertilization in orchards. Proceedings of the Workshop Fertilizer Management in Horticultural Crops: Implications for Water Pollution Hort Technology, 2(1): 112-119.

Wierenga, P. J., R. G. Hills, and D. B. Hudson, 1991. The Las Cruces trench site: Characterization, experimental results, and one-dimensional flow predictions. *Water Resour. Res.*, 27(10): 2695-2705.

Wildenschild, D., and K. H. Jensen, 1999. Laboratory investigations of effective flow behavior in unsaturated heterogeneous sands. *Water Resour. Res.*, 35(1): 17-27.

Zhu, J. and B. P. Mohanty, 2002a. Analytical solutions for steady state vertical infiltration. *Water Resour. Res.*, 38(8), 1145, doi:10.1029/2001WR000398.

Zhu, J. and B. P. Mohanty, 2002b. Upscaling of soil hydraulic properties for steady state evaporation and infiltration. *Water Resour. Res.*, 38(9), 1178, doi:10.1029/2001WR000704.

APPENDIX 1:

Reprint of

Onsoy, Y. S., T. Harter, T. R. Ginn, W. R. Horwath, 2005. Spatial variability and transport of nitrate in a deep alluvial vadose zone. Vadose Zone J. 4:41-55.

Reproduced from Vadose Zone Journal. Published by Soil Science Society of America. All copyrights reserved.

Spatial Variability and Transport of Nitrate in a Deep Alluvial Vadose Zone

Yuksel S. Onsoy, Thomas Harter,* Timothy R. Ginn, and William R. Horwath

ABSTRACT

Little empirical evidence exists about the spatial distribution of NO_3–N in deep vadose zones and about the associated fate and transport of NO_3–N between the root zone and the water table. We investigated NO_3–N occurrence in a deep alluvial vadose zone and its relation to geologic site characteristics, hydraulic properties, and fertilizer application rates via an intensive three-dimensional core-sampling campaign beneath an irrigated orchard in semiarid Fresno County, California. Statistical and geostatistical analyses were used to determine spatial variability of NO_3–N and water content, to estimate total NO_3–N mass in the vadose zone beneath each of three fertilizer treatments, and to compare NO_3–N occurrence with that predicted from standard agronomic analysis of N and water flux mass balances. Vadose zone NO_3 was highly variable and lognormally distributed. Fertilizer treatment had a significant effect on NO_3–N levels in the vadose zone. In all cases, deep vadose zone N mass estimated by kriging measured data totaled only one-sixth to one-third of the mass predicted by the N and water flux mass balance approach. Vadose zone denitrification estimates could not account for this discrepancy. Instead, the discrepancy was attributed to highly heterogeneous flux conditions that were not accounted for by the mass-balance approach. The results suggest that spatially variable vadose zone flow conditions must be accounted for to better estimate the potential for groundwater NO_3 loading.

Intensive use of agrochemicals such as fertilizers and pesticides has been recognized as a major source of nonpoint source pollution. Subsurface NO_3 transport is of particular interest because of the widespread application of inorganic and manure based NO_3 fertilizers. Highly mobile and persistent, NO_3 has become a primary groundwater pollutant (USEPA, 1990; Lunn and Mackay, 1994; Bransby et al., 1998; Ling and El-Kadi, 1998). Between 1945 and 1993, the use of NO_3 in commercial fertilizers in the USA increased 20-fold (Puckett, 1995). In semiarid regions with intensive irrigated agricultural production (e.g., in California and the southwestern USA), conflicts between water scarcity and NO_3 groundwater pollution have further highlighted concerns about soil N management (Owens et al., 1992).

Driven in part by pollution prevention measures that attempt to optimize the use of fertilizers, N budgeting methods for specific crop–fertilizer application scenarios have been widely used in agronomy to determine the fate of N in soils and the potential for N leaching to groundwater (Tanji and Gupta, 1978; Frissel et al., 1981; Legg and Meisinger, 1982; Willigen and Neeteson, 1985). These methods are driven by experimental studies of N cycling processes that have almost exclusively focused on the uppermost soil horizon (0–30 cm, Paustian et al., 1990; Tindall et al., 1995; Watkins and Barraclough, 1996; Simek and Kalcik, 1998; Sharmasakkar et al., 1999) or on the root zone (0–1.8 m, Lafolie et al., 1997; Trettin et al., 1999; de Vos et al., 2000; Allaire-Leung et al., 2001; Stenger et al., 2002). Some experiments examined the annual N budget with intensive field investigations, but were not of long enough duration for a proper assessment of the effects of land management practices on groundwater quality (e.g., Paustian et al., 1990; Aronsson, 2001).

Critical gaps remain in our understanding of the influence of the vadose zone *below* the root zone, where it exists, on the estimation of N loading to aquifers (Ling and El-Kadi, 1998). Mechanisms involved in N transfer in the (deep) vadose zone below the root zone are rarely measured. The dearth of information about the deeper vadose zone results partly from the misconception that little chemical and biological activities occur below the root zone (i.e., below 0.3–1.8 m) (Pionke and Lowrance, 1991; Krug and Winstanley, 2002), but the vadose zone of many agricultural regions is considerably deeper and may contain appreciable amounts of organic matter (OM) or NO_3 or both (Stevenson, 1986). Nitrate well below 1.8 m may be available to some plants (Smith and Cassel, 1991). Furthermore, denitrification between the root zone and the water table may significantly reduce N loading to groundwater, although this is difficult to quantify (Rees et al., 1995). Our current understanding of NO_3 fate and transport below the root zone is further limited by prohibitive experimentation costs (e.g., Rees et al., 1995), by potentially long travel times through deep vadose zones, and perhaps most importantly, by a large degree of spatial variability.

Spatial variability is caused by spatially variable water and N application rates (i.e., external variability) and by spatially variable vadose zone hydraulic and chemical properties (i.e., intrinsic variability). Both may lead to highly nonuniform distribution of NO_3 and other agrochemicals (Rao and Wagenet, 1985; Mohanty and Kanwar, 1994). Past studies have quantified spatial variability of NO_3 by geostatistical methods, but only within the root zone of agricultural field soils (Dahiya et al., 1984; Tabor et al., 1985; White et al., 1987; van Meirvenne and Hofman, 1989; Istok et al., 1993; Cambardella et al., 1994; Hofman et al., 1994; Mohanty and Kanwar, 1994; Sharmasakkar et al., 1999; Allaire-Leung et al., 2001; Ilsemann et al., 2001; Stenger et al., 2002).

Equivalent field work on the spatial variability and storage of NO_3 in the deep vadose zone (below the root zone) and analysis of its relationship to field-scale N mass balance and NO_3 leaching into groundwater has,

Y.S. Onsoy1, T. Harter, T.R. Ginn, and W.R. Horwath, Department of Land, Air, and Water Resources, One Shields Avenue, University of California, Davis, CA 95616-8628. Received 26 Apr. 2004. Original Research Paper. *Corresponding author (ThHarter@ucdavis.edu).

Published in Vadose Zone Journal 4:41–54 (2005).
© Soil Science Society of America
677 S. Segoe Rd., Madison, WI 53711 USA

Abbreviations: BNF, biological N fixation; K–S, Kolmogorov–Smirnov; MB, mass balance; OM, organic matter.

Reproduced from Vadose Zone Journal. Published by Soil Science Society of America. All copyrights reserved.

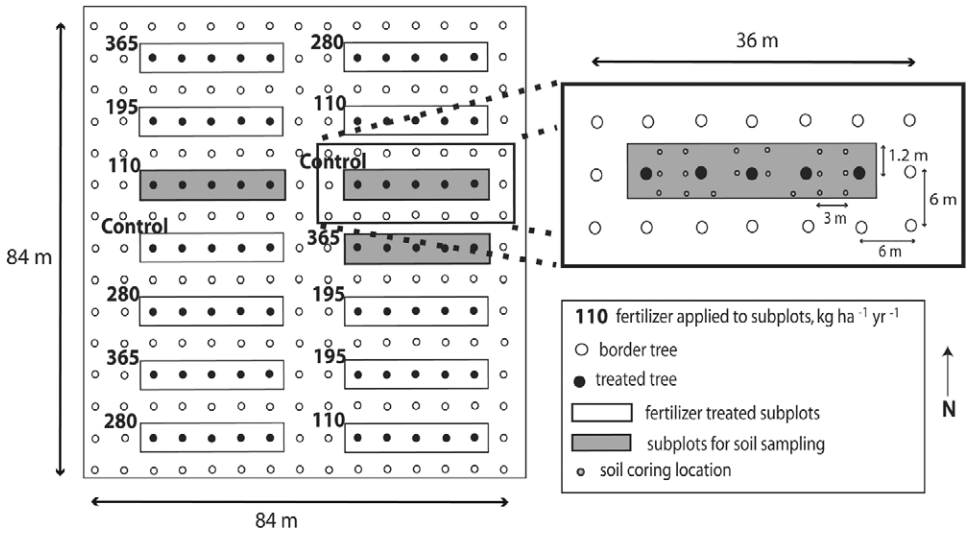

Fig. 1. The field experiment design showing the locations of five different fertilizer treatments at the project site. Three subplots with the 0, 110, and 365 kg N ha^{-1} yr^{-1} treatments were selected for vadose zone sampling. The three subplots were named "control," "standard," and "high," respectively.

to our knowledge, not yet been attempted. The goal of our work is therefore to provide a detailed field analysis of NO_3 occurrence in a deep alluvial vadose zone, its relationship to the geologic and hydraulic characteristics of the vadose zone and to fertilizer management, and to discuss the implications of our findings with respect to common interpretations of vadose zone data.

Recognizing that the study is site specific, we do not make a strong claim that our results can be quantitatively transferred to other sites and situations. However, the general site conditions (alluvial soils, semiarid Mediterranean climate, irrigated crops) are representative of many important agricultural regions around the globe. The fundamental conditions at the study site, namely the strong heterogeneity of the NO_3 distribution, the lack of significant denitrification, and the strong control of the heterogeneous hydraulic and flow conditions on the NO_3 distribution are therefore not unique to this site and provide universal insight into "real" deep vadose zones. Therefore, findings from this site provide important evidence for the fate and transport of NO_3 in deep vadose zones in general. In particular, we hope that studies like the one presented here will provide a useful basis for developing guidance on the role of monitoring devices in the deep vadose zone.

In the following, we give a brief description of the site and the experimental methods. We then implement a conventional field-scale root zone water and N mass balance (MB) analysis to estimate NO_3–N leaching from the root zone and to provide a predictive framework for the assessment of deep vadose zone NO_3–N. A statistical analysis of the measured water content and NO_3–N distribution is used to separate deterministic large-scale spatial variability that can be explained by depth, N treatment, and discrete lithofacies zonation from random smaller-scale spatial variability. For the nondeterministic residuals, we develop appropriate geostatistical models of the deep vadose zone water content and NO_3–N data to estimate the total deep vadose zone NO_3–N mass. In the discussion, we compare this estimate with the total NO_3–N mass predicted from the MB analysis to evaluate the deep vadose zone NO_3 fate and transport processes and the role of spatial variability in assessing potential NO_3 leaching to groundwater.

METHODS

Field Site

The site is a flood-irrigated, 0.8 ha (2 acres) 'Fantasia' nectarine [*Prunus persica* (L.) Batsch var. *nucipersica* (Suckow) C.K. Schneid. 'Fantasia'] orchard at the University of California Kearney Agricultural Center (http://www.uckac.edu), located 20 km southeast of Fresno, CA, on the Kings River alluvial plain (elevation: 103 m above sea level). The site has a semiarid, Mediterranean climate.

Fertilizer Treatments

Planted in 1975, the matured orchard was subject to a 12-yr fertilizer trial that began in September 1982. A complete random block design was used (Fig. 1) with application rates of 0, 110, 195, 280, or 365 kg N ha^{-1} yr^{-1} in several replicates. Fertilizer was broadcast in September of each year at a rate of 110 kg N ha^{-1} to all rows except the control treatments (0 kg N ha^{-1} yr^{-1}). During the following spring, the 195, 280, and 365 kg N ha^{-1} yr^{-1} treatments received additional applications at a rate of 85 kg N ha^{-1} (or 75 lb ac^{-1}) once, twice, and three times, respectively, to achieve the desired annual fertilization rate. In the first year, $(NH_4)_2SO_4$ was applied. To prevent soil acidification, NH_4NO_3 (33.5% N content) and $Ca(NO_3)_2$ (15.5% N content) were used throughout the remainder of the study. There was no application of fertilizer in 1995. In September 1996, 110 kg N ha^{-1} was applied throughout the entire orchard including the control plots in the usual broadcast application method. Vadose zone water quality analysis was not part of the original project's scope.

Irrigation and Climate Measurements

Flood irrigation dates were obtained from farm records at the Kearney Agricultural Center. Irrigation records indicate

Reproduced from Vadose Zone Journal. Published by Soil Science Society of America. All copyrights reserved.

that the approximate amount of applied water was 13.4 cm ha^{-1} (5.3 in ac^{-1}) per irrigation. Depending on spring precipitation patterns, 9 to 16 irrigations (average of 13 irrigations) were applied to the orchard each year. Daily reference evapotranspiration and precipitation data were measured at a California Irrigation Management Information System climate field station located within 1 km from the site. Crop evapotranspiration was computed from the product of the daily reference evapotranspiration rates and crop coefficients, k_c, for nectarine orchards (California Department of Water Resources, 2000). Over the past 20 yr, annual precipitation ranged from 160 to 490 mm, while groundwater levels during that period fluctuated between 12 and 20 m below ground surface.

Yield and Plant Nitrogen Uptake

The nectarine orchard blossoms in mid- to late February immediately before leafing out. Fruit ripening is completed by July. Using standard methods, crop yield (fruit weight) and leaf N concentrations were measured in 1983 through 1985 and in 1991 through 1994. Fruit N concentrations were only measured in 1983 (Johnson et al., 1995).

Vadose Zone Sampling

In 1997, three subplots with the 0, 110, and 365 kg N ha^{-1} yr^{-1} treatments were selected for sampling (Fig. 1). For convenience, the three subplots are named "control," "standard," and "high," respectively, throughout the text. Between July and October 1997, 60 undisturbed continuous soil cores were drilled with a Geoprobe Systems (Salina, KS) direct-push drilling rig to a depth of 15.8 m (52 ft), including 18 cores from each subplot (Fig. 1). Cores were obtained in approximately 1.2-m sections (4 ft), their sedimentologic characteristics were described, and then the cores were sampled. More than 1000 soil samples of 22.5 cm long and 4 cm in diameter were taken at 30- to 60-cm intervals depending on stratification. Subsamples were prepared and preserved for later analysis. During the drilling phase, groundwater was detected at approximately 16 m below the ground surface.

Vadose Zone Textures

The entire vadose zone at the site consists of unconsolidated sediments deposited on a stream-dominated alluvial fan. The textural groups range from clay and clayey paleosol hardpans to a wide range of silt and sand, including occasional coarse sand and gravel sediments. Coarse-grained materials are believed to represent channel deposits embedded within finer-grained floodplain and levee deposits. Sandy loam is the most common textural unit in the profile while clay was the least (48 and 8% of the vertical profile length, respectively). Ten major stratigraphic units were identified based on texture, color, and cementation and are referred to as "lithofacies." They exhibit vertically varying thicknesses, yet are laterally continuous across the experimental site. The measured saturated hydraulic conductivity data, best described by a lognormal distribution, indicate high hydraulic variability at the local scale (10^{-2}–10^{-1} cm, for details see Minasny et al., 2004).

Soil Water Content and Nitrate

Gravimetric water content θ_{dw} (g g^{-1}) was determined using measured values of oven-dried (105°C for 24 h) 1.25-cm (1/2-in)-long samples. Bulk density was measured on 119 core samples and varied from 1.3 to 1.9 g cm^{-3}, with an average of 1.6 g cm^{-3}. However, core samples, particularly finer-textured samples, were subject to variable compression during coring. Therefore, a more representative constant bulk density ρ_b of 1.45 g cm^{-3} (Hausenbuiller, 1985) and the measured values of θ_{dw} were used to compute volumetric water content θ (m^3 m^{-3}). Regardless of the specific number used for bulk density, the potential error introduced is small (<10%) compared with the large range of observed NO_3 concentrations (see below).

Nitrate concentration was measured in 0.5 *M* K_2SO_4 soil extractions (5/1 ratio, 1-h reciprocal shaking) prepared from 809 core subsamples sieved through a 1-mm screen (Horwath and Paul 1994). Soil extracts were analyzed by automated flow-injection colorimetry following the methods of the USEPA 353.2 (Wendt, 1999). At each subplot, the smallest horizontal sampling interval varied between 1.2 to 3 m (10 and 4 ft, respectively, Fig. 1). The average vertical sampling interval was approximately 0.6 m (2 ft). Two hundred twenty-four sample concentrations were below the limit of detection (LOD = 10^{-3} mg L^{-1} = 10^{-3} g m^{-3}) and recorded as zero. Measured values were converted to aqueous concentrations NO_3–N_{aq} in units of grams per cubic meter (or equivalently μg mL^{-1}), using measured water content data. Both, θ and NO_3–N_{aq} measurements contribute to the N mass estimate and are therefore both included in the statistical analysis. Results of core analyses for θ and NO_3–N_{aq} are summarized in Table 1.

FIELD-SCALE WATER AND NITROGEN FLUXES: NITROGEN BUDGET

The principle method for analyzing and predicting the NO_3 leaching potential is a field- or plot-scale MB analysis coupled with a simple uniform steady-state flow model. We applied the method to provide a basis of comparison for the amount of NO_3–N in the deep vadose zone from the three subplots. The vadose zone was conceptually divided into two compartments: soil root zone and deep vadose zone (Fig. 2). The root zone is considered to be 1.8 m (6 ft) deep. Approximately 90% of the tree roots in the nectarine orchard are contained in this zone, with some roots to depths of 3 m (6–10 ft). Individual roots are expected to grow as long as 6 to 9 m (20–30 ft) horizontally (Scott Johnson, personal communication, 2004). The deep vadose zone is bounded by the soil root zone at the top and the water table at the 15.8-m depth. A long-term root zone N mass balance yields annual NO_3–N leaching, $N_{leaching}$, from the root zone into the deep vadose zone:

$$N_{leaching} = N_{input} - N_{uptake} - N_{transformation} - \Delta N \qquad [1]$$

where N_{input} is the total N input to the root zone, N_{uptake} is the N used for plant uptake, $N_{transformation}$ is the N loss through various N transformations in the root zone other than N leaching, and ΔN is the change in the total amount of N (organic and inorganic) stored in the root zone. $N_{leaching}$ is equivalent to the long-term potentially leachable N (LPLN) described in Meisinger and Randall (1991).

Nitrogen Storage Changes

When soil, climate, and management factors are constant for an extended time (5–20 yr), annual mineralization of N from soil OM has been found to be approximately equivalent to organic N returned to the soil in crop residues plus microbial immobilization (Legg and Meisinger, 1982; Stevenson, 1982). Hence, annual changes in N storage reach a quasi-steady state, $\Delta N \approx 0$ (Meisinger and Randall, 1991). Warm, semiarid climate conditions with irrigation further accelerate the time required for a system to reach quasi-steady-state conditions with respect to annual N storage changes. The 12-yr duration of the fertilizer treatment was considered sufficient to assume that annual N storage changes were negligible ($\Delta N = 0$).

Reproduced from Vadose Zone Journal. Published by Soil Science Society of America. All copyrights reserved.

Table 1. Basic statistics of water content θ, nitrate–nitrogen NO_3–N_{aq}, and logtransformed NO_3–N_{aq}. The number of samples measured for water content are: 339 in the control, 391 in the standard, and 310 in the high subplot. During the data quality check, 27 water content samples were removed due to inconsistencies (10 from both the control and standard subplots and 7 from the high subplot), which reduced the number of samples used in geostatistical analysis to 1013. Also shown are basic statistics of NO_3–N_{aq} and logtransformed NO_3–N_{aq} categorized by subplots.

Data	Subplot	No. of data	Mean	Min.	Max.	Variance	SD	CV	Mean	Variance	Skewness
θ, $cm^3\ cm^{-3}$	–	1183	0.23	0.004	0.59	0.015	0.12	–	–	–	0.50
NO_3–N_{aq} w/ND, $g\ m^{-3}$†	–	809	3.28	0	129.72	62.74	7.92	–	–	–	9.51
NO_3–N_{aq} w/o ND, $g\ m^{-3}$‡	–	585	4.54	0.04	129.72	81.10	9.00	–	–	–	8.55
$lnNO_3$–N_{aq} w/ND, $g\ m^{-3}$†	–	809	−0.70	−4.61	4.87	6.97	2.63	–	–	–	−0.53
$lnNO_3$–N_{aq} w/o ND, $g\ m^{-3}$‡	–	585	0.80	−3.24	4.87	1.54	1.24	–	–	–	−0.46
NO_3–N_{aq} w/ND, $g\ m^{-3}$†	control	204	3.73	–	–	80.64	8.98	241%	–	–	–
	standard	406	2.10	–	–	20.79	4.56	217%	–	–	–
	high	199	5.22	–	–	123.99	11.13	213%	–	–	–
NO_3–N_{aq} w/o ND, $g\ m^{-3}$‡	control	158	4.82	–	–	99.00	9.95	207%	–	–	–
	standard	277	3.08	–	–	27.48	5.24	170%	–	–	–
	high	150	6.93	–	–	152.86	12.36	178%	–	–	–
$lnNO_3$–N_{aq} w/ND, $g\ m^{-3}$†	control	204	−0.51	–	–	6.40	2.53	NA§	NA§	NA§	–
	standard	406	−1.06	–	–	6.69	2.59	NA§	NA§	NA§	–
	high	199	−0.15	–	–	7.57	2.75	NA§	NA§	NA§	–
$lnNO_3$–N_{aq} w/o ND, $g\ m^{-3}$‡	control	158	0.69	–	–	1.91	1.38	240%§	5.17§	153.66§	–
	standard	277	0.59	–	–	1.22	1.11	155%§	3.31§	26.11§	–
	high	150	1.30	–	–	1.41	1.19	176%§	7.43§	170.66§	–

† Including nondetects, ND, which are set to zero for NO_3–N_{aq} data and to half the limit of detection (−4.605) for $lnNO_3$–N_{aq}.
‡ Excluding nondetects.
§ Sample NO_3–N_{aq} mean, m, and variance, s^2, estimated from mean, μ, and variance, σ^2, of the logtransformed dataset: $m = \exp(\mu + 0.5\ \sigma^2)$ and $s^2 = m^2[\exp(\sigma^2) - 1]$. Coefficient of variation estimated for NO_3–N_{aq} sample mean and variance. NA: No estimates were computed from $lnNO_3$–N_{aq} data with the nondetects included at −4.605 because the bimodal distribution of that dataset violates the normality assumption.

Nitrogen Inputs

Annual N inputs included fertilizer applications, and N received from irrigation, precipitation, dry deposition, and nonsymbiotic N_2 fixation. Table 2 lists average annual N inputs and margin of errors (95% confidence intervals) in the N mass balance analysis (e.g., Berthouex and Brown, 1994). Average NO_3–N concentration in irrigation water was 4 $g\ m^{-3}$ (Harter et al., 1999). Long-term average annual irrigation N input is therefore 70 kg N $ha^{-1}\ yr^{-1}$. A margin of error of ±10% primarily accounts for the lack of precise irrigation flow measurements and also for measurement errors of the NO_3–N concentration.

Wet and dry depositions and biological N fixation at the site are considered secondary N inputs because of their small contribution to the N budget. Wet and dry depositions were estimated as 2 and 14 kg N $ha^{-1}\ yr^{-1}$, respectively, based on data collected by the California Acid Deposition Monitoring Program at the nearest monitoring stations to our site, Lindcove, Tulare County and Bakersfield, Kern (e.g., Blanchard and Tonnessen, 1993; Mutters, 1995). Biological N fixation (BNF) is small due to readily available N, low OM, and the lack of plant growth that supports N-fixing bacteria fertilization. Stevenson (1982) reported BNF inputs to be in the range of 2 to 7 kg N $ha^{-1}\ yr^{-1}$.

Nitrogen Plant Uptake and Transformations

In the first year of the experiment, there were no significant differences in yield or average fruit weight among the subplots. In the second and third years, the control subplot dropped off in both yield and fruit size, but then remained at about the same level for the duration of the experiment. The 7-yr average yield was 36, 51, and 48 t ha^{-1} for the control, standard, and high subplots, respectively, indicating a negative response of the high subplot to overfertilization. Nitrogen content in dry fruit measured in 1983 was 0.71, 1.51, and 2.05% for the control, standard, and high subplots, respectively. Nitrogen uptake estimates are based on 7-yr average annual crop yield and the dry matter fruit N content measured in 1983:

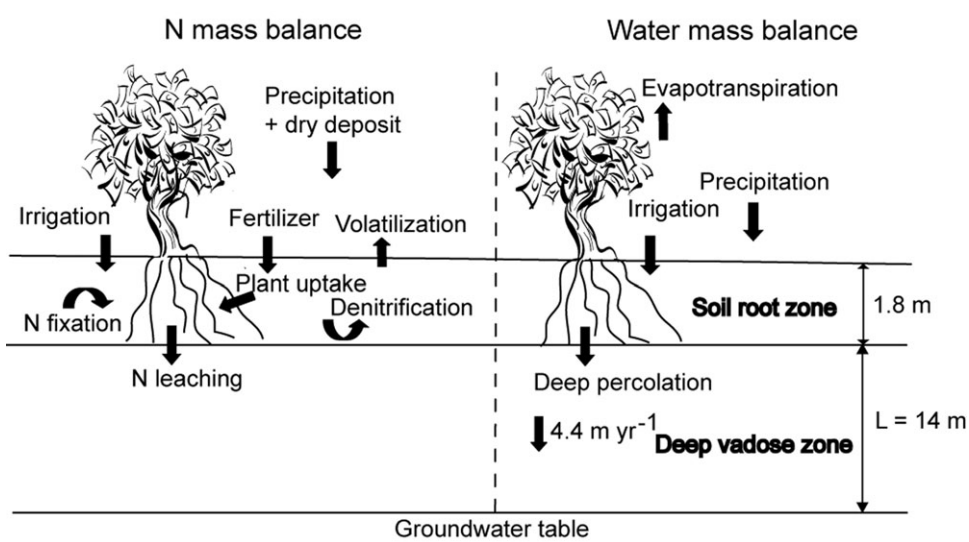

Fig. 2. A schematic representation of the components of the N budget and water mass balance.

Reproduced from Vadose Zone Journal. Published by Soil Science Society of America. All copyrights reserved.

Table 2. Root zone water balance, root zone N mass balance, and deep vadose zone N storage estimation by the mass balance method. The 95% confidence intervals are given in parentheses. For computed results, confidence intervals were obtained by standard, linear error analysis (Berthouex and Brown, 1994). Confidence intervals for deep vadose zone storage were computed at the lower and upper 95% confidence intervals for the mean travel time through the deep vadose zone, given the confidence intervals of $N_{leaching}$ and recharge.

	Control	Standard	High	All 3 subplots
Root zone water balance				
Irrigation I, cm yr^{-1}				174 (157/192)
Precipitation P, cm yr^{-1}				33 (32/35)
Evapotranspiration ET, cm yr^{-1}				98 (93/103)
Recharge = $I + P$ − ET, cm yr^{-1}				110 (91/128)
Root zone N balance				
Primary inputs				
Fertilizer appl., kg ha^{-1} yr^{-1}†	0	110	365	
Irrigation, kg ha^{-1} yr^{-1}†	70 (56/84)	70 (56/84)	70 (56/84)	
Secondary inputs				
Precipitation + dry deposit, kg ha^{-1} yr^{-1}‡	16 (11/21)	16 (11/21)	16 (11/21)	
Nonsymbiotic N fixing, kg ha^{-1} yr^{-1}‡	5 (2/7)	5 (2/7)	5 (2/7)	
Total, kg ha^{-1} yr^{-1}	91	201	456	
Primary outputs (transformations)				
Plant N uptake, kg ha^{-1} yr^{-1}†	25 (19/37)	77 (65/82)	98 (74/112)	
NH_3 losses, kg ha^{-1} yr^{-1}‡	–	11 (2/22)	37 (7/73)	
Denitrification, kg ha^{-1} yr^{-1}‡	9 (2/27)	20 (4/60)	46 (9/137)	
Secondary outputs				
Soil erosion + surface runoff, kg ha^{-1} yr^{-1}	–	–	–	
Total, kg ha^{-1} yr^{-1}	34	108	181	
ΔN change in organic/inorganic N pool, kg ha^{-1} yr^{-1}	–	–	–	
$N_{leaching}$ = inputs − outputs + ΔN, kg ha^{-1} yr^{-1}	57 (36/78)	93 (59/127)	275 (228/322)	
Potentially leachable N (LPLN) risk	low	medium	high	
Deep vadose zone N storage				
Measured, kg ha^{-1}	48 (42/62)	36 (33/47)	87 (79/107)	
Predicted for 1997, kg ha^{-1}	218 (130/334)	261 (147/427)	478 (271/784)	

† Measured.
‡ Estimated from literature reference values.

$$N_{uptake} = (\text{annual yield} \times 10\%) \times (\%N_{content}/100) \quad [2]$$

where 10% is the dry matter content in the fresh fruit. In the absence of multiyear measurements, fruit N concentrations (but not yield) were assumed to vary proportional to leaf N content (Scott Johnson, personal communication, 2004), which remained practically constant throughout the experiment. Annual yields varied among the 7 yr that N leaf content was measured. The measured range of annual yields provided a conservative basis for estimating the 95% confidence interval of the long-term average annual N uptake (Table 2).

Nitrogen in tree leaves is considered to be completely recycled into the root zone. Losses due to soil erosion and surface runoff are negligible since the ground surface at the orchard is flat and the basin irrigation system (surface flooding) generates no surface water return flow.

Denitrification and NH_3 losses were estimated from previous experimental studies (Meisinger and Randall, 1991) that took into account various controlling site conditions (e.g., irrigation, drainage, climate, soil OM, and pH). The observed range of 6 to 20% N loss from denitrification is consistent with the experimental findings of Dowdell and Webster (1984), who reported N loss of 2 to 19% during a long-term N balance study, but lower than the 15 to 30% loss estimates reported by Allison (1966) and Hauck (1981). We adopted an average N loss of 10% of N_{inputs} with the error margins equal to the range of reported loss percentages (2–30%, Table 2). Neutral to slightly acidic soil pH conditions at the site (not shown here) keep NH_3 volatilization at a minimum (Paustian et al., 1990). Average volatilization losses are approximately 10% with error margins equivalent to those of denitrification (Table 2) (Meisinger and Randall, 1991).

Water Mass Balance and Deep Vadose Zone Nitrogen

The average annual water budget, as illustrated in Fig. 2, is (Martin et al., 1991)

$$R = I + P - \text{ET} \quad [3]$$

where R (m yr^{-1}) is the average annual deep percolation (recharge) from the root zone, and I, P, and ET (m yr^{-1}) are average annual irrigation, precipitation, and (crop) evapotranspiration amounts for the 12 yr from 1984 to 1995. In the deep vadose zone, water flux is typically assumed to be at steady state and equal to the average water leaching rate from the root zone.

For predictive purposes, we applied a commonly used simple one-dimensional uniform steady-state flow concept. Average NO_3–N concentration (g m^{-3}) in the 14-m-deep vadose zone was obtained by multiplying annual NO_3–N leaching loss from the root zone with the recharge rate R. The total amount of NO_3–N (kg ha^{-1}) contained within the deep vadose zone was computed by multiplying the annual NO_3–N leaching loss, $N_{leaching}$, with the average time of travel, τ, through the deep vadose zone, where $\tau = 14\text{ m} \times \theta_{avg}/R$, and θ_{avg} is the average reported field capacity (25%) for the dominant soil texture (Martin et al., 1991).

STATISTICAL AND GEOSTATISTICAL ANALYSIS

Statistical Analysis

Statistical analysis was used to determine sample distributions and to identify deterministic factors controlling the spa-

Reproduced from Vadose Zone Journal. Published by Soil Science Society of America. All copyrights reserved.

tial variability of water content θ and NO_3–N_{aq}. Factors considered included depth, *N* treatments, and lithofacies distribution.

Depth-dependent trends were determined using a separate regression analysis of the θ and logtransformed NO_3–N_{aq} for each subplot treatment. After removing trends, a Kolmogorov–Smirnov (K–S) test (e.g., Davis, 1986; Olea, 1999) was used to test normality of the θ and logtransformed NO_3–N_{aq} distribution. The effects of subplot treatment (three groups: control, standard, and high) and lithofacies (10 sample groups, one for each lithofacies), and their interactions (30 groups) on θ and $\ln NO_3$–N_{aq}, were measured by a sigma-restricted ANOVA with effective hypothesis decomposition (Hocking, 1985) to account for the unbalanced design (unequal number of samples between groups). Homogeneity of variance was assumed if the ratio of the largest to smallest group standard deviation did not exceed 3. Where significant effects were observed ($p < 0.05$), Newman-Keuls and Duncan's multiple range tests were performed for post-hoc pair-wise comparison of means. Nitrate-N samples below the LOD were not included in the significance analysis. To check for potential bias from exclusion of nondetects, a nonparametric Kruskal–Wallis ANOVA was performed on the bimodally distributed dataset with nondetect samples recorded at one-half the LOD concentration (see below). A Kruskal–Wallis test was also performed to test for significant effects of subplot and vertical location on the probability of nondetects (using an indicator variable of 1 for "non-detects" and 0 for "detects"). All statistical analyses were performed with the Statistica software (Statsoft, 2002).

Geostatistical Analysis of Water Content and Nitrate Data

After trends were removed and appropriate variable transformations were done based on the results of the statistical analysis, geostatistical analysis was used (i) to quantify the amount of spatial variability in the θ and NO_3–N distributions unexplained by depth, treatment, and lithofacies location; (ii) to characterize differences in the NO_3–N distribution among the three different fertilizer treatments; and (iii) to quantify the field-scale N loading rate to groundwater from those local-scale measurements. The correlation coefficient between NO_3–N_{aq} and θ was −0.11; hence, θ and NO_3–N_{aq} were considered uncorrelated for purposes of the geostatistical analysis. Due to a large number of nondetect NO_3 concentrations, two sets of experimental NO_3–N_{aq} semivariograms were computed for the complete dataset and for the dataset that excluded nondetects.

Directional (horizontal and vertical), nested spherical semivariograms were fitted to the observed semivariograms by initially using a manual calibration followed by a least square optimization process (e.g., Davis, 1986; Olea, 1999). Directional semivariograms were constructed with appropriate lag intervals that were assigned according to average horizontal and vertical sampling scheme (Fig. 1).

Ordinary block kriging (Deutsch and Journel, 1992) was applied to estimate average volumetric block values of $\ln NO_3$–N_{aq} and residual (i.e., trend-removed) θ from their point measurements. The kriging domain size for each subplot was x = 24 m, y = 3 m, and z = 16 m (80, 10, and 53 ft, respectively), discretized into blocks with Δx = 0.75 m, Δy = 0.3 m, and Δz = 0.15 m.

RESULTS

Field-Scale Water and Nitrogen Balance: Long-Term Potentially Leachable Nitrogen

As expected, LPLN increases with N application rates since crop N uptake consumes only part of the increased amount of N fertilizer (Table 2). The LPLN computed for the high subplot represents a potentially high risk for groundwater pollution (Meisinger and Randall, 1991). The net percolating water to below the root zone (R) is 1.1 (±0.2) m yr^{-1} (Table 2), reflecting the low irrigation efficiency of the flood irrigation. The margin of error stems mostly from the large uncertainty about the mean irrigation rate, which was much larger than that for precipitation or crop evapotranspiration. The estimated net annual mean vertical solute travel distance is 4.4 (±0.8) m (θ_{avg} = 25%) and the mean travel time to groundwater, τ, is 3.2 (2.8–3.8) yr (Fig. 2). At τ = 3.2 yr, field-scale N concentration in the leachate (and recharge) is predicted to be 5, 9, and 25 g m^{-3} for the control, standard, and high subplots, respectively. Corresponding deep vadose zone N storage is predicted to be 180, 300, and 880 kg N ha^{-1}, respectively. For 1997, the deep vadose zone storage can be computed by considering that all subplots were subject to the "control" leaching rate in 1995 (no fertilizer application) and to the "standard" leaching rate in 1996 (uniform standard fertilizer application). Then, the predicted deep vadose zone N storage at the time of drilling in 1997 is 220, 260, and 480 kg N ha^{-1}. The wide confidence intervals for the deep vadose zone N storage, summarized in Table 2, reflect potential errors in both the recharge and the LPLN computation.

Statistical Analysis of Water Content and Nitrate Distribution

Water Content

Measured water content data follow an approximately symmetric, normal distribution (Table 1). Within all subplots water content is characterized by a significant linear increase with depth. Separate linear trend models were fit to each subplot dataset, as illustrated in Fig. 3. Trend residuals are shown to be normally distributed with K–S differences insignificant at the p = 0.1 significance level. Trends are essentially identical between the three subplots.

Water content residuals are significantly controlled by lithofacies (ANOVA testing, $p < 0.05$). Multiple range tests suggest that the thick sand S unit at approximately the 6- to 9-m depth is significantly drier (Fig. 3). Similarly, although only few samples were available, the clay and silt-textured C unit (from 2.75–3 m) and a clay-textured unit in Var3 (from 9–9.75 m) were found to be significantly wetter than the other lithofacies. Differences reflect varying field capacity between coarse, intermediate, and fine-textured lithofacies.

Nitrate

The NO_3–N_{aq} distribution is highly skewed (Fig. 4a) and lognormal (significance level, $p < 0.05$) after excluding nondetect samples (Fig. 4b). Resulting sample means (estimated from the moments of the logtransformed data, Table 1) are 5.2, 3.3, and 7.4 g m^{-3} for the control, standard, and high subplots, respectively. Detectable NO_3–N_{aq} concentrations range from 0.04 to 129.72 g m^{-3}

Reproduced from Vadose Zone Journal. Published by Soil Science Society of America. All copyrights reserved.

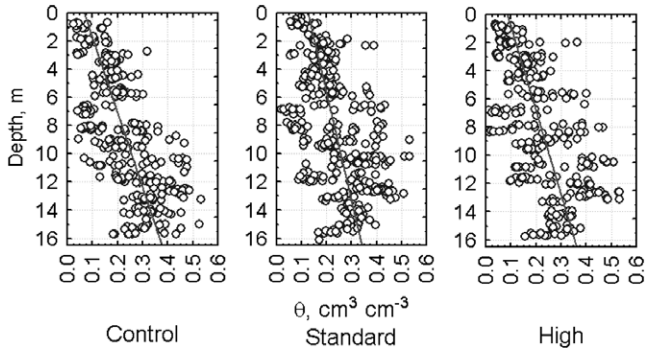

Fig. 3. Scatter plots of water content with depth for each subplot. Line represents linear regression models for the trend defined as a function of depth. Equations for the trends are $\theta_C = 0.069 + 0.019z$ for the control subplot (a correlation coefficient of $r^2 = 0.48$), $\theta_S = 0.127 + 0.013z$ for the standard subplot ($r^2 = 0.25$), and $\theta_H = 0.087 + 0.017z$ for the high subplot ($r^2 = 0.36$).

(Table 1). Of the samples with detectable concentrations, 21% measure <1 g m^{-3} and 10% exceed the maximum contamination level for drinking water (10 g m^{-3}). Significant differences exist between subplots. In the high subplot, the fraction of low NO_3–N_{aq} measurements is less than one-third of the fraction observed in the other two subplots. On the other hand, most of the high concentration samples, exceeding 10 g m^{-3}, are found in the high subplot, while only a small fraction (8%) of these are found below the root zone of the control plot.

Figure 5a shows the profiles of lithofacies-specific mean lnNO_3–N_{aq} in the three subplots. The lithofacies effect represents the combined influence of depth and sediment texture on NO_3–N_{aq} since the lithofacies are sorted in vertical sequence. At all three subplots, the highest average NO_3–N_{aq} levels occur in the root zone to approximately 3 m, which is mostly comprised of a fine sandy loam lithofacies (SL1). Below SL1, NO_3–N_{aq} concentrations are lower, but no significant vertical trends or contrasts were observed. The high subplot shows the largest NO_3–N_{aq} mean concentrations throughout most of the profile, which is consistent with the higher fertilizer applications. Differences between the control and standard subplot means are not significant. Coefficients of variation for each subplot range from 1.6 to 2.4 (Table 1) and similarly for individual lithofacies and lithofacies X subplot groups.

Almost one-third of the samples (28% of all samples) have nondetectable levels of NO_3–N_{aq} (Fig. 5b): 22% of the control, 32% of the standard, and 25% of the high subplot, and from 13% to 50% for individual facies. The fewest nondetects were observed at depths below 12 m (SL2, HP2) (Fig. 5b). The highest fractions of nondetects occurred in the coarse-textured, sandy lithofacies Var1, in the hardpan HP1, and in the sand lithofacies S, where approximately one-half of the samples had nondetectable levels of NO_3–N_{aq}.

Because of the large number of nondetects, replacing nondetects with a default value of −4.605 (one-half of the LOD) leads to a bimodal lnNO_3–N_{aq} distribution; the LOD for NO_3–N_{aq} is significantly lower than the extent of the left tail of the lnNO_3–N_{aq} distribution in Fig. 4b. In other words, the number of nondetects (224)

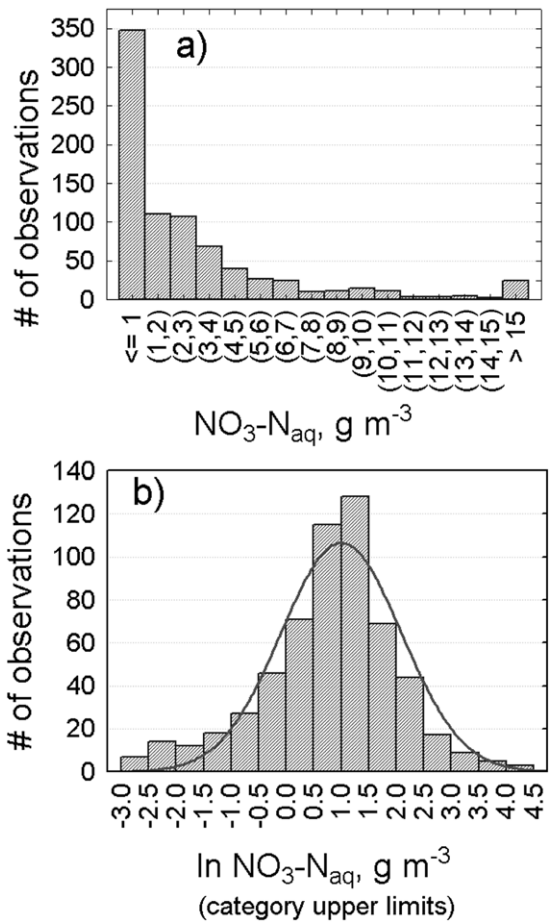

Fig. 4. (a) Frequency distribution of NO_3–N_{aq} (g m^{-3} = μg mL^{-1}) (includes 224 nondetects in the left-most class). (b) Logtransformed NO_3–N_{aq} data fitted to a normal distribution with a mean of 1.0 and variance of 1.095 (does not include nondetects).

far exceeds the (small) number that would be expected if the fitted lognormal distribution of Fig. 4b is considered to be censored to the left. Because of the large number of nondetects, the first two sample moments of lnNO_3–N_{aq} strongly depend on the concentration specified for nondetects (here one-half of LOD). Effectively then, the mean and variance become a measure of the mid-point and spread between the mode of the detect group and the level specified for the nondetect group (Table 1).

Geostatistical Analysis of Water Content and Nitrate Distribution

Separate water content and NO_3 semivariograms were computed for each subplot. Data density was not sufficient to derive well-structured separate semivariogram models for individual lithofacies within each subplot. But by applying a thin vertical bandwidth (<15 cm) in the search window, horizontal semivariograms were computed for data pairs containing only points within the same lithofacies (e.g., Deutsch and Journel, 1992).

Water Content

Semivariograms of the water content trend residuals exhibit not only a significant geometric anisotropy (un-

Reproduced from Vadose Zone Journal. Published by Soil Science Society of America. All copyrights reserved.

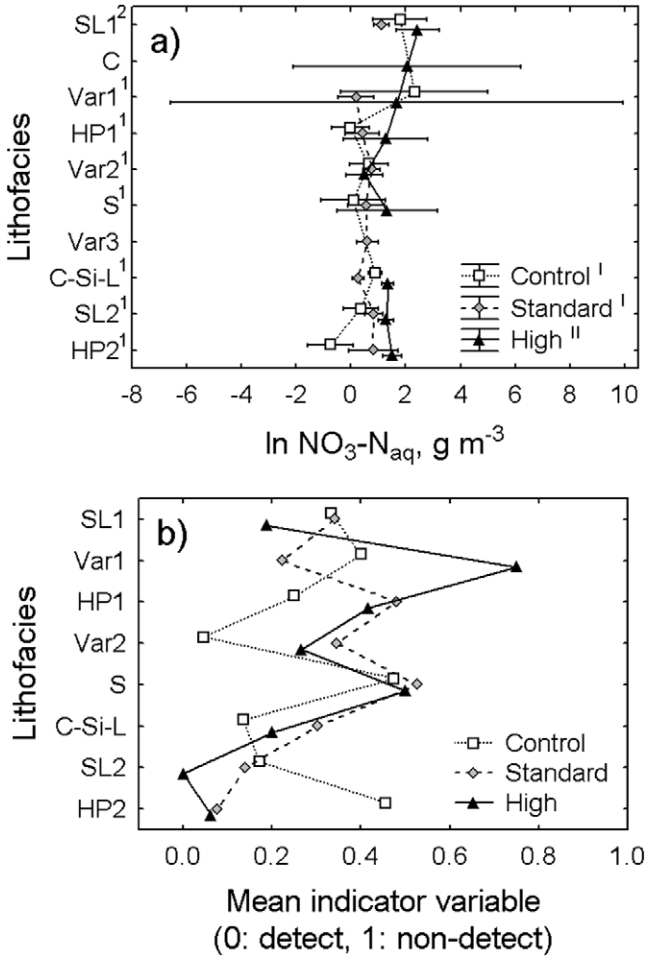

Fig. 5. (a) Facies X subplot group means and 95% confidence intervals for natural logtransformed NO_3–N_{aq} (g m^{-3}), not including nondetect samples. Facies are sorted in vertical sequence followed by their average depth interval in meters given in parentheses: SL1, sandy loam (0–2.75); C, clay (2.75–3); Var1, thin, predominantly sand (2.75–3); HP1, hardpan-like paleosol (3–3.65); Var2, various sandy loam to clay loam (3.65– 6.7); S, medium sand (6.7–9); Var3, various textures (9–9.75); C-Si-L, fine-textured floodplain deposits (9–12); SL2, sandy loam (12–15); and HP2, a hardpan-like paleosol (15–15.85). Lithofacies symbols followed by the same numbers (1, 2) indicate no significant differences between lithofacies groups at the 95% significance level (C and Var3 had less than four samples and those were from only one subplot and were therefore not included in the ANOVA). Fertilizer treatments (control, standard, high) followed by the same Roman numerals (I, II) indicate no significant difference between the fertilizer treatments at the 95% significance level. (b) Facies X subplot group means of the detect–nondetect indicator variable, that is, the fraction of nondetects in each group. No means were computed for C and Var3.

equal range), but also a strong zonal anisotropy (unequal sill) throughout all subplots. The sill in the horizontal direction (Fig. 6a–6c) is significantly smaller, while the range in the horizontal direction is significantly longer than in the vertical direction (Fig. 6d–6f).

Kriged θ, shown in Fig. 7, is much less variable than the distribution of NO_3–N_{aq} (see below). Due to the large horizontal correlation scale, water content distribution is fairly uniform, with predominantly horizontal layering (e.g., Hills et al., 1991). Although all three subplots exhibit a similar trend of soil moisture distribution, the depth profiles of water content data shown in Fig. 7b suggest that the deeper portion of the control and high subplots is wetter than that of the standard subplot.

Nitrate

Separate semivariograms for the complete dataset and for the detectable level dataset were computed and, for comparison, plotted after normalizing the semivariograms by their respective variances (Fig. 8). The semivariogram of the complete dataset with its strong bimodal distribution and large standard deviation (2.63, see Table 1) reflects the combined effect of two spatial variability structures: (i) the spatial variability structure between measurable $\ln NO_3$–N_{aq} levels (pattern of different colors in Fig. 9) and (ii) the spatial variability of the bimodal pattern of zones with nondetectable NO_3–N_{aq} and zones with detectable NO_3–N_{aq} (pattern of purple/dark vs. other colors in Fig. 9). Separate variograms were computed for the two datasets, to determine whether the pattern created by the bimodality dominated the semivariogram structure because of the large concentration difference between the two modes in the distribution. However, the normalized semivariograms of the two datasets were found to be essentially identical. Only the vertical nugget effect, especially in the high subplot, is notably smaller for the semivariograms of the smaller (detectable levels only) dataset. Hence, vertical spatial continuity is higher within zones of measurable NO_3–N_{aq} (triangles) than between zones of measurable and nondetectable NO_3–N_{aq} (diamonds). In the horizontal direction, differences between the two sets of semivariograms are not significant.

Kriged concentrations (using the semivariograms of the complete dataset) are found to be highly variable with several "plumes" of high concentration observed near the top and in the upper third of the profile of each subplot (Fig. 9). The total N mass in the vadose zone obtained from kriging is 52 (±9.7), 40 (±7), and 93 (±14.1) kg N ha^{-1} for the control, standard, and high subplots, respectively. Confidence intervals represent the average kriging error variance. The deep vadose N mass (without the root zone) is 48, 36, and 87 kg N ha^{-1}, respectively. These latter kriged ("measured") total N masses amount to 24% (15–40%), 15% (9–27%), and 19% (12–34%), respectively, of those predicted from the MB analysis for 1997 (values in parentheses account for estimation errors in the MB analysis).

These observations raise several issues to be discussed in the following section: What are the potential errors contributing to the difference between predicted and measured deep vadose zone N? How representative and significant is the amount of observed spatial variability of water content and NO_3? What does the observed spatial variability of water content and NO_3 indicate with respect to the spatial distribution of water flux and the expected fate of transport?

DISCUSSION

Measured vs. Predicted Nitrate Mass in the Deep Vadose Zone

Several reasons may explain the large discrepancy between the two estimates of deep vadose zone NO_3:

Reproduced from Vadose Zone Journal. Published by Soil Science Society of America. All copyrights reserved.

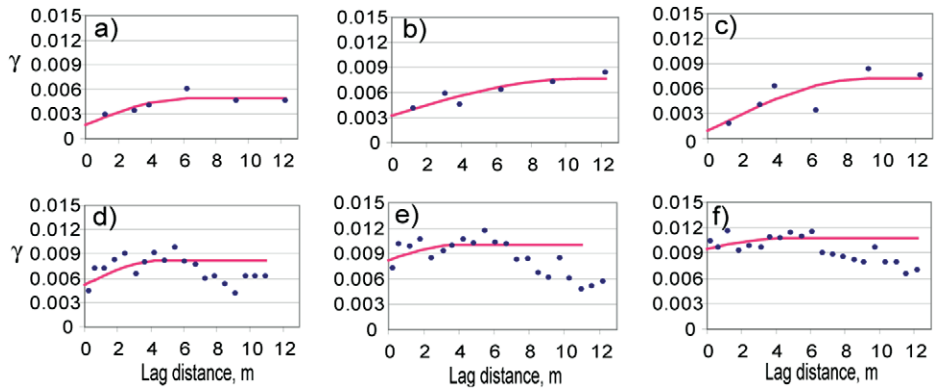

Fig. 6. Experimental and spherical model semivariograms for water content (trend residuals) in the horizontal direction for the (a) control, (b) standard, and (c) high subplot; and in the vertical direction for (d) the control, (e) standard, and (f) high subplot. Diamonds denote experimental values and lines denote spherical semivariogram models.

estimation errors in the MB method yielding an erroneous interpretation for LPLN, estimation errors in the geostatistical analysis of vadose zone N mass, significant N losses in the deep vadose zone not accounted for in the MB method, and nonuniform flow conditions in the vadose zone.

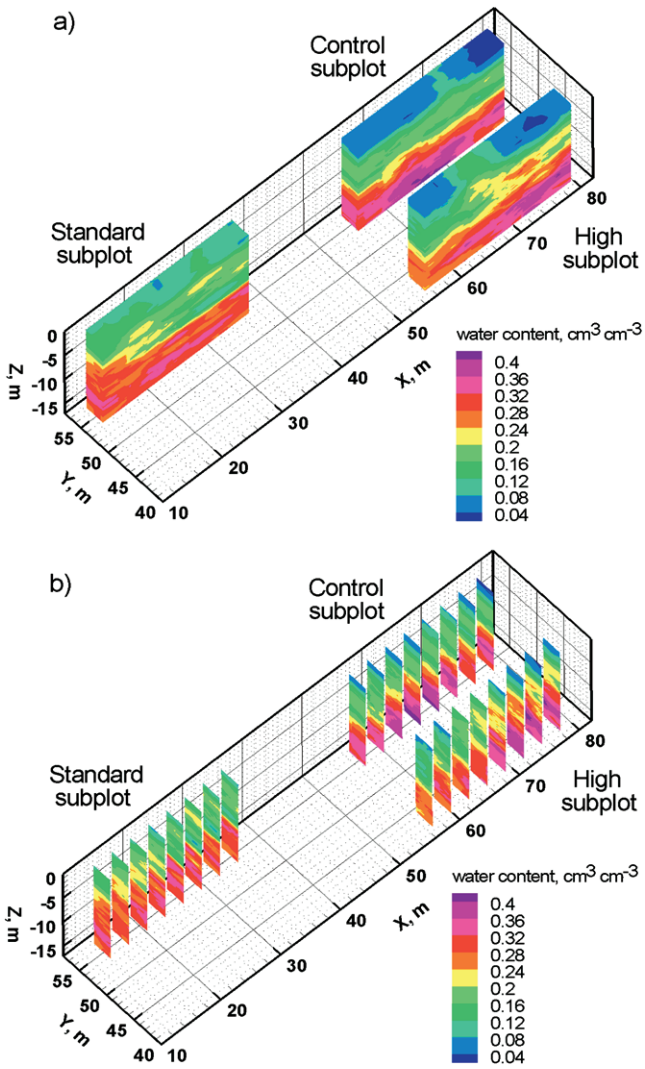

Fig. 7. Contour maps of the kriged (a) water content at the control, standard, and high fertilizer treatment sites; (b) various depth profiles of water content at each subplot.

The computed error margins for recharge, LPLN, and the resulting deep vadose zone storage (Table 2) are on the same order as the 30% of actual leaching losses suggested by Meisinger and Randall (1991). Although large, neither these errors nor those from the kriging analysis can explain the observed difference between MB predicted and measured deep vadose zone N.

If the differences were assumed to be primarily caused by denitrification (Bar-Yosef and Kafkafi, 1972; Aronsson, 2001) under predominantly uniform vertical flow conditions, the amount of N loss in the deep vadose zone should be on the order of one hundred to several hundred kilograms per hectare within one leaching cycle (i.e., 3.2 yr) with much higher denitrification rates under the high subplot than the other two subplots. Most of this denitrification would have had to occur in the shallowest zone because no significant depth-dependent decrease in NO_3–N was observed below the root zone and because several relatively high NO_3–N concentrations were measured even at depth. However, denitrification rates of more than 55 to 60 kg ha^{-1} yr^{-1} are unlikely, given the low organic C content of the root zone and its relatively coarse texture (e.g., Rolston et al., 1982; Aronsson, 2001; Sanchez et al., 2001; Krug and Winstanley, 2002). This is also consistent with the lack of significant vertical trends in the N isotope fractionation observed at the site (Harter et al., 2004).

While the denitrification processes in the deep vadose zone may be locally significant (Harter et al., 2004), other explanations, namely the role of heterogeneity and flow nonuniformity (not considered in the MB model) must be considered to explain the large discrepancy between field measured and MB estimated deep vadose zone N content. The site stratigraphy and hydraulic properties are highly variable both between facies and within facies (Minasny et al., 2004). The significant degree of layering observed at the site is typical of the alluvial fan architecture in the region, which contains laterally extensive hardpans and floodplain deposits intercalated between higher permeable sediments of varying texture representing channel and overbank deposits (Page and LeBlanc, 1969; Weismann et al., 1999). While

Reproduced from Vadose Zone Journal. Published by Soil Science Society of America. All copyrights reserved.

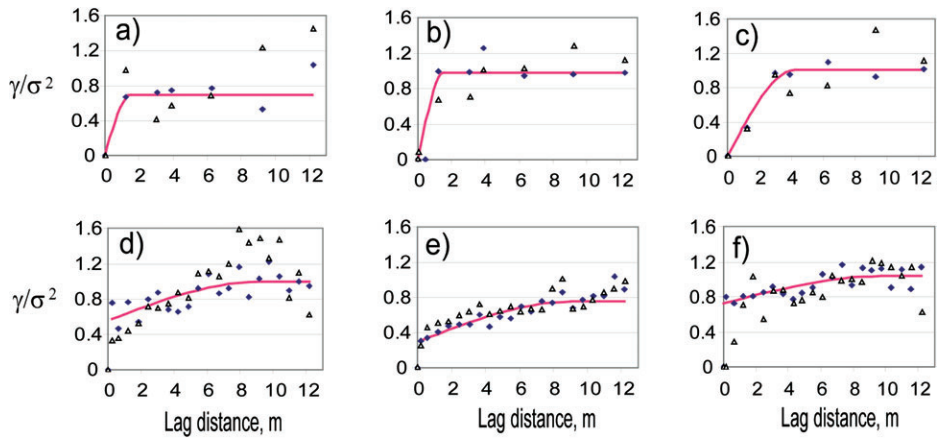

Fig. 8. Normalized experimental and spherical model semivariograms for $\ln NO_3$–N_{aq} in the horizontal direction for the (a) control, (b) standard, and (c) high subplot and in the vertical direction for the (d) control, (e) standard, and (f) high subplot. Diamonds represent the experimental semivariograms for the complete NO_3–N_{aq} dataset; triangles denote experimental semivariograms computed from the dataset without nondetect samples. Solid lines are the spherical semivariogram models fitted to the experimental variograms of the complete data set.

flow paths of NO_3 are thought to be predominantly vertical within one layer, the stratigraphic layering may contribute to lateral flows (Iqbal, 2000) leading to both, preferential flow pattern and potentially significant NO_3 exchange between subplots.

Spatial Variability of Water Content and Nitrate

Water Content

The geometric and zonal anisotropy (Fig. 6) are the result of the highly stratified conditions and strong horizontal layering of water content across the site, which is also evident in the kriged water content map (Fig. 7a, 7b). Such "layering" of moisture content can be the result of either layered strata with significant textural differences and also of transiency in the water flux. The significant contribution of textural layering to the water content distribution suggests that textural differences at the site are the main cause of the water content differences with depth. Similar phenomena have been observed in other field experiments and in numerical studies of vadose flow through heterogeneous media (e.g., Hills et al., 1991; Polmann et al., 1991).

Nitrate

Lognormal NO_3–N_{aq} distributions found at this deep vadose zone site are not unlike those reported in other studies focusing on the root zone (e.g., Tabor et al., 1985; Sharmasarkar et al., 1999; Ilsemann et al., 2001). However, CVs for each subplot treatment (Table 1) are significantly higher than those measured elsewhere, where reported CVs typically range from 20 to 50% and in few cases are as high as 70 to 100% (e.g., Mohanty and Kanwar, 1994; Sharmsarkar et al., 1999; Ilsemann et al., 2001). In part, the higher observed variability of NO_3–N_{aq} may be attributed to the small sample size (3.5-cm diameter by 7.5-cm length) relative to other typical soil samples (≈3.2-cm diameter by 30-cm length). It may also be a result of the fact that practically all samples are taken at depths well below the mechanical impact zone of agricultural practices. It cannot be attributed to lithofacies control, since no large concentration contrasts were observed between most lithofacies.

The significantly larger mean NO_3–N_{aq} of the high subplot indicates that higher than standard fertilizer treatment indeed affects NO_3 transport to groundwater. However, the difference must be interpreted carefully in light of the high degree of spatial variability. Some of the key patterns in NO_3–N_{aq} distribution are also due to other boundary effects:

- High concentrations of kriged NO_3–N_{aq} near the top and in the upper third of the profile of each subplot are attributed to the most recent fertilizer application in 1996 and explain the significant shift in the mean NO_3–N_{aq} in the upper 3 m (Fig. 5a). In the control subplot, we suspect that the higher NO_3–N_{aq} content is likely the result of poor root uptake. After 12 yr, tree roots of the control subplot were likely unable to capture the additional N of the one-time application because the root system had grown to capture nutrient supply primarily or exclusively from neighboring treatments (Scott Johnson, personal communication, 2004).
- Significant reduction of the number of nondetects below depths of 12 m is likely the result of the fact that the bottom of the vadose zone had been fully saturated (part of the shallow groundwater system) in some high water years before 1989. Shallow groundwater contains elevated levels of NO_3 (4 g m^{-3} or more).

Nitrate semivariograms exhibit a statistically significant spatial continuity as postulated in theoretical stochastic models of solute transport through the vadose zone (e.g., Harter and Yeh, 1996). The observed geometric anisotropy may be caused by nonuniform N applications (extrinsic variability). Possibly, such strong geometric anisotropy may also be the result of highly heterogeneous vadose flow processes (see below). While it is difficult to further facilitate the comparison of the results of spatial correlation that we observed for NO_3

Reproduced from Vadose Zone Journal. Published by Soil Science Society of America. All copyrights reserved.

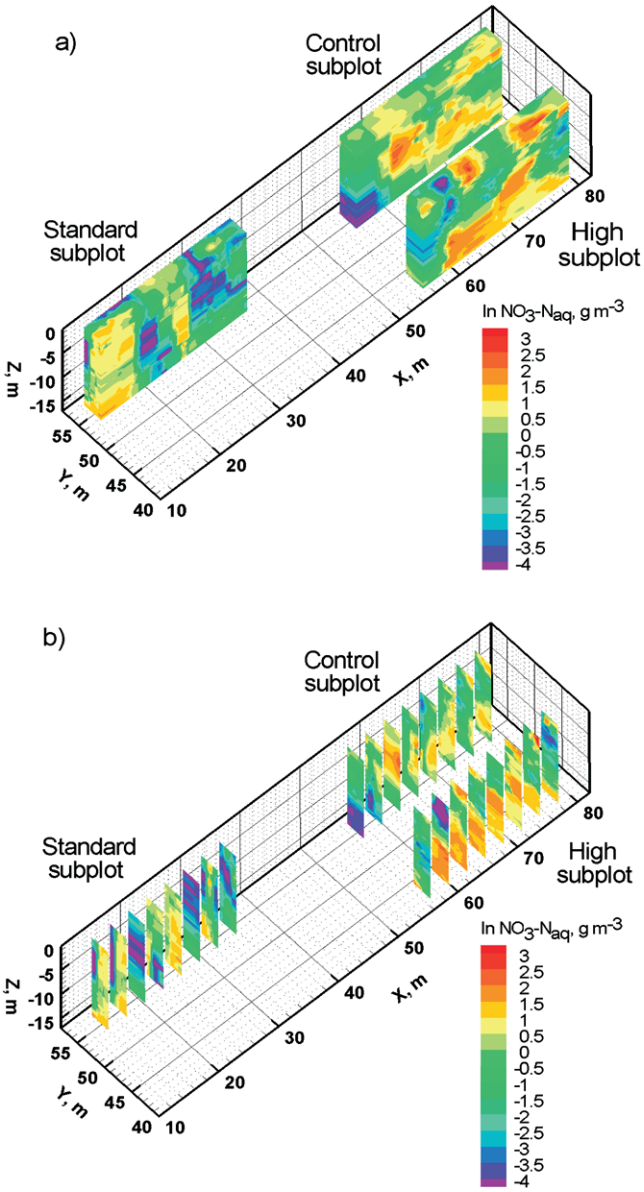

Fig. 9. Contour maps of the kriged (a) $\ln NO_3$–N_{aq} (g m^{-3} = μg mL^{-1}) at the control, standard, and high fertilizer treatment sites; (b) various depth profiles of $\ln NO_3$–N_{aq} at each subplot.

with those reported by previous studies, it is noteworthy to mention that some studies observed a finite range of spatial dependence (e.g., van Meirvenne and Hofman, 1989). Other studies found monotonically increasing semivariance with increasing lag distances (e.g., Tabor et al., 1985). In many studies with large sampling distances (10–500 m), a pure nugget effect (no spatial correlation) is observed (e.g., Hofman et al., 1994; Ilsemann et al., 2001; Stenger et al., 2002). This is consistent with our finding that correlation scales of core-measured NO_3–N_{aq} extend to a few meters at most.

Spatial Variability of Nitrogen Flux: Interpretation in the Context of Heterogeneous Flow Fields

The probability distributions of θ and NO_3–N_{aq} are consistent not only with root zone field studies but also with results obtained from stochastic models of flow and transport in heterogeneous porous media. Harter and Yeh (1998) and Harter and Zhang (1999) demonstrated that spatially variable soil properties lead to approximately normal distributed moisture distributions while the resulting vadose moisture velocity distribution is highly skewed (lognormal), which then leads to a skewed concentration distribution. Like its marginal probability distribution, the kriged NO_3–N_{aq} distribution pattern at the experimental site is also surprisingly similar to that found in other experimental studies (e.g., Hills et al., 1991; Roth et al., 1991) and to that postulated in numerical models (e.g., Harter and Yeh, 1996; Ünlü et al., 1990; Tompson and Gelhar, 1990) of transport in highly heterogeneous hydraulic conductivity fields. We observed zones with individual plumes apparently moving laterally in some locations and downward in others, high concentration variability, and large zones with negligible NO_3 concentrations.

The conceptual framework of lognormally distributed flow rates (e.g., Harter and Yeh, 1996) is in fundamental contrast to the uniform flow conditions assumed in the LPLN estimates of N mass in the deep vadose zone. Under the conditions of lognormal flow rates (i.e., strongly heterogeneous flux rates), quasipreferential flow paths exist (Polmann et al., 1991; Russo et al., 1994; Harter et al., 1996; Harter and Yeh, 1996), creating a flow pattern not unlike that in soils with a relatively low permeable matrix and a highly permeable macropore structure (Roth et al., 1991). Under such heterogeneous flux conditions, the majority of the pore space is occupied by regions with slow velocities (including stagnant zones that do not contribute significantly to active flow). Nitrate in those low flow regions can have tortuous flow paths, long travel times, and be subject to local denitrification, particularly in the shallow vadose zone after storm events (Pionke and Lowrance, 1991; Ryden and Lund, 1980; Xu et al., 1998; MacQuarrie and Sudicky, 2001). Largest flux contrasts between preferential flow paths and stagnant flow zones would be observed in coarse-textured material because of its low capillary potential. This is consistent with the fact that the largest amount of NO_3–N_{aq} nondetects at the site occurred in the sand lithofacies S located in the center of the vadose zone profile.

Theoretical models indicate that the relatively high flow zones are of only limited spatial extent (e.g., Fig. 9 in Harter et al., 1996), but their high flux rates lead to rapid NO_3 transfer through the vadose zone. Such effects of textural heterogeneity on flow nonuniformity are further enhanced by potentially unstable infiltration into the sandy loam root zone, which were documented for this site in Wang et al. (2003). Even stronger instabilities and fingering may occur at and below the interface of fine-textured lithofacies overlying coarse-textured lithofacies (Glass et al., 1988), such as in the deeper sand lithofacies S, which had relatively low water content and a high ratio of NO_3–N_{aq} nondetects.

The combined evidence of textural heterogeneity, lithofacies contrasts, hydraulic heterogeneity (Minasny et al., 2004), and spatial variability of water content and

Reproduced from Vadose Zone Journal. Published by Soil Science Society of America. All copyrights reserved.

NO_3–N_{aq} strongly suggests three major processes controlling the fate and transport of NO_3 in the vadose zone:

- limited, localized denitrification in the slow flow regions,
- lateral flow and N exchange between subplots, and
- preferential flow and perhaps fingering, which lead to rapid, highly localized N transport toward the water table.

These processes would explain both the large number of nondetects and the overall low N mass remaining in the deep vadose zone. The rapid NO_3–N_{aq} transport in localized flux channels significantly reduces the amount of N stored in the deep vadose zone, strongly limiting the role of denitrification. Our results suggest that the lack of N stored below the root zone should not automatically be interpreted as significant N attenuation due to denitrification (or other unquantified losses within the root zone). We point out that the conceptual framework of heterogeneous flow (as opposed to uniform deep vadose zone flow) also suggests the simultaneous occurrence of significantly older water next to very young water within the vadose zone. Hence, the NO_3 distribution at the site (Fig. 9a) represents as much average conditions during the long-term fertilizer treatment (in lower flux regions) as it represents only the most recent two N applications (in 1994, 1996), the latter of which was uniform across all treatments (in the localized high flux regions). This would explain the relative similarity in measured total N levels between subplots.

CONCLUSIONS

An intensive field sampling campaign resulted in a unique snapshot of the vadose zone NO_3–N distribution throughout its 16-m depth under three different 12-yr fertilization trials. While results are site specific, the site conditions are typical of many agricultural regions in alluvial basins. Our findings summarized below are therefore relevant to heterogeneous, alluvial vadose zone sites below agricultural production areas in general.

1. Significantly higher NO_3–N leaching occurs in overfertilized tree crops, when compared with those fertilized under standard or substandard conditions.
2. The field data reveal significant variability in water content and particularly in the NO_3–N distribution throughout the deep vadose zone, with measured NO_3 values varying by several orders of magnitude over relatively short distances. Almost one-third of the core samples had nondetectable levels of NO_3–N.
3. Despite the high variability, NO_3–N semivariograms discern the presence of a significant short-range spatial structure at the scale of a several decimeters, particularly in the vertical direction, normal to the horizontal layering in the sedimentary structure. The highly heterogeneous NO_3–N distribution is consistent with the significant textural and hydraulic heterogeneity observed in the vadose zone at the site.
4. The presence of strongly heterogeneous geologic formations at the site, highly variable hydraulic conductivity and water content, and the strongly log-normal, variable distribution of NO_3 concentrations suggest that highly heterogeneous, skewed or log-normally distributed flux conditions and, in coarse facies, finger-like flow dominate the vadose zone hydrology in these alluvial sediments.
5. The variability of NO_3–N concentrations underscores the importance of high spatial sampling frequencies when monitoring field-scale solute leaching with suction lysimeters or other common soil monitoring tools that measure relatively small volumes of soil water.
6. In alluvial sediments, the often used assumption of uniform flow in the deep vadose zone is inadequate to predict NO_3–N levels in the deep vadose zone below the root zone. Actual NO_3–N levels are potentially much lower due to rapid N transport in preferential flow paths of limited spatial extent.
7. Vice versa, measured NO_3–N levels below the root zone should not be used to validate a LPLN analysis or to close the mass balance of the LPLN framework assuming uniform field-scale flow conditions. Doing so would lead to significant underestimation of NO_3 leaching rates to groundwater.
8. Denitrification may locally occur throughout the deep vadose zone, but our data indicate that it is not likely to be a major process and cannot account for the relatively low N mass found in the deep vadose zone.
9. Given that field measurements of NO_3–N fluxes below the root zone remain difficult in light of the observed spatial variability, alternative methods for measuring NO_3–N leaching will continue to play a significant role. In particular, proper determination of the field-scale water and N mass balance, independent of root zone NO_3–N measurements, remains an important option. The results also suggest that groundwater quality measurements at the water table are a viable monitoring tool, as travel times through deep vadose zones may be shorter than previously assumed under uniform flow assumptions.

The results are consistent with, albeit not a direct proof of, theoretical work on the effects of soil and sediment heterogeneity on vadose flow and transport. The extensive deep vadose zone sampling campaign presented here provides the first extensive dataset to confirm the applicability of stochastic concepts of unstable flow to predicting solute flux in the deep vadose zone. Ongoing work to substantiate the role of heterogeneity and denitrification will include a detailed, site-specific modeling analysis.

ACKNOWLEDGMENTS

The research support for this project is provided by the State of California Department of Food and Agriculture Fertilizer Research Education Program, the California Center of Water Resources, and the California Tree Fruit Agreement. We would like to thank Scott Johnson, Katrin Heeren, Anthony Cole, Chad Pyatt, Rigo Rios, Andrea De Lisle, and Timothy

Reproduced from Vadose Zone Journal. Published by Soil Science Society of America. All copyrights reserved.

Doane for their help in the collection of the field data and analysis. In particular, we would like to thank Geoprobe Systems for the generous loan of their direct-push drilling rig for this study. We appreciate the helpful comments of several anonymous reviewers and our associate editor, Brian Andraski, which helped to greatly improve this manuscript.

REFERENCES

Allaire-Leung, S.E., L. Wu, and B.L. Sanden. 2001. Nitrate leaching and soil nitrate content as affected by irrigation uniformity in a carrot field. Agric. Water Manage. 48:37–50.

Allison, F.E. 1966. The fate of nitrogen added to soils. Adv. Agron. 18:219–259.

Aronsson, P.G. 2001. Dynamics of nitrate leaching and ^{15}N turnover in intensively fertilized and irrigated basket willow grown in lysimeters. Biomass Bioenergy 21:143–154.

Bar-Yosef, B., and U. Kafkafi. 1972. Rates of growth and nutrient uptake of irrigated corn as affected by N and P fertilization. Soil Sci. Soc. Am. Proc. 36:931–936.

Berthouex, P.M., and L.C. Brown. 1994. Statistics for environmental engineers. CRS Press Inc., Boca Raton, FL.

Blanchard, C.L., and K.A. Tonnessen. 1994. Precipitation chemistry measurements from the California Acid Deposition Monitoring Program, 1985–1990. Atmos. Environ. 27A:1755–1763.

Bransby, D.I., S.B. McLaughlin, and D.J. Parrish. 1998. A review of carbon and nitrogen balances in switchgrass grown for energy. Biomass Bioenergy 14:379–384.

California Department of Water Resources. 2000. California Irrigation Management Information System agricultural resource book. California Dep. Water Resour., Sacramento.

Cambardella, C.A., T.B. Moorman, J.M. Novak, T.B. Parkin, D.L. Karlen, R.F. Turco, and A.E. Konopka. 1994. Field scale variability of soil properties in central Iowa soils. Soil Sci. Soc. Am. J. 58: 1501–1511.

Dahiya, I.S., R. Anlauf, K.C. Kersebaum, and J. Richter. 1984. Spatial variability of some nutrient constituents of an alfisol from loess. I. Classical statistical analysis. Z. Pflanzenernaehr. Bodenkd. 147: 695–703.

Davis, J.C. 1986. Statistics and data analysis in geology. 2nd ed. John Wiley and Sons, New York.

Deutsch, C.V., and A.G. Journel. 1992. GSLIB: Geostatistical software library and user's guide. Oxford University Press, New York.

de Vos, J.A., D. Hesterberg, and P.A.C. Raats. 2000. Nitrate leaching in a tile-drained silt loam soil. Soil Sci. Soc. Am. J. 64:517–527.

Dowdell, R.J., and C.P. Webster. 1984. A lysimeter study of the fate of fertilizer nitrogen in spring barley crops grown on shallow soil overlying chalk: Denitrification losses and nitrogen balance. J. Soil Sci. 35:183–190.

Frissel, M.J., G.J. Kolenbrander, I. Shvytov, and U.F. Vasileu. 1981. Systematic comparison of the models described. *In* M.J. Frissel and J.A. Van Veen (ed.) Simulation of nitrogen behavior in soil–plant systems. Center for Agricultural Publishing and Documentation, Wageningen, the Netherlands.

Glass, R.J., T.S. Steenhuis, and J.-Y. Parlange. 1988. Wetting front instability as a rapid and far-reaching hydrologic process in the vadose zone. J. Contam. Hydrol. 3:207–226.

Harter, T., A.L. Gutjahr, and T.-C.J. Yeh. 1996. Linearized co-simulation of hydraulic conductivity, pressure head, and flux in saturated and unsaturated, heterogeneous porous media. J. Hydrol. (Amsterdam) 183:169–190.

Harter, T., K. Heeren, G. Weissmann, W.R. Horwath, and J. Hopmans. 1999. Field scale characterization of a heterogeneous, moderately deep vadose zone: The Kearney Research Site. p. 621–630. *In* Proceedings, Characterization and Measurement of the Hydraulic Properties of Vadose Porous Media. U.S. Salinity Lab., Riverside, CA.

Harter, T., Y.S. Onsoy, K. Heeren, M. Denton, G. Weissmann, J.W. Hopmans, and W.R. Horwath. 2004. Deep vadose zone hydrology in the eastern San Joaquin Valley: At the crossroads between life and mystery. California Agriculture.

Harter, T., and T.-C.J. Yeh. 1996. Stochastic analysis of solute transport in heterogeneous, variably saturated soils. Water Resour. Res. 32:1585–1595.

Harter, T., and T.C.J. Yeh. 1998. Flow in vadose random porous media nonlinear numerical analysis and comparison to analytical stochastic models. Adv. Water Resour. 22:257–272.

Harter, T., and D. Zhang. 1999. Water flow and solute spreading in heterogeneous soils with spatially variable water content. Water Resour. Res. 35:415–426.

Hauck, R.D. 1981. Nitrogen fertilizer effects on nitrogen cycle processes. p. 551–561. *In* F.E. Clark and T. Rosswall (ed.) Terrestrial nitrogen cycles. Ecol. Bull. 33. Swedish Natural Sci. Res. Counc., Stockholm, Sweden.

Hausenbuiller, R.L. 1985. Soil science principles and practices. Wm. C. Brown Publ., Dubuque, IA.

Hills, R.G., P.J. Wierenga, D.B. Hudson, and M.R. Kirkland. 1991. The second Las Cruces trench experiment: Experimental results and two-dimensional flow predictions. Water Resour. Res. 27: 2707–2718.

Hocking, R.R. 1985. The analysis of linear models. Brooks/Cole, Monterey, CA.

Hofman, G., J. De Smet, M. van Meirvenne, and P. Verstegen. 1994. Residual soil nitrate under intensive agriculture. Commun. Soil Sci. Plant Anal. 25:1197–1207.

Horwath, W.R., and E.A. Paul. 1994. Microbial biomass. p. 753–773. *In* Methods of soil analysis. Part 2. SSSA Book Ser. 5. SSSA, Madison, WI.

Ilsemann, J., S. Goeb, and J. Bachmann. 2001. How many soil samples are necessary to obtain a reliable estimate of mean nitrate concentrations in an agricultural field? J. Plant Nutr. Soil Sci. 164:585–590.

Iqbal, M. 2000. Effects of layered heterogeneity in subsurface geologic materials on solute transport under field conditions: A case study from northeastern Iowa, USA. Hydrogeol. J. 8:257–270.

Istok, J.D., J.D. Symth, and A.L. Flint. 1993. Multivariate geostatistical analysis of groundwater contamination: A case history. Ground Water 31:63–74.

Johnson, R.S., F.G. Mitchell, and C.H. Crisost. 1995. Nitrogen fertilization of Fantasia nectarine—A 12 year study. UC Kearney Tree Fruit Rev. 1:14–19.

Krug, E.C., and D. Winstanley. 2002. The need for comprehensive and consistent treatment of the nitrogen cycle in nitrogen cycling and mass balance studies: I. Terrestrial nitrogen cycle. Sci. Total Environ. 293:1–29.

Lafolie, F., L. Bruckler, and A.M. de Corkborne. 1997. Modeling the water transport and nitrogen dynamics in irrigated salad crops. Irrig. Sci. 17:95–104.

Lark, R.M. 2002. Modeling complex soil properties as contaminated regionalized variables. Geoderma 106:173–190.

Legg, J.O., and J.J. Meisinger. 1982. Soil nitrogen budgets. *In* F.J. Stevenson (ed.) Nitrogen in agricultural soils. Agron. Monogr. 22. ASA, CSSA, and SSSA, Madison, WI.

Ling, G., and A.I. El-Kadi. 1998. A lumped parameter model for nitrogen transformation in the vadose zone. Water Resour. Res. 34:203–212.

Lunn, R.J., and R. Mackay. 1994. An integrated modeling system for nitrate transport. *In* Dracos and Stauffer (ed.) Transport and reactive processes in aquifers. A.A. Balkema, Rotterdam, the Netherlands.

MacQuarrie, K.T.B., and E.A. Sudicky. 2001. Multicomponent simulation of wastewater derived nitrogen and carbon in shallow unconfined aquifers. I. Model formulation and performance. J. Contam. Hydrol. 47:53–84.

Martin, D.L., J.R. Gilley, and R.W. Skaggs. 1991. Soil water balance and management. *In* R.F. Follett et al. (ed.) Managing nitrogen for groundwater quality and farm profitability. SSSA, Madison, WI.

Meisinger, J.J., and G.W. Randall. 1991. Estimating nitrogen budgets for soil-crop systems. *In* R.F. Follett et al. (ed.) Managing nitrogen for groundwater quality and farm profitability. SSSA, Madison, WI.

Minasny, B., J.W. Hopmans, T. Harter, S.O. Eching, A. Tuli, and M.A. Denton. 2004. Neural networks prediction of soil hydraulic functions from multi-step outflow data. Soil Sci. Soc. Am. J. 68: 417–429.

Mohanty, B.P., and R.S. Kanwar. 1994. Spatial variability of residual nitrate-nitrogen under two tillage systems in central Iowa: A composite three-dimensional resistant and exploratory approach. Water Resour. Res. 30:237–251.

Mutters, R. 1995. Atmospheric deposition to agricultural soil. Final

Reproduced from Vadose Zone Journal. Published by Soil Science Society of America. All copyrights reserved.

Rep. 93-334. California Environmental Protection Agency, Air Resources Board Research Division, Sacramento, CA.

Olea, R.A. 1999. Geostatistics for engineers and earth scientists. Kluwer Academic Publ., Boston.

Owens, L.B., W.M. Edwards, and R.W. Vankeuren. 1992. Nitrate levels in shallow groundwater under pastures receiving ammonium nitrate or slow release nitrogen fertilizer. J. Environ. Qual. 21: 607–613.

Page, R.W., and R.A. LeBlanc. 1969. Geology, hydrology, and water quality in the Fresno area, California. USGS Open File Rep. USGS, Reston, VA.

Paustian, K., O. Andren, M. Clarhom, A.C. Hansson, G. Johansson, J. Lagerlof, T. Lindberg, R. Petterson, and B. Sohlenius. 1990. Carbon and nitrogen budgets for four agro-ecosystems with annual and perennial crops, with and without N fertilization. J. Appl. Ecol. 27:60–84.

Pionke, H.B., and R.R. Lowrance. 1991. Fate of nitrate in subsurface drainage water. *In* R.F. Follett et al. (ed.) Managing nitrogen for groundwater quality and farm profitability. SSSA, Madison, WI.

Polmann, D.J., D. Mckaughlin, S. Luis, L.W. Gelhar, and R. Ababou. 1991. Stochastic modeling of large-scale flow in heterogeneous unsaturated soils. Water Resour. Res. 27:1447–1458.

Puckett, L.J. 1995. Identifying major sources of nutrient water pollution. Environ. Sci. Technol. 29:408A–414A.

Rao, P.S.C., and R.J. Wagenet. 1985. Spatial variability of pesticides in field soils: Methods for data analysis and consequences. Weed Sci. 33:18–24.

Rees, T.F., D.J. Bright, R.G. Fay, A.H. Christensen, R. Anders, B.S. Baharie, and M.T. Land. 1995. Geohydrology, water quality, and nitrogen geochemistry in the saturated and vadose zones beneath various land uses, Riverside and San Bernadino Counties, California, 1991–93. USGS Water Resources Investigations Rep. 94-4127. USGS, Reston, VA.

Rolston, D.E., A.N. Sharply, D.W. Toy, and F.E. Broadbent. 1982. Field measurement of denitrifcation. III. Rates during infiltration cycles. Soil Sci. Soc. Am. J. 46:289–296.

Roth, K., W.A. Jury, H. Fluhler, and W. Attinger. 1991. Transport of chloride through an vadose field soil. Water Resour. Res. 27: 2533–2541.

Russo, D., J. Zaidel, and A. Laufer. 1994. Stochastic analysis of solute transport in partially saturated heterogeneous soil. 1. Numerical experiments. Water Resour. Res. 30:769–779.

Ryden, J.C., and L.J. Lund. 1980. Nature and extent of directly measured denitrification losses from some irrigated vegetable crop production units. Soil Sci. Soc. Am. J. 44:501–511.

Sanchez, L., J.A. Diez, A. Vallho, and M.C. Cartagena. 2001. Denitrification losses from irrigated crops in central Spain. Soil Biol. Biochem. 33:1201–1209.

Sharmasarkar, F.C., S. Sharmasakkar, R. Zhang, G.F. Vance, and S.D. Miller. 1999. Microspatial variability of soil nitrate following nitrogen fertilization and drip irrigation. Water Air Soil Pollut. 116:605–619.

Simek, M., and K.J. Kalcik. 1998. Carbon and nitrate utilization in soils: The effect of long-term fertilization on potential denitrification. Geoderma 83:269–280.

Smith, S.J., and D.K. Cassel. 1991. Estimate nitrate leaching in soil materials. *In* R.F. Follett et al. (ed.) Managing nitrogen for groundwater quality and farm profitability. SSSA, Madison, WI.

Statsoft, Inc. 2002. STATISTICA 6.0. Statsoft, Tulsa, OK.

Stenger, R., E. Priesack, and F. Beese. 2002. Spatial variation of nitrate-N and related soil properties at the plot scale. Geoderma 105:259–275.

Stevenson, F.J. 1982. Origin and distribution of nitrogen in soils. p. 1–42. *In* F.J. Stevenson (ed.) Nitrogen in agricultural soils. Agron. Monogr. 22. ASA, CSSA, and SSSA, Madison, WI.

Stevenson, F.J. 1986. Cycles of soil: Carbon, nitrogen, phosphorus, sulfur, micronutrients. Jon Willey and Sons, New York.

Tabor, J.A., A.W. Warrick, D.E. Myers, and D.A. Pennigton. 1985. Spatial variability of nitrate in irrigated cotton. II. Soil nitrate and correlated variables. Soil Sci. Soc. Am. J. 49:390–394.

Tanji, K.K., and S.K. Gupta. 1978. Computer simulation modeling for nitrogen in irrigated croplands. p. 79–131. *In* D.R. Nielsen and J.G. MacDonald (ed.) Nitrogen in the environment. Vol. 1. Academic Press, San Diego.

Tindall, J.A., R.L. Petrusak, and P.B. McMahon. 1995. Nitrate transport and transformation processes in vadose porous media. J. Hydrol. (Amsterdam) 169:51–94.

Trettin, C.C., D.W. Johnson, and D.E. Todd. 1999. Forest nutrient and carbon pools at Walker Branch Watershed: Changes during a 21-year period. Soil Sci. Soc. Am. J. 63:1436–1448.

Tompson, A.F.B., and L.W. Gelhar. 1990. Numerical simulation of solute transport in three-dimensional randomly heterogeneous porous media. Water Resour. Res. 26:2541–2562.

Ünlü, K., D.R. Nielsen, and J.W. Biggar. 1990. Stochastic analysis of vadose flow: One-dimensional Monte Carlo simulations and comparisons with spectral perturbation analysis and field observations. Water Resour. Res. 26:2207–2218.

USEPA. 1990. National water quality inventory. 1988 Report to Congress, EPA-440-4-90-003. USEPA, Washington, DC.

van Meirvenne, M.V., and G. Hofman. 1989. Spatial variability in topsoil micronutrients in a one ha cropland plot. Commun. Soil Sci. Plant Anal. 120:103–110.

Wang, Z., L. Wu, T. Harter, J. Lu, and W.A. Jury. 2003. A field study of unstable preferential flow during soil water redistribution. Water Resour. Res. 39(4):1075. doi:10.1029/2001WR000903.

Watkins, N., and D. Barraclough. 1996. Gross rates of N mineralization associated with the decomposition of plant residues. Soil. Biol. Biochem. 28:169–175.

Weismann, G.S., S.F. Carle, and G.E. Fogg. 1999. Three dimensional hydrofacies modeling based on soil surveys and transition probability geostatistics. Water Resour. Res. 35:1761–1770.

Wendt, K. 1999. Determination of nitrate/nitrite by flow injection analysis. QuikChem Method 10-107-04-1-A. Lachat Instruments, Milwaukee, WI.

White, R.E., R.A. Haigh, and J.H. Macduff. 1987. Frequency distribution and spatially dependent variability of ammonium and nitrate concentrations in soil under grazed and ungrazed grassland. Fert. Res. 11:193–208.

Willigen, P., and J.J. Neeteson. 1985. Comparison of six simulation models for the nitrogen cycle in the soil. Fert. Res. 8:157–171.

Xu, C., M.J. Shaffer, and M. Al-Kaisi. 1998. Simulating the impact of management practices on nitrous oxide emissions. Soil Sci. Soc. Am. J. 62:736–742.

APPENDIX 2:

Reprint of

Harter, T., Y. S. Onsoy, K. Heeren, M. Denton, G. Weissmann, J. W. Hopmans, W. R. Horwath, 2005. Deep vadose zone hydrology demonstrates fate of nitrate in eastern San Joaquin Valley, California Agriculture 59(2):124-132.

Deep vadose zone hydrology demonstrates fate of nitrate in eastern San Joaquin Valley

Thomas Harter
Yuksel S. Onsoy
Katrin Heeren
Michelle Denton
Gary Weissmann
Jan W. Hopmans
William R. Horwath

The sustainability of water resources is key to continued prosperity in the San Joaquin Valley and California. The vadose zone is an often-ignored layer of wet but unsaturated sediments between the land surface and the water table. It plays an important role in groundwater recharge and in controlling the flux and attenuation of nitrate and other potential groundwater contaminants. In a former orchard at the UC Kearney Research and Extension Center, we investigated the processes that control the movement of water, nitrate and other contaminants through the deep vadose zone. These processes were found to be controlled by the alluvial sedimentary geology of the vadose zone, which is highly heterogeneous. This heterogeneity should be considered when interpreting soil and deep vadose zone monitoring data and assessing of the leaching potential of agricultural chemicals. The transport of contaminants through the vadose zone may be significantly faster than previously assumed, while denitrification is likely limited or insignificant in the oxic, alluvial vadose zone of the eastern San Joaquin Valley.

Nearly 3,000 feet of continuous soil cores were obtained between July and October 1997 using the Geoprobe direct-push drilling method. This method allowed for complete recovery of undisturbed cores throughout the 52-foot deep vadose zone. *Above*, UC Davis vadose zone hydrology professor Jan Hopmans (left) and Fresno State geology undergraduate Anthony Cole operate the coring equipment.

For decades, the leaching of agricultural chemicals (fertilizer, especially nitrate, and pesticides) has been a concern of agronomists, soil scientists and hydrologists. Federal legislation first recognized the potential impacts to water resources in the early 1970s, when the Clean Water Act, the Safe Drinking Water Act, the Federal Insecticide, Fungicide, and Rodenticide Act and other legislation related to water pollution were enacted. Since then, countless efforts have been mounted by both the scientific-technical community and the agricultural industry to better understand the role of agricultural practices in determining the fate of fertilizer and pesticides in watersheds (including groundwater) and to improve agricultural management accordingly.

Much of the scientific work related to subsurface nitrate and pesticide leaching has focused on two areas: documenting the extent of contamination in groundwater; and investigating the fate of these chemicals in the soil root zone (including the potential for groundwater leaching) as it relates to particular agricultural crops and management practices. Rarely are these two research areas linked within a single study.

In California's valleys and basins, particularly in Central and Southern California, groundwater levels are frequently much deeper than 10 feet (3 meters) and sometimes as deep as 150 feet (45 meters) or more. Hydrologists refer to the unsaturated zone above the water table as the vadose zone. In general, only the uppermost 4 to 6 feet (1 to 2 meters) is described in soil surveys and investigated in soil studies; the deep vadose zone below the root zone remains largely outside the area of research and regulatory activity.

Yet, the vadose zone below the root zone stores significant moisture. All water and contaminant transport from the land surface to groundwater passes downward through the vadose zone. Few studies have investigated the fate or potential fate of, for example, nitrate and other contaminants in such deep vadose zones. Key questions include, What is the time of travel through the deep vadose zone? And, is there significant denitrification (natural attenuation) of nitrate in the deep vadose zone?

Pioneering work on nitrate in deep soil profiles was presented by Pratt et al. (1972) who investigated nitrate profiles in a Southern California citrus orchard to depths of 100 feet (30 meters); they estimated that it would take between 10 and 50 years for nitrate to leach to that depth. Average nitrate-nitrogen levels

Preferential flow paths, which are responsible for most of the water and solute transport from the root zone to the water table, quickly flush nitrogen to deeper portions of the vadose zone and to the water table, allowing for little or no denitrification.

below the root zone varied from 15 to 35 milligrams per liter (mg/L) under a 50 pounds per acre (lb/ac) treatment and from 35 to 55 mg/L under an excessive 350 lb/ac treatment. Based on gross mass-balance estimates, denitrification at that site was estimated to account for up to 50% of nitrate losses in the thick unsaturated zone profile where application rates were high.

Lund et al. (1974), supported later by Gilliam et al. (1978), Klein and Bradford (1979) and Rees et al. (1995), argued that nitrate losses in the deep vadose zone (due to denitrification) were strongly correlated with the textural properties of the soil. High losses were found in soils with pans or textural discontinuities, while losses were limited in relatively homogeneous, well-draining soils in other areas of Southern California. In contrast, Rolston et al. (1996), using isotope analysis at sites in the southern Sacramento Valley and the Salinas Valley, found little evidence of significant denitrification, even in thick unsaturated zones.

To study deep unsaturated zone hydrology, we established a research site in a former 'Fantasia' nectarine orchard at the UC Kearney Research and Extension Center (KREC) in Fresno County. The objective of our work is to provide a comprehensive assessment of the fate of nitrate in a 52-foot (16-meter) deep alluvial vadose zone that is typical of many agricultural areas in California. The assessment included detailed geologic, hydraulic and geochemical characterization, using nitrate as an example.

Field sampling

A 12-year fertilizer management experiment (from 1982 to 1995) was implemented in a 'Fantasia' nectarine orchard (Johnson et al. 1995). The fertilization experiment consisted of five application treatments in a random block design with triple replicates. Treatments included annual nitrogen application rates ranging from 0 to 325 pounds per acre (0 to 365 kilograms per hectare [kg/ha])(fig. 1). For the vadose zone characterization, three treatment subplots (0, 100 and 325 pounds per acre) were selected in 1997 (2 years after termination of the experiment), which we refer to as the control, standard and high subplot, respectively.

To start, we conducted a conventional root-zone nitrogen (N) mass-balance analysis from application and harvest records for the 12-year experiment in the three subplots. The analysis showed that the annual nitrogen leaching of excess nitrogen fertilizer from the root zone into the deep vadose zone was 51 (± 19), 83 (± 30) and 245 (± 42) pounds per acre. Water losses from the root zone to the deep vadose zone in the flood-irrigated orchard amounted to 1,100 (± 180) millimeters

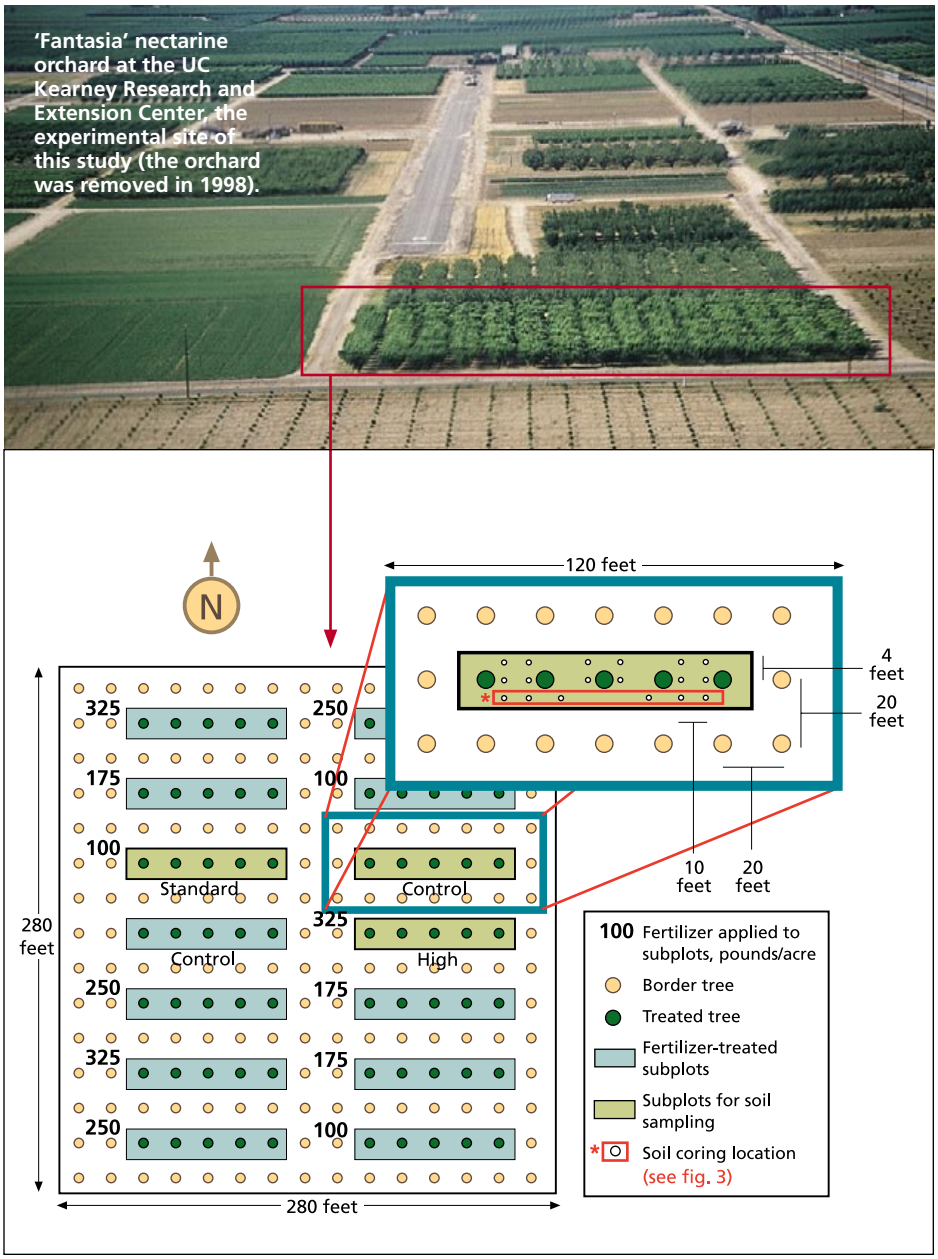

Fig. 1. In 1997, extensive core drilling was conducted, 2 years after the completion of three orchard nitrate-management trials at KREC with annual fertilizer rates of 0, 100 and 325 pounds nitrogen per acre. The complete random block design of the management trial and the three subplots selected for the deep vadose zone drilling are shown.

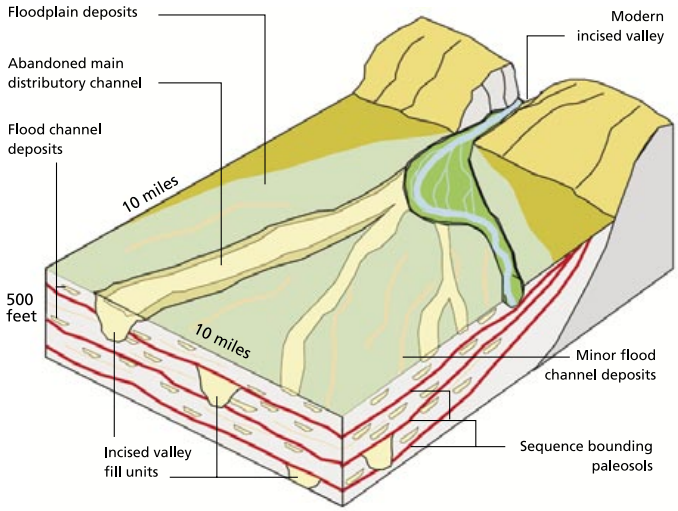

Fig. 2. Schematic diagram of the Kings River alluvial fan and its geologic elements.

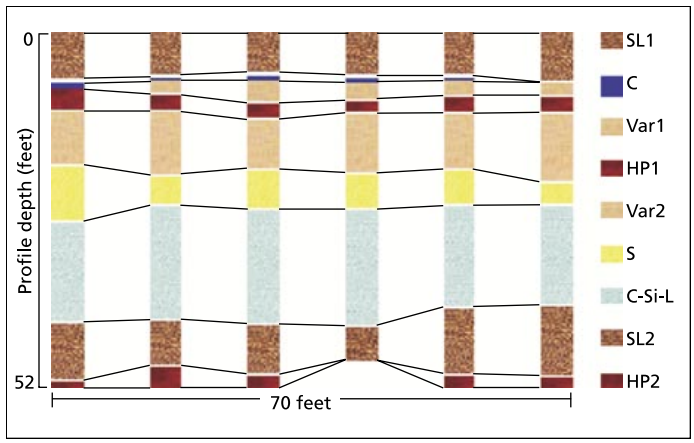

Fig. 3. The 10 major lithofacies identified at the two east-west cross sections, 140 and 144 feet from the southern edge of the orchard. The lithofacies, classified in the field according to color, texture and cementation, exhibit vertically varying thicknesses, yet are laterally continuous over the experimental site. Sandy loam is the most frequent textural unit, while clay is the least.

per year (Onsoy et al. 2005). Assuming uniform flow conditions throughout the deep vadose zone at an average soil moisture content of 25%, the travel time through the deep vadose zone was projected to be 3.2 (± 0.5) years. Based on the leaching rate and travel time, and taking into account that the experiment ended 1 year prior to drilling, we estimate that the deep vadose zone nitrogen storage at the time of drilling would be on the order of 195, 233 and 426 pounds nitrogen per acre in the control, standard and high subplot, respectively.

To confirm this estimate and to determine the applicability of the uniform flow concept, 60 undisturbed sediment cores were obtained in 1997 by drilling to the water table at a depth of 52 feet (16 meters) using a Geoprobe direct-push drilling technique. After geologic characterization of the complete core sections, 1,200 samples were collected (approximately one every 2.5 feet [0.8 meters]). Samples were collected for each sedimentologic stratum or substratum. The soil samples were preserved and stored for later analysis of their texture, hydraulic properties (water content, unsaturated hydraulic conductivity and water retention functions) and biochemical properties (pH, dissolved organic carbon, nitrate-nitrogen, ^{15}N isotope analysis).

Geologic framework

The site is located on the Kings River alluvial fan, approximately 2 miles (3.2 kilometers) west of the current river channel. The quaternary alluvial sediments (that is, sediments deposited by a stream) are derived exclusively from the hard, crystalline Sierran bedrock. Stratigraphically, the quaternary deposits in this part of the valley can be divided into five units (Marchand and Allwardt 1981): the post-Modesto (youngest), Modesto, Riverbank, Upper and Lower Turlock Lake deposits. Except for the post-Modesto, which is less than 10,000 years old (Holocene), these deposits are of Pleistocene age (2 million to 10,000 years old).

Most of the stratigraphic units (sediment facies) found at the site are believed to represent separate alluvial episodes related to several Sierran glaciations. In cores from the study site, these deposits appear as intercalated, thick and thin lenses of clayey silt, silt, sand and gravel from fluvial deposition. Channel sediments consist of moderately to well-sorted, subangular to subrounded sand and gravel. These channel deposits are surrounded by muddy sand and silts of floodplain deposits (fig. 2)(Page and LeBlanc 1969; Huntington 1980; Weissmann et al. 2002). Deposits from the various periods of Sierran glaciations are vertically separated by paleosols. Paleosols are buried soil horizons that were formed on stable upper-fan or terrace surfaces during interglacial periods, when no sediment deposition took place (fig. 3).

The vadose zone sediments are most easily classified by their texture, which ranges from clay to small gravel and includes a wide spectrum of predominantly silty to sandy sediments. The colors of the sediments range from grayish brown to yellowish brown, and more randomly to strong brown (no significant reduction zones). The thickness of individual beds varies from less than 0.4 inch (1 centimeter) for some finely layered clayey floodplain deposits to more than 8 feet (2.5 meters) for sandy streambed deposits. Sharp as well as gradual vertical transitions are present between texturally different units. The relative proportion of the five major textural categories found in the sediment cores was 17.2% sand, 47.8% sandy loam, 13.8% silt loam/loam, 8.3% clay loam/clay and 12.9% paleosol (see sidebars, pages 128 and 129; fig. 4).

KEY (figs. 3, 4): The major lithofacies are:

- **SL1 — recent Hanford sandy loam**
- **C — clay, very thin**
- **Var1 — variable sedimentary structures, predominantly sand**
- **HP1 — shallow paleosol (hardpan), red**
- **Var2 — various textures, sandy loam to clay loam**
- **S — medium sand**
- **C-Si-L — clay/clayey silt/clay loam, fine-textured floodplain deposits**
- **SL2 — sandy loam and**
- **HP2 — deep clayey paleosol (hardpan), red**

Hydraulic properties variability

Hydraulic properties of the unsaturated zone, such as the hydraulic con-

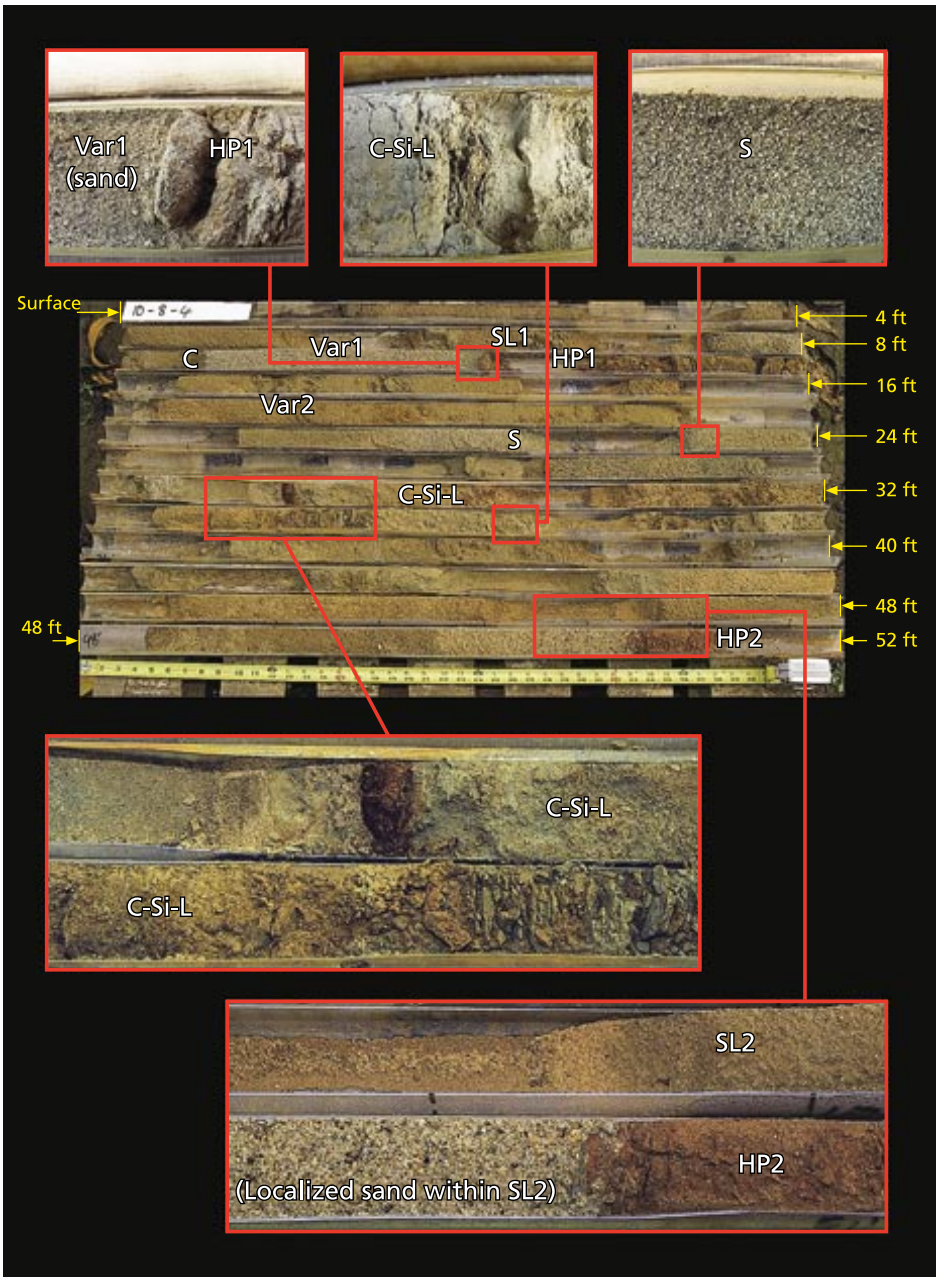

Fig. 4. Individual core sections were collected in 4-foot (1.2 meter) plastic tubes (see fig. 1). This image shows all 13 sections of a 52-foot (15.6-meter) core, lined up from the ground surface (*upper left*) to the bottom of the core (*lower right*). Missing subsections represent soil sampling locations for hydraulic and chemical analysis.

ductivity/moisture curve and the water retention curve — and the spatial distribution of these properties — strongly control the flow of water and the transport of nitrate and other solutes in the deep vadose zone. (Hydraulic conductivity is a measure of how fast water can percolate through the sediments; the higher the moisture and the coarser the sediments, the higher the hydraulic conductivity.) Hydraulic properties were determined in the laboratory on more than 100 undisturbed sediment core samples (3.5 inches [9 centimeters] long by 1.5 inches [3.8 centimeters] diameter) taken from various locations and depths at the orchard site. The laboratory tests involved measuring the water percolation rates in each core at six to 10 different moisture conditions, then determining the hydraulic properties by computer analysis.

Given the large amount of textural variability observed in the cores, it was not surprising that we found the hydraulic properties to also vary significantly, both with depth and laterally across the site (Minasny et al. 2003). The saturated hydraulic conductivity, for example, varied over nearly four orders of magnitude. Within some sedimentary layers (facies) we observed nearly as much hydraulic variability within individual facies as between facies. By far the highest conductivity was observed in sandy facies ("S" and "Var1" in figs. 3 and 4).

Heterogeneity of water flow

Traditionally, water flow between the root zone (at depths of 6.6 feet ([0 to 2 meters]) and the water table (here a depth of 52.8 feet [16 meters]) has been considered essentially a uniform, vertically downward flow process in a more or less homogeneous vadose zone. Within this conceptual framework, water from individual rainfall or irrigation events is thought to be initially stored in the root zone. There, it is available for uptake by the roots. Surplus water then gradually drains into the deeper vadose zone. Individual rainfall or irrigation events create pulses of moisture that penetrate the root zone profile. Through root water uptake and vertical spreading, the moisture pulse dampens out as it travels downward. In the deeper portions of the vadose zone, the downward flow rate has therefore been thought to be equal to the annual recharge rate.

However, the highly heterogeneous geology of the alluvial sediments observed at the orchard site, coupled with the associated heterogeneity of the hydraulic properties, suggest that this traditional conceptual framework is inadequate to describe how water and chemicals are transported through the vadose zone to the water table. Using our field data and computer simulation, we reconstructed two-dimensional cross-sections of the vadose zone that reasonably reflect the spatial variability

Major facies in the study-site vadose zone

The **sand** ("S" and "Var1") is quartz-rich, and contains feldspar, muscovite, biotite, hornblende and lithic fragments consistent with the granitic Sierran source (see figs. 3 and 4). Cross-bedding at the scale of few inches (centimeters) could be observed in some fine-grained sand samples. The dominant color of the sand is a light gray to light brown, the brown hue increasing with increasing loam content. The thickness of the sand beds is as much as 8 feet (2.4 meters), though thickness varies across the study site. Very coarse sand and particles up to pebble grain-size (up to 0.4 inch or 1 centimeter) could occasionally be observed at the bottom of the sand units, but were not present in all the cores. The sand units typically show a subtle fining-upward succession. The basal contact is typically sharp. The texture and distribution of these sandy deposits are consistent with deposition in a fluvial distributary channel on the Kings River fluvial fan. One ancient river channel was observed in cores collected from the orchard site, and it appears to have had a northeast-southwest orientation. The mean thickness of this channel deposit is nearly 6 feet (1.7 meters). The basal coarse sand and pebbles probably represent channel lag deposits that were laid down in deeper parts of the channels.

Sandy loam ("SL1," "SL2") is the most frequent lithofacies within the profile. The color is usually light olive to yellowish brown. Some of the sandy loam sediments are considered to be weakly developed paleosols because of their stronger brownish color, root traces and presence of aggregates. Mean bed thickness is 20 inches (50 centimeters), though individual beds can be as much as 7 feet (2 meters) thick. The sorting is moderate to good. Clay flasers and thin (fractions of an inch, 0.5 to 1 centimeter) clay laminae occur in some sandy loam units. Sandy loam sediments are assumed to have developed at the edge of channels, as levee or as proximal floodplain deposits near the channels.

Silt loam, loam and silty clay loam (portions of "C-Si-L" and "Var2") are usually slight olive brown to brownish gray in color. The bed thickness is within a range of a few inches to a foot (centimeters to decimeters). Fine-grained sediments often show sharp contacts between the units. Changes from one unit to the next exist on small distances. Lamination can more frequently be observed within silty sediments than in fine sands. Root traces and rusty brown–colored mottles are quite common. The depositional environment was presumably the proximal to distal floodplain of the fluvial fan, an area dissected by distributary streams.

The finest sediments are grouped in the fourth category: **silt, clay and clay loam** (portions of "C," "C-Si-L" and "Var2"). These are believed to have been deposited in the distal floodplain and in ponds that developed in abandoned channels. The main color is brownish gray to olive brown. Fine, less than 1-millimeter-diameter root traces and rusty brown mottles are common in the clay sediments. Statistics for the thickness of clay layers in the unit between 27 and 43 feet (8 and 13 meters) depth show a mean thickness of 5 inches (12.8 centimeters), but the mode is about 2.2 inches (3 centimeters). A 20-inch (50-centimeters) thick clay bed was observed at approximately 8 feet (2.5 meters) depth in most of the cores.

Paleosols ("HP1," "HP2") were recognized in different stages of maturity. They show a brown to strong brown, slightly reddish color, exhibit aggregates, ferric nodules and concretions, few calcareous nodules and hard, cemented layers. They also display a sharp upper and a gradual lower boundary as is typical for paleosols (Retallack 1990). Clay content decreases downward in the paleosols. Another feature is fine root traces, though these are typically obliterated in the more mature paleosols. Paleosols formed in periods of stasis marked by nonerosion and nondeposition, during the interglacials (Weissmann et al. 2002). The thickness of the paleosol horizons ranges from 20 inches (50 centimeters) to about 7 feet (2 meters).

of the hydraulic properties observed in the field, then we simulated water flow through this reconstructed vadose zone. Figure 5 illustrates the spatial distribution of the water flux through a hypothetical cross-section at 40 feet, similar to that observed at the orchard site. It captures important features that are characteristic of water flow in heterogeneous vadose zones (Russo et al. 1998; Harter and Yeh 1996). Understanding that flow occurs in this highly irregular pattern is important for interpreting the field data.

In particular, figure 5 shows that even though the simulated water application at the surface was uniform, the heterogeneity of the vadose zone forces water into distinct preferential flow paths (warm colors), separated by large areas of relatively stagnant flow (cooler colors). The preferential flow paths have highly irregular shapes, but are continuous and extend to the water table. The preferential flow paths occupy only a small portion of the vadose zone. In contrast, areas with relatively stagnant water flow occupy most of the vadose zone. Soil moisture differences between these two zones are small. Soil moisture is therefore not a particularly sensitive indicator and may not be useful for identifying the presence and location of these preferential flow paths.

In our study, further field work and computer simulations indicate that the location of these preferential flow paths does not change over time, even though they may partially or completely dry out between infiltration events. A new event will recreate the same set of preferential flow paths.

Preferential flow paths are not only created by the sediment heterogeneity. Other conditions may also trigger and support preferential flow paths: macropores in the root zone; flow instability during infiltration into sand or loamy sand soils (Wang et al. 2003); flow through or above embedded clay or sand lenses ("funneling")(Kung 1990); and "fingering" as a result of a sharp textural boundary within the vadose zone where the finer-textured (silt/clay) layer is located above a coarse-textured (sand) layer (Glass and Yarrington 2003).

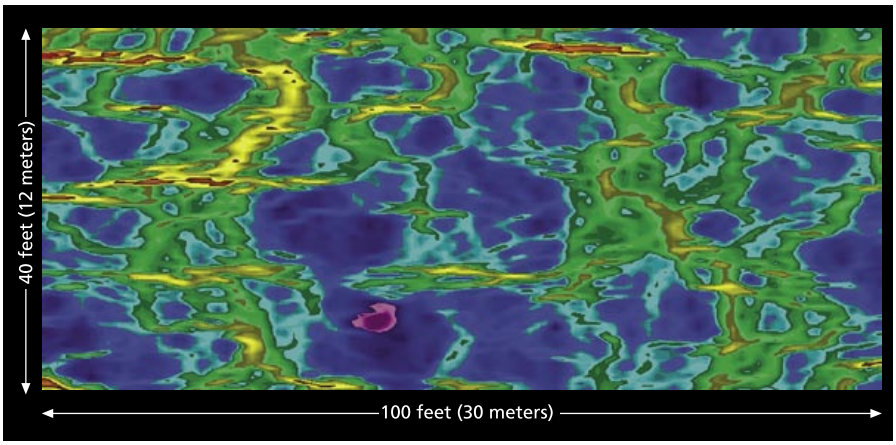

Fig. 5. Hypothetical, computer-simulated, unsaturated water flow rates through a heterogeneous vadose zone, illustrating how heterogeneity in the unsaturated zone generates preferential flow paths: Warmer colors (red, orange, yellow) represent high flow rates, and cooler colors (blue, violet, black) represent lower flow rates. The unsaturated hydraulic properties used for the simulation are similar to those found at the KREC research site.

Since much of the annual recharge occurs through these preferential flow paths, the actual downward flow rate is locally much higher than that estimated when assuming that the entire vadose zone uniformly participated in the downward water flow. Hence, solute travel times through deep vadose zones are likely shorter than if flow were indeed uniform. Because of the shorter travel time, nitrogen storage in the deep vadose zone should be significantly lower than estimated based on the uniform flow concept. On the other hand, under heterogeneous conditions, relatively old water may be trapped in the more stagnant portions of the vadose zone for extended periods. Do the measured nitrate distribution and water chemistry in the deep vadose zone at the Kearney site support this alternative conceptual framework of water and solute flow through the vadose zone?

Nitrogen distribution

To address this question, nitrate-nitrogen (NO_3-N) concentrations were measured in 809 subsamples of our cores. We found that the data were indeed highly variable and log-normally distributed (the logarithms of the data were normally distributed). Nitrate-nitrogen concentrations ranged from less than the detection limit of 0.05 milligram per liter (mg/L)(224 samples or 28% of the sample population) to more than 100 mg/L (two samples). Approximately 10% of the samples exceeded the maximum contamination level for drinking water (10 mg/L), set by the U.S. Environmental Protection Agency under the Safe Drinking Water Act. More than half of those occurred in the subplot with the highest nitrogen application. Mean nitrate-nitrogen concentrations (not including nondetects) in the control, standard and high subplot vadose zone were estimated to be 5.2, 3.3 and 7.4 mg/L, respectively (Onsoy et al. 2005). The nitrate-nitrogen coefficient of variation (CV) ranged from 1.6 to 2.4 within each subplot. The difference between the control and standard subplots was statistically not significant due to the large variability. But the high subplot yielded significantly larger mean nitrate-nitrogen concentrations throughout the profile, consistent with the overapplication of fertilizer.

Within all three subplots, slightly higher nitrate-nitrogen levels were observed in the root zone than in the deep vadose zone below the root zone, possibly due to the last fertilizer application in fall 1996, prior to our drilling. Other than that, we observed no significant vertical nitrate-nitrogen trend in the deep vadose zone.

The highest number of nondetects occurred in the coarse-textured, sandy lithofacies and in the sand lithofacies (above historic water level). There, approximately half of the samples had nondetectable nitrate-nitrogen levels. This is consistent with findings that fingering or preferential flow is particularly dominant in sandy unsaturated sediments. In other words, much of the sand facies does not participate in the flow (stagnant moisture) and would see little or none of the nitrate-nitrogen that is passing through the preferential flow paths.

Study-site geologic profile

A number of distinct sedimentologic units are recognized in the vadose zone profile throughout the orchard and are used to construct a field-scale geologic framework for the research site (see figs. 3 and 4).

The deepest parts of the cores (between 50 and 52 feet [15 and 15.8 meters]) display a strong brownish-colored, clay-rich paleosol. This paleosol marks the top of the upper Turlock Lake deposits (Weissmann 2002). Directly above this paleosol, from depths between 40 and 50 feet (12 to 15 meters) below the surface, the main textural units are sandy loam to fine sandy loam, with some coarse sand and gravel or fine-grained sediments. In the cores with fine sediment at the bottom of this unit, a coarsening-upward succession was observed in this zone; in the other cores a fining-upward cycle was observed.

Between 27 and 40 feet (8 and 12 meters) depth, the sediments are vertically and laterally quite heterogeneous with relatively thin bedding (thickness of a few inches [centimeters] to a couple of feet [few decimeters]), consisting mainly of clayey, silty and loamy material. Another strong brownish paleosol occurs at a depth of 30 to 33 feet (9 to 10 meters). Between 20 and 30 feet (6 and 9 meters) below the surface, a distinct sand layer, representing a former stream channel bed, is found. This unit has laterally varying thickness averaging nearly 6 feet (1.7 meters). A weak, mostly eroded paleosol was developed on top of the sand unit.

From about 10 to 13 feet (3 to 4 meters) to 20 feet (6 meters) below the surface, sandy loam with intercalated sand, clayey and silty material is found. Different trends of upward-fining and upward-coarsening are found on top of each other and laterally next to each other within this unit.

Immediately above the unit, at a depth of about 10 to 13 feet (3 to 4 meters), a nearly foot thick (0.2 meter) to more than 10 feet (1 meter) thick paleosol hardpan occurs. This paleosol marks the top of the Riverbank formation. Recent ground-penetrating radar surveys indicate that this paleosol is laterally extensive across the orchard site.

Sandy loam and subordinated loamy sand and loam are present from the top of the paleosol to the surface, and represent the Modesto deposits at the site. About 8 feet (2.5 meters) below the surface, a laterally continuous clay horizon with a thickness of few inches (centimeters) is found in most of the cores.

Most importantly, the total nitrogen mass estimated directly from the measured nitrate-nitrogen distribution in the deep vadose zone was only 46 (± 9), 37 (± 6) and 83 (± 12) pounds per acre annually for the control, standard and high subplots, respectively. This is less than one-quarter of the total nitrogen mass in the deep vadose zone that was indirectly estimated from the mass balance described above, which is based on the conventional uniform flow concept.

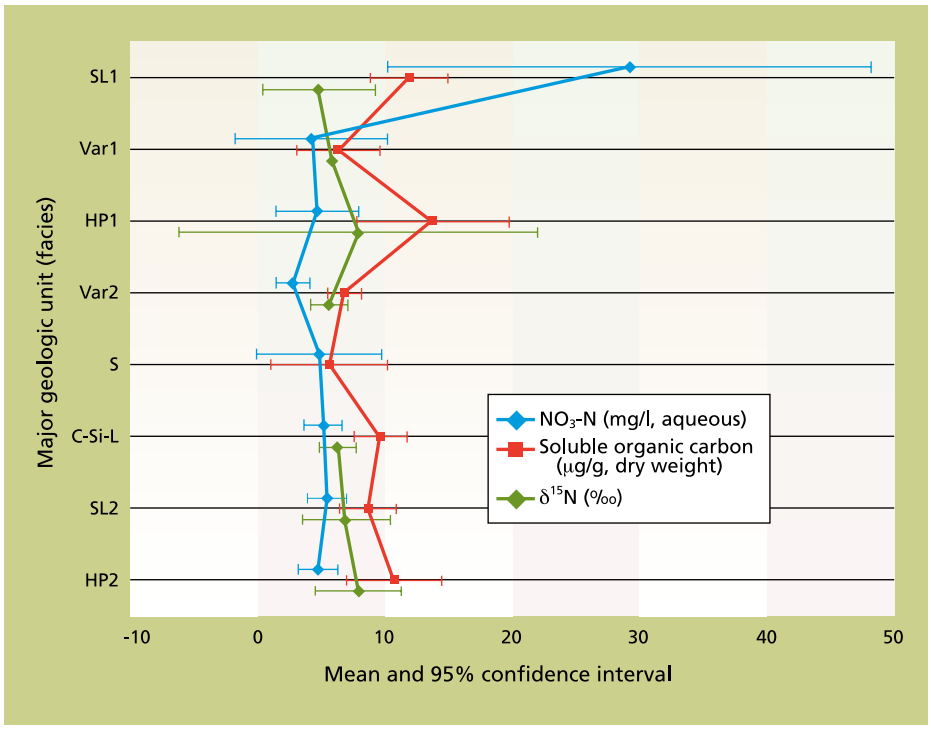

Fig. 6. Composite nitrate-nitrogen, dissolved organic carbon (DOC) and δ^{15}N profiles from borings at the orchard study site. Higher DOC indicates a higher potential for denitrification. Higher δ^{15}N levels (above 10) indicate the occurrence of partial denitrification.

Role of denitrification

Traditionally, such low nitrate-nitrogen mass in the deep vadose zone has been attributed to denitrification (the microbial breakdown process of nitrate by soil microbes). However, the lack of a significant vertical trend in the average nitrate-nitrogen concentration does not support that hypothesis (denitrification in the deep vadose zone would create a nitrate-nitrogen profile that shows decreasing concentration with depth). To further evaluate whether denitrification played a significant role in the deep vadose zone, we measured the amount of soluble organic carbon (a microbial food source) and the amount of δ^{15}N (a rare nitrogen isotope that increases in relative abundance when denitrification occurs) in the nitrate-nitrogen of samples from four cores (three from the high subplot and one from the standard subplot). (The concentration of isotopes is not reported in absolute values, but rather as a relative concentration, hence the notation "delta" or "δ" ^{15}N. A value of δ^{15}N = 5‰ indicates that the ^{15}N concentration is 5 permil above normal [1 permil = 0.1 percent].)

Soluble carbon was found to be very low, not favoring high rates of microbial degradation anywhere in the vadose zone profile. The δ^{15}N values varied from 0‰ to 12‰ and averaged 6‰ (fig. 6). Without denitrification, δ^{15}N levels are expected to be in the range of –5‰ to 5‰ (Rolston et al. 1996). Denitrification decreases nitrate-nitrogen concentrations, but increases the relative amount of isotopically heavy NO_3– δ^{15}N. Indeed, there was a very weak trend ($R^2 < 0.1$) to support the hypothesis that a limited amount of denitrification may occur in the vadose zone: samples with 2 mg/L to 10 mg/L nitrate-nitrogen had relative δ^{15}N levels of 5‰ to 12‰, while samples with higher nitrate-nitrogen contained from 0‰ to 6‰ of δ^{15}N. (No δ^{15}N measurements could be made on samples with less than 2 mg/L nitrate-nitrogen.)

There was significant scatter in these data, corroborating the concept of highly heterogeneous transport. Furthermore, just as there was no significant decrease in nitrate-nitrogen with depth, there was no significant increase in δ^{15}N with depth, similar to isotopic results at geologically similar Yolo County and Salinas Valley sites (Rolston et al. 1996). Then why was the total nitrogen storage in the deep vadose zone so low?

The nitrate distribution pattern that we found (fig. 7) was similar to that postulated in other experimental studies specifically designed to assess transport in heterogeneous soils as well as that predicted by numerical models of flow and transport in highly heterogeneous vadose zones (Harter and Yeh 1996). Hence, the proposed conceptual framework of preferential flow in the deep vadose zone may provide the answer: preferential flow paths, which are responsible for most of the water and solute transport from the root zone to the water table, quickly flushed nitrate-nitrogen to deeper portions of the vadose zone and to the water table, allowing for little or no denitrification. This would explain the occurrence of high nitrate-nitrogen levels and low δ^{15}N levels throughout the depth of the vadose zone profile.

Lower nitrate-nitrogen would occur in stagnant water zones outside preferential flow paths. Due to their longer residence time, nitrate-nitrogen in these zones was apparently subject to a small amount of denitrification, which would explain the higher levels of δ^{15}N that were also found, scattered throughout most of the profile.

The importance of this finding is that while limited denitrification took place in the stagnant water areas of the vadose zone, the majority of the

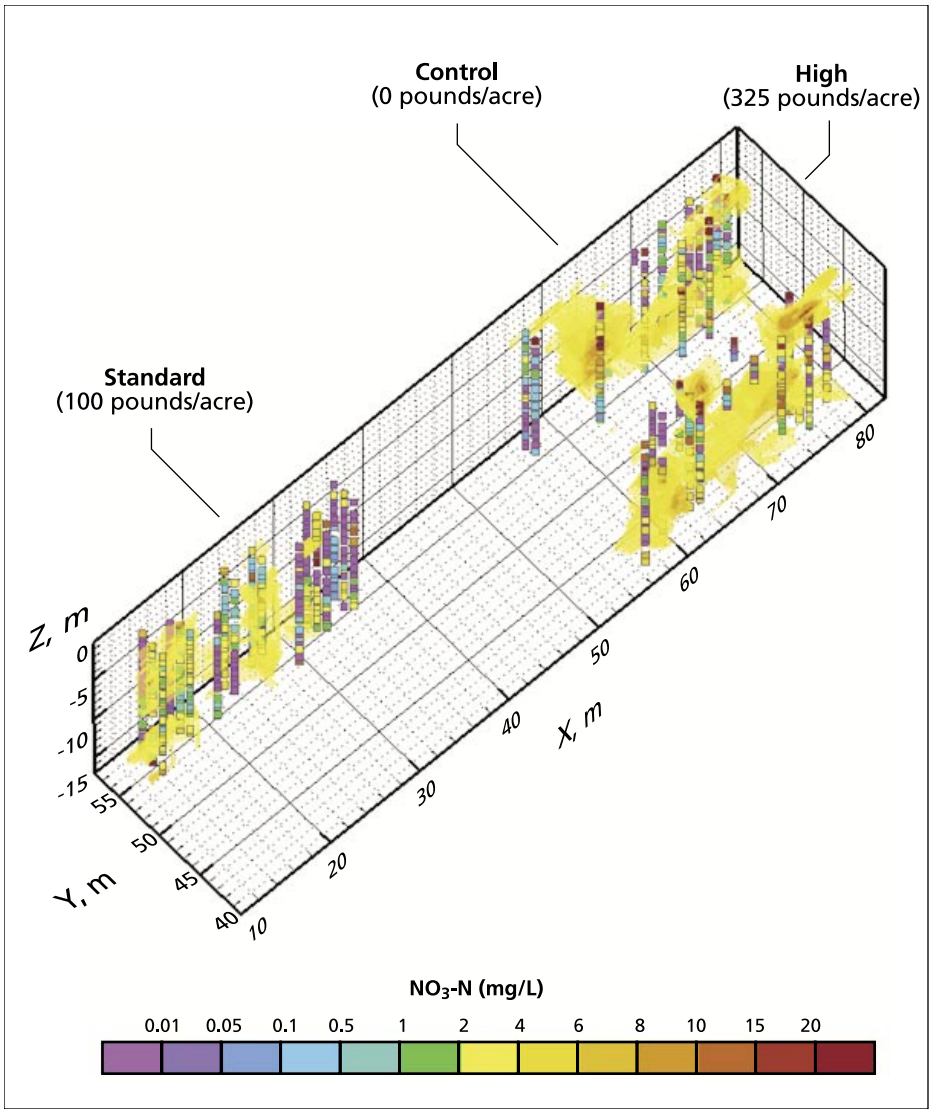

Fig. 7. Measured core nitrate-nitrogen data (squares) and three-dimensional, kriged (yellow) contours of nitrate-nitrogen data. The kriged isosurfaces (only for NO_3-N > 1 mg/L) are obtained from geostatistical analyses of the water content and nitrate measurements at the sampling locations. The standard subplot yielded the largest areas of negligible nitrate concentrations (NO_3-N < 1 mg/L) among the three subplots. High concentrations are seen in the upper profile and near the water table.

nitrate-nitrogen transport occurred in preferential flow paths, where no significant denitrification appears to have taken place. Hence, the low average nitrate-nitrogen concentration in the vadose zone pore water should not be interpreted as an indicator for high denitrification and low nitrate impact on groundwater. Rather, it may be the result of swift, unattenuated nitrate-nitrogen transport to the water table (the same may apply to the root zone).

Analysis shows variability

Our detailed geologic, hydraulic and geochemical analysis of a typical deep vadose zone in the eastern San Joaquin Valley demonstrated that alluvial vadose zones are subject to significant geologic variability, which in turn causes the hydraulic properties and water flow in the vadose zone to exhibit strong spatial variability. While such variability is expressed to only a limited degree in the variability of the observed moisture content, it leads to highly variable concentrations of chemicals, such as nitrate. Our research presents new evidence indicating that unsaturated water flow and transport of nitrate and other agrochemicals (such as pesticides) in the deep vadose zone below the root zone may be subject to significant preferential flow patterns with significantly faster travel times than would be estimated under uniform flow assumptions. Faster travel times not only decrease the potential for denitrification, but also decrease the potential for natural attenuation of pesticides.

Our work suggests that the traditional interpretation of deep vadose zone measurements should be reconsidered. The assumption of uniform flow is not applicable to many alluvial vadose zone sites. The common practice of compositing soil samples taken from immediately below the root zone provides an estimate of the average nitrate-nitrogen concentration at that depth. However, our work indicates that recharge water may constitute only a minor portion of that vadose zone water and is not effectively represented by composite soil samples. It appears that the average or composite nitrate-nitrogen concentrations are also not appropriate for estimating the amount of denitrification as a closure term to the nitrogen mass balance. We are currently implementing detailed heterogeneous flow and transport simulations to further support these findings and to develop guidelines for sampling the deep vadose zone.

T. Harter is Associate Groundwater Quality Hydrologist (UC Cooperative Extension), Department of Land, Air and Water Resources, UC Davis; Y.S. Onsoy is consultant and Doctoral Candidate, UC Davis; K. Heeren is freelance geologist in environmental education, Germany; M. Denton is

Before it is pumped to the surface for agricultural or other uses, groundwater percolates through the geologically variable vadose zone. Based on this study, current assumptions about transport of nitrate from fertilizers and other agricultural chemicals need to be reexamined.

consultant and obtained a master's degree in hydrologic studies, Department of Land, Air and Water Resources, UC Davis; G. Weissmann is Assistant Professor of Hydrogeology, Department of Geological Sciences, Michigan State University; and J.W. Hopmans is Professor of Vadose Zone Hydrology, and W.R. Horwath is Associate Professor of Soil Biogeochemistry, Department of Land, Air and Water Resources, UC Davis.

The California Fertilizer Research and Education Program, California Tree Fruit Agreement, UC Water Resources Center, Geoprobe Systems and Studienstiftung des Deutschen Volkes provided support for this project. We would like to thank Kevin Pope, formerly with Geoprobe Systems, Jean Chevalier with his crew at KREC, and Dick Rice and R. Scott Johnson at the UC Kearney Agricultural Center for their support during the field work; Anthony Cole, Chad Pyatt and Rigo Rios for drilling the 3,000 feet of vadose zone cores at the site; Andrea DeLisle and Timothy Doane for their analytical chemistry work; Jim MacIntyre for implementation of the multistep outflow experiments needed to determine the hydraulic properties at the site; and Atac Tuli for his support in developing the necessary software to use in conjunction with the multistep outflow experiments.

References

Gilliam JW, Dasberg S, Lund LJ, Focht DD. 1978. Denitrification in four California soils: Effect of soil profile characteristics. Soil Sci Soc Amer 42:61–6.

Glass RJ, Yarrington L. 2003. Mechanistic modeling of fingering, nonmonotonicity, fragmentation, and pulsation within gravity/buoyant destabilized two-phase/unsaturated flow. Water Resour Res 39(3):1058, DOI:10.1029/2002WR001542.

Harter T, Yeh T-CJ. 1996. Stochastic analysis of solute transport in heterogeneous, variably saturated soils. Water Resour Res 32(6):1585–95.

Huntington GL. 1980. Soil-land form relationships of portions of the San Joaquin River and Kings River alluvial depositional systems in the Great Valley of California. Ph.D. dissertation, UC Davis. 147 p.

Johnson RS, Mitchell FG, Crisosto CH. 1995. Nitrogen fertilization of Fantasia nectarine: A 12-year study. UC Kearney Tree Fruit Rev 1:14–9.

Klein JM, Bradford WL. 1979. Distribution of nitrate and related nitrogen species in the unsaturated zone, Redlands and vicinity, San Bernardino County, California. USGS Water Resourc Invest Rep 79–60. 81 p.

Kung K-JS. 1990. Preferential flow in a sandy vadose zone: 1. Field observations. Geoderma 46:51–8.

Lund LJ, Adriano DC, Pratt PF. 1974. Nitrate concentrations in deep soil cores as related to soil profile characteristics. Environ Qual 3:78–82.

Marchand DE, Allwardt A. 1981. Late Cenozoic stratigraphic units, northeastern San Joaquin Valley, California. USGS Bull 1470.

Minasny B, Hopmans JW, Harter T, et al. 2003. Neural networks prediction of soil hydraulic functions from multi-step outflow data. Soil Sci Soc Amer 68:417–29.

Onsoy YS, Harter T, Ginn T, Horwath WR. 2005. Spatial variability and transport of nitrate in a deep alluvial unsaturated zone. Vadose Zone J 4(1):41–54.

Page RW, LeBlanc RA. 1969. Geology, hydrology and water quality in the Fresno area, California. USGS Open-File Rep. 70 p.

Pratt PF, Jones WW, Hunsaker VE. 1972. Nitrate in deep soil profiles in relation to fertilizer rates and leaching volume. Environ Qual 1:97–102.

Rees TF, Bright DJ, Fay RG, et al. 1995. Geohydrology, water quality, and nitrogen geochemistry in the saturated and unsaturated zones beneath various land uses, Riverside and San Bernardino Counties, California, 1991–93. USGS Water Resour Invest Rep 94–4127. 267 p.

Retallack GJ. 1990. *Soils of the Past — An Introduction to Paleopedology*. Hyman U (ed.). Winchester, MA. 520 p.

Rolston D, Fogg GE, Decker DL, et al. 1996. Nitrogen isotope ratios identify nitrate contamination sources. Cal Ag 50(2):32–6.

Russo D, Zaidel J, Laufer A. 1998. Numerical analysis of flow and transport in a three-dimensional partially saturated heterogeneous soil. Water Resour Res 34(6):1451–6.

Wang Z, Wu L, Harter T, et al. 2003. A field study of unstable preferential flow during soil water redistribution. Water Resour Res 39(4), 10.1029/2001WR000903, 01 April 2003.

Weissmann GS, Mount JF, Fogg GE. 2002. Glacially-driven cycles in accumulation space and sequence stratigraphy of a stream-dominated alluvial fan, San Joaquin Valley, California. J Sediment Res 72:270–81.

APPENDIX 3:

SPATIAL VARIABILITY OF SCALING FACTORS

APPENDIX 3:
SPATIAL VARIABILITY OF SOIL HYDRAULIC PROPERTIES AND SCALING FACTORS

Y. Sevim Onsoy, Thomas Harter
Dept. Land, Air, and Water Resources
University of California
Davis, CA 95616-8628

Spatial Variability of Soil Hydraulic Properties by Lithofacies

The importance of sedimentary structure as a control on the soil properties and more specifically on hydraulic conductivity is evident from the findings of previous studies. Davis et al. (1993) suggest that sedimentary structures can be used to better evaluate and quantify the subsurface heterogeneity. The relationship between depositional structures and soil properties can then be used to infer a suite of soil hydraulic properties corresponding to various lithofacies. Some investigators focused on the description of aquifer properties with a particular interest in saturated hydraulic conductivity, by measuring saturated *K* for several sedimentary facies (e.g., Davis et al., 1993; Johnson and Dreiss, 1989; Davis et al., 1997). They delineated the spatial distribution of K using facies distributions and then suggested a quantifiable relationship between sedimentary facies and soil hydraulic properties. Kolterman and Gorelick (1996) provided a comprehensive review for sedimentologic approaches as they related to fluid transport properties in aquifers. Although less studied than *K*, the spatial variability of other soil properties are also investigated in relation to facies distributions. More recently, Allen-King et al. (1998) have emphasized the importance of characterizing heterogeneity of both soil physical and geochemical properties by evaluating the correlation between hydraulic conductivity and sorption coefficient in relation to sedimentary facies in a vertical core of the Borden aquifer. Their results have demonstrated that facies are significant explaining the variability in data and suggested that a facies-based approach can be used to identify zones of distinct statistical behavior of transport properties. Herein, spatial variability of soil hydraulic functions is analyzed by accounting for the lithofacies descriptions.

Soil Hydraulic Functions Grouped by Lithofacies

Soil samples measured for soil hydraulic properties were grouped by their lithofacies classes according to the locations of the samples with respect to the boundaries of lithofacies. Specific attention was given to those samples located near the facies boundaries (i.e., ~ within 15 cm of the facies boundaries) to ensure that samples belong to the appropriate lithofacies group. Three samples near the lithofacies boundaries were moved to the adjacent neighboring lithofacies since their water retention and hydraulic conductivity curves matched the hydraulic functions of those samples in the neighboring lithofacies better. The C facies contained only one sample whose soil hydraulic functions were in close resemblance of hydraulic curves of soil samples in the adjacent facies HP1. For simplicity in the further analysis, this sample was assumed to be part of the HP1 facies. Eight lithofacies with existing soil hydraulic properties (also referred to as *layers* interchangeably) were constructed.

Figure 1 displays two cross sections of lithofacies where most of the undisturbed soil samples were extracted from. The locations of samples with the measured saturated hydraulic conductivities are

superimposed on the cross sections. To show the spatial variability of water retention and unsaturated hydraulic conductivity functions ($K(\theta)$ and $h(\theta)$, respectively) in relation to the lithofacies, $K(\theta)$ and $h(\theta)$ functions were plotted according to the eight lithofacies descriptions, SL1, Var1, HP1, Var2, S, C-Si-L, SL2, and HP2. Figure 2 shows plots of unsaturated hydraulic conductivity $K(\theta)$ and water retention $h(\theta)$ functions corresponding to 10 samples that were extracted from the top layer SL1 lithofacies. Effective saturation Θ, instead of water content θ, was plotted on the x axes against to K and h data. This provides a common basis for comparing hydraulic conductivity functions between and within the groups over the whole range of saturation.

Evidently, when samples are categorized by lithofacies, they appear to form distinguishable subpopulations of hydraulic curves. However, there is still significant variability within each lithofacies as shown by the wide range of curves. The range of variability observed within lithofacies is interpreted as a sign of the local heterogeneity (within each lithofacies). Samples of the HP1, Var2 and C-Si-L facies show a larger range of curves than samples located in the Var1, S, SL2, and HP2 facies. The SL1 facies contains a moderate range of curves. The variability observed in the hydraulic curves together with the results from the close visual examination of the soil textures lead to the conclusion that among the lithofacies, the C-Si-L exhibits the largest spatial variability of soil hydraulic properties.

Effects of Lithofacies on Soil Hydraulic Parameters

Analysis of soil hydraulic parameters based on basic statistics, as presented earlier in this chapter, is an initial assessment of the spatial variability of data, yet it is of little value in numerical modeling of a layered (or lithofacies) system because of the lack of relation between the parameters and the existing lithofacies. Similar to the approach applied by previous studies (e.g., Allen-King et al. (1998), we used the facies-based approach as a tool to quantify the spatial variability of soil hydraulic parameters in the form of the van Genuchten model. Analysis of variance (ANOVA) was implemented to evaluate the source of variability of soil hydraulic parameters within and between lithofacies. In ANOVA, spatial variability is measured by what is called “sum of squares”, or SS for short. SS is similar to sample variance such that they are both computed from the sum of square deviations from mean. Thus, ANOVA examines the differences in the means of parameters through variances.

ANOVA applied to the soil hydraulic data produces SS partitioned into two components: 1) SS due to the differences in means between lithofacies groups and 2) SS due to within lithofacies variability. The former is usually referred to as “effect” variance. The latter is known as ”error” variance which does not mean mistakes made in the experiment, but signifies any differences among samples within a facies that cannot be explained by the design of the analysis.

As part of the ANOVA, the Post Hoc Tukey HSD comparison technique was applied to determine whether the means of various lithofacies groupings of the van Genuchten parameters are significantly different from each other. This analysis generates a table of correlations between the van Genuchten parameters grouped by lithofacies.

Figure 3 shows the mean and range of the van Genuchten parameters for each of the lithofacies. Observable trends exist particularly for log K_s, log n, and log α. Large values of these parameters coincide with the Var1 and S lithofacies. This outcome supports our earlier analysis based on the grain size distributions, which indicates that the S and Var1 facies contain coarse-textured materials and are found to be different from the other facies. The situation is rather different for residual water content. Consistent with its fine-textured materials, the C-Si-L facies retains more moisture than the other facies, thus has the highest mean and variance of residual water content. For saturated water content, both the S and C-Si-L facies have a higher mean than the other facies, but the latter exhibits the largest variation among all facies. The SL2 has the smallest mean for both residual and saturated water content.

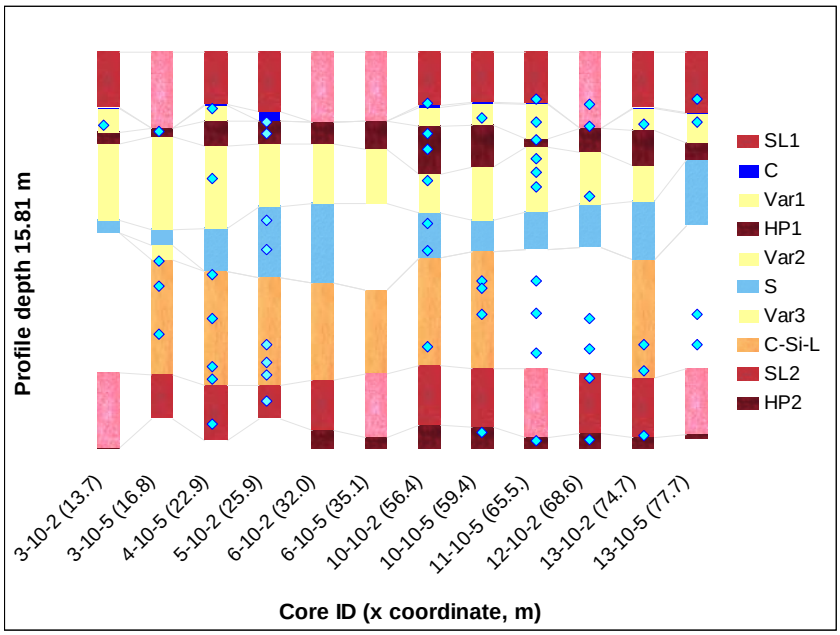

a)

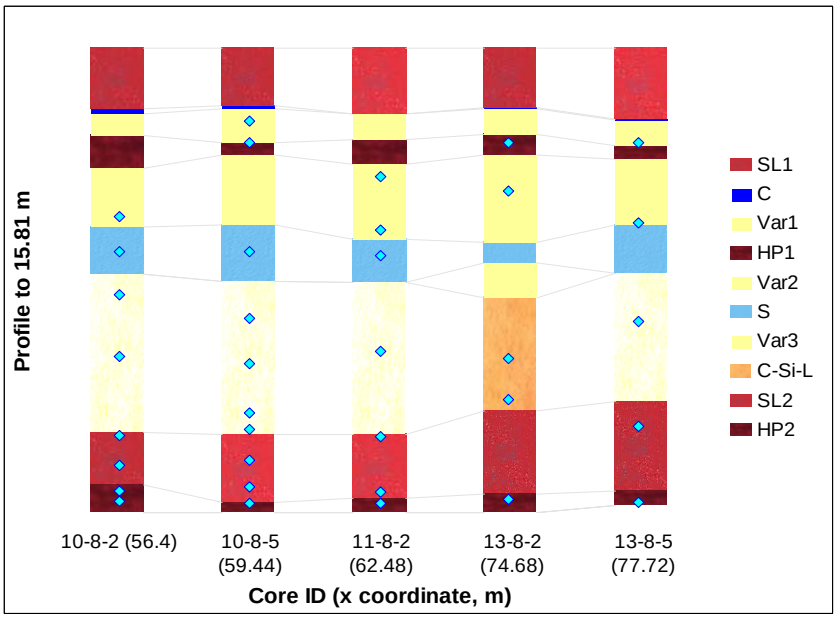

b)

Figure 1: Locations of undisturbed soil samples superimposed on two lithofacies cross sections, a) y = 54.86 m (57 samples) in the standard subplot and b) y = 53.64 m (35 samples) in the high subplot). Eight samples collected from the transect at y = 42.57 m are not shown here.

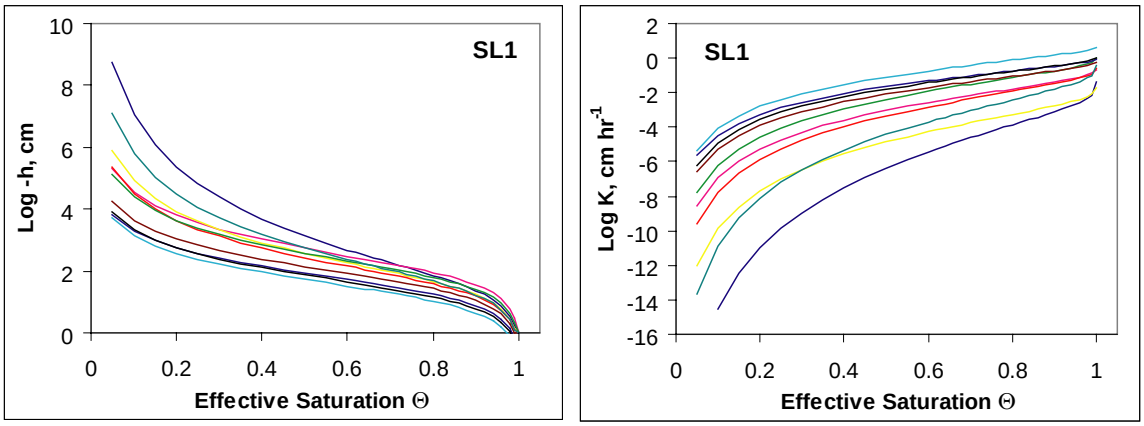

Figure 2: Unsaturated hydraulic conductivity $K(\theta)$ and water retention $h(\theta)$ functions for 10 soil samples extracted from the SL1 lithofacies.

(REMAINDER OF THIS PAGE IS BLANK)

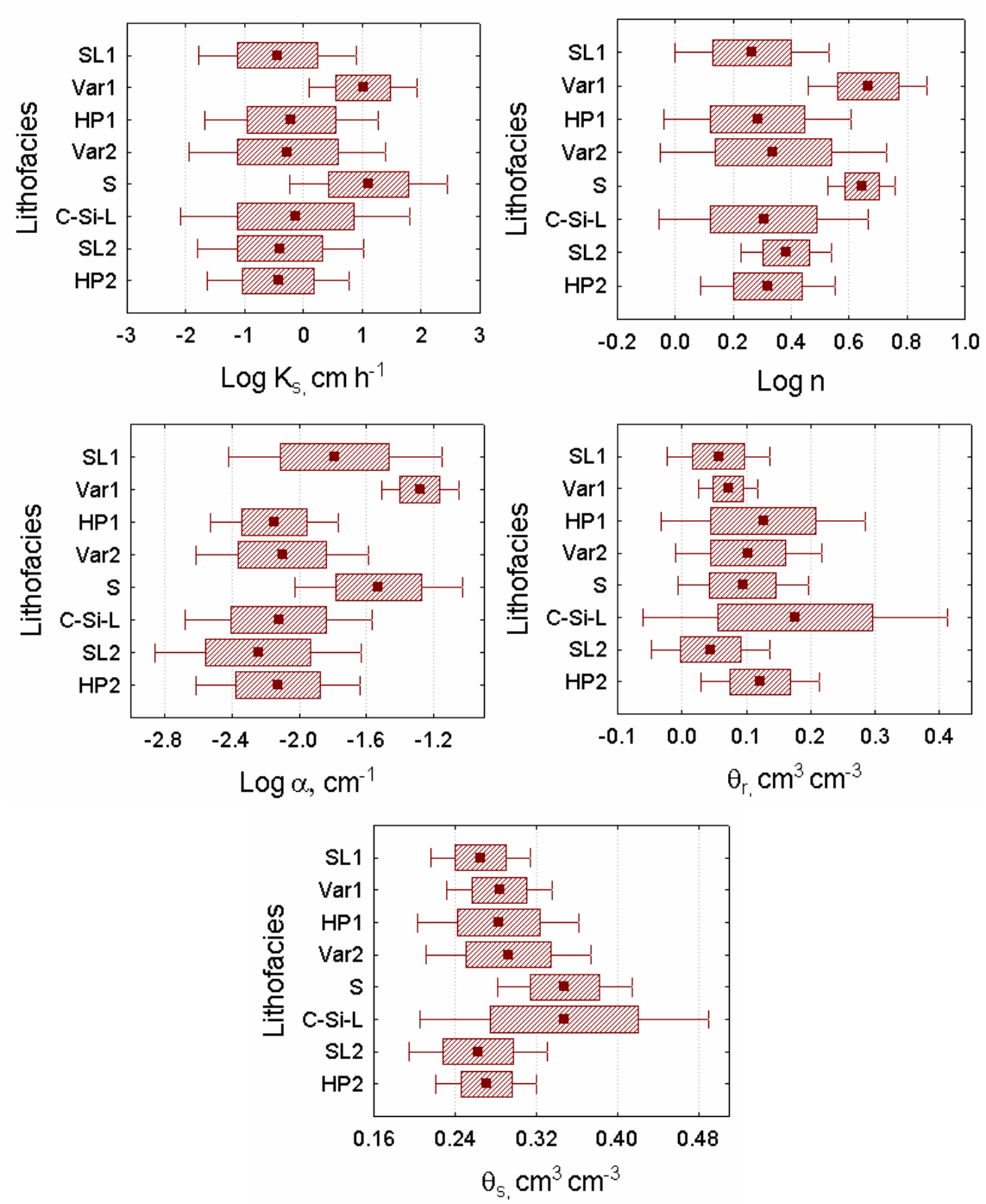

Figure 3: Means and ranges of the van Genuchten parameters categorized by the lithofacies. The center in each box is the mean; the box encloses the $\pm$ standard deviation, and the whiskers show the range of the samples that fall within $\pm 1.96 \cdot$ standard deviation.

Table 1 shows descriptive statistics of the van Genuchten parameters categorized by the lithofacies. The C-Si-L contains the largest portion of the data set (30 samples, almost 1/3 of the entire dataset). Evidently, for the C-Si-L facies within-facies variations, log K_s, log n, log α, θ_r, and θ_s, are nearly equal to or larger than those evaluated for the entire data. This further confirms that the C-Si-L unit that forms the thickest stratigraphic layer is the most variable unit in the subsurface. The Var2 facies, with less samples, shows the log K_s and log n variance that are comparable with those obtained for the entire data. For the other facies, variability increases with sample size.

Analysis of Variance

ANOVA results are summarized in Table 2. Following the same terminology given earlier, between-lithofacies variability is called the *effect* or *mean square effect* and within - lithofacies variability is called the *error* or *mean square error* (MS effect and MS error, respectively). MS effect and error are obtained by dividing the SS effect and error by the degrees of freedom. Within-lithofacies variation is a significant fraction of the total variation for log K_s, log n, θ_r, and θ_s. Significant within-facies variability suggests the existence of multiple individual layers of strata occurring at the scale of cm within facies leading to a heterogeneous structure within facies. This outcome is indicative of correlation lengths of the soil physical parameters less than the dimension of the facies boundaries (Davis et al., 1997). Overall, however, the MS error (variability within-facies) is an order of magnitude smaller than the MS effect (between-facies variability) (Table 2). Hence, differences in the van Genuchten parameters between the facies are statistically significant (Table 2), indicating that lithofacies exerts a quantifiable control on the spatial distribution of soil hydraulic properties.

Correlations between Lithofacies Soil Hydraulic Properties

Hydraulic properties of HP1, Var2, C-Si-L, SL2, and HP2 are significantly correlated. Correlations between θ_r and θ_s parameters and facies are nonlinear. For θ_r, the S unit shows strong correlations with all the facies except C-Si-L which has a moderate correlation with the HP1 and HP2 units. In terms of θ_s, the situation is reversed. The S has a weak or no correlation with the other facies except the C-Si-L. Apparently, a strong correlation exists among the other facies with respect to θ_s parameter.

Post Hoc Tukey HSD technique specifies the correlations between two facies for a given van Genuchten parameter by a pairwise comparison of parameters between facies. A correlation table is shown in Table 3. Significant differences between facies pairs occur for probabilities $\leq$ 0.05. Probabilities < 0.001 are reported as 0.000.

Compared to the visual representations of the means and variances of the van Genuchten parameters with facies (Figure 3), this analysis better demonstrates the relations between facies with respect to the parameters. The key results, noted for *log K*, areas follows: the S and Var1 are highly correlated and significantly different from the other facies. Differences in the SL1, HP1, Var2, C-Si-L, SL2, and HP2 are insignificant. The same test yield similar trends for log n: the S is significantly different from all the other facies except Var1. The SL1, HP1, Var2, C-Si-L, and HP2 are highly correlated with each other. For log α, the results are slightly different from those for log K_s and log n. The S unit shows a moderate correlation with the Var1 and SL1 facies.

Table 1: Basic statistics of the van Genuchten parameters categorized by the lithofacies identified at the site. Standard errors are shown in parentheses.

Lithofacies	# of Data	Mean		Variance	Confidence -95%	Confidence 95%
			log K_s			
All samples	90	-0.122	(0.096)	0.828	-0.313	0.068
SL1	10	-0.440	(0.217)	0.471	-0.931	0.051
Var1	3	1.013	(0.271)	0.221	-0.156	2.181
HP1	8	-0.208	(0.266)	0.567	-0.837	0.422
Var2	12	-0.277	(0.246)	0.729	-0.819	0.265
S	7	1.099	(0.259)	0.470	0.465	1.733
C-Si-L	30	-0.136	(0.181)	0.987	-0.507	0.235
SL2	11	-0.400	(0.217)	0.520	-0.885	0.084
HP2	9	-0.430	(0.205)	0.378	-0.903	0.042
			log n			
All samples	97	0.371	(0.020)	0.039	0.331	0.410
SL1	11	0.264	(0.041)	0.018	0.172	0.355
Var1	8	0.665	(0.037)	0.011	0.577	0.753
HP1	8	0.284	(0.058)	0.027	0.147	0.421
Var2	12	0.338	(0.058)	0.040	0.211	0.465
S	8	0.644	(0.021)	0.003	0.595	0.694
C-Si-L	30	0.305	(0.034)	0.034	0.236	0.374
SL2	11	0.384	(0.024)	0.006	0.330	0.437
HP2	9	0.321	(0.040)	0.014	0.229	0.412
			log α			
All samples	97	-1.979	(0.039)	0.149	-2.056	-1.901
SL1	11	-1.788	(0.100)	0.105	-2.005	-1.570
Var1	8	-1.282	(0.041)	0.014	-1.380	-1.185
HP1	8	-2.149	(0.069)	0.038	-2.311	-1.986
Var2	12	-2.099	(0.075)	0.068	-2.264	-1.933
S	8	-1.527	(0.090)	0.064	-1.739	-1.315
C-Si-L	30	-2.121	(0.052)	0.080	-2.227	-2.015
SL2	11	-2.242	(0.094)	0.098	-2.452	-2.032
HP2	9	-2.125	(0.083)	0.062	-2.317	-1.934
			θ_r			
All samples	97	0.114	(0.009)	0.008	0.096	0.133
SL1	11	0.057	(0.012)	0.002	0.030	0.084
Var1	8	0.072	(0.008)	0.001	0.053	0.091
HP1	8	0.126	(0.029)	0.007	0.058	0.194
Var2	12	0.104	(0.017)	0.003	0.067	0.141
S	8	0.095	(0.018)	0.003	0.051	0.138
C-Si-L	30	0.176	(0.022)	0.015	0.131	0.221
SL2	11	0.045	(0.014)	0.002	0.014	0.076
HP2	9	0.121	(0.016)	0.002	0.085	0.157
			θ_s			
All samples	100	0.305	(0.006)	0.004	0.293	0.317
SL1	11	0.266	(0.008)	0.001	0.249	0.282
Var1	8	0.284	(0.009)	0.001	0.262	0.306
HP1	8	0.283	(0.014)	0.002	0.249	0.317
Var2	12	0.293	(0.012)	0.002	0.266	0.319
S	8	0.348	(0.012)	0.001	0.320	0.376
C-Si-L	33	0.348	(0.013)	0.005	0.322	0.373
SL2	11	0.262	(0.010)	0.001	0.239	0.286
HP2	9	0.271	(0.008)	0.001	0.251	0.290

Table 2: Spatial variability of the van Genuchten parameters within and between the lithofacies.

Sources of Variation	df	SS	MS	F	P
		log K_s			
Between Lithofacies	7	17.367	2.481	3.612	0.002
Within Lithofacies	82	56.324	0.687	…	…
Total	89	73.691	…	…	…
		log n			
Between Lithofacies	7	1.643	0.235	10.028	0.000
Within Lithofacies	89	2.084	0.023	…	…
Total	96	3.727	…	…	…
		log α			
Between Lithofacies	7	7.876	1.125	15.621	0.000
Within Lithofacies	89	6.410	0.072	…	…
Total	96	14.286	…	…	…
		θ_r			
Between Lithofacies	7	0.222	0.032	4.841	0.000
Within Lithofacies	89	0.583	0.007	…	…
Total	96	0.805	…	…	…
		θ_s			
Between Lithofacies	7	0.132	0.019	7.347	0.000
Within Lithofacies	92	0.235	0.003	…	…
Total	99	0.367	…	…	…

df: degrees of freedom; SS: sum of squares; MS: Weighted mean square error (= SS/df); F: F test (no significant variations in the parameters between the two groups if $F < 1$); P: degree of significance (at the 95% confidence level, significant differences occur between and within facies for $p < 0.005$). Probabilities < 0.001 are reported as 0.000.

In general, our results indicate that a facies-based approach provides a good basis to conceptualize the subsurface heterogeneity and to identify distinct statistical behavior of parameters. In other words, large scale spatial variability of soil hydraulic properties can be explained by discrete lithofacies separating regions with different soil hydraulic properties.

Table 3: Results of Post hoc pairwise Tukey HSD comparison identifying the correlations between the van Genuchten parameters categorized by the lithofacies .

	SL1	Var1	HP1	Var2	S	C-Si-L	SL2	HP2
				log K_s				
SL1	1.000	…	…	…	…	…	…	…
Var1	0.149	1.000	…	…	…	…	…	…
HP1	0.999	0.378	1.000	…	…	…	…	…
Var2	1.000	0.250	1.000	1.000	…	…	…	…
S	0.007	1.000	0.059	0.017	1.000	…	…	…
C-Si-L	0.973	0.312	1.000	1.000	0.014	1.000	…	…
SL2	1.000	0.165	1.000	1.000	0.008	0.985	1.000	…
HP2	1.000	0.167	0.999	1.000	0.010	0.982	1.000	1.000
				log n				
SL1	1.000	…	…	…	…	…	…	…
Var1	0.000	1.000	…	…	…	…	…	…
HP1	1.000	0.000	1.000	…	…	…	…	…
Var2	0.939	0.000	0.994	1.000	…	…	…	…
S	0.000	1.000	0.000	0.001	1.000	…	…	…
C-Si-L	0.994	0.000	1.000	0.998	0.000	1.000	…	…
SL2	0.596	0.004	0.856	0.997	0.010	0.828	1.000	…
HP2	0.991	0.000	1.000	1.000	0.001	1.000	0.984	1.000
				log α				
SL1	1.000	…	…	…	…	…	…	…
Var1	0.003	1.000	…	…	…	…	…	…
HP1	0.086	0.000	1.000	…	…	…	…	…
Var2	0.115	0.000	1.000	1.000	…	…	…	…
S	0.430	0.603	0.000	0.000	1.000	…	…	…
C-Si-L	0.015	0.000	1.000	1.000	0.000	1.000	…	…
SL2	0.004	0.000	0.995	0.905	0.000	0.904	1.000	…
HP2	0.108	0.000	1.000	1.000	0.000	1.000	0.978	1.000
				θ_r				
SL1	1.000	…	…	…	…	…	…	…
Var1	1.000	1.000	…	…	…	…	…	…
HP1	0.597	0.880	1.000	…	…	…	…	…
Var2	0.866	0.989	0.999	1.000	…	…	…	…
S	0.974	0.999	0.994	1.000	1.000	…	…	…
C-Si-L	0.002	0.036	0.787	0.168	0.204	1.000	…	…
SL2	1.000	0.996	0.386	0.665	0.888	0.000	1.000	…
HP2	0.651	0.915	1.000	1.000	0.998	0.638	0.429	1.000
				θ_s				
SL1	1.000	…	…	…	…	…	…	…
Var1	0.994	1.000	…	…	…	…	…	…
HP1	0.996	1.000	1.000	…	…	…	…	…
Var2	0.904	1.000	1.000	1.000	…	…	…	…
S	0.016	0.190	0.177	0.254	1.000	…	…	…
C-Si-L	0.000	0.038	0.033	0.036	1.000	1.000	…	…
SL2	1.000	0.985	0.989	0.842	0.010	0.000	1.000	…
HP2	1.000	1.000	1.000	0.977	0.045	0.003	1.000	1.000

Scaling Factors

The scaling procedure has been extensively used as a physical-based method to express the spatial variability of soil hydraulic properties by a single parameter called *scaling factor* λ (Sposito, 1998). The scaling factor concept originates from *similar media theory* (Miller and Miller, 1956). This theory is based on the laws of viscous flow in porous material and assumes that the structure of void spaces is geometrically similar among different locations. In principal, according to similar media theory, a scale factor is the ratio of the local characteristic length of a soil at location i and the characteristic length of a reference soil. Then soil water retention and hydraulic conductivity curves (h and K) at any location i can be related to a reference h_r and K_r curves with a singke scaling factor:

$$h_r = h_i \cdot \lambda_i \tag{1a}$$

$$K_r = \frac{K_i}{\lambda_i^{\,2}} \tag{1b}$$

where subscript i = 1, …, N denote sample locations and r indicates the reference curve. Early scaling studies presented by Warrick et al. (1977) and Russo and Bresler (1980) applied a regression analysis to either soil water retention or unsaturated hydraulic conductivity data to determine scale factors. These studies emphasized that independent scaling of h and K curves for the same dataset may result in different distributions of scaling factors. It was Clausnitzer et al. (1992) who introduced an alternative scaling approach in which both hydraulic functions are scaled simultaneously, thus yielding a single set of scaling factors. Applications of various scaling methods can be found in Hopmans et al. (1987) and Clausnitzer et al. (1992).

Spatial distribution of scaling factors have been effectively used to assess the effect of variable soil hydraulic properties on soil water flow (Peck et al., 1977; Ahuja et al., 1984; Hopmans and Stricker, 1989; Kim et al., 1997) and on solute transport (Hopmans et al., 1988; van Ommen et al., 1989; Roth and Hammel, 1996). Provided that the assumption of geometric similarity theory is valid, the Miller and Miller scaling offers significant advantage for stochastic modeling by expressing the spatial variability of soil hydraulic properties using only one parameter as opposed to the van Genuchten model requiring five parameters (K_s, n, α, θ_r, and θ_s), each of which varies spatially and may show intercorrelations.

Following the similar media theory, Denton et al. (2004) implemented scaling analysis to scale the soil water retention and unsaturated hydraulic conductivity curves for 97 samples (70 samples with transient data and 27 samples with equilibrium data) using an existing model, SCALE (Clausnitzer et al., 1990, 1992). The scaling yields a set of scaling factors corresponding to each location (or sample). Then, reference functions in Eqn. (1a) and (1b), defined in the form of the van Genuchten-Mualem model, were determined simultaneously at 97 sample locations. To investigate the capability of scaling analysis in capturing the observed variability of soil hydraulic properties, samples were grouped in four ways:

- Soils divided into two groups based on data quality: 1) both good and poor data and 2) only good data.
- Soils divided into four groups based on soil texture classifications: 1) no prior knowledge on soil texture, 2) lithofacies classifications, 3) core scale classifications within lithofacies, and 4) mechanical classifications by the ANR.
- Soils all together without a prior knowledge on data quality and soil texture.

Data from each sample was considered to be of either good or poor quality. Transient multistep outflow data for 70 samples were considered to be "good" data. Static equilibrium data

available for 27 samples were denoted to be relatively "poor" data. Combination of the data quality and the soil texture classes yields seven subgroups, each scaled with two of the scaling methods available in SCALE: Method 1 includes a simultaneous scaling analysis of soil water pressure and log transformed unsaturated hydraulic conductivity, i.e., h and ln K. Method 2, on the other hand, is a simultaneous scaling of log transformed h and K (i.e., ln h and ln K). Samples when scaled according to the two data quality groups, four soil textural groups, and two scaling methods produce 14 sets of scaling factors, each including 97 scaling factors. Each subgroup has a scaled mean curve defined by the van Genuchten parameters.

The success of scaling analysis in presenting the local heterogeneity is determined based on two criteria: 1) the percent reduction in sum of squared deviations between the scaled mean hydraulic functions and individual scaled data for each sample location and 2) the degree of correlation between the original and de-scaled pressure head and conductivity values. The parameters of the scaled mean curve and scaling factors are used to de-scale the individual scaled curves to the original curves. The differences between original and de-scaled values are referred to as scaling errors in the text and are indicative of the amount of spreading around the mean curve. A protocol for the implementation of the scaling procedure and different scaling methods are discussed in detail elsewhere (Denton et al., 2004).

Spatial Variability of Scaling Factors

ANOVA was applied to determine the effect of the scaling methods on the spatial distribution of scaling factors and scaling errors associated with the scaling analysis. The ANOVA results, which are described elsewhere (Denton et al., 2004), indicated that neither the data quality nor the soil textural classifications has a significant effect on the distribution of scaling factors and errors. However, the scaling method plays a significant role in minimizing the error: scaling ln h and ln K data together yields less errors than scaling h and ln K data. Therefore, 97 scaling factors that were derived from simultaneous scaling of ln h and ln K functions without grouping with respect to data quality and soil texture descriptions were selected to be used in the numerical modeling of the subsurface heterogeneity. One outlier was identified, thus discarded for further analysis.

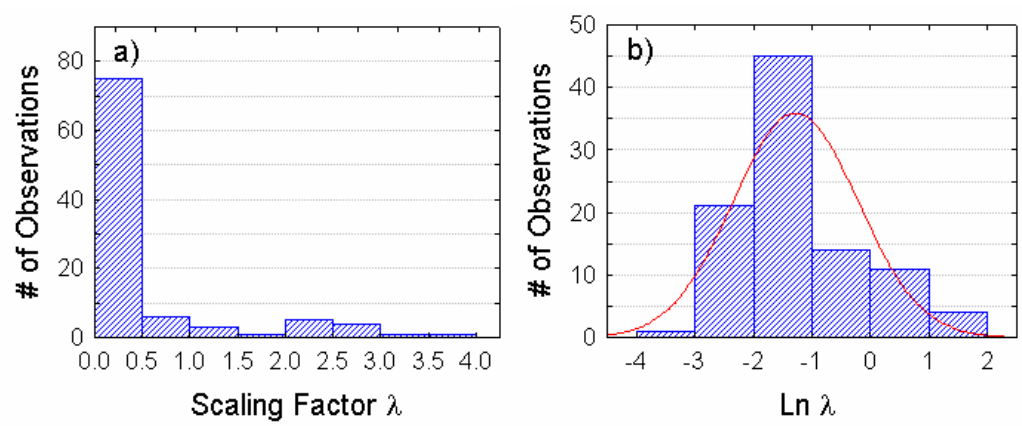

Figure 4: Frequency distribution of scaling factors. a) scaling factors λ, and b) log transformed scaling factors, ln λ, histogram fitted to a normal distribution with a mean of -1.28 and variance of 1.07.

Scaling factors λ have a large range (from 0.04 to 3.88) with a mean of 0.55 and a variance of 0.67. The frequency plot in Figure 4a shows a long tail to the right, with most samples falling below 0.5. The shape of the histogram combined with a high positive skewness coefficient of 2.32 implies that log transformed scale factors (ln λ) can be approximated by a normal distribution as shown in Figure 4b. Log-normal distributions of scaling factors that we observed at our site are consistent with those reported in other studies that examined the spatial variability of unsaturated hydraulic properties through scaling analysis (Warrick et al., 1977; Simmons et al., 1980; Rao and Wagenet, 1985; Vachaud et al., 1988; Hopmans and Stricker, 1987; Hopmans et al., 1988; Tseng and Jury, 1994; Braud et al., 1995; Zavattaro et al., 1999). The coefficient variation (CV) is found to be 146%, much higher than those reported elsewhere (47 - 57%, Hopmans (1993); 53%; Zavaratto et al., 1999). Higher observed variability can be a result of a larger sampling area and a smaller sampling size. Sample mean and variance, estimated based on the mean μ and variance σ^2 of the ln λ are m = exp(μ + 0.5 σ^2) = 0.49 and $s^2 = m^2$ (exp(σ^2)-1) = 0.52, respectively.

From a modeling point of view, the analysis of scaling factor variability and its relationship to the lithofacies is of significance. The relationship between the lithofacies and scaling factors can be used to infer a suite of scaling factors with distinct statistical properties Figure 5 displays the mean distribution of scaling factors categorized by the lithofacies. The lithofacies effect represents the combined influence of depth and sediment texture on scaling factors since the lithofacies are sorted in vertical sequence. The results suggest the existence of three subgroups of regions in the subsurface with a similar distribution of scaling factors. S and Var1 facies show similarities, with a much higher mean and a variance. Mean scaling factors in the SL1 facies is nearly equal to that in the SL2 facies. Evidently, the remaining four facies, the HP1, Var2, C-Si-L, and HP2, appear to fall in the same group with small means and variances. The delineation of these zones may control flow and nitrate transport and will provide a basis to conceptualize the subsurface heterogeneity of the numerical model.

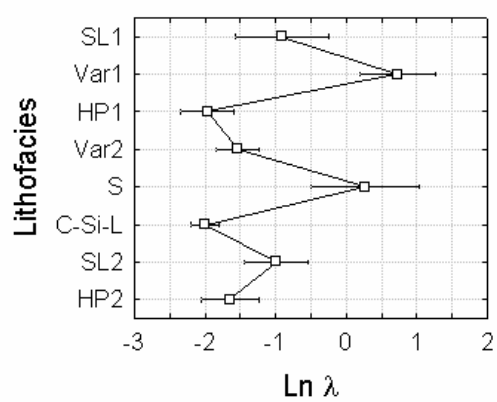

Figure 5: Lithofacies means of log transformed scaling factors λ with 95% confidence intervals around the means

Geostatistical Analysis of Scaling Factor Spatial Variability

Geostatistics has been used for spatial estimation in a variety of disciplines in the earth sciences, including hydrology. This technique has an important role in the development and application of stochastic methods as it introduces relevant improvements on the definition of spatial variability of data. Within the framework of geostatistical approach, a given property is

recognized as a regionalized variable (RV) that is a function describing natural phenomena with a spatial distribution. As opposed to the conventional statistical approach, in geostatistics, spatial structure inherent in data is incorporated to describe spatial variability. Following earlier work by Krige (1951), Matheron (1963) developed the theory of regionalized variables to improve ore grade estimation. The basic concepts and underlying principles of geostatistics have been extensively described in the literature (Journel and Huijgreghs, 1978; Isaak and Srivastava, 1989; Deutsch and Journel, 1992).

In this section, geostatistical analyses are implemented to quantify the amount of spatial variability that is unexplained by depth (or lithofacies location). Variogram analysis provides the model of spatial continuity λ. Scaling factors were described by a log-normal distribution with no spatial trends.

Experimental Semivariograms for Scaling Factors

For scaling factors, which were derived from scaling analysis on the undisturbed core samples, sampling locations were widely scattered over the sampling domain and the sampling interval was much coarser than for the nitrate and water content sampling intervals (see appendix A). To evaluate horizontal semivariograms for scaling factors, the vertical bandwidth was extended to approximately 30 cm (1 foot) to ensure enough number of pairs.

Since lithofacies boundaries delineate areas with a different distribution of scaling factors (Figure 5), vertical semivariograms for scaling factors were evaluated by pairing only data points that belong to the same lithofacies. This was done by adding an artificial vertical distance (300 m = ~ 1000 ft), which is much larger than the maximum lag distance (30 m), to separate samples from different lithofacies.

The **gamv** algorithm in Geostatistical Software Library, GSLIB (Deutsch and Journel, 1992) was used to compute the semivariogram models. Azimuth angle was chosen to be 90° because there is more data continuity; and in turn more pairs, in the E-W direction than N-S. Directional semivariograms were contructed with lag intervals appropriately assigned proportional to average horizontal and vertical sampling distance. Maximum lag distances were set to no more than one half the maximum sampling dimensions (the horizontal sampling domain is the entire orchard lengthm, i.e., 37 m or 170 ft). Semivariance values with too few pairs (< 2 pairs) were discarded.

Theoretical Directional Semivariograms

The theoretical semivariogram model is a mathematical expression to represent the experimental semivariogram when generating random fields in numerical modeling. In our analysis, the widely used spherical model is considered to be most suitable to fit to the experimental data:

$$\gamma(h) = c\left(\frac{1}{2}\frac{h}{a} - \frac{1}{2}\left(\frac{h}{a}\right)^3\right), \text{ if } 0 \le h < a \tag{2a}$$

$$\gamma(h) = c\,, \text{ if } h \ge a \tag{2b}$$

where c and a are the parameters corresponding to the sill and the range, respectively. Parameter estimation of the individual semivariogram models is obtained by a least squares optimization process giving the best-fit values of c and a. The fitting is performed per direction and per subplot. Under ideal conditions, when the distance between pairs become very large, the sample

values are considered to be stochastically independent. Then, semivariogram values at sufficiently large *h* become more or less constant. The range is the lag distance at which the semivariogram reaches this constant value referred to as sill that describes the total variance between sets of independent samples. The sample variance serves as a good approximation of the magnitude of the sill when the observations are evenly distributed over the area of interest and the dimension of the area is at least three times as large as the range (Isaak and Srivastava, 1989). Sometimes, another parameter referred to as nugget effect is used to quantify spatial variation occurring at distances smaller than the shortest sampling distance.

Results: Variograms of Scaling Factors

Scaling factors, despite their high variability, exhibit a statistically significant spatial continuity. The horizontal semivariogram shows an oscillatory nature as the lag interval increases. Perhaps, pairs located near the facies boundaries were matched, although they are from different depositional events, causing high variation. Horizontal layering seems to create pronounced anisotropy, with a scale of horizontal correlation longer than the vertical one (a range of 5.4 m in the vertical direction as opposed to a range of 1.7 m in the horizontal direction), as is also reported in earlier studies (Byers and Stephans, 1983; Sudicky, 1986). The vertical semivariogram shows a fairly clear structure with a range of 1.7 m that covers the average thickness of lithofacies (Figure 6b). The sill of the vertical direction is comparable to the variance of the entire dataset (1.14). The sill in the horizontal direction (0.77) is nearly half the sill in the vertical direction (Figure 6a).

Previously, only a few studies analyzed scaling factors with geostatistical tools and considered them as a realization of a stochastic function (Jury et al., 1987; Russo, 1991; Zavaratto et al., 1999). The analysis of Hopmans et al. (1988), based on 52 measurements of K within 2-m^2 site (with spacing of 0.25 m) in loamy sand soil at the Hupselse Beek watershed in Netherlands, suggested that a horizontal correlation scale of 0.5 m for log-transformed scaling factors. Due to the lack of sufficient data, they assumed equal distribution of scaling factors in the vertical direction. Zavattaro et al. (1999) used similar media theory to characterize spatial variability of hydraulic functions near saturation that were measured at 37 locations. They observed a clear spatial dependence of the scale factors within distances of at least 8 to 10 m and uncorrelated variance (i.e., nugget) of ~13% of the total variability.

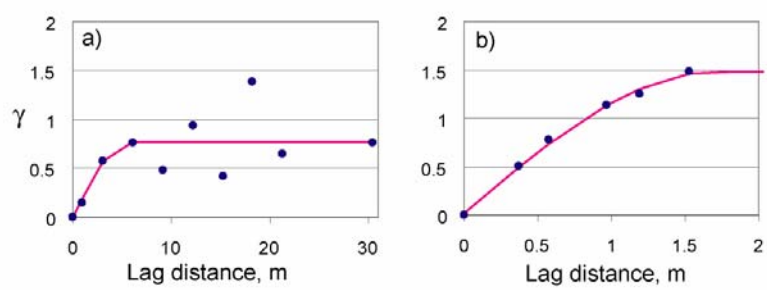

Figure 6: Experimental and spherical model semivariograms for log-normally distributed scaling factors, ln λ, a) in the horizontal and b) in the vertical directions. Solid circles represent the experimental semivariograms while solid lines are the spherical semivariogram models fitted to the experimental semivariograms.

References

Ahuja, L. R., J. W. Naney, and D. R. Nielsen, 1984. Soil-water properties and infiltration modeling. *Soil Sci. Soc. Am. J.*, 48(5): 970-973.

Allen-King, R. M., R. M. Halket, and D. R. Gaylord, 1998. Characterizing the heterogeneity and correlation of perchloroethene sorption and hydraulic conductivity using a facies-based approach. *Water Resour. Res.*, 34(3): 385-396.

Braud, I., A. C. Dantas-Antonio, and M. Vauclin, 1995. A stochastic approach to studying the influence of the spatial variability of soil hydraulic properties on surface fluxes, temperature, and humidity.*J. Hydrol.*, 165(1-4): 283-310.

Byers, E., and D. B. Stephans, 1983. Statistical and stochastic analysis of hydraulic conductivity and particle size in a fluvial sand. *Soil Sci. Soc. Am. J.*, 47: 1072-1081.

Clausnitzer, V., J. W. Hopmans, and D. R. Nielsen, 1990. A comprehensive scaling procedure allowing to scale both soil water retention and hydraulic conductivity data simultaneously. Pap. 100018, Dept. of Land, Air, and Water Resources, University of California, Davis.

Clausnitzer V., J. W. Hopmans, and D. R. Nielsen, 1992. Simultaneous scaling of soil-water retention and hydraulic curves. *Water Resour. Res.*, 28(1): 19-31.

Davis, J. M., R. C. Lohmann, F. M. Philips, J. L. Wilson, and D. W. Love, 1993. Architecture of the Sierra Ladrones Formation, central New Mexico. Depositional controls on the permeability correlation structure, *Geol. Soc. Am. Bull.*, 105: 998-1007.

Davis, J. M., L. J. Wilson, F. M. Philips, and M. B. Gotkowitz, 1997. Relationship between fluvial bounding surfaces and the permeability correlation structure. *Water Resour. Res.*, 33(8): 1843-1854.

Denton, M. A., 2004. Hydraulic Characterization of a Heterogeneous, Deep vadose Zone Beneath an Orchard in the Eastern San Joaquin Valley. M.S. Thesis. University of California, Davis.

Denton, M. A., Y. S. Onsoy, T. Harter, J. W. Hopmans, and W. R. Horwath, 2004. Long-term Nitrate Leaching Below the Root Zone in California Tree Orchards. Technical Completion Report to University of California Water Resources Center, 122 pp.

Deutsch, C. V., and A. G. Journel, 1992. *GSLIB: Geostatistical Software Library and User's Guide*. Oxford University Press, New York, 340 pp.

Hopmans, J. W., and J. N. M. Stricker, 1987. Soil hydraulic properties in the study area Hupselse Beek as obtained from three different scales of observation: An overview, Res. Rep., Dep. Hydraul. Catchment Hydrol., Wageningen.

Hopmans, J. W., H. Schukking, P. J. J. F. Torfs, 1988. Two-dimensional steady state unsaturated water flow in heterogeneous soils with autocorrelated soil hydraulic properties. *Water Resour. Res.*, 24(4): 2005-2017.

Hopmans, J. W., and J. N. M. Stricker, 1989. Stochastic analysis of soil water regime in a watershed. *J. Hydrol.*, 105(1-2): 57-84.

Hopmans, J.W., 1993. Scaling applications in soil characterization. *In*: M. Th. van Genuchten and F. L. Ley (eds.) Indirect Methods for Estimating the Hydraulic Properties of Unsaturated Soils. University of California, Riverside, p. 539-552.

Isaak, E. H., and R. M. Srivastava, 1989. Applied Geostatistics. Oxford University Press.

Johnson, N. M., and S. J. Dreiss, 1989. Hydrostratigraphic interpretation using indicator geostatistics. *Water Resour. Res.*, 25(12): 2501-2510.

Journel, A. G., and C. J. Huijbregts, 1978. Mining Geostatistics. London, Academic Press.

Jury, W. A., D. Russo, G. Sposito, and H. Elabd, 1987. The spatial variability of water and solute transport properties in unsaturated soil: II. Scaling models of water transport. *Hilgardia*, 55: 33-56.

Kim, C. P., J. N. M. Sticker, and R. A. Feddes, 1997. Impact of soil heterogeneity on the water budget of the unsaturated zone. *Water Resour. Res.*, 33(5): 991-1000.

Kolterman, C. E., and S. M. Gorelick, 1996. Heterogeneity in sedimentary deposits: A review of structure-imitating, process-imitating, and descriptive approaches. *Water Resour. Res.*, 32(9): 2617-2658.

Krige, D. G., 1951. A statistical approach to some basic mine valuation problems in the Witwater Srand. *J. Chem. Metalurgical and Mining Soc. South Africa*, 52: 119-139.

Matheron, G., 1963. Principles of Geostatistics, Economic Geology, No: 58. p. 1246-1266.

Miller, E. E., and R. D. Miller, 1956. Physical theory for capillary flow phenomena. *J. Apply. Phys*., 27(4): 324-332.

Peck, A. J., R. J. Luxmoore, and J. C. Stolzy, 1977. Effects of spatial variability of soil hydraulic properties in water budget modeling. *Water Resour. Res.*, 13(2): 348-354.

Roth, K., and K. Hammel, 1996. Transport of conservative chemical though an unsaturated two-dimensional Miller-similar medium with steady state flow. *Water Resour. Res.*, 32(6): 1653-1663.

Sposito, G., 1998. Scale Dependence and Scale Invariance in Hydrology. Cambridge University Press, 423 pp.

Rao, P. S. C., and R. J. Wagenet, 1985. Spatial variability of pesticides in field soils: methods for data analysis and consequences. *Weed Sci*., 33(2): 18-24.

Russo, D., and E. Bresler, 1980. Scaling soil hydraulic properties of a heterogeneous field. *Soil Sci. Soc Am. J.*, 44: 681-684.

Russo, D., 1991. Stochastic analysis of simulated vadose zone solute transport in a vertical cross section of heterogeneous soil during nonsteady water flow. *Water Resour. Res.*, 27(3): 267-283.

Sudicky, E. A., 1986. A natural gradient experiment on solute transport in a sand aquifer: Saptial variability of hydraulic conductivity and its role in the dispersion process. *Water Resour. Res.*, 22: 2069-2082.

Tseng, P. -H., and W. A. Jury, 1994. Comparison of transfer function and deterministic modeling of area-averaged solute transport in a heterogeneous field. *Water Resour. Res.*, 30(7): 2051-2064.

Vachaud, G., M. Vauclin, and P. Balabanis, 1988. Stochastic approach of soil water flow through the use of scaling factors: Measurement and simulation. *Agric. Water Manag*., 13: 249-261.

van Ommen, H. C., J. W. Hopmans, S. E. A. T. M Van der Zee, 1989. Prediction of solute breakthough from scaled soil physical properties.*J. Hydrol.*, 105(3-4): 263-273.

Warrick, A. W., G. J. Mullen, D. R. Nielsen, 1977. Scaling field measured soil hydraulic properties using a similar media concept. *Water Resour. Res.*, 13(2): 355-362.

Zavaratto, L., N. Jarvis, and L. Persson, 1999. Use of similar media scaling to characterize spatial dependence of near-saturated hydraulic conductivity. *Soil Sci. Soc Am. J.*, 63: 486-492.